

Porphyrin-Phthalocyanine triple-deckers; open, linked and caged systems

*A Thesis Presented to University of East Anglia in Partial Fulfilment of the
Requirements for the Degree of Doctor of Philosophy*



Submitted by

Abdulaziz Musaad A Almohyawi

Supervised by

Prof. Andrew N Cammidge

©This copy of the thesis has been supplied on condition that anyone who consults it is understood to recognise that its copyright rests with the author and that use of any information derived there from must be in accordance with current UK Copyright Law. In addition, any quotation or extract must include full attribution.

Declaration:

This research described in this is, to the best of my knowledge, original except where due reference is made.

Abdulaziz Musaad Almohyaw

Abstract

Open and linked heteroleptic triple deckers (TD) based on porphyrin-phthalocyanine-porphyrin order are investigated toward obtaining cage systems. They have potential applications in electronic devices such as molecular motion, switches, recognition, biomimetic chemistry, and nanoreactors. This model aims to increase the stability of phthalocyanine in that high order of assembly. Series of porphyrins were newly designed to investigate different routes to the cage system. The cage systems are found easily achievable through open and linked triple-deckers using lanthanum as a template for heteroleptic TD. The highest yield was achieved from linked TD through porphyrins' dyad, but its preparation is a challenge. On the other hand, the instability of the TDs based on the rest of the lanthanides was a barrier to achieving caged models that encapsulated Pc.

Access Condition and Agreement

Each deposit in UEA Digital Repository is protected by copyright and other intellectual property rights, and duplication or sale of all or part of any of the Data Collections is not permitted, except that material may be duplicated by you for your research use or for educational purposes in electronic or print form. You must obtain permission from the copyright holder, usually the author, for any other use. Exceptions only apply where a deposit may be explicitly provided under a stated licence, such as a Creative Commons licence or Open Government licence.

Electronic or print copies may not be offered, whether for sale or otherwise to anyone, unless explicitly stated under a Creative Commons or Open Government license. Unauthorised reproduction, editing or reformatting for resale purposes is explicitly prohibited (except where approved by the copyright holder themselves) and UEA reserves the right to take immediate 'take down' action on behalf of the copyright and/or rights holder if this Access condition of the UEA Digital Repository is breached. Any material in this database has been supplied on the understanding that it is copyright material and that no quotation from the material may be published without proper acknowledgement.

Acknowledgement

Firstly, I would like to express my special thanks of gratitude to my primary supervisor Prof. Andrew Neil Cammidge for his unlimited support during the past years. His guidance and advice were the light for my scientific life in UEA and beyond. Cammidge has shaped me into the researcher that I am today; words are not enough to reward his patience and professional supervision.

Also, I would like to extend my thanks to the past and present of my supervisory team for their valuable comments and supports Prof. Richard Stephenson, Dr. Isabelle Fernandes and Dr. Chris Richards.

Also, I would like to express my sincere gratitude to my parents and my brothers and sisters for encouraging and supporting me throughout my study in the UK.

I want to also thank the past and current members of the Cammidge team for a wonderful work environment. Extending that to all people in chemistry school, especially those who work on the third floor.

Thanks are also due to Umm Alqura University for funding my PhD research and providing me with an opportunity to achieve my goal. Thanks are extended to the Saudi Arabia Cultural Bureau in London for their support during my PhD.

A special thanks to my friends in the UK and back home who make this journey simple, extended that to Saudi Students Society in Norwich.

List of abbreviations

Ac	Acetate
acac	Acetylacetonate
AcOH	Acetic Acid
br	Broad
b.p	Boiling point
C ₁₀	Decane
DTD	Direct (open) Triple deckers
°C	Degrees Celcius
cm	Centimetre
COSY	Correlation spectroscopy
δ	Chemical Shift
d	Doublet
d-	Deuterated
dd	Doublet of doublets
DCM	Dichloromethane
DDQ	2,3-Dichloro-5,6-dicyano-1,4-benzoquinone
DMF	Dimethyl formamide
DMSO	Dimethyl sulfoxide
DNA	Deoxyribonucleic acid
dt	Doublet of triplets
ε	Extinction coefficient
eq	Equivalent
g	Grams
h	Hours
HOMO	Highest occupied molecular orbital
Hz	Hertz
IR	Infrared
J	Coupling constant
K	Kelvin
L	Ligand
Ln	Lanthanide
TD(La)	Lanthanum linked Triple deckers
LUMO	Lowest unoccupied molecular orbital
m	Multiplet

M (in structures)	Metal (any)
M	Molarity
MALDI-ToF-MS	Matrix-assisted laser desorption/ionization (time of flight)
Me	Methyl
MHz	Megahertz
min	Minutes
mg	Milligrams
ml	Millilitres
mm	Millimetres
mmol	Millimol
m.p.	Melting point
MS	Mass spectrometry
Mwt	Molecular weight
nm	Nanometres
NMR	Nuclear Magnetic Resonance
oi	<i>Ortho</i> -inside
oo	<i>Ortho</i> -outside
Pc	Phthalocyanine
PDT	Photodynamic therapy
Pet.	Petroleum
pm	Picometre
Por	Porphyrin
ppm	Parts per million
py	Pyridine
pyr	Pyrrole
q	Quadruplet
r.t.	Room temperature
RCM	Ring-closing metatheses
s	Singlet
S	Solvent
SMM	Single-Molecule Magnets
t	Triplet
^t Bu	<i>tert</i> -butyl
^t py	4- <i>tert</i> -butyl Pyridine

TD	Triple decker
Tc	Coalescence temperature
THF	Tetrahydrofuran
TLC	Thin Layer Chromatography
TPP	Tetraphenylporphyrin
TPPOH	5,10,15-tris-phenyl-20-(<i>p</i> -hydroxyphenyl)porphyrin
THxTPPOH	5,10,15-tris- <i>p</i> -(hex-5-ene-1oxy)phenyl-20-(<i>p</i> -hydroxyphenyl)porphyrin
TBnTPP	5,10,15,20-Tetra- <i>p</i> Benzyloxyphenylporphyrin
TBnTPPOH	5,10,15-tris- <i>p</i> -(benzyloxy)phenyl-20-(<i>p</i> -hydroxyphenyl)porphyrin
HxBnTPP	5,10,15-tris- <i>p</i> -(benzyloxy)phenyl-20-(hex-5-ene-1oxy)phenylporphyrin
tt	Triplet of triplets
UV-vis	Ultraviolet-visible

Table of Contents

ABSTRACT	II
ACKNOWLEDGEMENT	III
LIST OF ABBREVIATIONS	IV
TABLE OF CONTENTS	VII
1. PREFACE	1
2. AIMS	2
3. INTRODUCTION	4
3.1 MECHANICAL ENTRAPMENT.....	4
3.2 HOST SYSTEMS BASED ON CYCLIC PORPHYRIN DIMERS	4
3.3 CYCLIC PORPHYRIN CAGE	10
3.4 SYNTHESIS OF PORPHYRIN CAGE	12
3.6 THE CHEMISTRY OF PORPHYRIN	20
3.7 THE CHEMISTRY OF PHTHALOCYANINES	32
3.8 DYADS	34
4. RESULTS AND DISCUSSION	43
4.1 PRE-ORGANIZED PORPHYRIN CAGE	43
4.1.1 INTRODUCTION	43
4.1.2 PREPARATION OF <i>p</i> -HEX-5-EN-1-OXYBENZALDEHYDE	46
4.1.3 PREPARATION OF 10,15,20-TRIHEX-5-EN-1-OXY- <i>p</i> -PHENYL-5- <i>p</i> -HYDROXYPHENYLPORPHYRIN	47
4.1.4 TETRAKIS- <i>p</i> -METHOXY PHENYL PORPHYRIN	49
4.1.5 DYAD INTERMEDIATE.....	51
4.1.6 IMPROVEMENT ATTEMPTS:	56
4.1.7 PREPARATION OF 10,15,20-TRIBENZYLOXY PHENYL- <i>p</i> -HYDROXYPHENYL PORPHYRIN	59
4.1.8 PHTHALOCYANINE	61
4.1.9 TRIPLE DECKERS (TD)	62
4.1.10 CYCLIC TRIPLE DECKERS (CTD).....	66
4.1.11 REDUCTION OF CTD	70
4.1.12 CONCLUSION.....	72
4.2 SELF-ORGANIZED PORPHYRIN CAGE.....	73
4.2.1 INTRODUCTION	73
4.2.2 DIRECT TRIPLE DECKERS (DTD) FORMATION	73
4.2.3 CYCLIC DIRECT TRIPLE DECKERS (CDTD).....	77

4.2.4 REDUCTION OF ALKENE LINKERS OF CDTD	79
4.2.5 PORPHYRIN CAGE THROUGH DABCO TEMPLATE	80
4.2.5.1 PREPARATION OF ZINC TETRAKIS P-HEX-5-EN-1-OXY-PHENYL PORPHYRIN.....	80
4.2.5.2 PREPARATION OF ZINC PHTHALOCYANINE.....	81
4.2.5.3 TRIPLE DECKERS USING DABCO	81
4.2.6 CONCLUSION	83
4.3 LANTHANIDES' EFFECT	84
4.3.1 INTRODUCTION	84
4.3.2 NEODYMIUM TRIPLE DECKERS DTD(Nd)	86
4.3.3 SAMARIUM TRIPLE DECKERS DTD(Sm)	88
4.3.4 EUROPIUM TRIPLE DECKERS DTD(Eu)	89
4.3.5 GADOLINIUM TRIPLE DECKERS DTD(Gd)	90
4.3.6 DYSPROSIUM TRIPLE DECKERS DTD(Dy).....	92
4.3.7 YTTERBIUM TRIPLE DECKERS DTD(Yb).....	93
4.3.8 LUTETIUM TRIPLE DECKERS DTD(Lu)	94
4.3.9 CONCLUSION AND FUTURE WORK	96
5. EXPERIMENTAL SECTION.....	98
5.1 GENERAL METHODS.....	98
5.2 EXPERIMENTAL PROCEDURES	99
6. REFERENCES	132
7. APPENDIXES	136

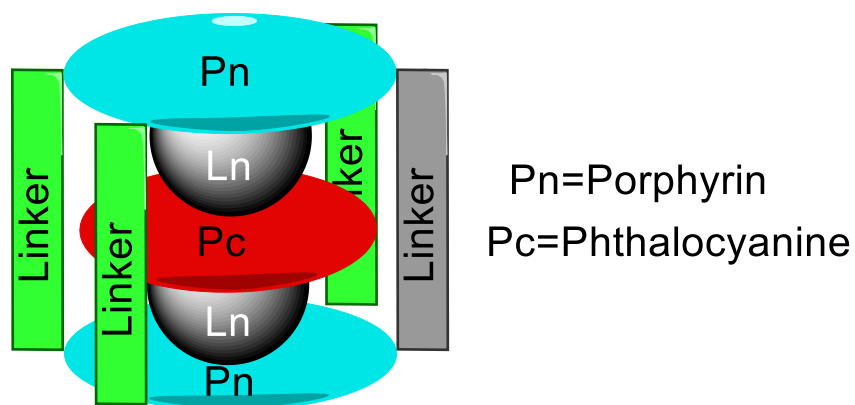
1. Preface

Beyond classical chemistry, the supramolecular field focuses on designing a component with mechanical ambitions like molecular machines, single molecular magnets and nanoreactors. The demand for new solutions for energy sources, data storage, electronic devices and, of course, medical treatment increased in recent decades. Supramolecular chemistry is defined by multicomponent molecular assemblies in which the component structural units are typically held together by a variety of weaker (non-covalent) interactions, such as the metal-donor bonds, that hold organic components together forming larger assemblies¹. Lehn described supramolecular chemistry as ‘the designed chemistry of the intermolecular bond’²

Unlike polymerisation, the selective binding of a substrate by a molecular receptor to form a supramolecular compound involves molecular recognition which rests on the molecular information stored in the interacting species. The functions of supramolecular assemblies cover recognition materials, catalysis field and charge transport in the same way, complementing porous organic frameworks (POF), metal-organic frameworks (MOF) and covalent organic frameworks (COF). In combination with polymolecular organisation, they open ways towards molecular and supramolecular devices for information processing and signal generation. The development of such devices requires the design of molecular components performing a given function such as photoactive, electroactive, ionoactive, thermoactive, or chemoactive and suitable for assembly into an organised array. This thesis will cover attempts to synthesise encapsulated phthalocyanines within porphyrin cages, towards investigating controlled assembly of triple-deckers in the order of porphyrin-phthalocyanine-porphyrin, and assessing their behaviour for potential application in electronic devices.

2. Aims

In recent years, porphyrin cages have been highlighted as potential models in advanced applications such as catalysts, molecular machines and organic single-molecule magnets, which attracted researchers to design models that meet the demands of new solutions for quantum computing, environmental issues, photodynamic therapy and energy resources. Porphyrin cages are known in the field, but there are rare examples due to several factors such as low yielding reactions, and difficult separation. We take a step toward contributing to the field and investigating its chemistry in the research journey. Our ambition was to build a cage from porphyrins that host a large molecule such as phthalocyanine to study its synthesis and open the gate for researchers in this direction. The model that we planned to prepare is new in the field, but there is a similarity in the approach in some studies.



The assembled order is varied due to the similarity in their electronic properties and reactivity³. Therefore, pre-organization led toward controlling the synthesis and increasing the overall yield⁴. The magnetic property of simple triple-deckers has been investigated by several studies that confirmed their favourable characteristics.

In the first aspect, we will design new porphyrin derivatives toward examining the best way toward making the cage. Encapsulating Pc into the cage cavity will be unique in the field, which may have potential applications in PDT or SMM. Also, we will study the effects of some lanthanide metals as a template on the formation of triple-decker intermediates.

Chapter 3

Introduction

3. Introduction

3.1 Mechanical entrapment

To start defining the phrases of the area, chemists defined mechanical bonds as entanglement in space between two or more molecular entities (component parts) such that they cannot be separated without breaking or distorting chemical bonds between atoms. Whereas they defined *component part* as a group of atoms, or '*molecular entity*', comprised of chemical bonds, which is mutually engaged in mechanical bonding with another molecular entity. Therefore, a *mechanomolecule* is a molecule possessing one or more mechanical bonds⁵. The importance of mechanical bonds is their uses in a variety of contexts and dynamic properties to build molecular machines and new materials⁶. Mechanical bonds are also known to efficiently absorb mechanical energy at low forces, but their behaviour at high forces is still under investigations⁶. That led us to define the Mechanical entrapment as a guest component encapsulated by host component mechanically (without bonds between cage and trapped guest).

3.2 Host systems based on Cyclic Porphyrin Dimers

Cyclic Porphyrin Dimers CPD are constrained host systems where two linkers join two porphyrins in a macrocycle. They gained attention due to their unique conformational properties. They can be considered as cofacial dyad and have been significantly exploited in the fields of molecular motion, switches, recognition, biomimetic chemistry, and nanoreactors. The properties of two porphyrin units together are affected by the kind of linker that connect them. It is possible to form molecular clefts with different shapes and sizes that can host various guest molecules and control their orientation inside the cavity of the cyclic dimer.

Also, the presence of different metal cations plays significant role in the cyclic dimers that can tune their properties either as reactive sites or as regulation sites. Therefore, various cyclic porphyrin dimers have been developed and successfully utilised for numerous spectacular applications depending upon the cavity size, metal cations and the substrate interactions within the host frameworks (**figure 3.1**).

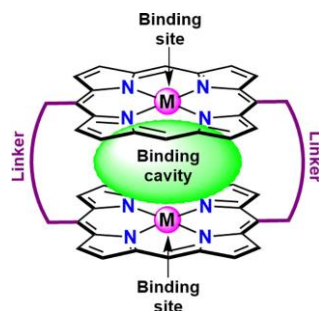
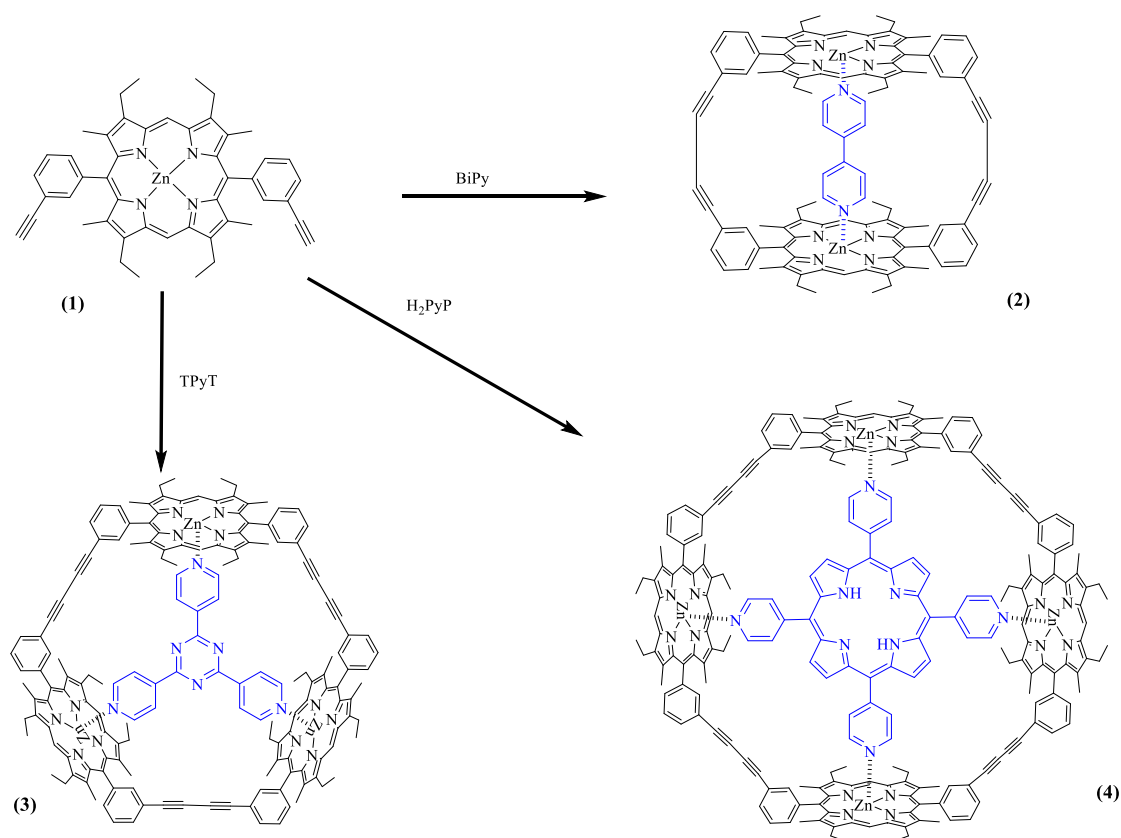


Figure 3.1: The general structure of cyclic porphyrin dimer, adapted from Mondal and Rath⁷

The molecular assembly functions are changed depending on what is encapsulated into the CPD cavity. The binding sites of porphyrin are active toward boosting chemical reaction and access to various applications. CPD was mentioned in catalytic field⁸, polymer field^{9,10}, single-molecule magnet (SMM)¹¹ and photodynamic therapy (PDT)¹². These potential applications encourage researchers to investigate the CPD model and their guests.

Harry Anderson and Jeremy Sanders also widely investigated the cyclic porphyrins using pyridine derivatives as a template to hold porphyrin units in proximity.¹³ There are significant observations under their methods such as ligands formation constant, kind of linkers, the cyclic size, and the ability of π bonds extension through meso positions. For example, the highest product yields of cyclic porphyrin dimers (**2**) were achieved using 4,4-bipyridine (BiPy), whereas the highest products yield of cyclic porphyrin trimers (**3**) was achieved using 2,4,6-tri(pyridine-4-yl)-1,3,5-triazine (TPyT) template (**scheme 3.1**).¹⁴

Under the same principles, the cyclic porphyrin can be extended by designing a special template that allows more porphyrin units to be assembled. For instance, cyclic porphyrin tetramer (**4**) was achieved using tetrakis-4-pyridyl porphyrin that prevents dimer from being observed. Also, Anderson and his co-workers successfully designed and applied two units of T6ef template, (1,2,3,4,5,6-hexakis((4'-((4'-(pyridin-4-yl)-2',5'-bis(trifluoromethyl)-[1,1'-biphenyl]-4-yl)ethynyl)phenyl)ethynyl)benzene), toward synthesis of the largest porphyrin cycle using twelve molecules (**figure 3.2**).¹⁵



Scheme 3.1: The pyridyl template effects on assembling multi porphyrin components in cyclic shapes.¹⁴

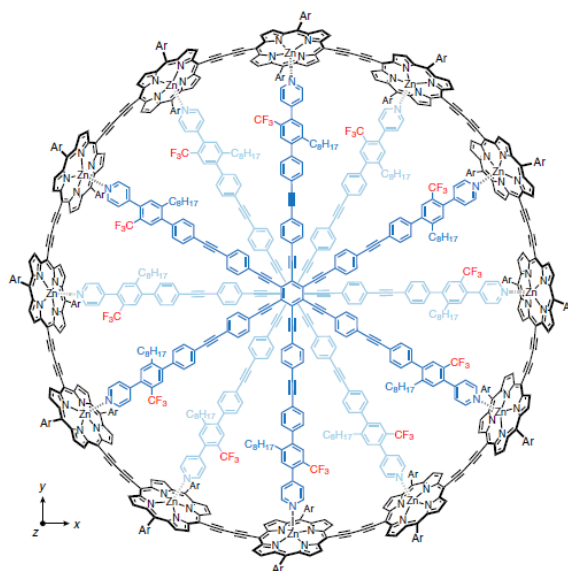


Figure 3.2: The largest cyclic porphyrin (adapted from Anderson *et al.*¹⁵)

Kang *et al.*⁸ examined the reactivity and binding of *p*-nitrophenyl diphenyl phosphate (PNPDPP) (Sarin gas) in the CPD (**figure 3.3**). They found that the decomposition of Sarin gas in the presence of CPD is faster by 1300x than normal conditions.

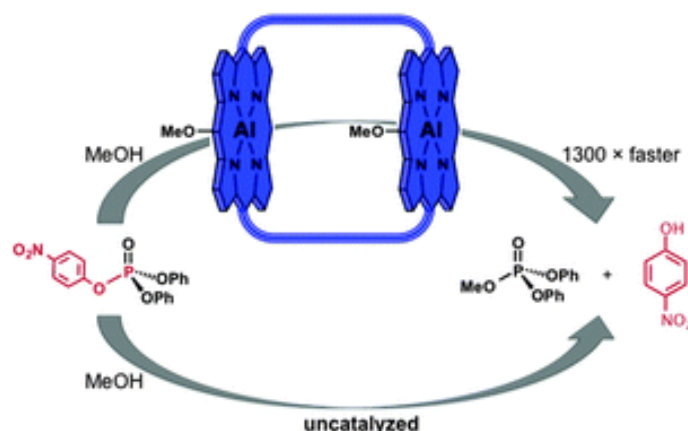


Figure 3.3: The reactivity of porphyrin cage toward catalysing of PNPDPP decomposition⁸

Also, Kang *et al.*¹⁶ have found that the CPD can be binding selectively with fullerenes. Different shapes and sizes of CPD were achieved by modulating the cavity shape and rigidity of cyclic dimeric and tetrameric porphyrin hosts as well as their metal sites. They found that the cavity of the dimeric system can host a large guest like fullerene C₇₀ due to its rectangular shape. Increasing the rigidity of the linkages increases the selectivity towards C₇₀ over C₆₀ due to the interaction between the cavity and the guest, especially when the porphyrins are metallated (**figure 3.4**). In contrast, they found that the tetrameric porphyrin can only host one fullerene C₆₀ due to the expansion of the first site making the other site smaller to fit the second as proposed (**figure 3.5**).

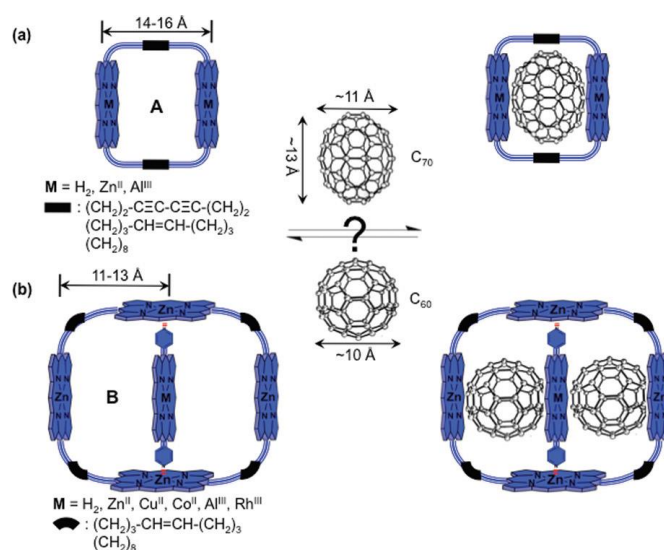


Figure 3.4: Adapted from Kang *et al.*¹⁶, the cavity size is different in the two models, affecting the binding and leading to selective behaviour toward the guest size and shape.

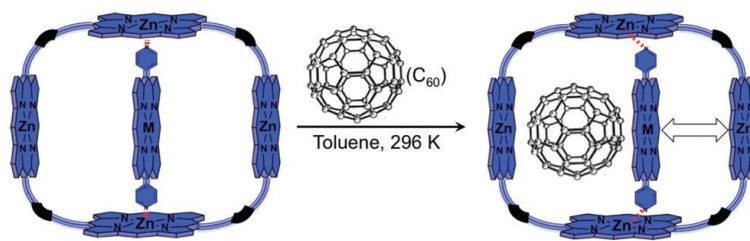
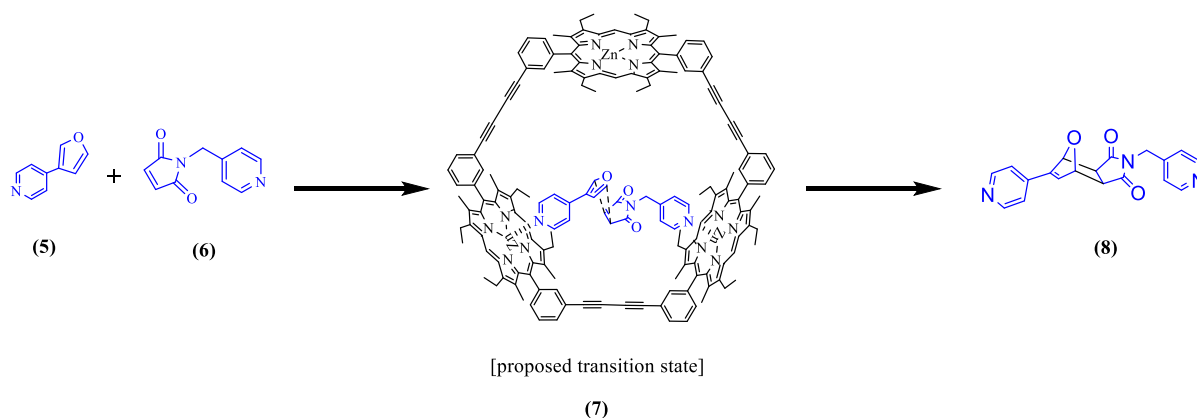


Figure 3.5: The tetrameric cavity is smaller and selective toward fullerene C_{60} , Totten *et al.*¹⁶

Regarding investigating the reactivity of cyclic porphyrin trimer toward its catalytic uses, Diels-Alder reaction was found to be selectively directed to form only *exo* isomer (**scheme 3.2**)¹⁷. The kinetic and thermodynamic studies of cyclic porphyrin trimer suggested that the reactants coordinated with the inner cavity, which accelerated the reaction by 6000 times more than the uncatalysed reaction¹⁷.



Scheme 3.2: Diels-Alder reactions can form only *exo* products in the presence of cyclic porphyrin trimer.

A cyclic porphyrin also was investigated by Ooyama *et al.*¹² toward generating singlet oxygen (1O_2) under visible light irradiation to evaluate its efficiency in photochemistry and its potential applications in photodynamic therapy (PDT). Their methodology measured the quantum yield (Φ) for the free base porphyrin dimer hosting fullerene C_{60} to determine the favourable pathway for electrons during excitation (**figure 3.6**). The evidence that they found from kinetic and thermodynamic data appears that the Φ value was lower for C_{60} hosted by the porphyrin cage. They concluded that as a result of charge-separated state formation $C_{60}^{\cdot-}$ -CPD $^{\cdot+}$, intersystem crossing (ISC) efficiency increased due to the formation of triplet excited state $^3(CPD)^*$. Therefore, the porphyrin cage hosting C_{60} can generate 1O_2 under visible light irradiation.



Figure 3.6: Singlet oxygen generation is increased under visible light due to the guest effect, adapted from Ooyama *et al.*¹²

3.3 Cyclic Porphyrin Cage

Chemists have also successfully synthesised a porphyrin cage, known as nanocage or nanoreactor, by several methods. Metallic binding sites, linker type, and binding cavity (**figure 3.7**) create active sites for photoreaction, thermo-reaction, or redox reactions, opening pathways to investigate the model systems.

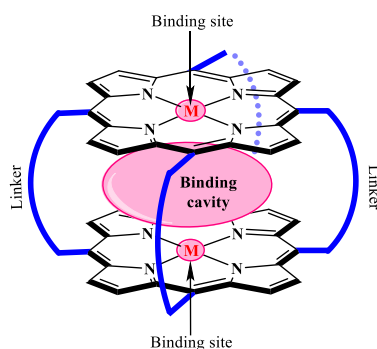
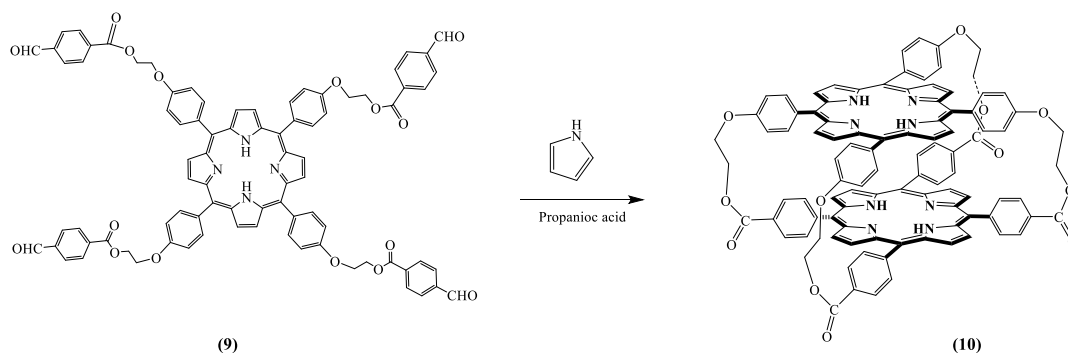


Figure 3.7: The general structure of porphyrin cage

One of the earliest attempts of synthetic porphyrin cage was reported by Kagan *et al.*¹⁸. Their method resulted in low yields due to hydrolyses of ester bonds in acidic conditions (**scheme 3.3**). They also noted that the interaction between components had broadened the Soret band in the UV-vis spectra in absorption and emission, but no shift was indicated. Whereas the Q bands of absorption and fluorescence intensity were red-shifted beside broadened. They suggested that the reduction of absorption energy has led to the shifts. Later, Sanders *et al.*¹⁹ introduced a special pair theory which suggested that there could be two Soret band signals, but they might overlapped as π system stabilises the radical cation formed in the initial charge separation step in the centre.



Scheme 3.3: The earliest method of cage preparation (adapted from Kagan *et al.*¹⁸).

Investigation into the cavity of nanocage systems resulted in several uses; for example, Cristina *et al.*²⁰ developed a washing based method (**figure 3.8**) to extract pure fullerene C₆₀ from a solid sample of cage charged with a mixture of fullerenes. Based on their results, extracting C₆₀ from fullerene mixtures selectively proved possible, providing a platform to design cages for selective extraction of different fullerenes and compounds. They called their method a sponge-like system which encapsulated and released fullerene in solid-phase.

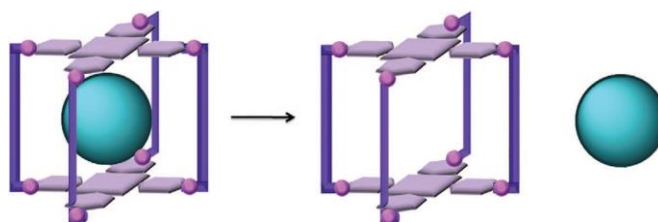


Figure 3.8: Schematic representation of the method developed by Cristina *et al.*²⁰

When homogeneous catalyst RhH(CO)₃ was encapsulated in their model by Reek *et al.*²¹, the selectivity toward higher *enantiomeric excess* (*ee*) was significantly increased in the hydroformylation of styrene derivatives (**figure 3.9**). There was obvious evidence of the effect of catalyst encapsulation on their selectivity that can be controlled by the cage as a second coordination sphere.

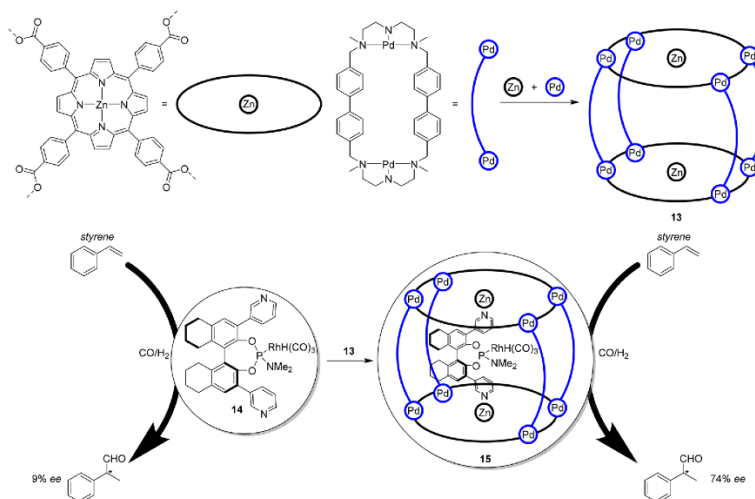


Figure 3.9: Adapted from Reek *et al.*²² encapsulation of ligand template RhH(CO)₃ in porphyrin cage gives an increase in confined space that leads to an increase in *ee* from 9% for the nonencapsulated catalyst RhH(CO)₃ to 74% (R) for the encapsulated catalyst²³.

Toward continuing overlook at porphyrin cages, Lanthanide encapsulated into fullerene C_{82} that itself is encapsulated in the cavity of porphyrin cage was investigated by Hajjaj *et al.*¹¹ toward studying its magnetic property. As $La@C_{82}$ and cyclo porphyrins that host copper on its binding sites are considered a paramagnetic component, they found that its magnetic state was reversed to ferromagnetic due to the interaction between Cu and carbon radical delocalised over the spherical network of C_{82} . Further reversal was recorded when the cage was locked by metathesis, making the analogue component generate a ferrimagnetic property (**figure 3.10**). Their study opens a new way to develop the single molecular magnets by investigating the interaction between Ln and TM into a Porous Organic Framework (POF) provided by porphyrin cage, which locks the metals closer to each other to interact.

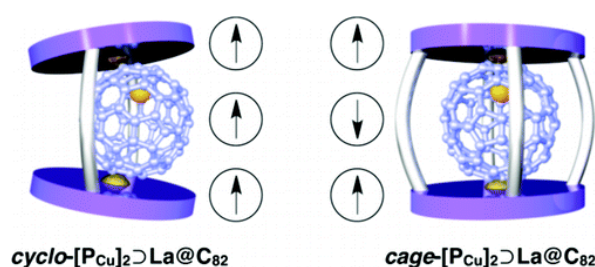


Figure 3.10: The spin ground state of $cyclo-[P_{Cu}]_2 \supset La@C_{82}$ is found quartet (left), and $cage-[P_{Cu}]_2 \supset La@C_{82}$ is found doublet in its spin ground state (right) as determined by DFT and Electron Spin Transient Nutation spectroscopy (ESTN) due to the geometrical position of fullerene between the two copper metals (adapted from Hajjaj *et al.*¹¹); ESTN spectroscopy is a pulsed ESR method that allows the investigation of the spin states of diluted analytes in frozen solvents¹¹. It is a powerful tool for determining the spin quantum number in order to identify the origin of the continuous wave electron spin resonance²⁴. Also, it is known as a two dimensional ESR spectroscopy²⁵.

3.4 Synthesis of porphyrin cage

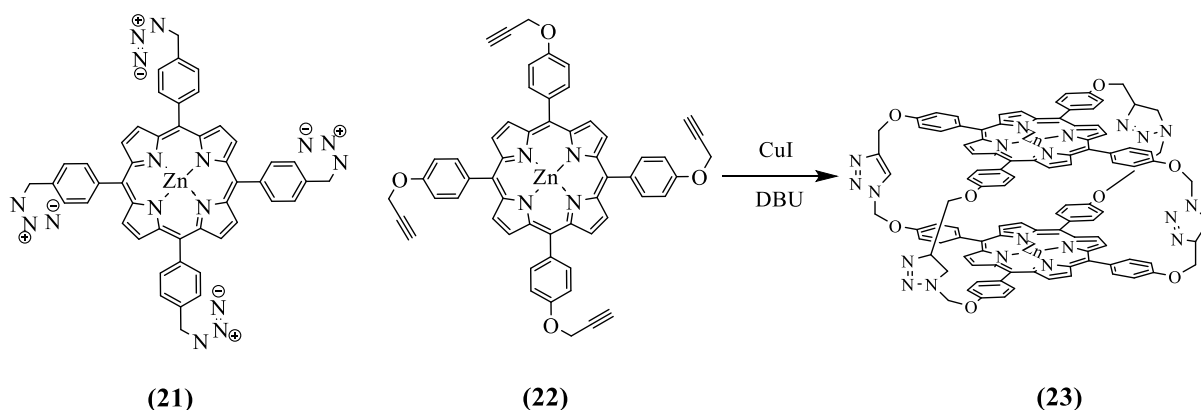
The synthetic method for preparing CPD is crucial for building an entrapment. Therefore we will introduce the synthesis of CPD toward understanding its nature and choose our pathway for the project. It is challenging to design three-dimensional (3D) components that can encapsulate a guest in their cavity. Due to their active binding sites, there are significant conformational changes in cage-like systems. It is expected to be efficient toward controlling guest capture and release as well as their chemical reactivity. Controlling the cavity size in 3D structures was achieved in a few systems using a chemical or a photochemical signal²⁶. In our

case, we will focus on porphyrins and their metallated forms, which have been involved in various covalent or non-covalent cage-like structures to stabilise guest molecules.

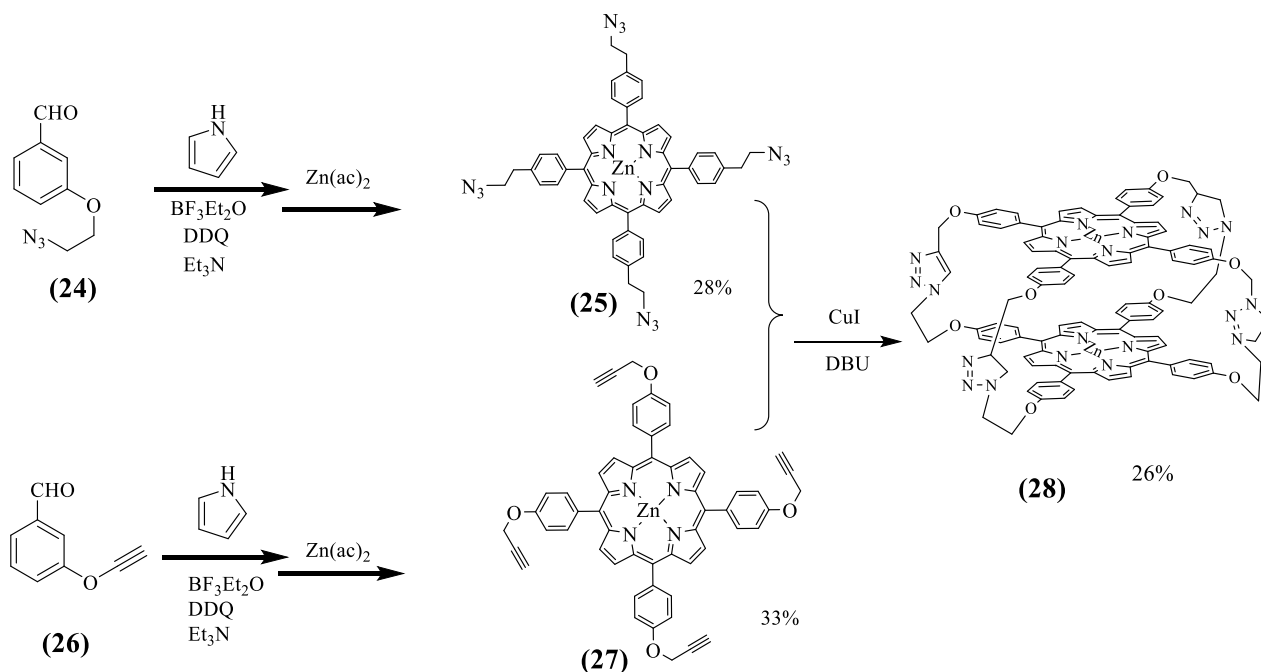
The porphyrin cage-like reactivity is shown to be affected by cavity size change. The type of linkers can also increase the reactivity, which can introduce extra reactive sites. Therefore, two main types of linkers control the porphyrin cavity (i) flexible linkers, which allow the cavity to be adjustable to fit the guest, and (ii) rigid linkers that fix the cavity at a specific size. Those linkers are based on self-assembly or building block synthesis, which will be discussed in detail.

The synthesis of porphyrin is well known previously, but its caged models have mainly gained attention in the last decade when Hajjaj *et al.*¹¹, followed by Zhang *et al.*²⁷, successfully synthesised the cages based on two porphyrin units. They studied the cage compared with cyclic analogues, which were previously described, and the differences were clear. Compared to the synthesis of cyclic compounds, the organic cage compounds formed with only covalent bonds are relatively rare because the synthesis of most cage compounds requires multiple steps and often has low overall yields. The example for the synthesis through covalent bonds was obtained by Hajjaj *et al.*¹¹ (**scheme 3.4**). Therefore, it was clear that the steps toward the target affected the final yield.

To reduce the steps of porphyrin cage preparations and obtain a higher yield, Zhang *et al.*²⁷ applied click methodology (**scheme 3.5**). They used cycloaddition procedure through Cu-catalysed alkyne-azide coupling (CuAAC) reaction, which successfully obtained covalent porphyrin cages of various sizes and rigidity²⁷ and ²⁶. Their first example was too smaller for hosting fullerene, but it was extended later on by the same approach, and they successfully obtained the required cavity size for that²⁸ (**scheme 3.6**).

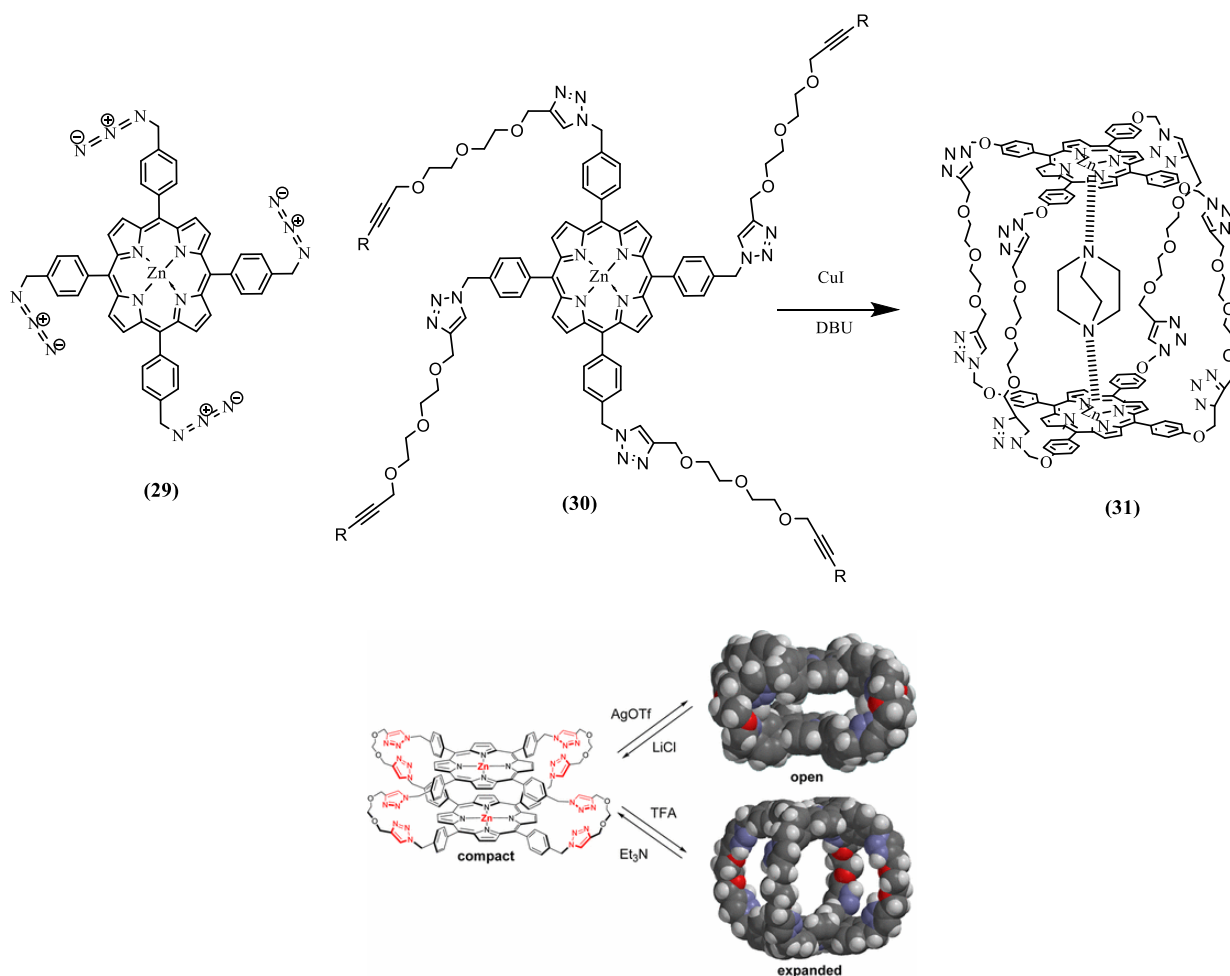


Scheme 3.5: The synthetic method of cage preparation developed by Zhang *et al.*²⁷



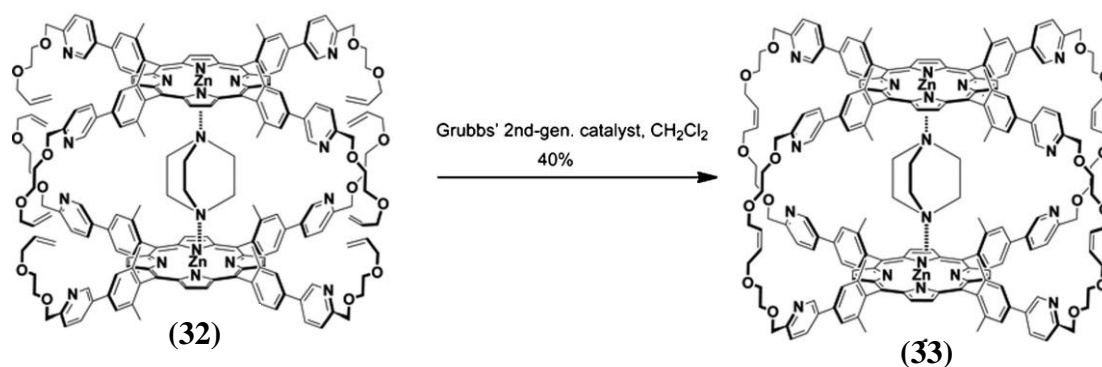
Scheme 3.6: The expansion of cavity size to host fullerene²⁸

The cavity was also extended by Kosher *et al.*²⁶ and examined toward controlling cage size. They successfully managed to control the eight triazole ligands as additional active sites toward resizing the cavity (**scheme 3.7**). The flexibility of the linkers allowed the cage to be coordinated by silver cation, bringing porphyrin units closer, or expanded when treated by acid that extracted the metal. They called it a chemically induced breathing based on reversible complexation or protonation reaction.



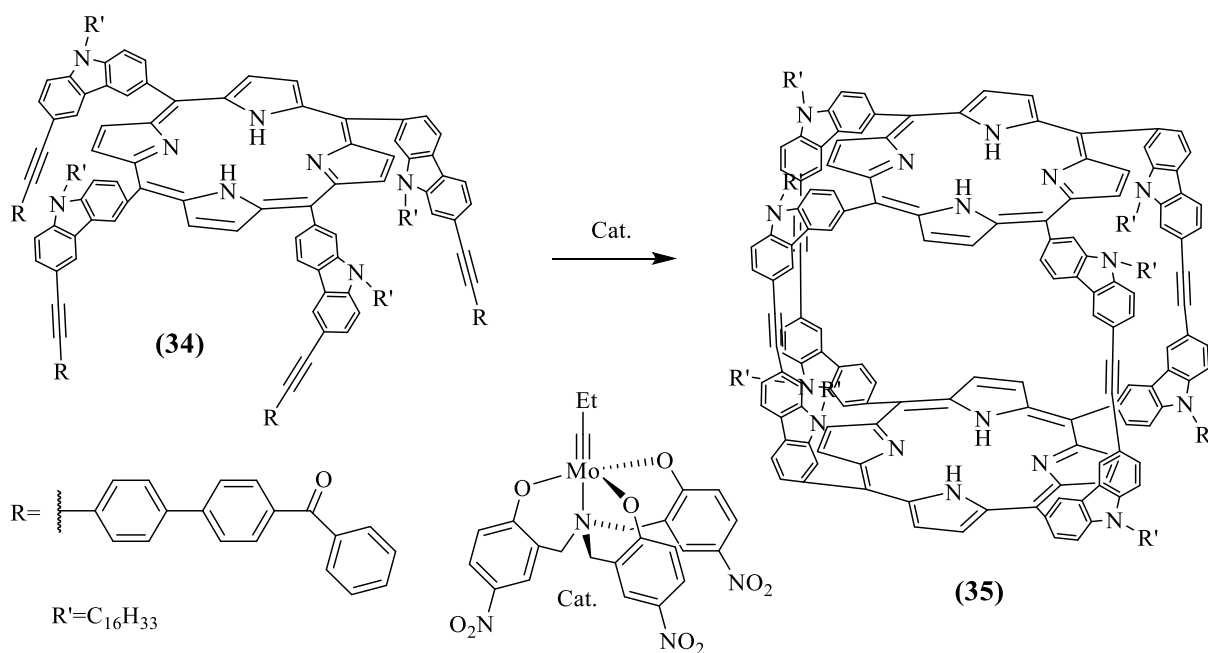
Scheme 3.7: The control of cavity size using silver (Ag) ligands developed by Kosher *et al.*²⁶

Toward extra control, 1,4-diazabicyclo[2.2.2]octane (DABCO) was employed to assemble the porphyrin dimer through binding sites allowing ring-closing metathesis, making the covalent cage model²⁹ (**scheme 3.8**). DABCO binding is reversible, and it is easily removed to obtain the hollow analogues, improving the yield obtained and raising its efficiency³⁰. The reactive sites inside the cavity are fascinating, particularly toward kinetic and photophysical studies due to the long triplet excited state lifetime in the system²⁹. The assemblies of porphyrins are also achievable through naked silver (Ag) cation³¹, which allow pyridyl to bond coordinately with the cation.



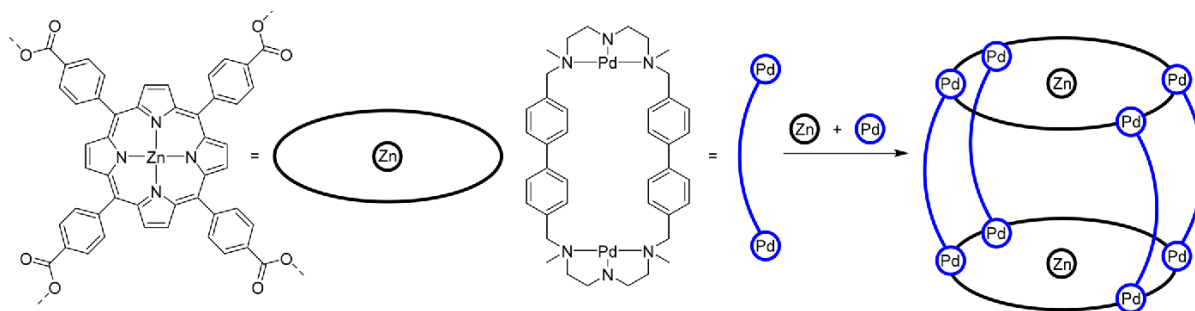
Scheme 3.8: The cage achieved by alkene metathesis adapted from Taesch *et al.*²⁹

A rectangular porphyrin cage that is highly selective toward encapsulating fullerene C₇₀ was achieved by Zhang *et al.*³² through one-step alkyne metathesis using Mo-catalyst³³ (**scheme 3.9**). The rigidity of the linkers they had used significantly increased the selectivity of separation. It is classified as a covalent porphyrin cage that is highly stable thermally and chemically.



Scheme 3.9: Rigid cage through alkyne metathesis.

Also, porphyrin cage is achievable by metal-directed self-assembly methodology yielding around 38%²⁰ (**scheme 3.10**). As the method is based on symmetrical porphyrin, it may be considered easy access to the cage model. The rigidity and shape of the cavity are controlled by the linkers, which could be modified to the shape of its guest.



Scheme 3.10: Self-assembled cage

An attempt toward stimulated self-assembly for achieving porphyrin cage, by Singh *et al.*,³⁴ successfully obtained a unique model through hydrogen bonds (**figure 3.11**). Thermodynamic studies found that this model is highly rigid because four connections and alkyl chains drove the system toward assembly on surfaces.

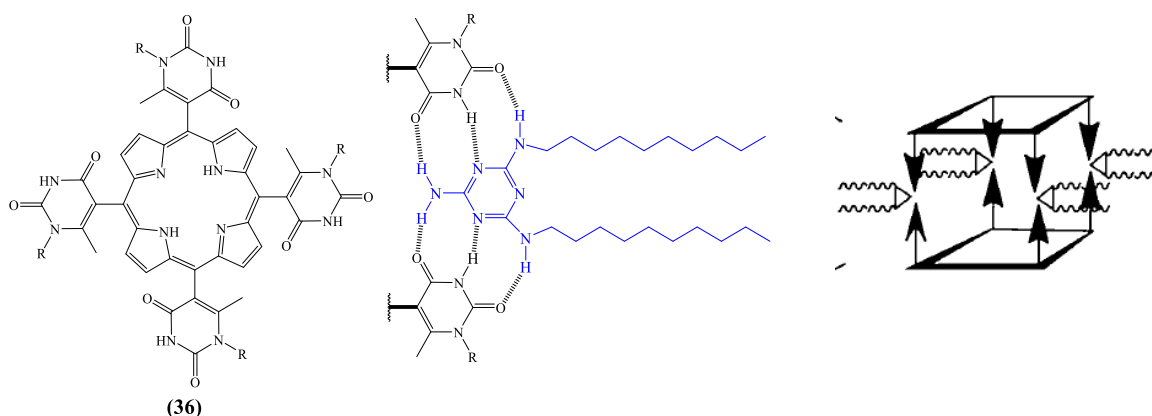
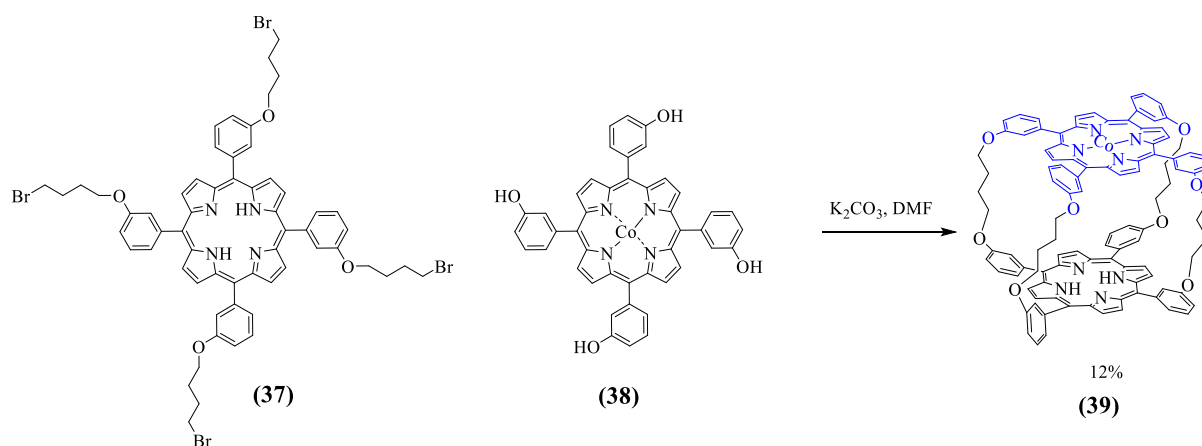


Figure 3.11: Porphyrin cage formation through hydrogen bonds

Also, the cofacial porphyrin dyad (cage) attracted Rogers *et al.*³⁵ due to its photosynthesis applications, a suitable model for multielectron redox reactions. Therefore, they developed an approach and applied it to the synthesis of cofacial porphyrin cages by using flexible alkyl chains. They chose such linkers to achieve a degree of flexibility that could be imparted into the cage system. The flexibility of the cage system may enable the molecule to fulfil the optimum metal-metal distance, which is needed for a catalytic activity or substrate binding (**scheme 3.11**).



Scheme 3.11: Flexible cage system achieved by Roger *et al.*³⁵

The evidence from the literature concluded that the interaction between the porphyrin cage and its guest in the cavity has resulted in new properties. Although choosing the guest toward encapsulation in the cavity requires considering its size for increasing overall efficiency, the binding sites also require consideration for their stability. Therefore, the linkers control the cavity size between porphyrin units, whereas the binding sites are responsible for interaction with its guest. The stability of covalent cages is much greater than self-assembled cages toward extreme conditions such as high temperature, water and acids. Therefore, there is a great potential opportunity to study its phenomenon that might result in new applications. Thus, we will investigate encapsulation of phthalocyanine as one of the most common companions of porphyrin that previously reported⁴ in triple-deckers, in the order of Porphyrin-Phthalocyanine-Porphyrin.

From the previous section, studying porphyrin is important for developing this science. There is a high possibility for applying its derivatives in many projects. Therefore, porphyrin structure and preparation will be discussed in more chemical detail.

3.6 The chemistry of porphyrin

3.6.1 Definition

Porphyrins are an example of a macrocyclic compound. One of the first studies that led to the discovery of porphyrin was done by Verdeil in 1844 when he recognised the relation between haemoglobin and chlorophyll. He studied those compounds by UV-vis spectroscopy and found a strong signal at 420 nm. Later, the analysis suggested that there are twenty carbon and four nitrogen atoms joined in an aromatic system with 22π electrons, 18π of them are conjugated. In addition, it can be described as a poly-pyrrole because there are four pyrrole groups linked by four methene bridges (**figure 3.12**).

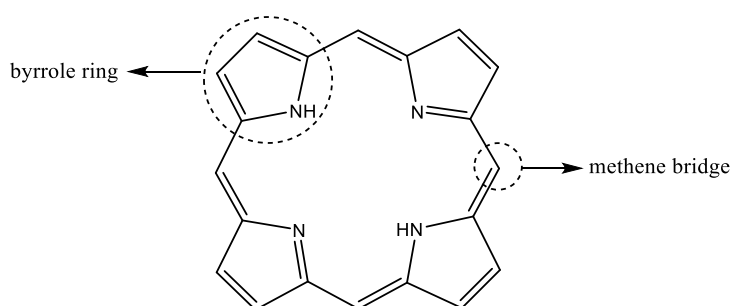


Figure 3.12: porphyrin structure

The unique structure of porphyrin has attracted scientists. It exists in many natural resources with minor structure differences, but that leads to different biological functions. The porphine (**40**) is the main structure block in the famous natural derivatives such as haemoglobin (**41**) (blood protein), chlorophyll (**42**) (plants' green pigment and light harvester toward photosynthesis reaction that is producing food), peroxidases (**43**) (reductant enzyme for peroxide), vitamin B12 (**44**) (animal-based food that helps to produce red blood cells), and cytochromes (**45**) (redox active protein in heme) etc³⁶. That similarity gives a wide range of opportunities for chemists to investigate the formation of porphyrin naturally in the way of developing laboratorian methods of its synthetic preparation (**Figure 3.13**).

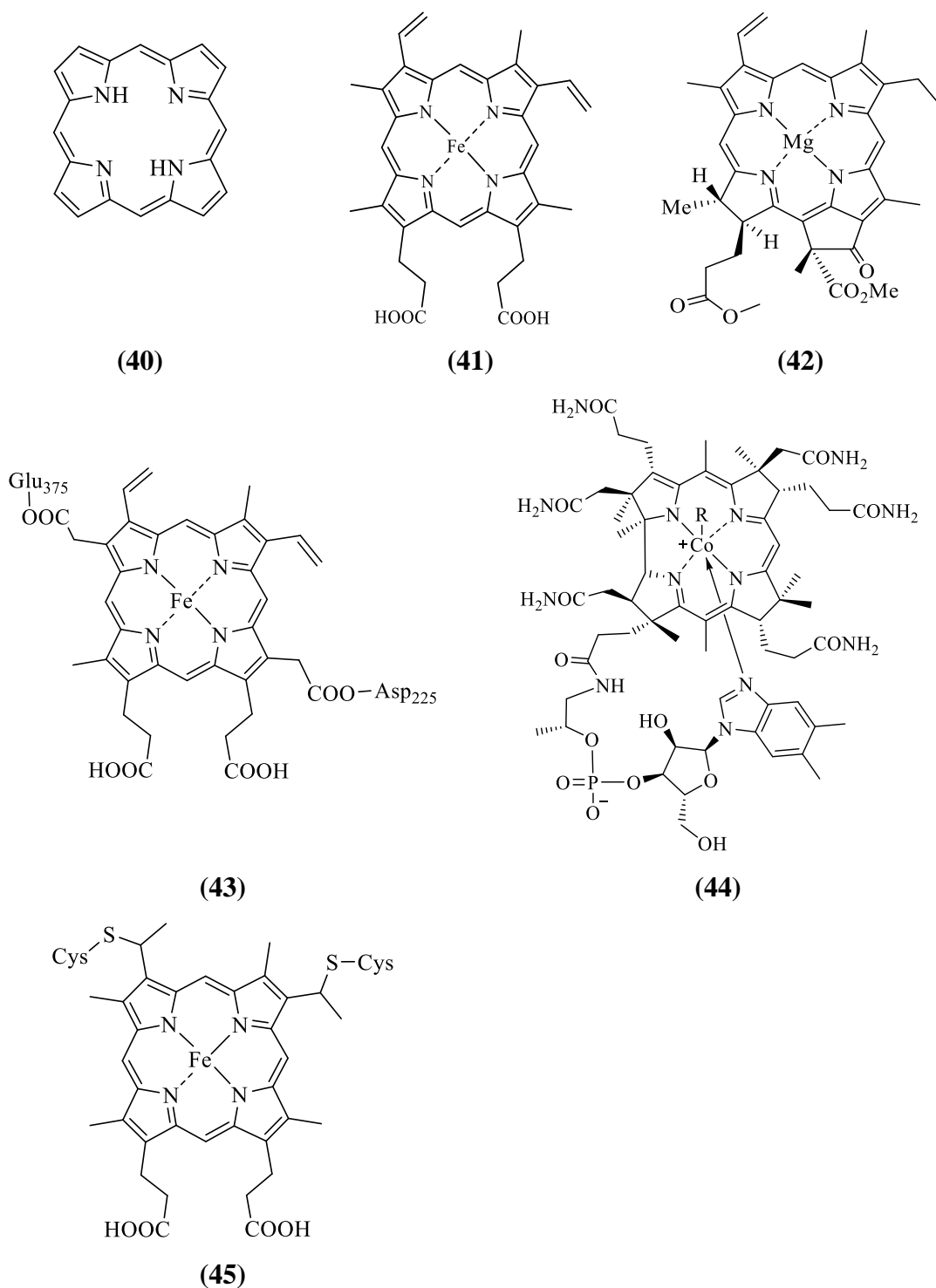


Figure 3.13: Chemical structure of various kinds of porphyrins, porphine (40), haemoglobin (41), chlorophyll (42), peroxidases (43), vitamin B12 (44), and cytochromes (45)

Research in the porphyrin field demonstrates the kinetics of bioprocesses and opened the gate for medical researchers to simulate natural processes. Also, the investigation into protein

and biosystems also shows that porphyrins are responsible for redox reactions and other catalytic activities into bioprocesses through chemical energy³⁷.

There are many examples of the porphyrin component inside protein structures biosystems. Therefore, scientists examined porphyrin to find evidence related to how blood transfers the oxygen in the body and DNA transfers genes, as well as how energy forms and moves into the biosystem. The data collected from the porphyrin studies show that the energy transfer is extremely efficient (95-99³⁸).

The formation of porphyrin into cells was one of the main questions in the biochemistry field toward understanding how and where the reactions are happening. The first pathway of biosynthesis of porphyrin was published by Shemin, D and Wittenberg, J in 1951³⁹ that found the tricarboxylic acid is the first step of the series toward porphyrin formation. This pathway was summarised by Brody⁴⁰ as heme synthesis forms in eight steps.

Starting from glycine and succinyl-CoA, the formation of aminolevulinic acid is the initial product toward producing porphobilinogen (pyrrole unit). The source of succinyl-CoA is an intermediate product of the Krebs cycle (citric acid cycle)³⁹ (**figure 3.14**), whereas glycine can be derived from the diet or serine. The dehydratase of aminolevulinic acid is the second step that forms a porphobilinogen (pyrrole unit).

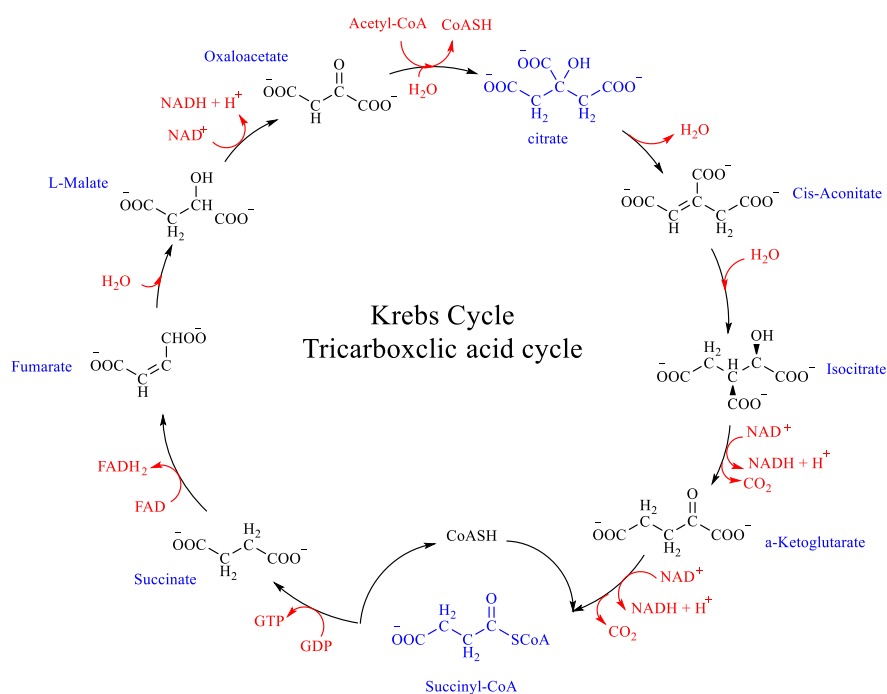
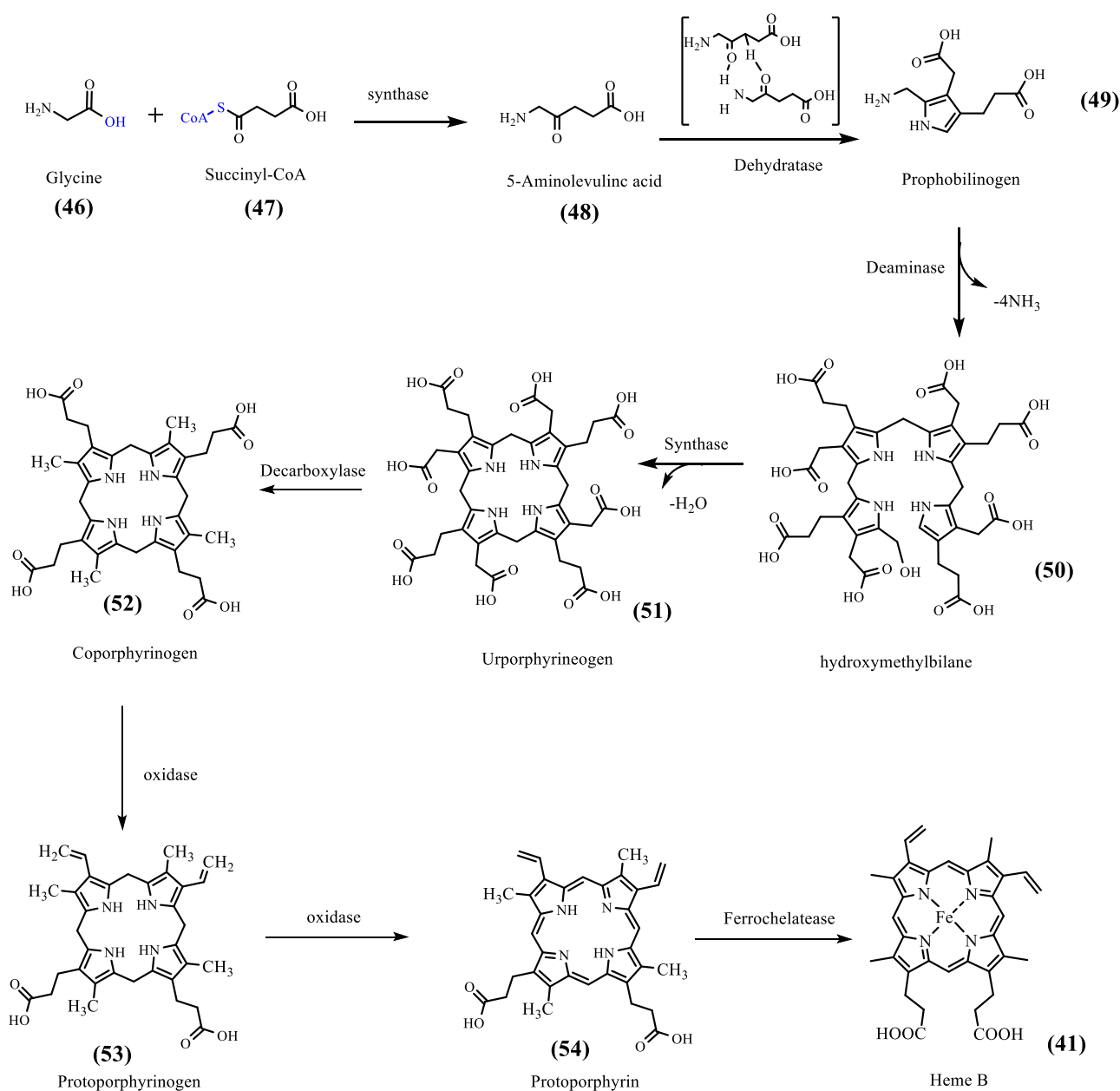


Figure 3.14: Kerbs cycle shows the mechanism of the natural formation of Succinyl-CoA.⁴¹

Four pyrrole units (porphobilinogen) are then joined in polymerase step by deaminase of amino group forming hydroxymethylbilane. The polymerase step was followed by cyclisation of the tetrapyrrole units (hydroxymethylbilane) to form a large ring, the porphyrin ring. This is followed by modification of the ring by decarboxylations and oxidations. The final step involves the insertion of ferrous iron into protoporphyrin to form heme (**scheme 3.12**). The heme biosynthetic pathway is distinguished by the fact that the first and final three steps take place in the mitochondrion, whereas the intermediate steps take place in the cytosol.⁴⁰



Scheme 3.12: Bio-synthetic pathway of porphyrin (Heme) formation into cells⁴⁰

3.6.2 Structure

Since the first signal from UV-vis, determining the structure was a challenge because it existed in a complex environment. As previously mentioned, there are 18π electrons that gives the porphyrin macrocycle a highly conjugated environment. Porphyrin is examined under Hückel's rule of aromaticity ($4n+2$) and results from finding ($n=4$), which means the porphyrin is a stable aromatic system. According to Hollingsworth⁴², there are six different delocalised pathways porphyrin with 18π electrons (**figure 3.15**).

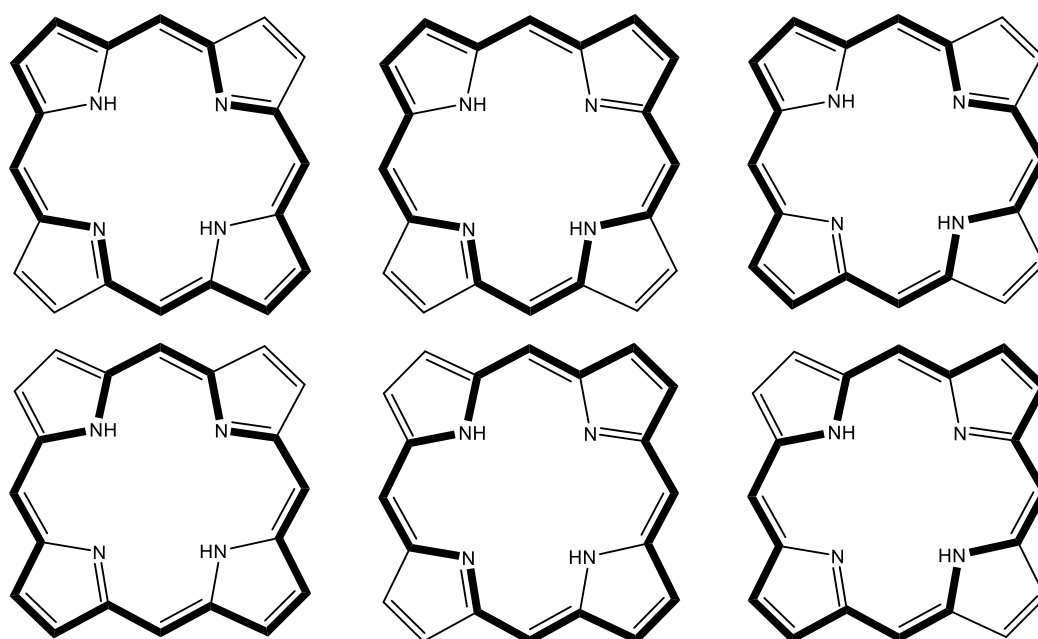


Figure 3.15: different delocalised pathways for porphyrin with 18π electrons.

These highly conjugated π electron systems are responsible for porphyrins' intensity and colour. This feature of porphyrins can be studied by their characteristic UV-vis spectra, consisting of two distinct regions: one in the near-ultraviolet and the other in the visible. The first involves the transition from the ground state to the second excited state ($S_0 \rightarrow S_2$). Its corresponding band is called the Soret or B band, with a range of absorption between 380 and 500 nm depending on whether the porphyrin is (β) or meso-substituted. Whereas the second region consists of a weak transition to the first excited state ($S_0 \rightarrow S_1$) in the range between 500-750 nm (the Q bands). Also, the wavelength and the absorption intensity values of those regions are affected relatively by substituents position on the porphyrin ring.

The absorption spectrum of porphyrins has long been understood in terms of the highly successful “four-orbital” (two highest occupied π orbitals and two lowest unoccupied π^* orbitals) model first applied by Gouterman⁴³ that has discussed the importance of charge localisation on electronic spectroscopic properties. According to this theory, the absorption bands in porphyrin systems arise from transitions between two HOMOs and two LUMOs (**figure 3.16**). The energy of those orbitals is affected by the metal centre and the substituents on the ring, which are applied to identify the relevant changes.

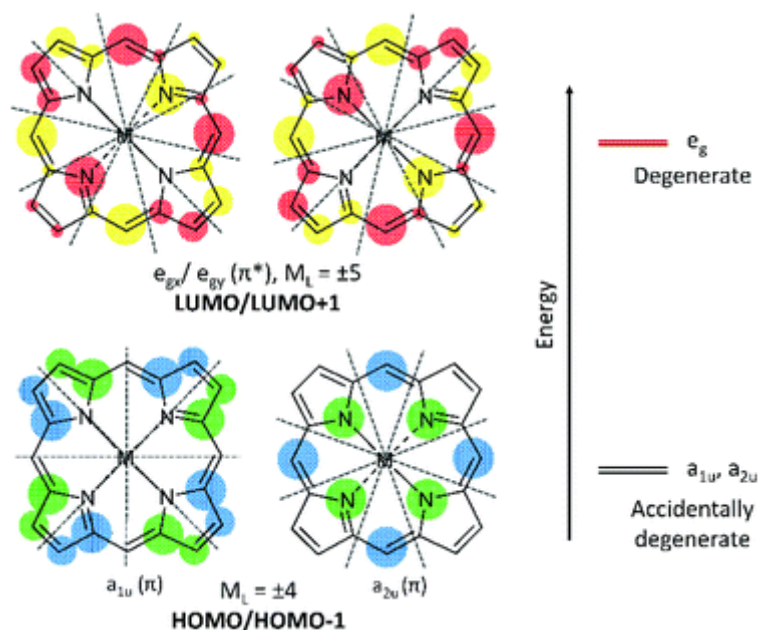


Figure 3.16: The nodes for the HOMOs and LUMOs for a metallated porphyrin with an 18 π electron aromatic ring, shown with grey dotted lines, represents the four Gouterman orbitals⁴³. The blue and green shading indicates the electron density of the occupied π MOs while the red and yellow shading shows the electron density map of the unoccupied π^* MOs (adapted from Stillman, M *et al.*⁴⁴).

In contrast to minor changes to the intensity and wavelength of the absorption features caused by variations of the peripheral substituents on the porphyrin ring, protonation of two of the inner nitrogen atoms or the insertion/change of metal atoms into the macrocycle usually strongly change the visible absorption spectrum. There is a more symmetrical situation than in the free base porphyrin, which simplifies the Q bands pattern and the formation of two Q bands.

Porphyrin has two different sites that electrophilic substitution can take place with different reactivity: positions 5, 10, 15 and 20, called *meso*-positions and also 2, 3, 7, 8, 12, 13, 17 and 18, named β -pyrrole positions (**figure 3.17**). According to that, the substitution can affect porphyrin classification as symmetric or asymmetric (**figure 3.18**).

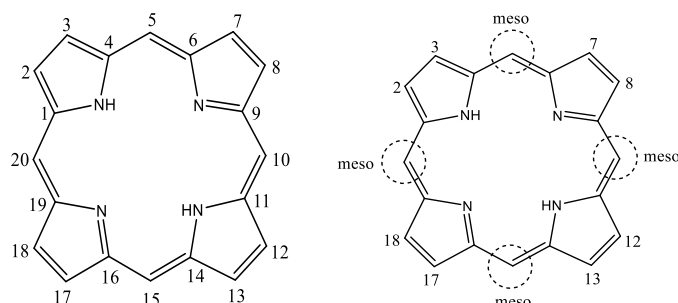


Figure 3.17: Porphyrin numeration that applies for its description.

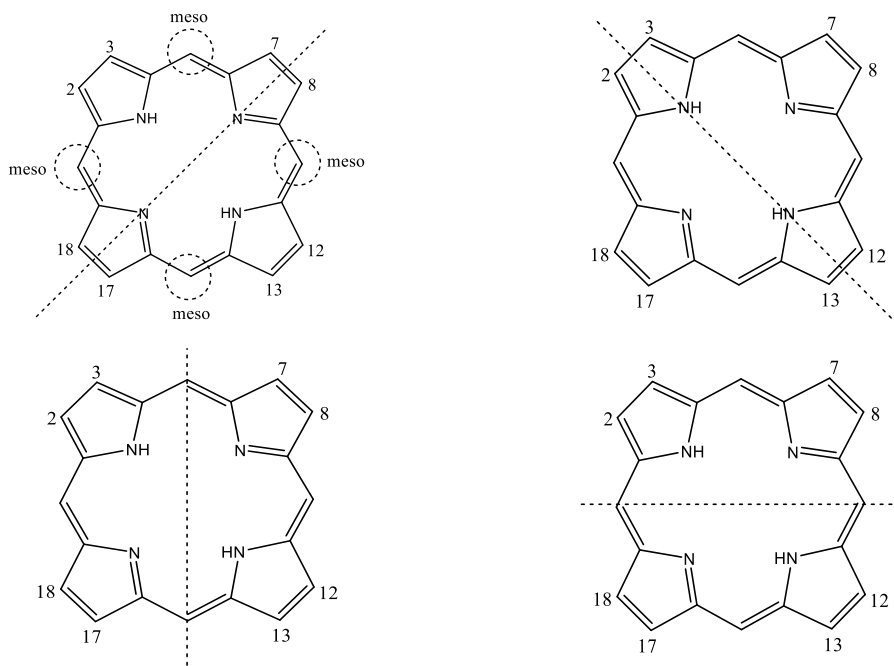


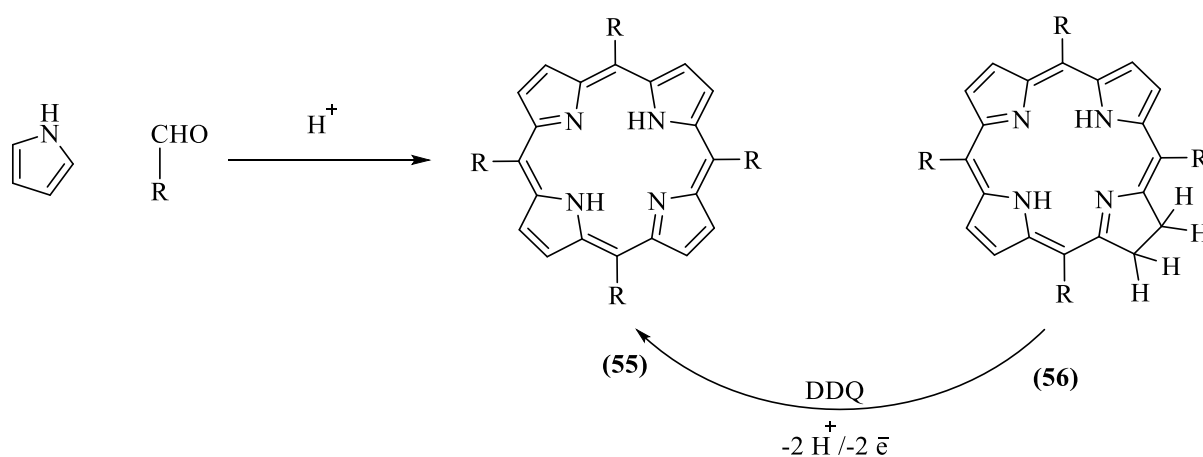
Figure 3.18: The axes show the possibility of a symmetrical environment.

3.6.3 General porphyrins preparation

There are several methods for preparing porphyrins. It has been developed over a long time to obtain a higher yield and less by-product and usefulness method. The most popular methodologies in the field are Rothmund, Alder and Lindsey. These methodologies can be summarised as pyrroles are reacted with aldehydes under acidic conditions. General information about these preparation methodologies will be given below.

3.6.3.1 Rothmund methodology⁴⁵

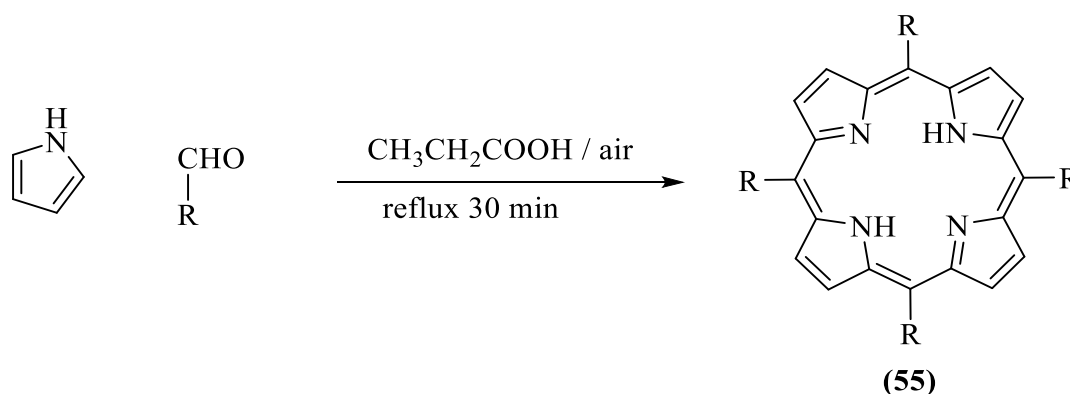
Rothmund invented the first methodology for preparing porphyrins in 1935. His method is based on reacting a mixture of benzaldehyde and pyrrole in pyridine in one step (**scheme 3.13**). The reaction was done in a sealed flask at 150 °C for 24 h. Although the experimental conditions are severe, a few benzaldehydes could be converted to the corresponding substituted porphyrin. The yield was low because the reaction's primary (non-polymeric) by-product was meso-substituted chlorin (**56**). To understand the nature of its formation, Calvin *et al.*⁴⁶ discovered that adding metal salts to the reaction mixture, such as zinc acetate, increases the yield of porphyrin (**55**) from 4-5% for the free-base derivative, and decreases the amount of (**56**)⁴⁷. In addition, changing reactant, the reaction conditions, and substituents on the benzaldehyde derivative are the way to improve the reaction.



Scheme 3.13: Porphyrin preparation by Rothmund's methodology

3.6.3.2 Adler's methodology

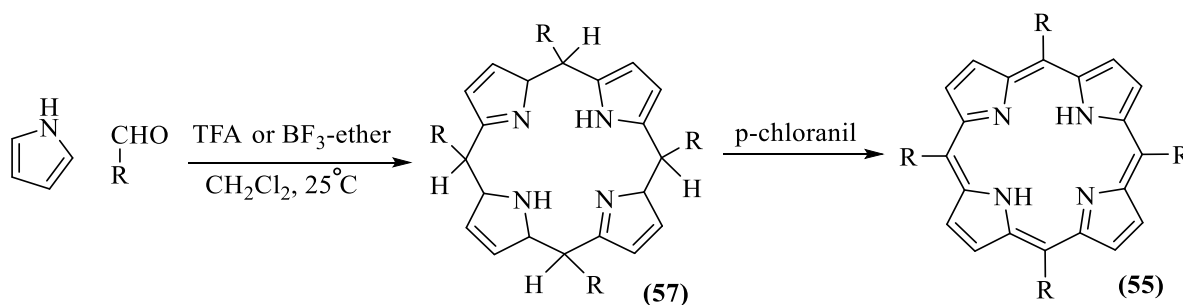
The second methodology for porphyrin preparation was invented by Adler, Longo and coworkers^{48,49}. They re-examined the synthesis of mesosubstituted porphyrins and developed an alternative approach (**scheme 3.14**). Their methodology involves an acid catalysed pyrrole-aldehyde condensation in glassware open to the atmosphere in the presence of air as an oxidant. Under the general meth, the reaction requires high temperature and propionic acid as a solvent. The yield of porphyrin was 30-40 %, and the chlorin contamination lower than that obtained with the Rothemund methodology.



Scheme 3.14: A general methodology of Adler-Longo for preparing porphyrins.

3.6.3.3 Lindsey's methodology^{50,51}

The third methodology for preparing porphyrin was developed by Lindsey. The innovative method is based on two steps at room temperature. In the first step, a mixture of aldehyde and pyrrole are dissolved in dry DCM under a flow of nitrogen. The concentration has to be considered due to its effect on the yield. Then, the reaction required covering from light, and trifluoride boron etherate was added to start the reaction. In the second step, under refluxing, p-chloranil was added as an oxidative agent to convert propphyrinogen to porphyrin. This strategy attempts to avoid side reactions in all steps of the porphyrin-formation process (**scheme 3.15**).



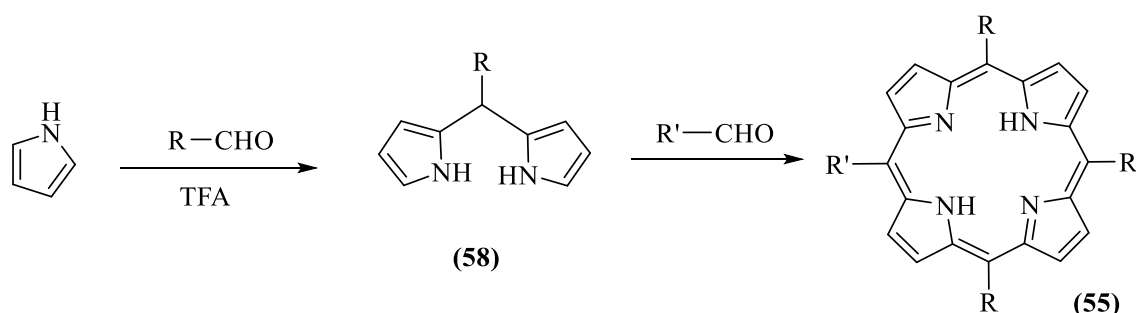
Scheme 3.15: Two-step one-flask room-temperature synthesis of porphyrins.

3.6.4 Preparation development

There are two significant developments in the methodology of preparing porphyrin, which are related to functional groups around the porphyrin ring. According to that, porphyrin can be characterised as symmetrical or asymmetrical, as mentioned in the structure section. Therefore, the general approach for these kinds of porphyrins will be discussed below.

3.6.4.1 Symmetrical porphyrins preparation

The methodologies that discussed in the previous part can be employed efficiently for preparing tetra-meso-substitutions by using one kind of aldehyde. On the other side, there are two options to prepare di meso substitutions. In the first approach, a mixture of two types of aldehyde can be used in the reaction under the conditions of any porphyrin preparation methodology in the last part. The second approach can be done in multiple steps⁵⁰ (scheme 3.16).



Scheme 3.16: explanation of symmetrical porphyrin preparation in two steps

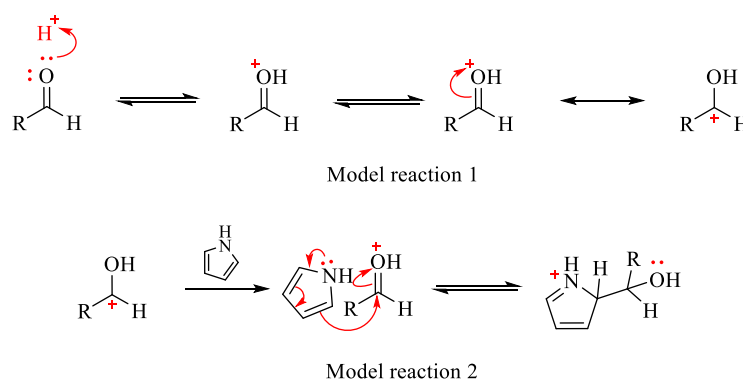
3.6.4.2 Asymmetrical porphyrins preparation

There are several methodologies that have been developed to prepare asymmetrical porphyrins. The importance of this kind of porphyrins is to functionalised one position selectively. The asymmetrical porphyrin can be employed in various applications such as derivatising proteins and DNA⁴². The methodology of their preparation can be similar to previous methods but with varying aldehyde components. The straightforward procedure is mixing two aldehydes (1:3), where 1 refers to the aldehyde with a different functional group than others, which aim to be applied in further steps. In addition, reacting a symmetrical porphyrin with a nucleophilic or electrophilic substitution can result in asymmetrical porphyrin.

3.6.5 General mechanism of porphyrin formation

The mechanism of porphyrin formation (**scheme 3.18**) was investigated by several studies toward identifying the specific effect of solvents, acids and oxidation agents in the reaction that has affected the overall yield. Also, electronic environment of aldehyde was found playing significant role in the formation of porphyrin. For example, electron-donating aryl groups on aldehyde tend to be reducing the overall yield of porphyrin due to the formation of scrambling, whereas the yield is increasing where substituted of aldehyde are electron-withdrawal⁵².

As the formation of the carbocation is the initial step in the mechanism, Li *et al.*⁵³ suggested two model reactions for carbocation formation (**scheme 3.17**) (model reaction 1) and its reaction with pyrrole (model reaction 2) to calculate their formation energy (**figure 3.19**).



Scheme 3.17: the possible model reactions for the initial carbocation formation

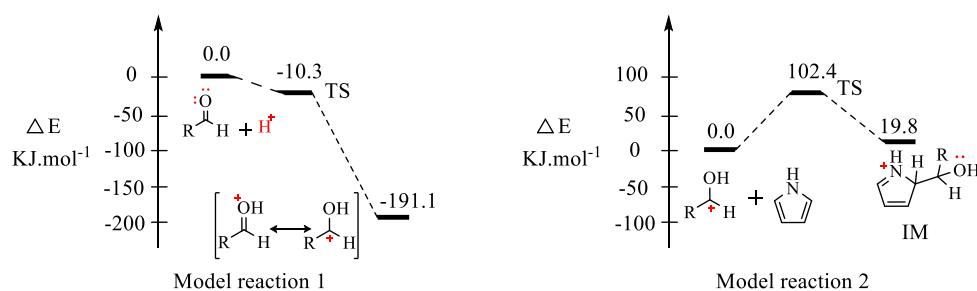
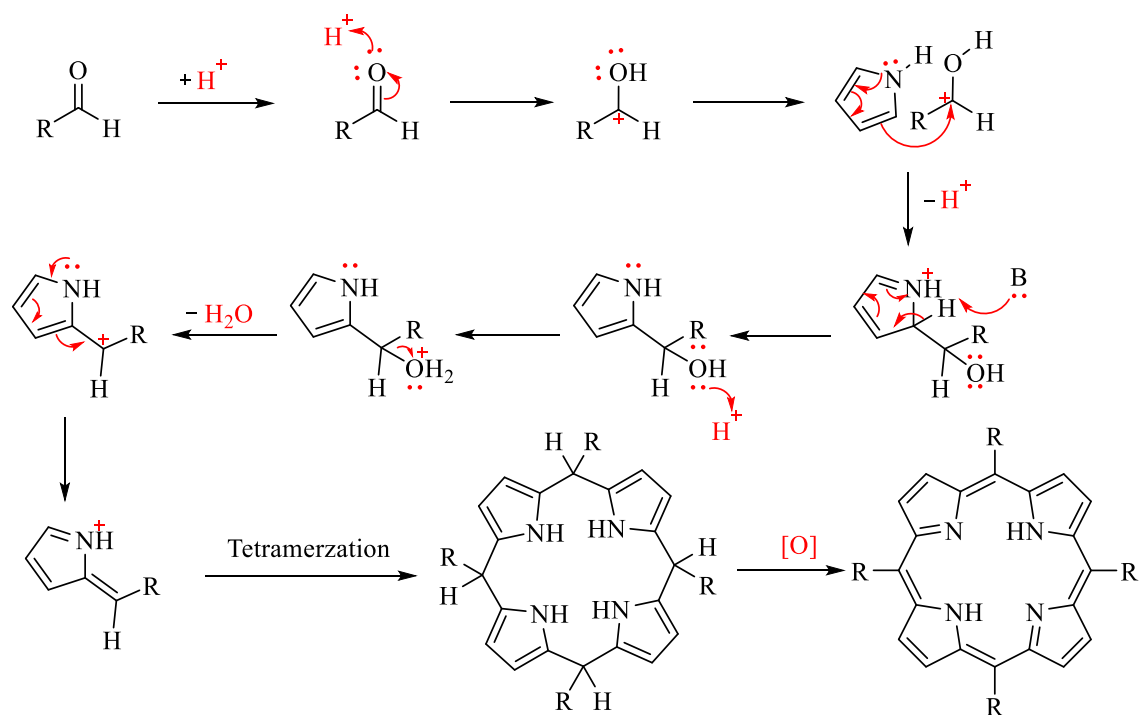


Figure 3.19: The potential energy profiles for the formation of carbocation intermediate (model reaction 1) and the addition reaction between carbocation intermediate and pyrrole (model reaction 2)⁵³



Scheme 3.18: the general mechanism of porphyrin formation⁵³

3.7 The chemistry of phthalocyanines

Like porphyrins, phthalocyanine (Pc) and its family (**figure 3.20**) are another example of a macrocycle system. It was synthesised by Braun and Tcherniac in 1907, which could be the first attempt toward preparing a macrocyclic template. Until the 1960s, there was less attention about substituted macrocycles due to the low yield, many side products, and a large volume of solvent needed.⁵⁴ Since then, thousands of publications have mentioned it due to its unique structure and revolutionary applications.

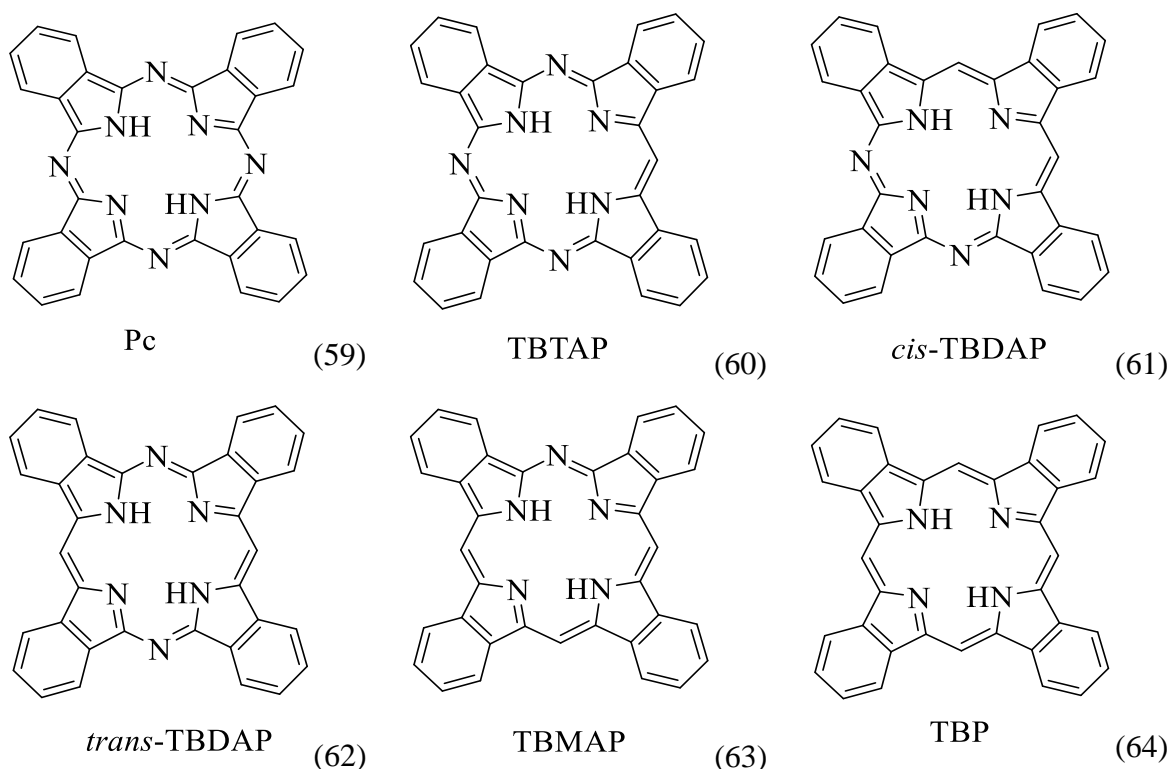
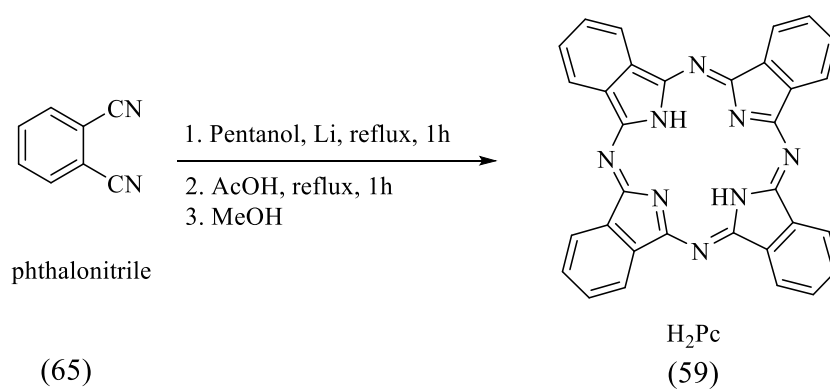


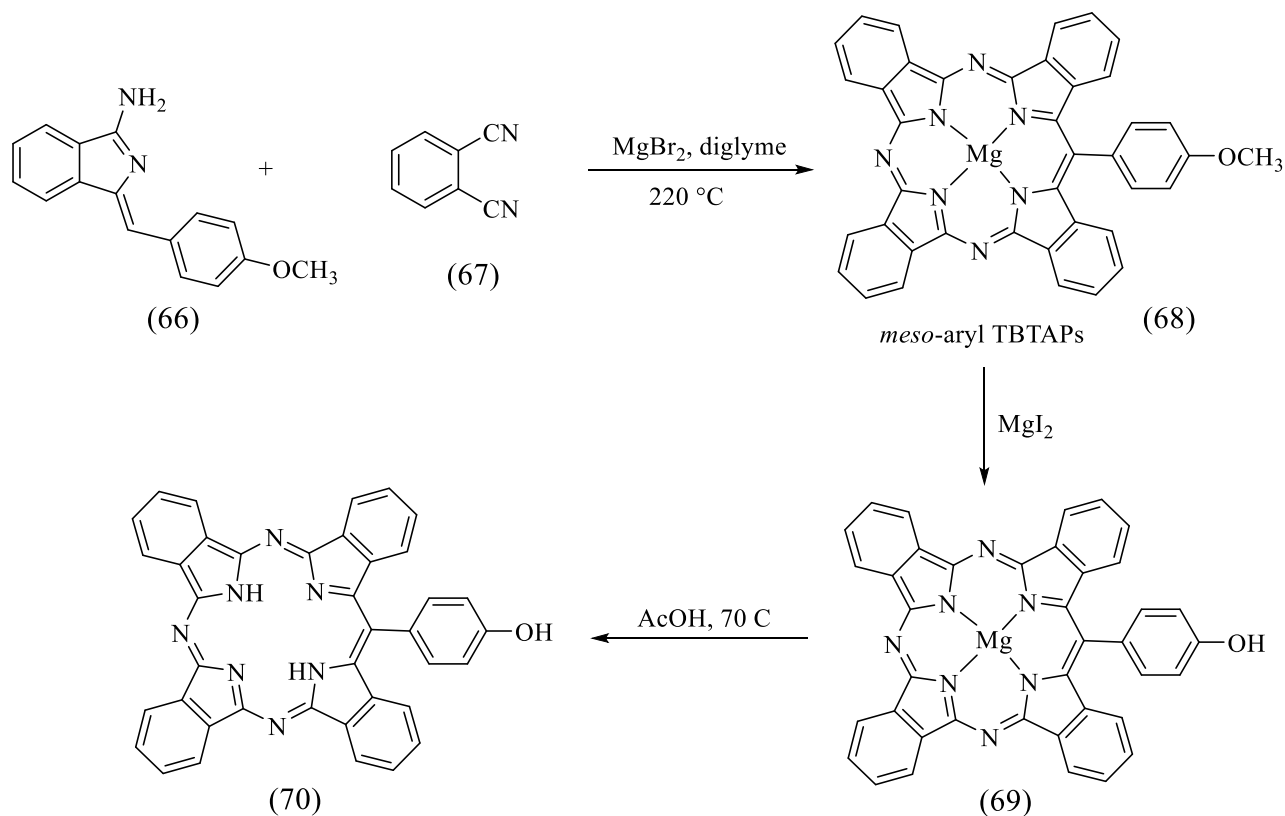
Figure 3.20: The structures of phthalocyanine (Pc) and its family

Chemically, there are several procedures toward preparing Pc and other relative molecules based on phthalonitrile (**scheme 3.19**). Like porphyrin, phthalocyanine can be synthesised as a symmetrical or asymmetrical component by functionalising one position or more around the ring⁵⁵. That will give access toward preparing further reactions after the target molecule is designed.



Scheme 3.19: the general procedure toward Pc formation

Toward preparing asymmetrical phthalocyanine macrocycles, the recent focus was on tetrabenzotriazaporphyrin (TBTAP) as an example, and its synthetic method was developed by Cammidge *et al.*⁵⁶ (scheme 3.20).

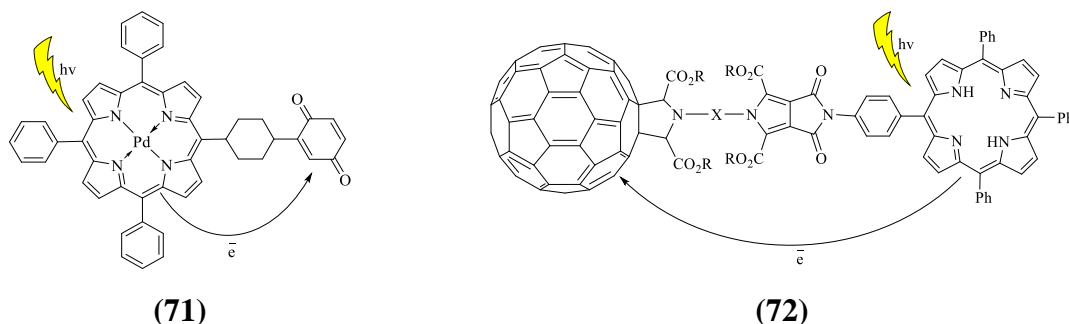


Scheme 3.20: The preparation of TBTAPs that was developed by Cammidge *et al.*⁵⁶.

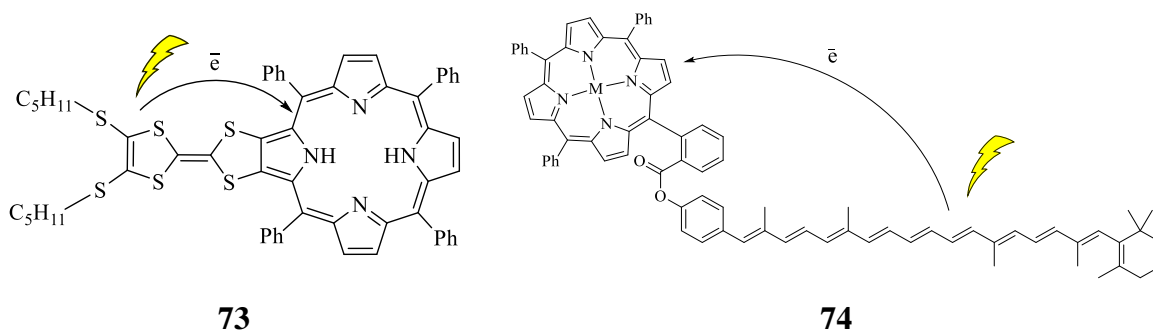
3.8 Dyads

Porphyrins can be produced as complex compounds by methods including electrophilic substitution reactions. Further procedures can yield more complex compounds such as dimers, dyads and triads. Porphyrin dyads have been examined for transferring energy within the molecular machine principles. Many porphyrin dyads have been reported as simulating the electron transfer and energy transfer in nature, which gives a very useful way to understand the process of photosynthesis⁵⁷.

Depending on the components that are connected, the porphyrin can work as an electron donor or acceptor. In the first examples, porphyrin units act as electron donors in such molecules as porphyrinequinones (**71**), and porphyrinC₆₀ (**72**), where electrons can be moving from porphyrin subunit to acceptors.



In the second example, porphyrin units act as electron acceptors such as porphyrin tetrathiafulvalene (TTF) (**73**), and porphyrin carotenes (**74**)⁵⁸, where electrons move to the porphyrin ring. These systems can be used as light-harvesting materials⁵⁷.



Porphyrin dyads are also produced from two units of the same compound symmetrically like dimers by several kinds and lengths of spacers, or two different units asymmetrically on the same principles. They can act by themselves in the role of the donor-acceptor system in the case where spacer length is short, and their centres are close enough to each other. In the case where the spacer length is large, they may need a third unit to act as a triad.

There are several ways to design dyads and triads based on the differences in the way toward connecting porphyrin molecules. As porphyrin molecules are planer, they can link by their edges (**figure 3.21**) using hydrocarbon chains, whether from meso or β positions. However, researchers found the electron transfer from those positions is weaker. Moreover, in the presence of an active functional group on one of the porphyrin molecules, the ability to connect metallic centres of the other molecule is allowed (**figure 3.22**). Also, porphyrin molecules can be connected face-face (cofacial dyad) in the presence of large metallic ions to coordinate with (**figure 3.23**). All these systems were examined toward electron and energy transfer by several publications that concluded the highest values recorded were for face to face models, which we will discuss later. This kind of dyad opens the gate toward investigating double and triple- models without spacers.

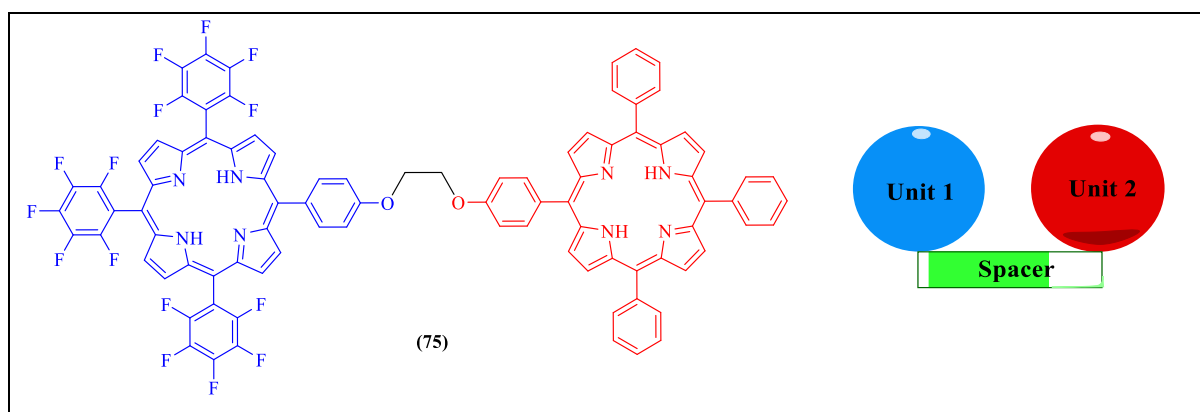


Figure 3.20: An example of edge-edge dyads

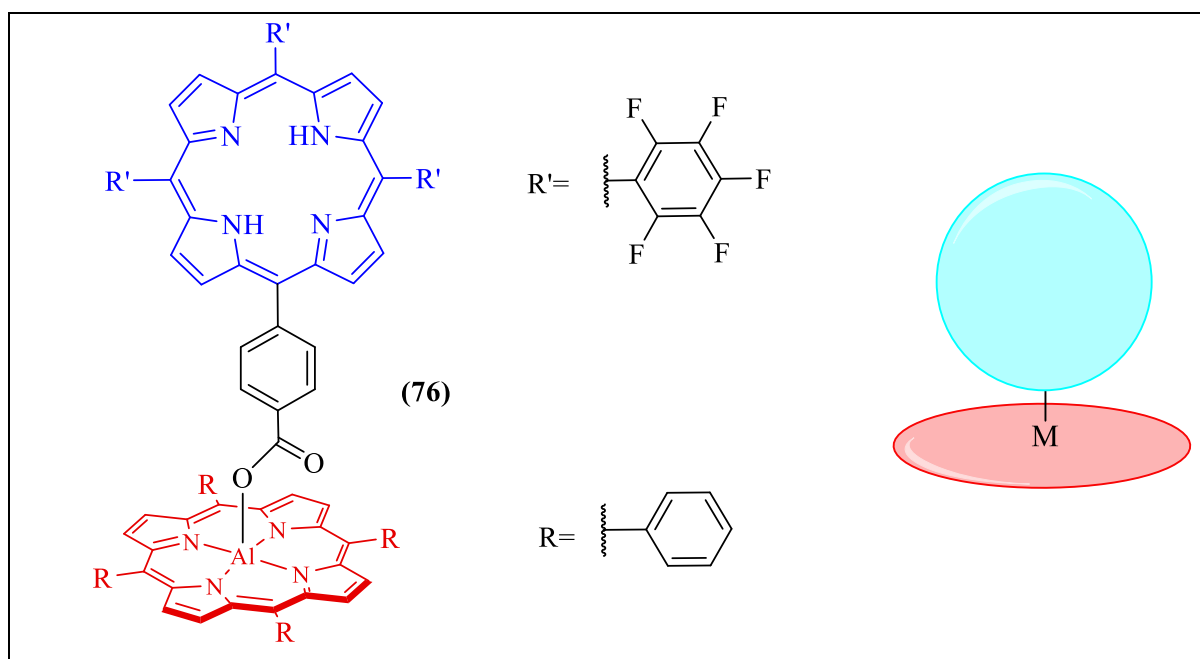


Figure 3.21: An example of centre-edge dyads

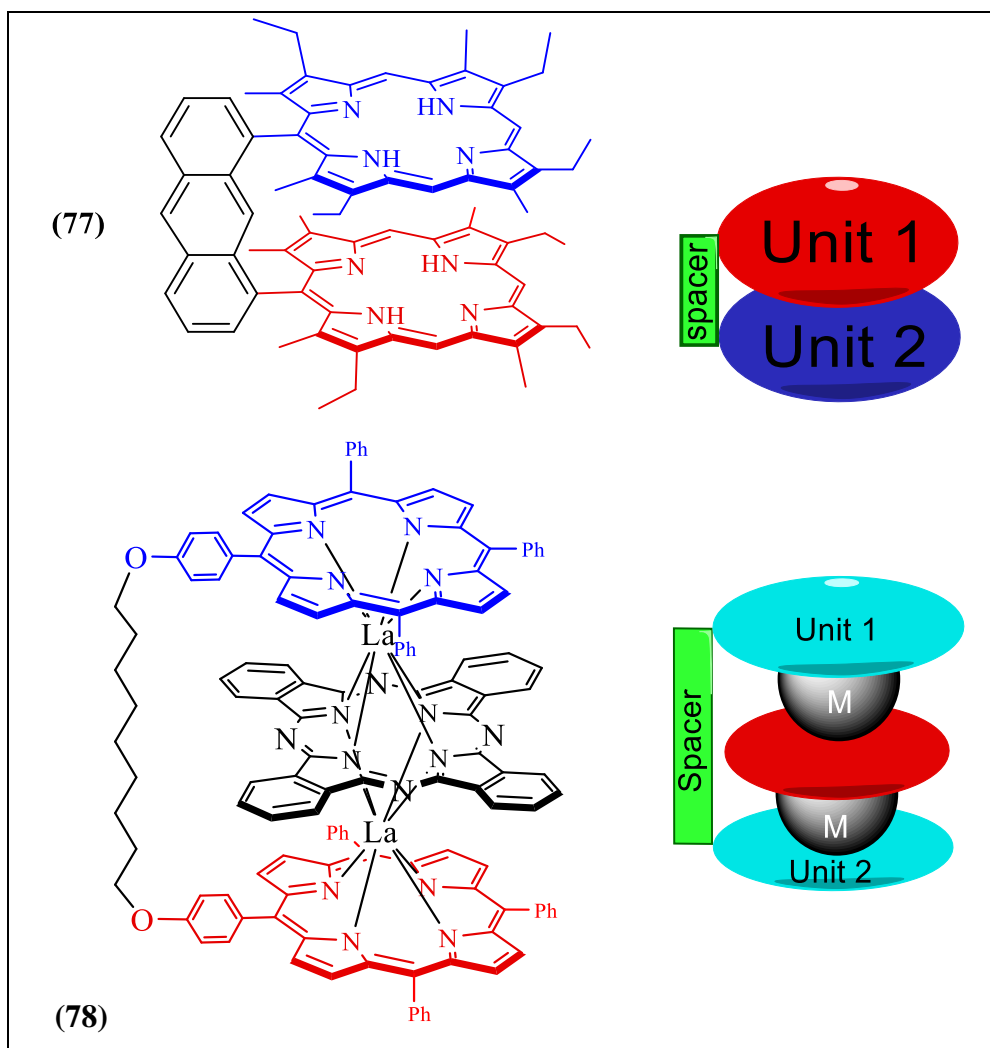


Figure 3.22: The examples of face-face dyad and triad, known also as double and triple-deckers.

There is more attention on macrocycle organic components like porphyrin and phthalocyanine on hosting a metal on their inner space or in between two units where this is possible. The interaction between metal and π electrons is well known and studied widely. Therefore, chemists have been developing a dyad's designs for collecting more information toward understanding the porphyrin framework behaviours⁴. As porphyrin and phthalocyanine can absorb visible light, they can be used as photocatalysts toward activating the reaction centre, such as an antenna function.

Toward understanding the energy transformation mechanism, several publications have discussed this, which was reviewed by Faure, S. *et al.* (2004)⁵⁹. The main finding is that: (i) the energy transfer through chemical bonds is weaker due to the electronic density at meso position, (ii) the distance between donor and acceptor components centres is important, and (iii) energy transformation is accepted within the distance of 10\AA via Forster and Dexter

mechanisms (**Figure 3.23**).⁵⁹ As the short distance between macrocyclic components is responsible for a fast rate of energy transfer⁵⁹, cofacial dyads (**Figure 3.24**) provide an excellent opportunity toward this goal that allows π orbitals to be overlapping⁶⁰. Accordingly, redox reactions (electron transfer) can be promoted with short distances between the porphyrins, but photoreactions are rather quenched than promoted⁶¹.

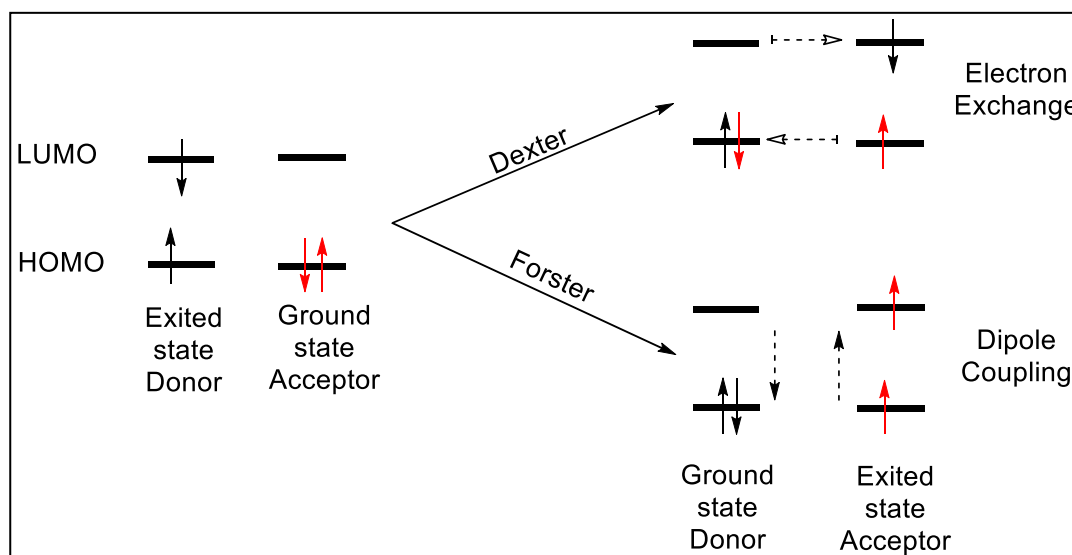


Figure 3.23: The mechanism of energy transfer into donor-acceptor system⁶²

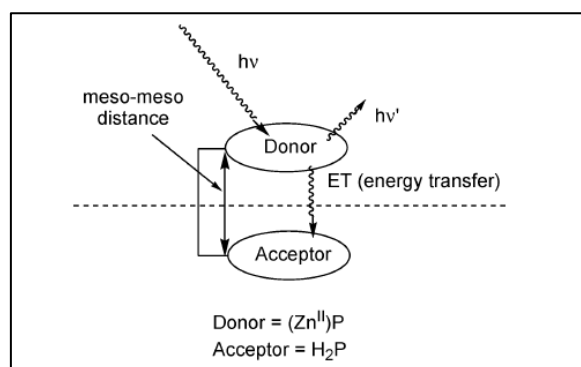


Figure 3.24: Adapted from Faure *et al.*⁵⁹, the electron transfer is allowed within 10Å between donor and acceptor

One of the principles that followed to make molecular machines is adding metallic atoms to allow rotation. The similarity of porphyrins and phthalocyanine (**59**) toward hosting a transition metallic ion gives an opportunity to study their rotation and design complex structures based on face-face dyads and triads such as double or triple-deckers as "sandwich". In this case, the atom's size is important to connect the molecules, whether through oxygen bond (**79**) or coordinating bonds (**80**). The reason for that is the metallic atom with the ionic radius over the range of 80-90 pm cannot be fitting into the hole in the centre of the macrocycle (**figure 3.25 and 3.26**).

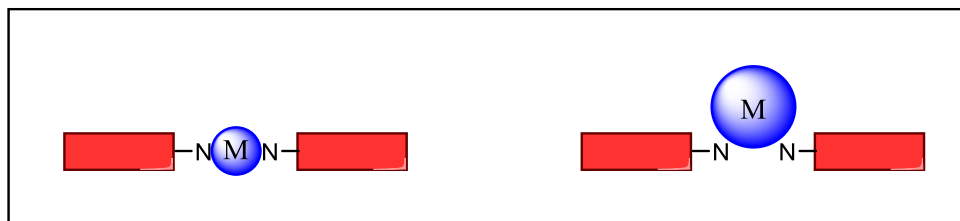


Figure 3.25: explanation of the position of the metal atom based on its ionic radius.

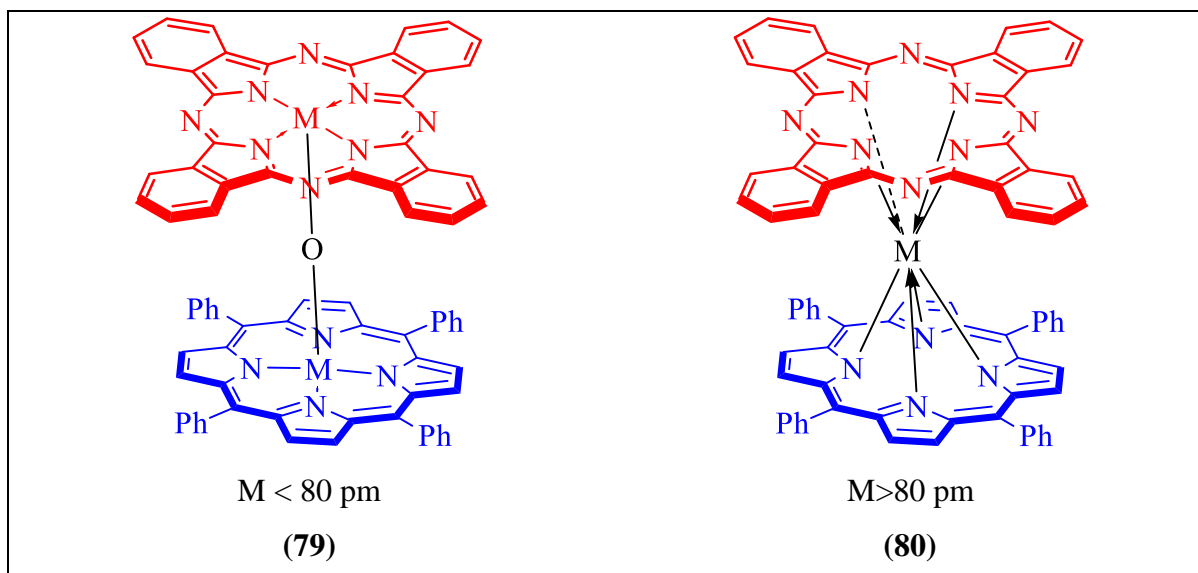


Figure 3.26: the examples of metallic atoms' position depending on their size.

Several researchers investigated the effect of transition metals on porphyrin and phthalocyanine in terms of understanding their behaviours⁶³. In the molecular orbital aspect, the energy of π orbital in porphyrin and πd orbital in transition metals are relative (**figure 3.27**). Therefore, the number of electrons in orbital d affects the energy gap (ΔH) between π and π^* . In the case of ($d^m=1-5$), the effect in the energy gap is small, whereas the significant shift toward the hypsochromic region appears in the case of ($d^m=6-9$) due to the increase of (ΔH) value.⁶⁴

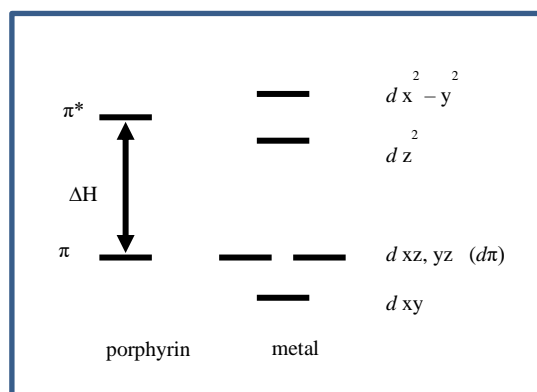


Figure 3.27: Molecular orbital diagram for d -metal-porphyrin interaction (Adapted from Prushan⁶⁴)

On the side of larger metals such as f orbital elements, the interaction between porphyrin and metal is more complex to analyse due to limited studies in the fields. They are affected by several factors such as (i) the f orbital is shielded by $5s^25p^6$ sub-shells, (ii) the transition between d and f orbitals may occur, (iii) f - f transitions, and (iv) the free electrons in the macrocyclic framework of porphyrin and phthalocyanine. According to Mironove review⁶⁵, the intrinsic luminescence of lanthanide ions (Ln) is relatively weak, but it is highly amplified in complexes with porphyrins due to the energy transfer from the excited macrocycle to the Ln^{+3} ion. The investigations of porphyrin-lanthanide complexes concluded that erbium, neodymium and ytterbium are the only metals that able to be characterised by near-infrared spectroscopy due to the intramolecular energy transfer from the triplet level of porphyrin, which is located higher than resonant levels of Er^{+3} , Nd^{+3} and Yb^{+3} (**figure 3.28 and 3.29**)⁶⁵.

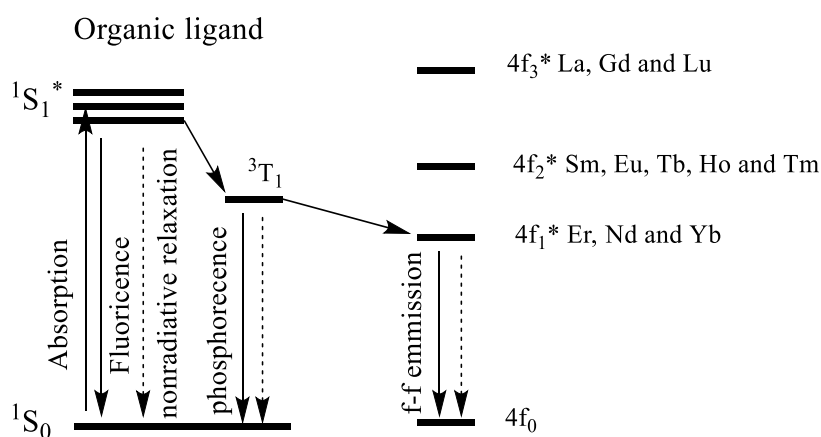


Figure 3.28: Modified energy diagram describing the luminescence of lanthanide complexes^{66 65}

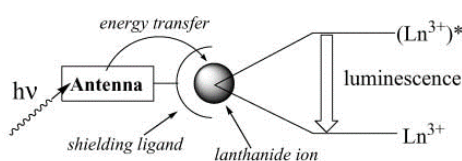
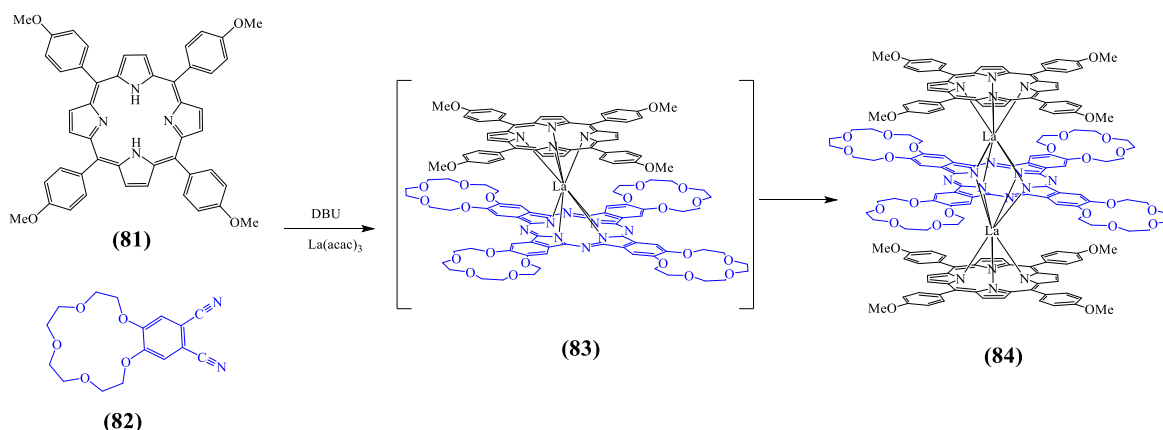


Figure 3.29: Porphyrin complexes shield lanthanide ions and works as an antenna for harvesting light and transferring it to lanthanides ion (Adapted from Werts *et al.*)⁶⁷

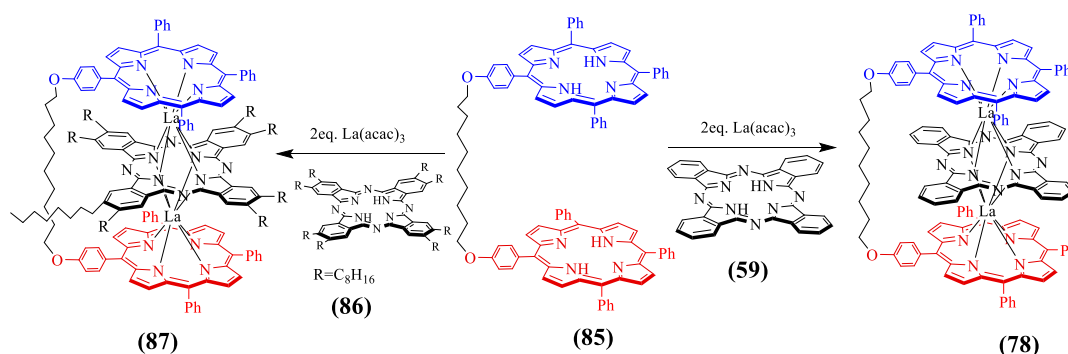
As mentioned earlier, the highest value of electron transfer was recorded for cofacial models; the researchers were fascinated by increasing the layers of porphyrin toward collecting more information. The attempts to produce multi-deckers such as triple, quadruple and quintuple were successfully achieved, but the synthetic method leads to a mixture of products. More attention is given to triple-deckers to cross the energy barrier for other lanthanide metals besides accessing a new magnetic material using lanthanide.

Accordingly, porphyrin-phthalocyanine-porphyrin TD was not achieved in sufficient yield till Tsivadze and co-workers developed a protocol for this kind of complex. They obtained a 30% yield by refluxing a mixture of tetrakis-meso-(4-methoxyphenyl)-porphyrin, 4,5-dicyanobenzo-15-crown-5, lanthanide acetylacetonate (La, Ce, Pr) and DBU in 1-octanol, which leads to a selective formation of a heteroleptic triple-decker complex of symmetrical structure (**scheme 3.21**).



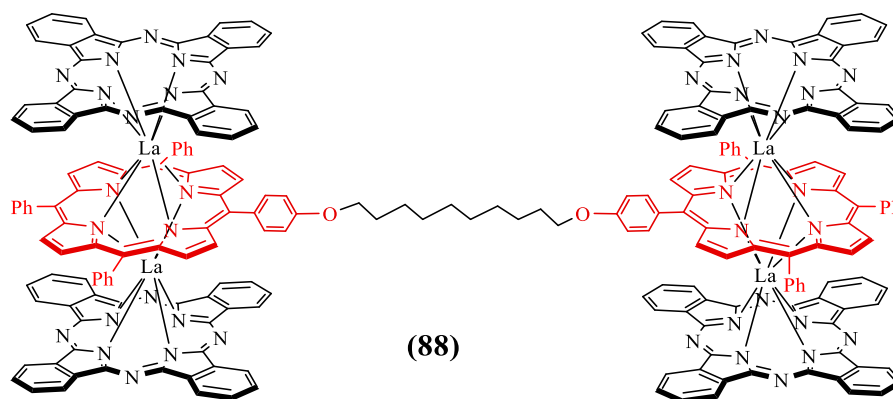
Scheme 3.21: Tsivadze *et al.*⁵⁸ general protocol for TD formation.

In recent years, our team developed a protocol for preparing TD in excellent yield⁴. My colleagues achieved TD through dyad intermediate to control synthetic processes by connecting porphyrin units with an *n*-alkyl chain. They found that the suitable length is *n*-decane, which can host phthalocyanine and two lanthanide atoms. Within molecular machine principles, the large lanthanide atoms allowed phthalocyanine units to rotate freely. Also, the rotation of phthalocyanine can be stopped by the porphyrins' linker if phthalocyanine has substituents attached (**scheme 3.22**). Even though the porphyrins bridge controls the formation of porphyrin-phthalocyanine-porphyrin TD, an open bis-triple decker can also be produced by increasing the equivalent of phthalocyanine and lanthanide ions (**scheme 3.23**).



Scheme 3.22: Cammidge *et al.*⁴ general protocol for bridge TD model

(right: rotation is allowed; left: rotation is prevented)



Scheme 3.23: Open bis-triple decker model

As large naked cations of lanthanides cannot interact directly; phthalocyanine is templated them between porphyrin units. Therefore, magnetic properties may be achieved due to the effect of free electrons at f orbital as well as magnetic dipole interactions. Hosting Pc shows an intricate balance of steric, geometric and ion-size effects, which can open the area for highly functional single-molecule materials (**figure 3.30**).

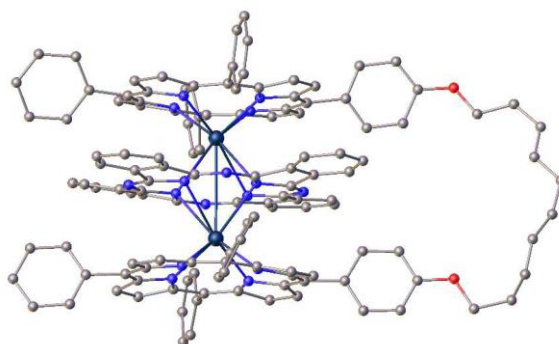


Figure 3.30: Pc hosted between the porphyrin dimer using lanthanide metals, adapted from Cammidge *et al.*⁴

Chapter 4

Results and discussion

4. Results and discussion

4.1 Pre-organized Porphyrin cage

4.1.1 Introduction

In recent years, porphyrin cages have been highlighted as a potential model in advanced applications such as catalysts, molecular machines and organic single-molecule magnets. They attracted researchers to design models that meet the demands of new solutions for quantum computing, environmental issues, photodynamic therapy and energy resources. Porphyrin cages are known in the field due to their reactive sites, leading to a unique property. Also, porphyrin cages can be modified based on binding sites, linkers, or binding cavities (**figure 4.1**).

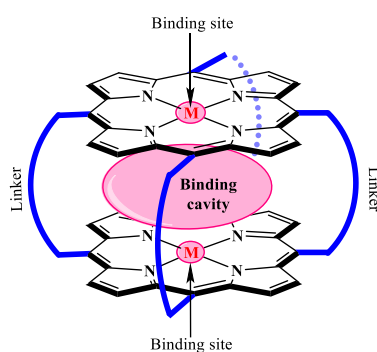


Figure 4.1: The general structure of porphyrin cage

Previous studies demonstrated that changing the guest at the cavity is affecting its behaviour. Therefore, our ambition is to build a cage from porphyrins that host large molecules such as phthalocyanine. Due to the similarity with porphyrin, researchers found Pc can be self-assembled with porphyrin in double and triple-deckers structures in the presence of large metals such as lanthanides. The assembled order is varied due to the similarity in their electronic properties and reactivity³. Therefore, pre-organization will control the synthesis and increase the overall yield⁴.

The starting point for our design toward encapsulated phthalocyanine into the porphyrin cage, the target in this work, is finding the suitable linkers for obtaining the goal. Cammidge *et al.*⁴ found that the length of n-decane chain is suitable for preparing porphyrin-phthalocyanine-porphyrin which is like our target (**figure 4.2**). Therefore, we concluded that the length of C₁₀ will be suitable for our investigation.

Hence, taking advantage of the active centres of porphyrin and phthalocyanine by hosting large metal such as lanthanide⁴ may be essential to hold the component together, but there is a specific requirement due to metal size limitation⁴. Thus, we must design porphyrin units to be linked firstly from one side to encapsulate the Pc molecule in between as mentioned in literature⁴ to avoid any side reactions occurring during the formation of triple-deckers TD.

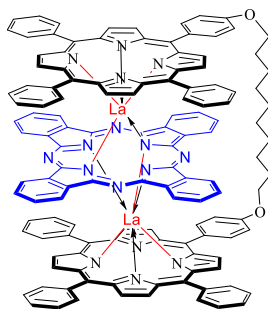
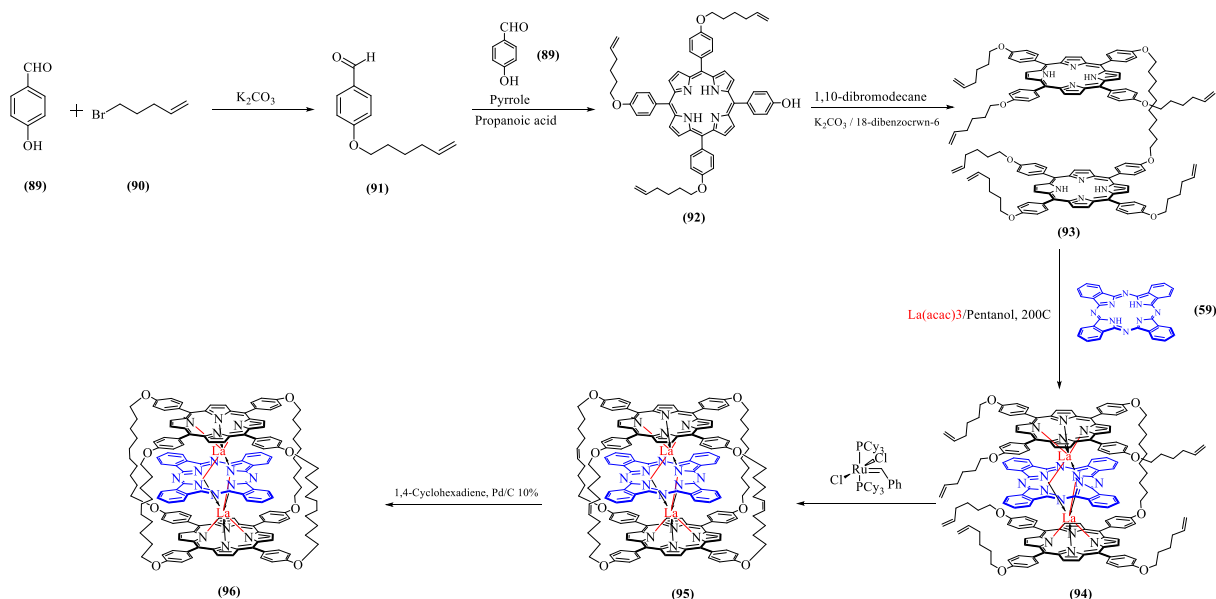


Figure 4.2: Controlled assembling of TD in a correct order of Porphyrin-Phthalocyanine-Porphyrin using a bridged diporphyrin⁴

The linker that we chose is 1,10-dibromodecane based on successful previous work on similar analogues in our team. As the distance is known, the length of the other linkers to make a cage should be considered identical to the first linker. Encapsulated Pc into porphyrin cage through the mentioned methods in literature is not considered. Therefore, the protocol toward the goal will be modifying the porphyrin components to meet the cage target through TD general protocol.

Porphyrin formation was studied heavily, and it concluded that the formation of asymmetrical porphyrin requires modifying aldehyde units starting material toward obtaining satisfactory results. We went through that toward accessing dyad intermediate as a straightforward and controlled synthetic method of porphyrin-phthalocyanine-porphyrin heteroleptic triple-deckers (TD) assemblies. Therefore, designing our cage on that approach required linkers that can be locked after TD formation with the same length. Thus, 5-hexene was nominated to be the precursors to the linkers due to its ability for alkene ring-closing through metatheses (**scheme 4.1**).

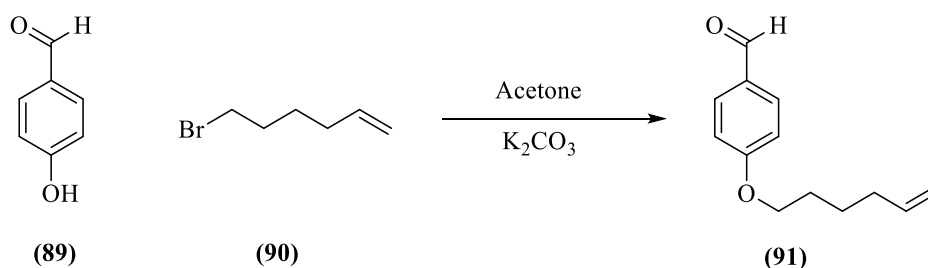


Scheme 4.1: The general hypothesis toward encapsulating Pc into the porphyrin cage

Addressing the sequence of the hypothesis in detail will provide understanding toward improving the methodology and emphasis on the background literature. Also, the unique geometry structure of TD cages may increase the stability of Pc, which provides access toward dipolar magnetic fields by bridging lanthanide metals. The only other example of allowing direct Ln–Ln bonding is in dimetallofullerenes C_{80} , which had been investigated by Popov *et al.*⁶⁹. The joint advantages between lanthanides and Pc in TD cages can be summarised in two points: (i) Ln templating Pc in the cavity centre, and (ii) Pc provides extra ligands to Lanthanides which act as a radical bridge between them. Thus, this assembly results in overlapped π electrons that increase the absorption to the near-infrared region as a consequence.

4.1.2 Preparation of *p*-hex-5-en-1-oxybenzaldehyde

The title compound was synthesised to meet the target of required linkers length as an initial step for pre-organising starting material of asymmetrical porphyrin. It was firstly mentioned by Mazumder. Unlike his method, we had done this reaction by one-pot step as a modified version of a Williamson reaction procedure (**scheme 4.2**). The activity of the aldehyde function group limited the choice of base to obtain a higher yield. We also optimised this reaction due to the need of collecting starting material on a large scale (**table 1**). Compared to the literature, we obtained sufficient yield at a very short time by using DMSO or DMF as a result of the optimisation that we had made.



Scheme 4.2: Synthesis of *p*-hex-5-en-1-oxybenzaldehyde

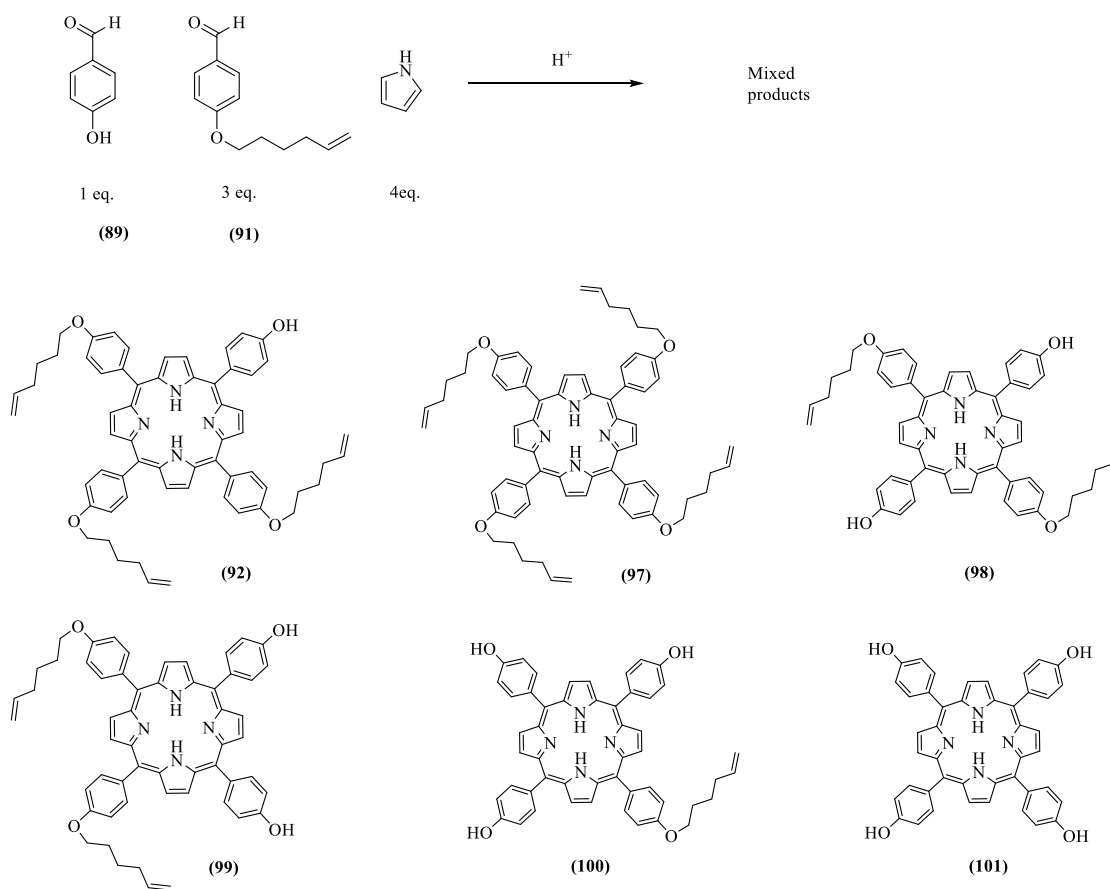
	1 (g)/eq.	2 (g)/eq.	Time(h)	Solvent / Vol.(ml)	T (°C)	3 yield (%)
1	6.1 / 1eq.	10.2 / 1.25 eq.	48	Acetone (50)	reflux	85.5
2	6.1 / 1eq.	12.23 / 1.5 eq.	48	Acetone (100)	reflux	93
3	6.1 / 1eq.	10 / 1.22 eq.	1	DMSO (20)	100	85
4	24.4 / 1eq.	35.3 / 1.08 eq.	2.5	DMF (80)	100	90.50

Table 1: Representation of the different reaction conditions screened

The reaction completion was monitored by TLC and ^1H NMR; then, the organic phase was extracted by DCM. The pure product was collected by distillation under reduced pressure and required a high temperature of 182°C.

4.1.3 Preparation of 10,15,20-trihex-5-en-1-oxy-*p*-phenyl-5-*p*-hydroxyphenylporphyrin

Toward the target, a new class of asymmetrical porphyrin (**92**) was designed to meet the goal. We followed the general method for synthesising the title compound using a mixture of aldehydes (**89**) and (**91**) in a 1:3 ratio. As with any asymmetrical porphyrins, it is expected to obtain a mixture of products that need further purification (**scheme 4.3**). The major products were obtained (**92**) and (**97**), separated by a common method for purification over silica gel column chromatography.



Scheme 4.3: General method of asymmetrical porphyrin preparation.

As there are different methods for porphyrin synthesis, we started by examining Lindsey preparation methodology because it is recognised to give higher yield often. We examined both conditions they mentioned; neither BF_3 nor TFA provided a satisfactory product. Even increasing time and temperature were applied, the reaction mixture was not improved. That might indicate that this kind of acid may result in alkoxy hydrolysis byproducts to form. As we ended with oily tar which was hard to analyse, we suspended this method and moved to alternative Adler methodology.

In contrast to Lindsey's porphyrin preparation methods, the Adler-Longo methodology appears to give fair progression toward **(92)** preparation with an average yield between 4% to 6%. The major product in the crude mixture were **(92)** and **(97)**, which were separated by column chromatography. The optimisations of this reaction appeared nearly the same result with slightly higher at a lower amount of propanoic acid (**table 4.2**).

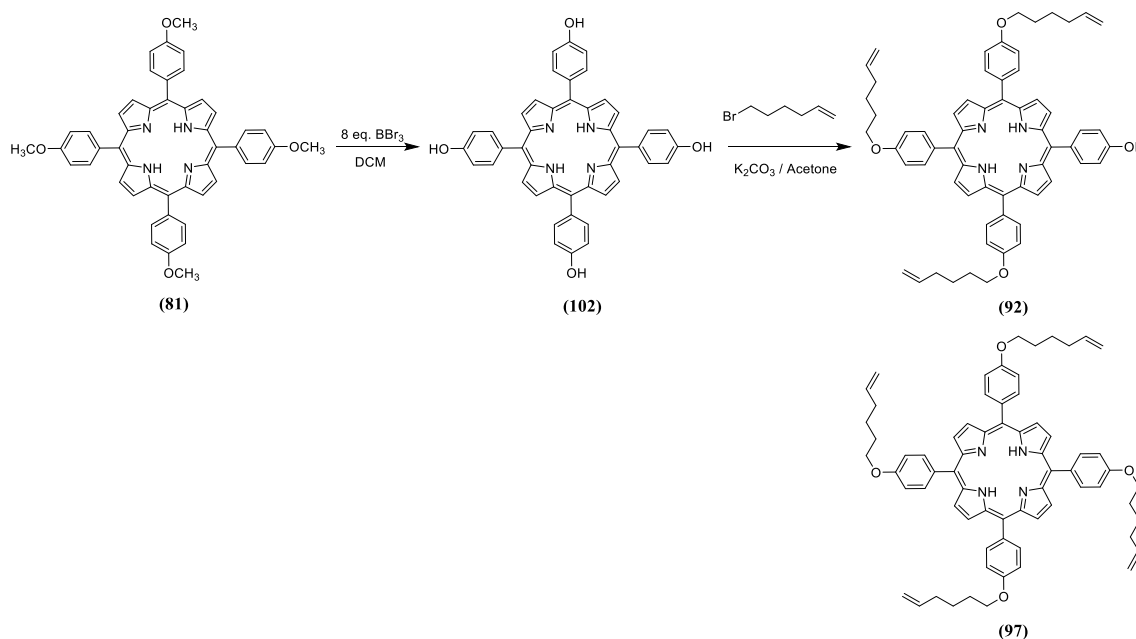
	scale (mmol)	(89) (1 eq.)(g)	(91) (3 eq.)(g)	Pyrrole (4 eq.)(g)	Propanoic acid (ml)	T (°C)	yield (%)
A	15	0.457	2,298	1.007	100	140	4.2
B	50	1.525	7.65	3.35	100	Reflux 180	5.3
C	50	1.528	7.67	3.35	120	Reflux 180	5
D	50	1.526	7.66	3.35	150	Reflux 180	5.2
E	61	1.87	9.40	4.11	150	Reflux 180	6
F	100	3.06	15.3	6.7	400	Reflux 180	3.2

Table 4.2: Optimization of porphyrin **(92)** preparation using Adler-Longo method

As mentioned earlier, the crude product was precipitated from the reaction mixture selectively by methanol followed by column chromatography separating **(92)** and **(97)** in pure forms. Even though the separation on the TLC plate seems smooth, preparative separation on column chromatography proved extremely challenging because it required a high amount of eluent system. (DCM/Hexane 1:1) then (DCM/EtOAc 9:1), is very slow, and gives results that are not consistent. Accordingly, we managed to find another suitable elute systems (EtOAc/DCM/Hexane 1:9:40) to collect **(97)** then (EtOAc/DCM 1:9) to collect **(92)**, which not comparable with the first elute system. It required less solvent, and fast separation was achieved, which reduced time and waste. However, the procedure again proved difficult to reproduce each time, and we decided to investigate alternative syntheses of this key intermediate.

4.1.4 Tetrakis-*p*-methoxy phenyl porphyrin

In the line of preparing **(92)** in large quantity, we attempted to obtain higher yield through symmetrical porphyrin because it can be achieved in higher yield easily. Preparing tetrakis-*p*-methoxy phenyl porphyrin **(81)** followed by demethylation will give hydroxy analogues **(102)**. This method was proposed because tetrakis-*p*-hydroxyphenyl porphyrin **(102)** is hard to separate from the crude mixture if prepared directly. The proposal was then to react the resulting compound with three equivalents of 6-bromo-1-hexene to achieve **(92)** (scheme 4.4).



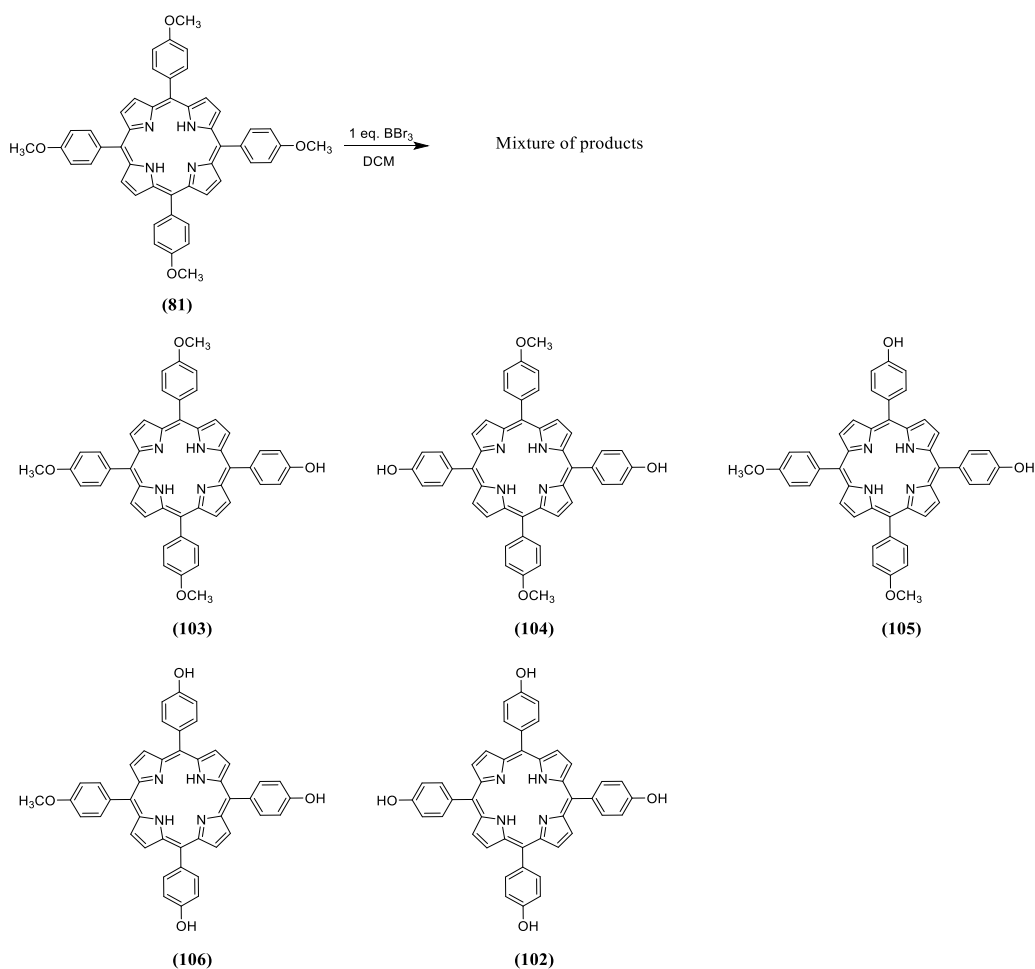
Scheme 4.4: The proposal of preparing **(92)** in multi-steps to increase overall yield.

Preparation of **(81)** was carried out through the Adler-Longo methodology with an overall yield of over 32%. The reason for obtaining a higher yield is that symmetrical porphyrin tends to form one product which is statistically reasonable. It was easily crystallised and used without further purification in the demethylation step.

The demethylation was done following the general procedure of ether cleavage using boron tribromide BBr_3 ⁷⁰. We followed the recommendation of McOmin⁷¹ to use more than one equivalent of BBr_3 for each methoxy group. Therefore, the reaction was carried under N_2 , and the temperature was controlled to -20 C upon the addition of double equivalents of BBr_3 . The completion was obtained within one day and quenched by water. The addition of triethylamine was required to neutralise **(102)** for recovering the purple colour. Further purification was unnecessary as the analysis confirmed its purity that is suitable for direct application.

In the line toward (**92**), three equivalents of 6-bromo-1-hexene were reacted with (**102**) in a similar way to prepare (**91**). The reaction was monitored by TLC, which showed the formation of (**97**) instead and unreacted (**102**) after two days. It seemed that the reactivity of porphyrin increases when it starts attaching alkenes as the solubility increases as well.

Attempting to demethylate only one group of methoxides to obtain asymmetrical analogues on the same principle resulted in all six possibilities, including unreacted starting material (**scheme 4.5**). The plan was to obtain a dyad from (**103**) then demethylate the rest of the methoxy groups. However, this pathway was suspended because the resulting mixture was not sufficiently soluble to separate by chromatography at a reasonable scale.

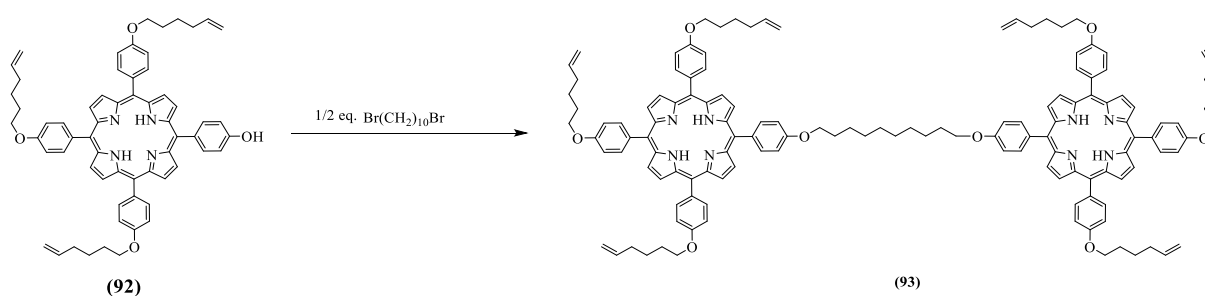


Scheme 4.5: Attempts to prepare (**103**) by ether cleavage methodology

The alternative pathway to achieve (**103**) is through the general methodology of Adler to prepare porphyrin. Mixtures of 4-methoxybenzaldehyde and 4-hydroxybenzaldehyde were examined. The crude products were a mixture of (**81**) and (**103**) with an overall yield of ~11%. However, the yield of (**103**) was found to be only around 3.5%. For that reason and the concern of cleavage of alkyl linker of the dyad when later removing methoxide groups, investigation of this approach was suspended.

4.1.5 Dyad intermediate

As mentioned earlier, preparing dyad intermediate (**93**) is expected to increase the selectivity toward encapsulated Pc into the porphyrin cage. Therefore, linking porphyrin units will be reducing the side products toward selective assembly. The required bridging chain length was concluded from an earlier study carried by Cammidge *et al.*⁴, and it has been modified to meet our goal (**scheme 4.6**). Even though preparing a dyad seems straightforward protocol, dealing with the formation of unwanted side-products proved to be a major challenge. This reaction is highly sensitive to kind of base, solvent, temperature and symmetry status, which need to be optimised to find the best conditions (**table 4.3**).



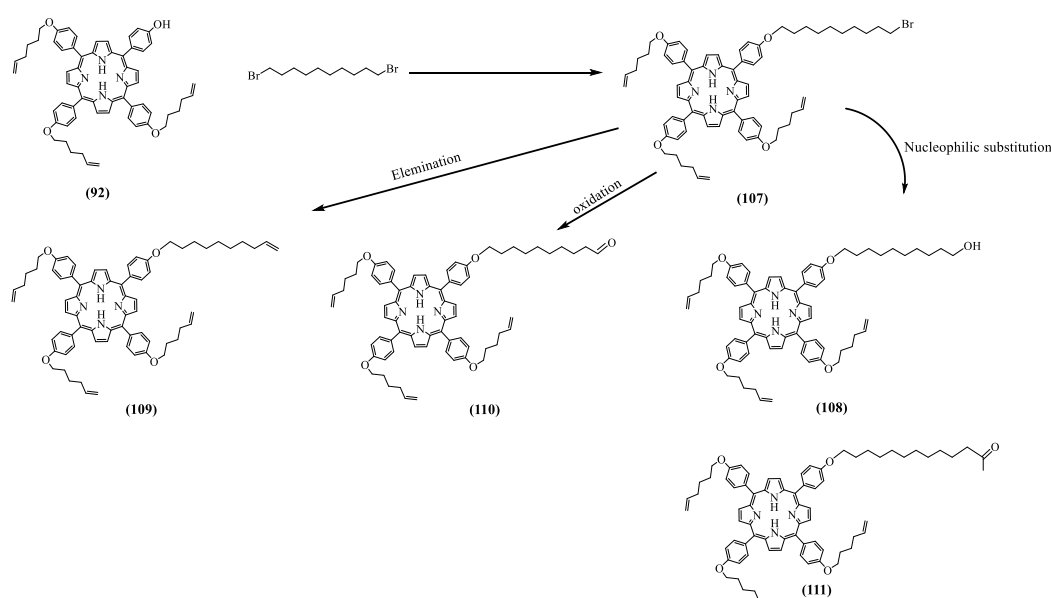
Scheme 4.6: general proposal of preparing dyad intermediate.

Entry	(92) (eq.)/ mg	$\text{Br}(\text{CH}_2)_{10}\text{Br}$ (eq.)/mg	Time	solvent	Temp. (°C)	Base (mg)	(93) Yield%
1	(2) 50	(1) 8.1	4 d	Acetone	70 (reflux)	K_2CO_3 (3.73)	18%
2	(2.1) 24.5	(1) 3.8	4 d	Acetone	70 (sealed tube)	K_2CO_3 (ex.)	20%
3	(2.1) 203	(1) 32.9	6 d	Acetone	70 (sealed tube)	K_2CO_3 (ex.)	~22%
4	(2.2) 205	(1) 30	24h	Acetone	70 (sealed tube)	K_2CO_3 (30.3), KI(10)	trace
5	(2.02) 98	(1) 15.8	3h	Acetone	RT (sealed tube)	NaOH (ex)	trace
6	(2.05) 195	(1) 30.8	2d	Acetone	RT (sealed tube)	K_2CO_3 (ex), 18-crown-6	trace
7	(2.05) 195	(1) 30.8	6d	Acetone	70 (sealed tube)	K_2CO_3 (ex), 18-crown-6	34%
8	(2.38)1.1g	(1) 162	24h	DMF	70 (under N_2)	K_2CO_3 (ex), 18-crown-6	20 %
9	(2.01) 105	(1) 17	8h	DMSO	100 (under N_2)	K_2CO_3 (ex), 18-crown-6	13%
10	(3) 0.88g	(1) 95	3d	MEK	90 (sealed tube)	K_2CO_3 (ex), 18-crown-6	28%

Table 4.3: Optimization of dyad (**93**) formation in one step.

The optimization did not increase the overall yield due to the formation of side reactions from intermediate product **(107)** (scheme 4.7). The reaction was monitored by MALDI-ToF-MS because **(108)** appeared on TLC overlapping with **(92)**, R_f (DCM/pet.ether 1:1) = 0.05 and 0.1 respectively, which makes the judgment hard whether it is SM or by-product. Also, **(109)** appears very close to **(107)**, R_f (DCM/pet.ether 1:1) = 0.6 and 0.55 respectively, which is another complication. Identification of those products carried by scratching the TLC toward analysing each spot separately by MALDI-ToF-MS. **(92)** ($C_{62}H_{61}N_4O_4$)⁺ [M+H]⁺ calcd: 925.46 found: 925.55; **(107)** ($C_{72}H_{80}N_4O_4Br$)⁺ [M]⁺ calcd: 1143.54 found: 1143.15; **(93)** ($C_{134}H_{137}N_8O_8$)⁺ [M+K]⁺ calcd: 2026.67 found: 2026.28; **(108)** ($C_{72}H_{81}N_4O_5$)⁺ [M+H]⁺ calcd 1081.62 found: 1081.14; **(109)** ($C_{72}H_{78}N_4O_4$)⁺ [M]⁺ calcd 1062.60 found 1062.62; **(111)** ($C_{75}H_{85}N_4O_5$)⁺ [M+H]⁺ calcd 1121.65 found 1121.13; **(110)** ($C_{72}H_{79}N_4O_5$)⁺ [M+H]⁺ calcd 1079.60 found: 1079.43;.

However, the presence of those by-products is different from one condition to another, but some are always there. The reasons for that vary between elimination reactions, nucleophilic substitutions, and oxidation. Those by-products resulted from the kind of base and the kind of solvent which provides suitable conditions for the side reactions to occur. The evidence from crude MALDI-ToF-MS showed peaks for these mentioned by-products, and results were confirmed by ¹H NMR for some of them, which support this observation. (chart 4.1 and 4.2).



Scheme 4.7: The side products that had been indicated in the MALDI-ToF-MS spectrum.

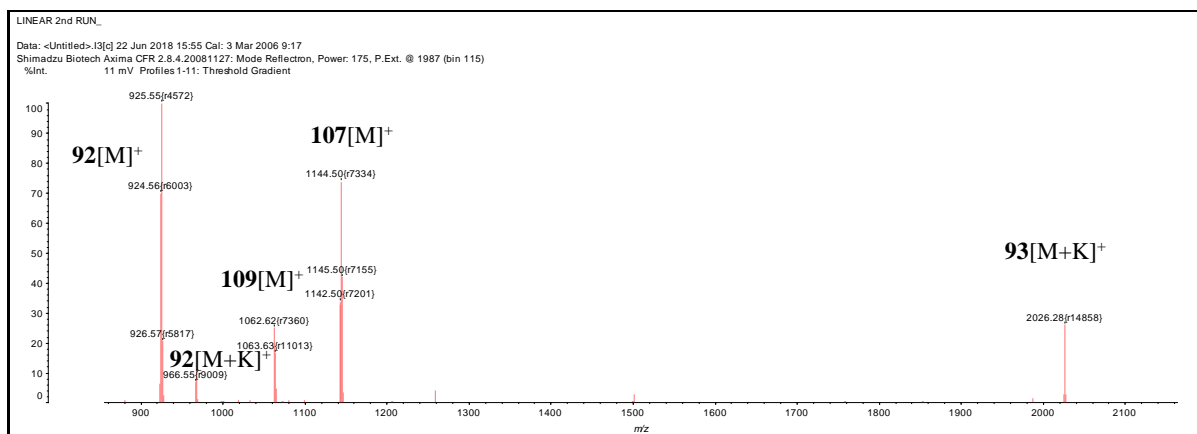
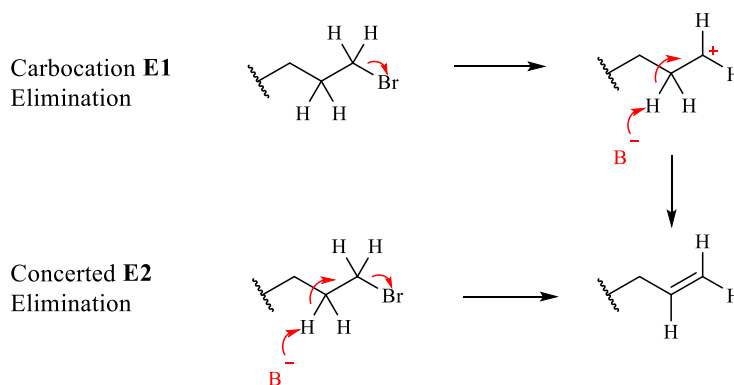


Chart 4.1: The crude analysis of dyad reaction peaks appears elimination byproducts

Elimination reactions are possible by removing a proton at the position next to a leaving group. This type of elimination can be occurred following two model mechanisms (**scheme 4.8**): (i) it can occur in a single concerted step when proton removed at β carbon occurring at the same time as α carbon bromide C-Br bond cleavage, or (ii) in two steps when α carbon bromide C-Br bond cleavage occurring first to form a carbocation intermediate, which is then quenched by proton removed at the β carbon⁷².



Scheme 4.8: Proposed elimination mechanism pathways of (109).

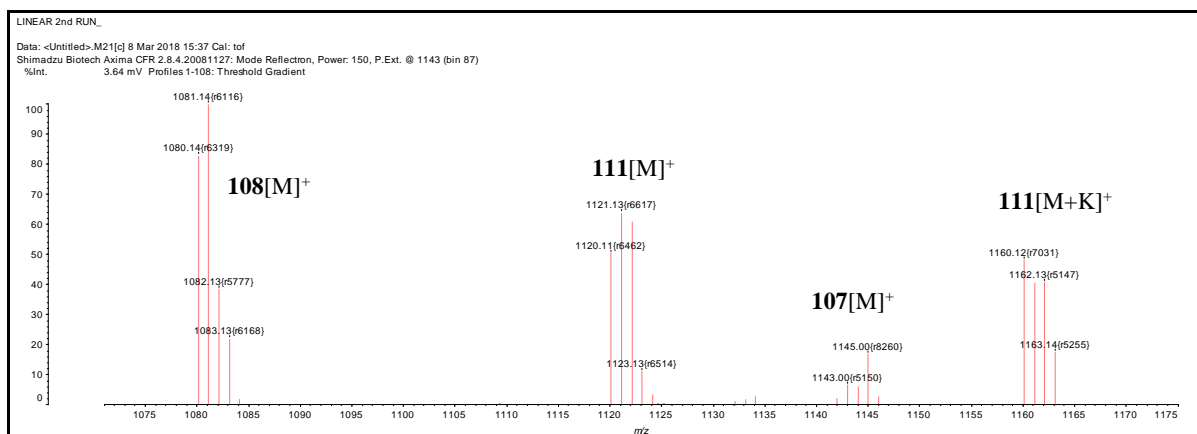
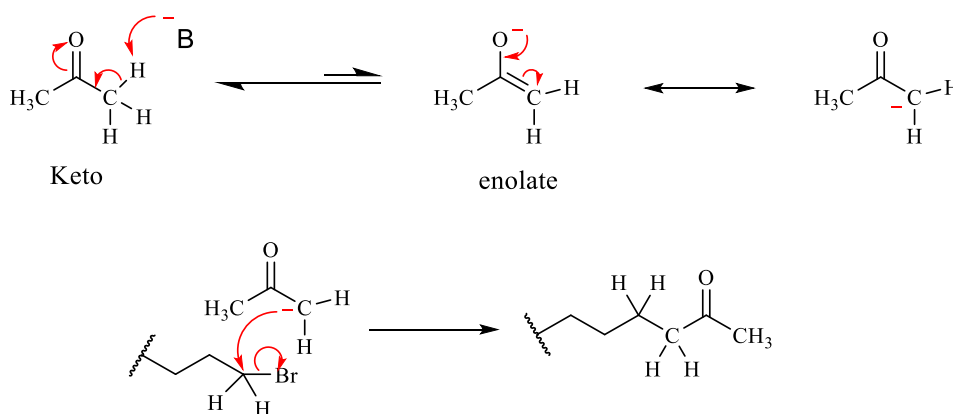


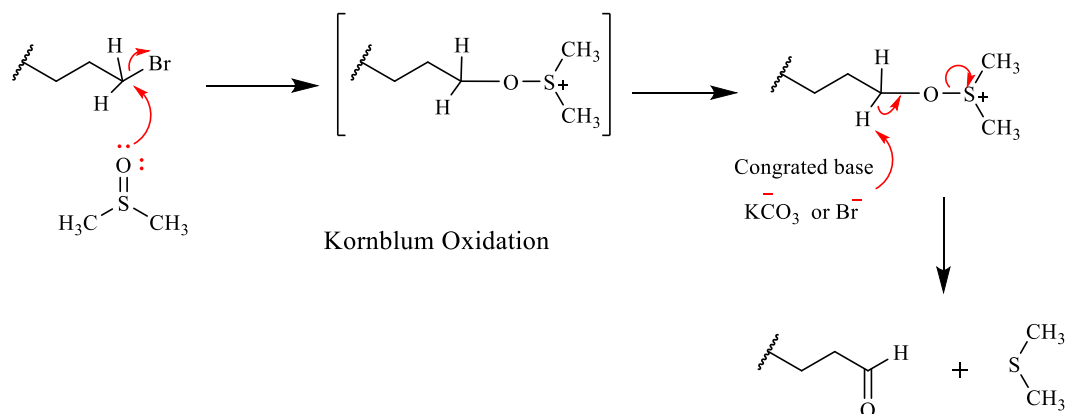
Chart 4.2: The crude analysis of dyad reaction peaks appears nucleophilic substitution byproducts

The by-product (**110**) is highly likely to form when overheating the reaction in acetone in the base condition, forming an enolate anion (**scheme 4.9**). The enolate anion attacks the α carbon halide as a nucleophile, which is stabilised later by bond cleavage of carbon halide C-X. This by-product may result from the S_N2 mechanism as a potential pathway of the reaction.⁷³ In the same way, the by-product (**108**) could be formed from the moisture in the system over the time of heating or when a strong base like KOH is used.



Scheme 4.9: Proposed pathway of enolate anion formation in order to form (**111**).

The by-product (**110**) is highly likely to form when using DMSO reagent as a result of Kornblum oxidation occurrence (**scheme 4.10**). Notably, (**110**) may be water-soluble as it was indicated in the crude run, but it cannot be isolated after the workup process. We examined the reactant 1,10-dibromo-decane toward elimination and other reactions under the reaction conditions to investigate side reactions. Aldehyde and alkene side products did indeed appear to form. Even though DMSO observed the highest yield, it is not a suitable solvent for preparing dyads. Therefore, we moved toward investigating two-steps formation with the aim of increasing overall yield.



Scheme 4.10: The general mechanism of Kornblum oxidation⁷⁴ that may lead to reduce the yield of our target.

^1H NMR shows that the peaks of SM (**91**) are different from (**92**) and (**93**), whereas (**92**) and (**93**) are not moved. However, 18 shows duplication of the peaks even though the symmetry of the compound (**chart 4.3**).

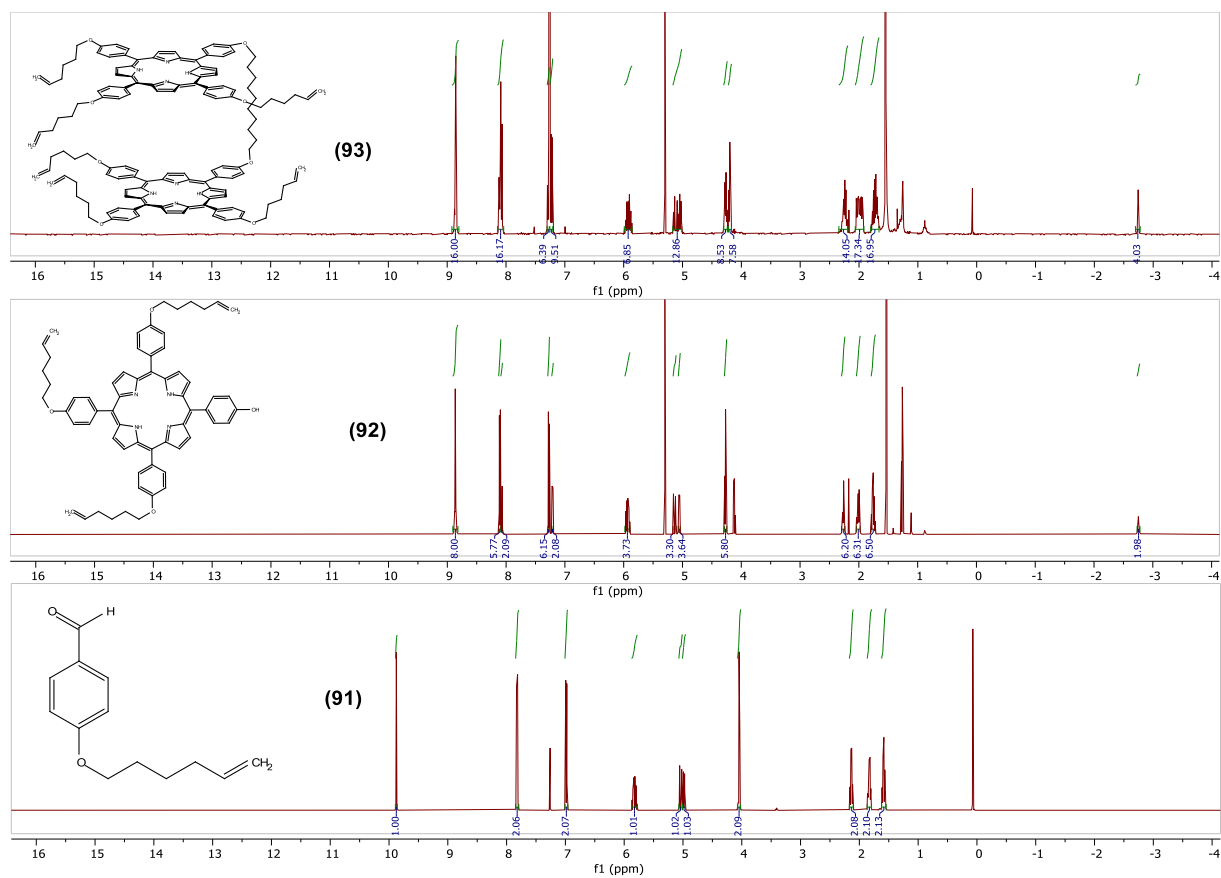
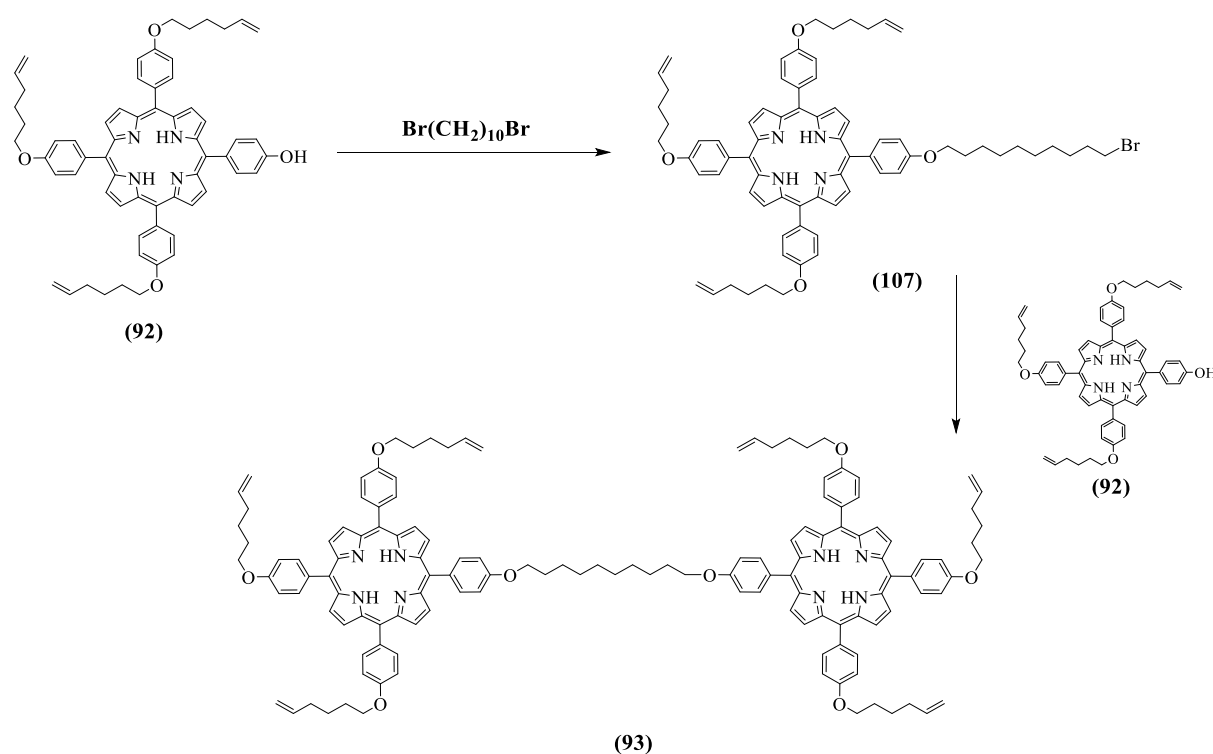


Chart 4.3: The ^1H NMR chart of the reaction progression

4.1.6 Improvement attempts:

Toward increasing the dyad's yield and understanding why it takes such a long time, we divided the reaction into two steps instead (**scheme 4.11**). As the previous approach did not show a completion point due to complications of side-products formed rather than our proposed product, we aimed to increase the efficiency by this approach. The focus remained on this particular dyad because it meets the length of the required linkers to close the cage in forwarding steps. The drop in the overall yield that we faced was wasting starting material (**92**), which itself needed a laborious two-step synthesis and challenging purification. Therefore, addressing this issue may help to avoid side-products and long formation time.



Scheme 4.11: the two steps approach toward dyad's formation

In the first step toward achieving **(107)**, the general approach was to react **(92)** with an excess amount of 1,10-dibromodecane with the aim of increasing the reaction's rate to direct it toward product formation. We optimised this reaction as it may provide a hint about the behaviour of **(107)** intermediate in the reaction (**table 4.4**).

Entry	(92) (eq.)/ mg	Br(CH ₂) ₁₀ Br (eq.)/mg	Time	solvent	Temp. (°C)	Base (mg)	(107) Yield%
1	(1) 203	(10) 650	6d	Acetone	70 (sealed tube)	K ₂ CO ₃ (ex.)	85.3
2	(1) 57	(10) 180	17h	Acetone	70 (sealed tube)	NaOH	trace
3	(1) 100	(5) 150	24h	THF	rt (under N ₂)	LiHMDS	N/C
4	(1) 153	(10) 530	3d	Acetone	70 (sealed tube)	K ₂ CO ₃ (ex), 18-crown-6	84%
5	(1) 200	(30) 2 g	2 min	N/C	100 (MW)	K ₂ CO ₃ (ex), 18-crown-6	80%
6	(1) 110	(10) 330	1 h	DMSO	100 (under N ₂)	K ₂ CO ₃ (ex), 18-crown-6	32%

Table 4.4: Optimization of mono intermediate **19** formation

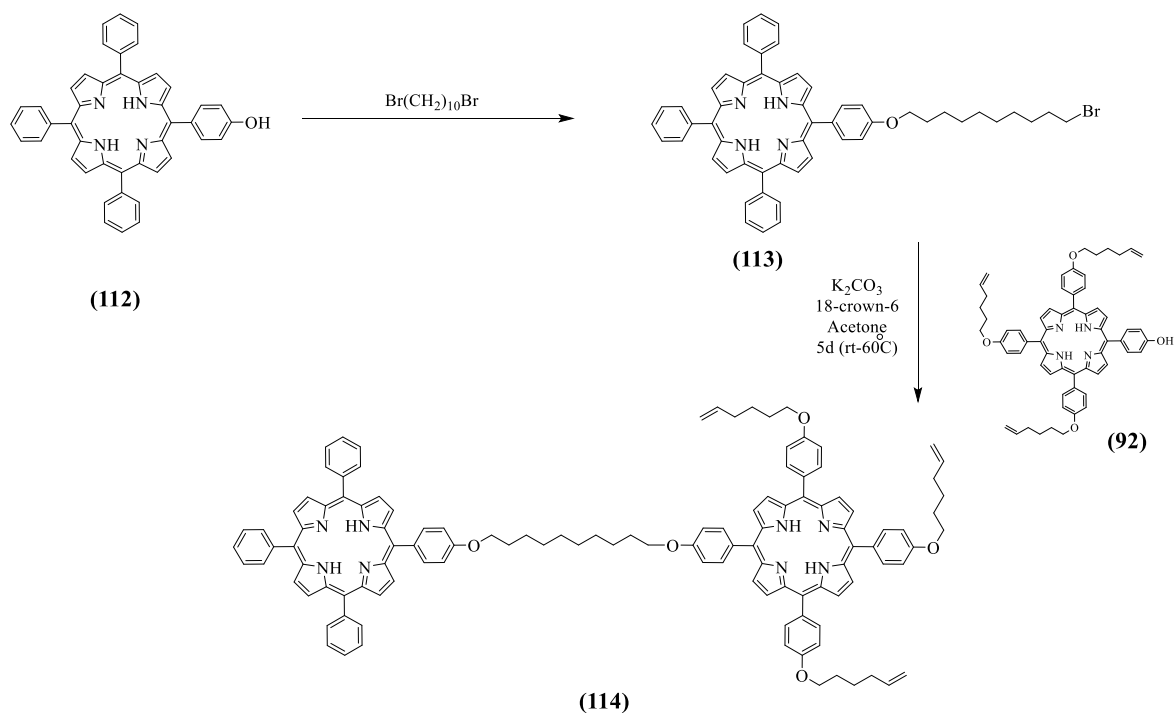
The comparison between these results appeared to show a strong evidence of the effect of solvent and the base in the formation of (**107**), which concluded from the time of completion. Also, the elimination by-products were not indicated in a significant amount in this step. However, the elimination test for the product (**107**) showed three spots on TLC using DMSO, which explained the drop in the yield compared to the acetone and solvent-free method. Thus, the higher yield that was obtained from the acetone and solvent-free method is similar to the approach toward dyad (**93**) formation. However, we cannot apply the solvent-free method for the next step as (**92**) and (**107**) are solid, which limits the choice to acetone as a proper solvent.

Moving toward the second step of the synthesis approach, in a similar way, optimisation may provide more answers for obtaining the best conditions to prepare (**93**). According to previous optimisations, this step always seems to take extra time compared with (**107**). Therefore, we aimed to increase overall yield and preparation efficiency besides answering the fundamental question that why the side-reactions are happening during the formation of the dyad (**93**). The optimisations (**table 4.5**) are based on reacting (**107**) with (**92**) at various conditions in aim to avoid side reaction occurrence.

Entry	(92) (eq.)/ mg	(107) (eq.)/mg	Time	solvent	Temp. (°C)	Base (mg)	(93) Yield%
1	(1.03) 162	(1) 190	9d	Acetone	70 (sealed tube)	K ₂ CO ₃ (ex)	17.1
2	(1.35) 54	(1) 50	9d	Acetone	rt. to 90 (sealed tube)	K ₂ CO ₃ (ex), 18-crown-6	31.9
3	(1.15) 12	(1) 13	2h	DMF	100 (under N ₂)	K ₂ CO ₃ (50)	28
4	(1.45) 195	(1) 166	24h	DMSO	100 (under N ₂)	K ₂ CO ₃ (ex), 18-crown-6	~13

Table 4.5: Optimization of dyad intermediate (**93**) formation in two steps

According to the results we obtained, an unsymmetrical dyad (**114**) was examined in the same approach to determine whether the formation is affected by the alkenyl chain surrounding porphyrin or the reaction conditions (**scheme 4.12**). We found that the reaction observed the completion without eliminations were indicated by TLC or ^1H NMR with yield over 70%.

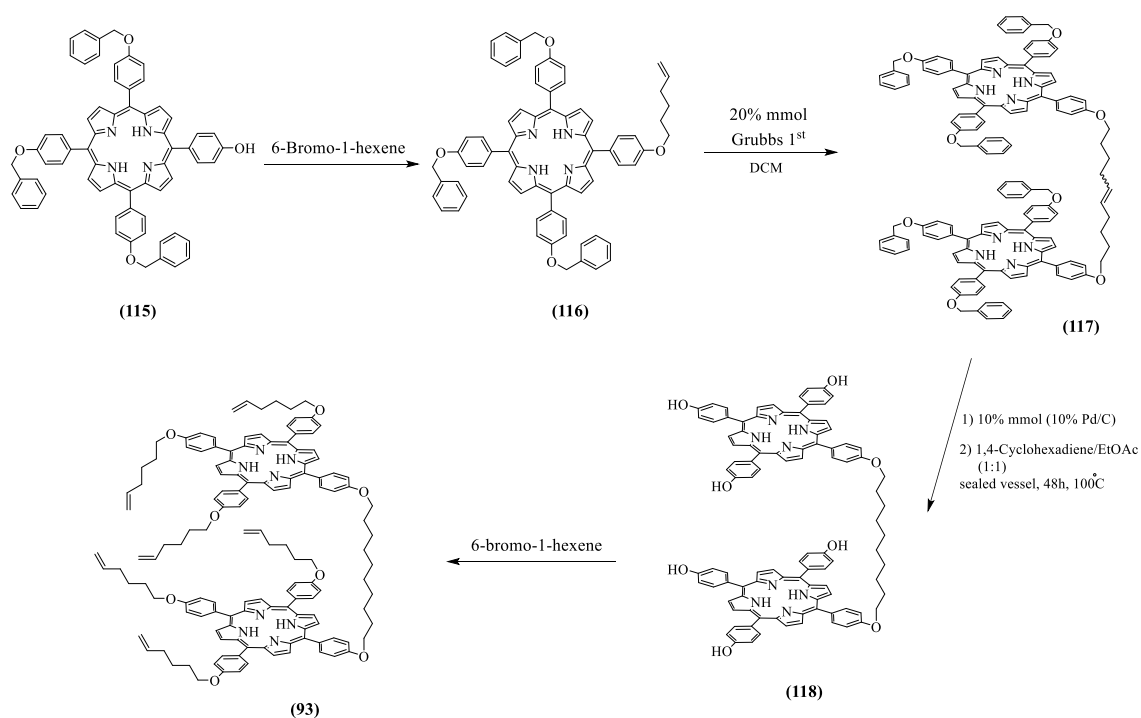


Scheme 4.12: The pathway of unsymmetrical dyad (**114**) formation

To conclude, the fundamental question is why the eliminations are happening during the formation of the dyad (**93**), and can conditions be found that prevent this and other side reactions from competing. The suggestions are that whether the reactive centres are blocked by the alkyl chains, which delay the formation of (**93**), or the solubility of (**107**) is more than (**92**) which increase its reactivity with reagents. Moreover, the reaction rate is increased dramatically with rising nucleophilicity of the base and temperature. However, the elimination by-products are increased as well under those conditions, especially, with strong bases. Even though the difficulties of (**93**) formation could not be fully solved, we continued to the following steps with the amount that had been collected.

4.1.7 Preparation of 10,15,20-tribenzyloxy phenyl-*p*-hydroxyphenyl porphyrin

Toward increasing the selectivity and avoiding the side-reactions and by-products, a new approach was designed to obtain a symmetrical dyad (**93**). As this dyad was required to obtain a higher yield of TD, the aim is to increase its overall yield besides avoiding side-products that observed from one-step and two-steps dyad (**93**) formation. Our aim is to link two porphyrin units before adding the rest of the linkers that are required to complete the cyclisation of the cage (**scheme 4.13**). This pathway was designed to investigate the steric hindrance occurrence from the presence of hexenyl linkers to avoid it. The starting materials that we started with are commercially available, which reduce the initial steps to obtain (**115**). The ability of benzyl cleavage and alkene reduction by palladium in one step selectively will yield the dyad spacer within the required length to form TDs.



Scheme 4.13: general proposal of achieving dyad through metathesis

Preparing unsymmetrical porphyrin (**115**) was carried out in a similar method of preparing (**92**), which resulted in a mixture of products. We found that the crude yield was much higher than (**92**) analogues by almost two times. The solubility of (**115**) is less than the rest of the products in the crude, which makes the purification easier. The crude mixture was dissolved in DCM and loaded over short column chromatography to be separated using DCM eluent. The pure product of **27** was reacted with 6-bromo-hexene to prepare (**116**). The reaction was monitored by TLC, and the completion was observed in 24h in DMF. By-products were not indicated in this step which made it encouraging to continue.

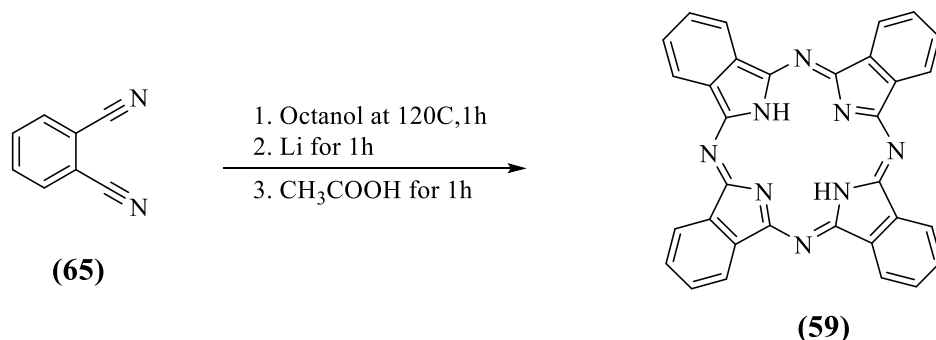
The dimerisation (dyad) (**116**) was obtained by metathesis coupling methodology using Grubbs 1st generation catalyst. This reaction was monitored by TLC, and ¹H NMR till completion was observed in which was obtained in 48h. As this generation of Grubbs catalyst is not stereoselective, the formation of *cis* and *trans* isomers are expected in an approximately (1:1) ratio. Both isomers were used in the next step as the reduction will be resulting only one product. We obtained (**116**) in a high yield after purification to recover the product from the catalyst.

The reduction of alkene and benzyl deprotection were taken place in one step to obtain (**117**) using Pd/C 10%. Examining isopropanol as a source of hydrogen was only valid for alkene reduction. Therefore, the best source of hydrogen for this reaction was 1,4-cyclohexadiene in a straightforward step of hydrogen transfer methodology that afforded one product. The reaction was monitored by ¹H NMR, and the completion was observed in 24h.

As the final stage in this plan, obtaining (**93**) again in an alternative method was not carried due to the solubility of (**117**) being the barrier to separate the product from Pd catalyst. Even though the extra steps in this pathway toward dimerisation, the overall yield almost doubled compared to the one-step pathway. It may indicate that the existence of the hexenyl chain in (**92**) might delay the formation of (**93**) as a result of steric hindrance effects. Hence, taking a shortcut toward dimerisation is possible from (**115**) to (**117**) using 1,10-dibromodecane; we did not follow that pathway due to the consideration of the solvent effect, side reactions formations and solubility issues.

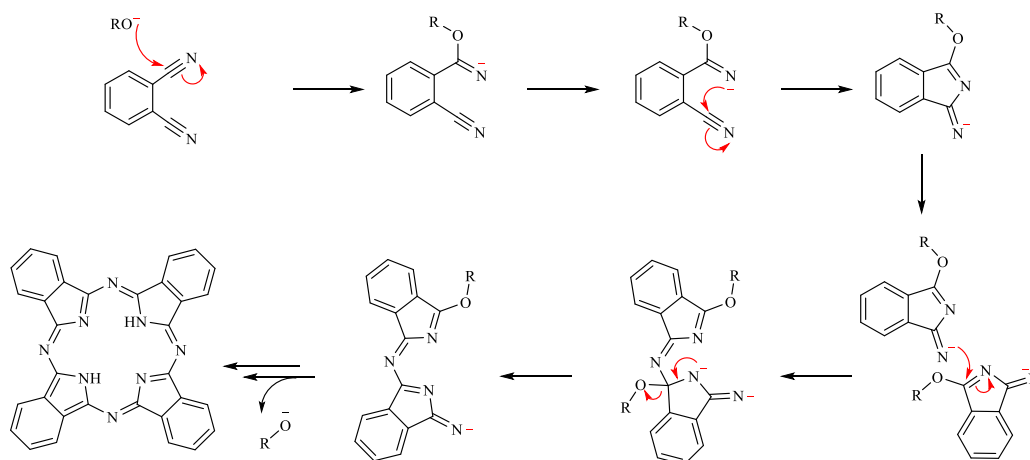
4.1.8 Phthalocyanine

As we are targeting phthalocyanine on encapsulation, preparation of Pc was performed following the general methodology mentioned by Galanin and Shaposhnikov⁷⁵. Even though there are several protocols for preparing phthalocyanine, we followed this method because high yield can be obtained besides short time formation (**scheme 4.14**). Our aim will target Pc and dyad (**93**) toward forming TDs.



Scheme 4.14: general procedure to prepare phthalocyanine

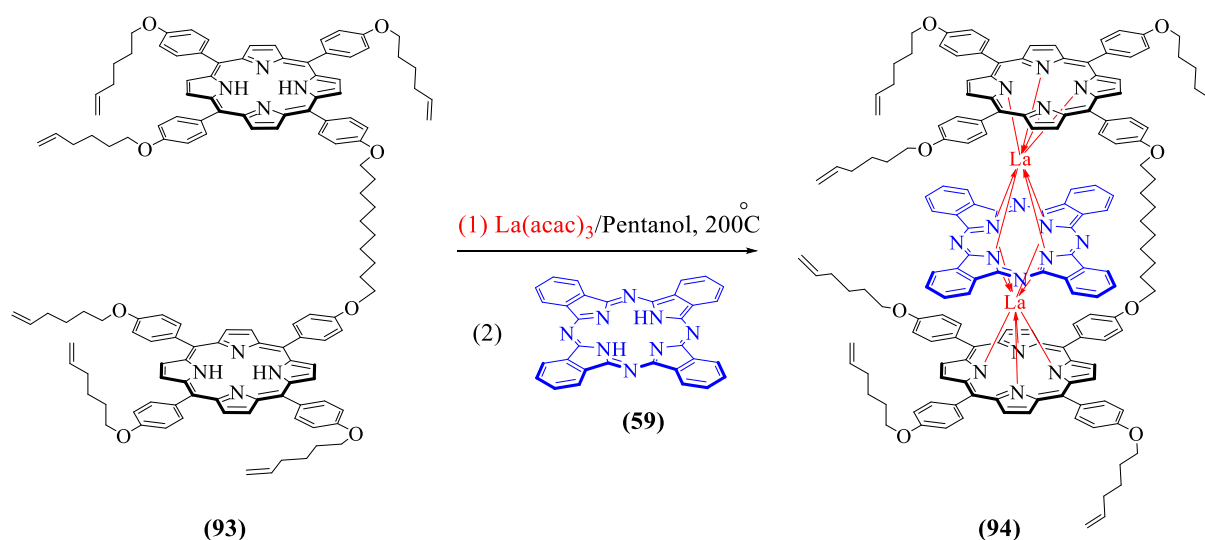
The procedure of Pc formation is straightforward, and it yielded over 40%. The general mechanism of the formation is based on the reaction of phthalonitrile with lithium-pentanolate in refluxing pentanol (**scheme 4.15**)⁷⁶. Acetic acid is acting to quench the reaction by removing the excess of the metal to form free phthalocyanine⁷⁷. The Pc was precipitated by MeOH and collected by filtration, and washed several times by MeOH. The Pc is slightly soluble in THF, which is only enough to record its UV-vis absorption to confirm its formation beside the MALDI-ToF-MS.



Scheme 4.15: the proposed mechanism of Pc formation

4.1.9 Triple deckers (TD)

Toward encapsulating phthalocyanine into the porphyrin cage cavity, the hypothesis was designed to prepare triple-deckers (TD) (**94**) as an intermediate in the order of porphyrin-phthalocyanine-porphyrin. The general protocol that developed by Cammidge *et al.*⁴ was followed, which required two equivalents of lanthanide salt to be added to dyad in hot pentanol followed by Pc addition for resulting intermediate TD (**scheme 4.16**). This methodology will pre-organise the component in the required order, which holds Pc in the middle between porphyrin units. This methodology is valid on Ln elements with large radii⁴, therefore, we first attempted the reaction using lanthanum (La), dyad (**93**) and Pc (**59**).



Scheme 4.16: general procedure toward TD formation

The formation of TDs is sensitive to moisture⁶⁵; therefore, the reaction was done under Argon and repeated in a sealed tube. The higher yield can be obtained when metalation takes place before Pc addition to avoid the formation of bis triple-deckers and Pc double-deckers. When the metalation was completed, Pc was added to the mixture. The reaction was monitored by UV-vis, and the metalations were observed in 36h, whereas Pc complexation took another 24h. Even though the concern was about the alkene bonds to be oxidised as a result of the long heating time, these bonds were found to be stable and survived, which was encouraging to continue.

The analysis of ^1H NMR peaks appears that the symmetry is affected by Pc, La, and alkyl chain bridge. The Pc and inner protons were deshielded as a result of the effect of electron density near Lanthanum atoms. In contrast, the porphyrin β protons and outer protons were

shielded due to the opposite reason of low electrons density. The protons of phenyl rings that connected by alkyl linkers are distinguished from the rest due to their geometry position (**chart 4.4**). For more clarifications, (**figure 4.3**) illustrates the geometry positions of protons. The protons were assigned from studying ^1H NMR, 2D-COSY NMR, ^{13}C NMR, dept135 NMR, and HSQC NMR, which compared with the similar model (**78**) in the literature from Cammidge *et al.*⁴.

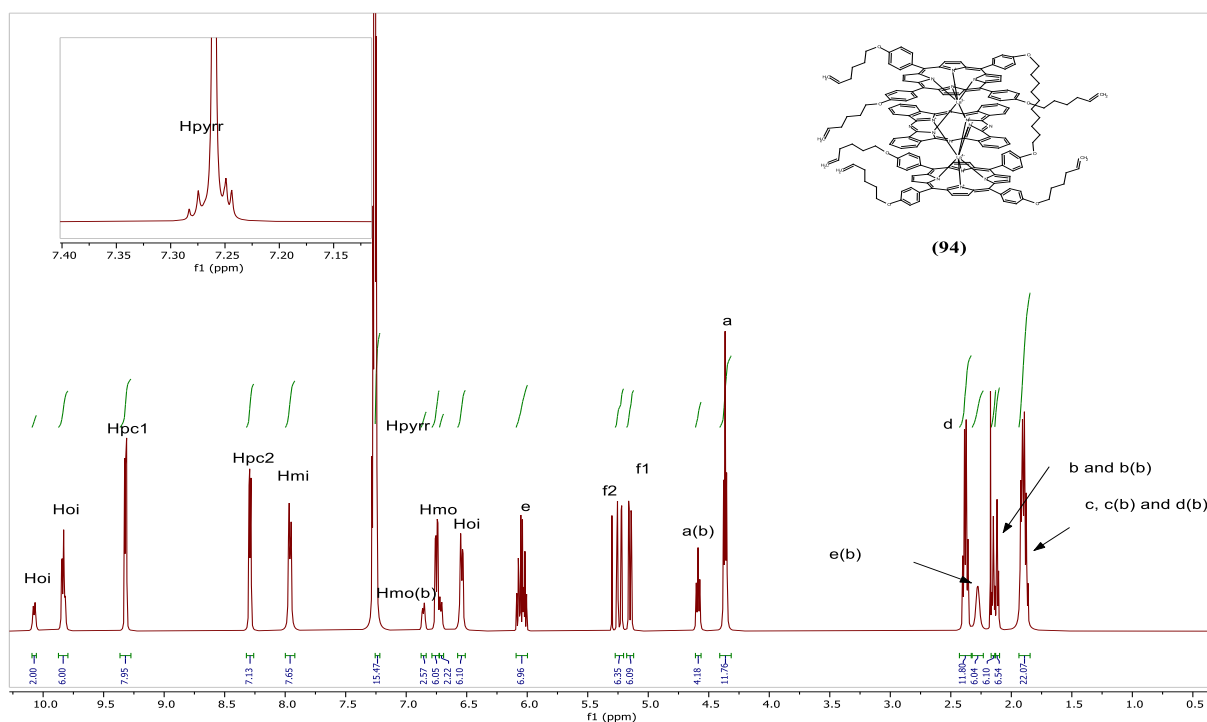


Chart 4.4: ^1H NMR indicates the TD formation; Porphyrin peaks in the frame (overlapped with chloroform) show the unsymmetrical environment of the molecular.

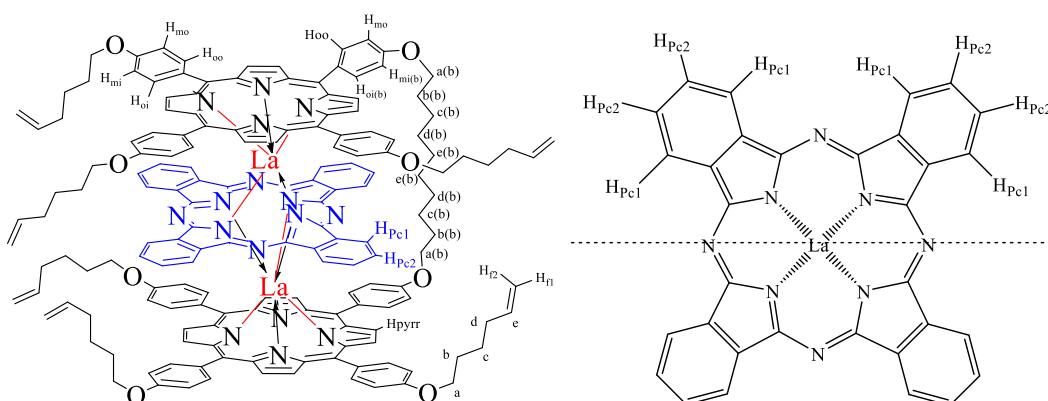


Figure 4.3: Representation of the TD(La) (**94**), (b in bracket refer to bridge) (left); Representation of Pc in TD(La) (right) with porphyrins omitted for clarity. The dotted line represents a plane of symmetry

The analysis of TD(La) (**94**) in MALDI-ToF-MS calcd: 2772.99 found: 2772.55 shows an almost identical match to isotopes' pattern in the theoretical calculation (**chart 4.5**). That confirms the ¹H NMR data discussed earlier of the formation of (**94**).

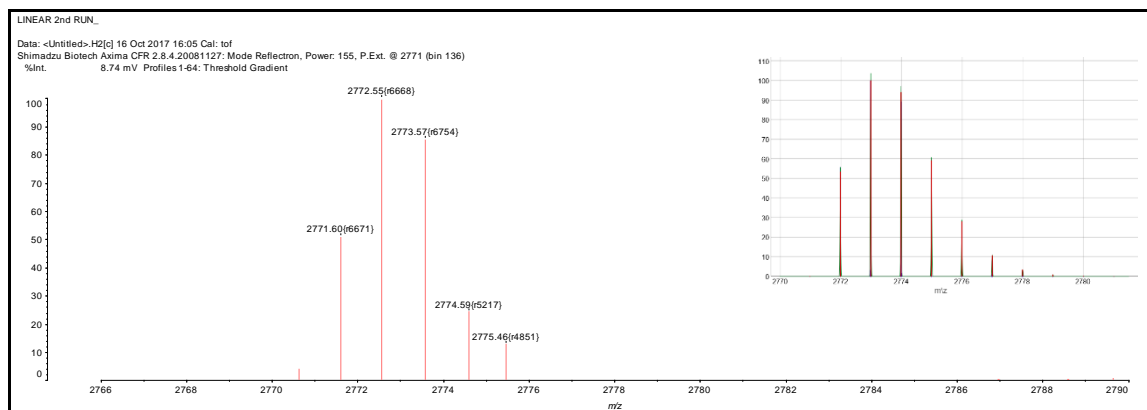


Chart 4.5: MALDI-ToF-MS chart confirms the formation of TD(La) (**94**); theoretical isotopes' pattern in the frame.

The indication of TD formation can be detected by UV-vis (**chart 4.6**), as the new compound has unique absorbance peaks that are different from SM. It is also clear from TLC analysis as the TDs are deep green/brown in colour. This can be the indication of π overlap due to the distance between layers being within the limitation of allowance. The spectra of (**94**) is consistent with (**78**) from literature⁴, and result from the π - π overlap of the three rings.

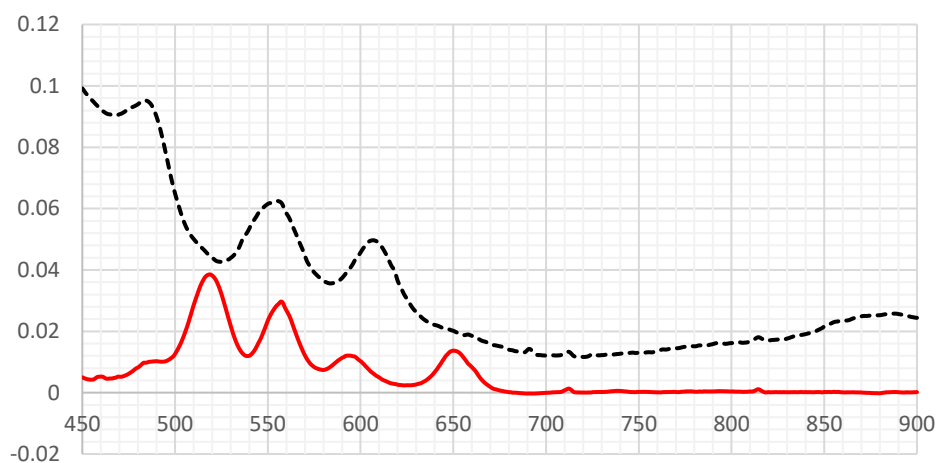
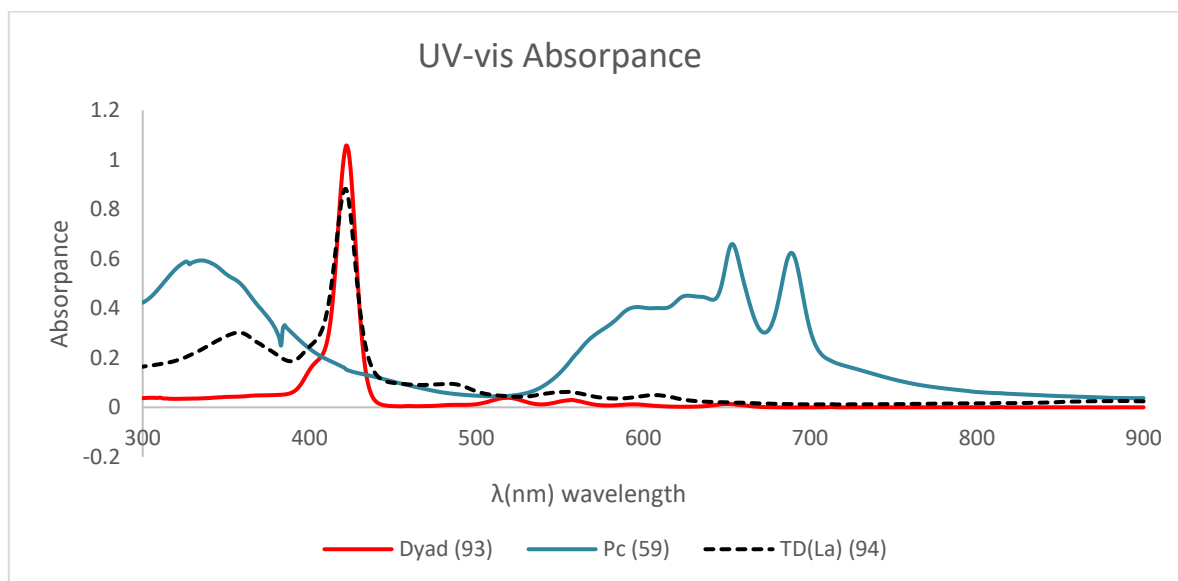
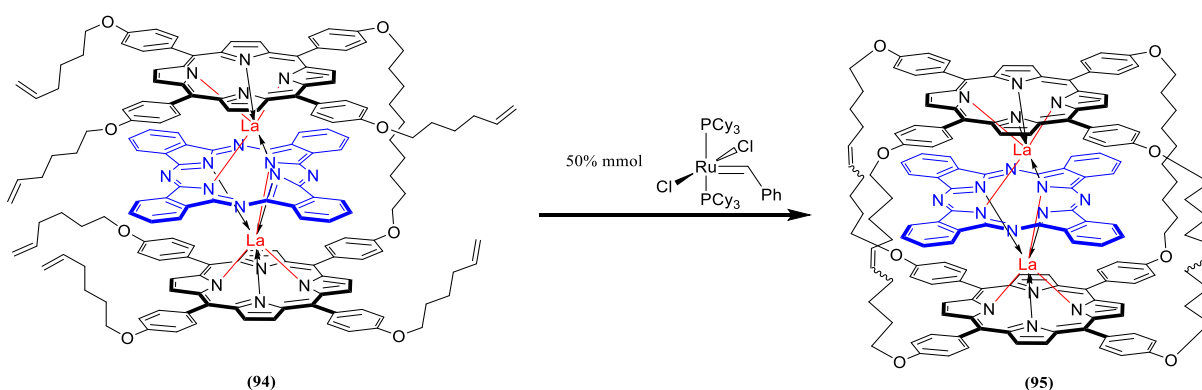


Chart 4.6: UV-vis absorption shows the new compound TD(La) (**94**) is different than the starting materials (**93**) and (**59**), which indicated the occurrences of overlapped between heteroleptic components (top); Focus on low absorbance region (bottom).

4.1.10 Cyclic Triple Deckers (CTD)

The success of the previous steps is essential to reach this stage of the project. Thus, the preparation of TD(La) (**94**) in the previous step allowed Pc (**59**) to be set into the proposed cavity. The examination of porphyrin ring-closing by metathesis in the presence of Pc was not previously known. Therefore, Grubbs catalyst⁷⁸ was chosen to achieve the goal as several examples of cyclic porphyrin dimer were successfully obtained by this method. Even though the concerns were whether TD(La) (**94**) fall apart or metal exchanged may occur, the cyclisation (**95**) in the presence of Pc has been achieved smoothly. This reaction was done by following the general procedure of ring-closing metathesis (RCM)⁷⁸, which required dissolving the catalyst in dry DCM then adding them to pre-dissolved TD(La) (**94**) in DCM as well (scheme 4.17). The mixture was stirred at room temperature for 24h then it was checked by ¹H NMR to observe completion.



Scheme 4.17: The general procedure for cage formation that hosting Pc

The general mechanism of RCM was proposed by Grubbs *et al.*⁷⁹ (figure 4.4) followed by intensive kinetic studies⁸⁰ toward investigating the role of ligands, solvent, reaction temperature, kinetic selectivity, and catalyst decomposing rate in the catalytic activities. The conclusion of those studies showed the effect of catalytic ligands on the products. As we are targeting ring close metathesis, the lack of control over the newly formed double bond configuration constitutes a significant hindrance when applied to the macrocyclic series.⁸¹ Therefore, the resulting bonds will be a mixture of *E* and *Z*, which is considered as a drawback because this catalyst generation is not stereoselective.⁸¹

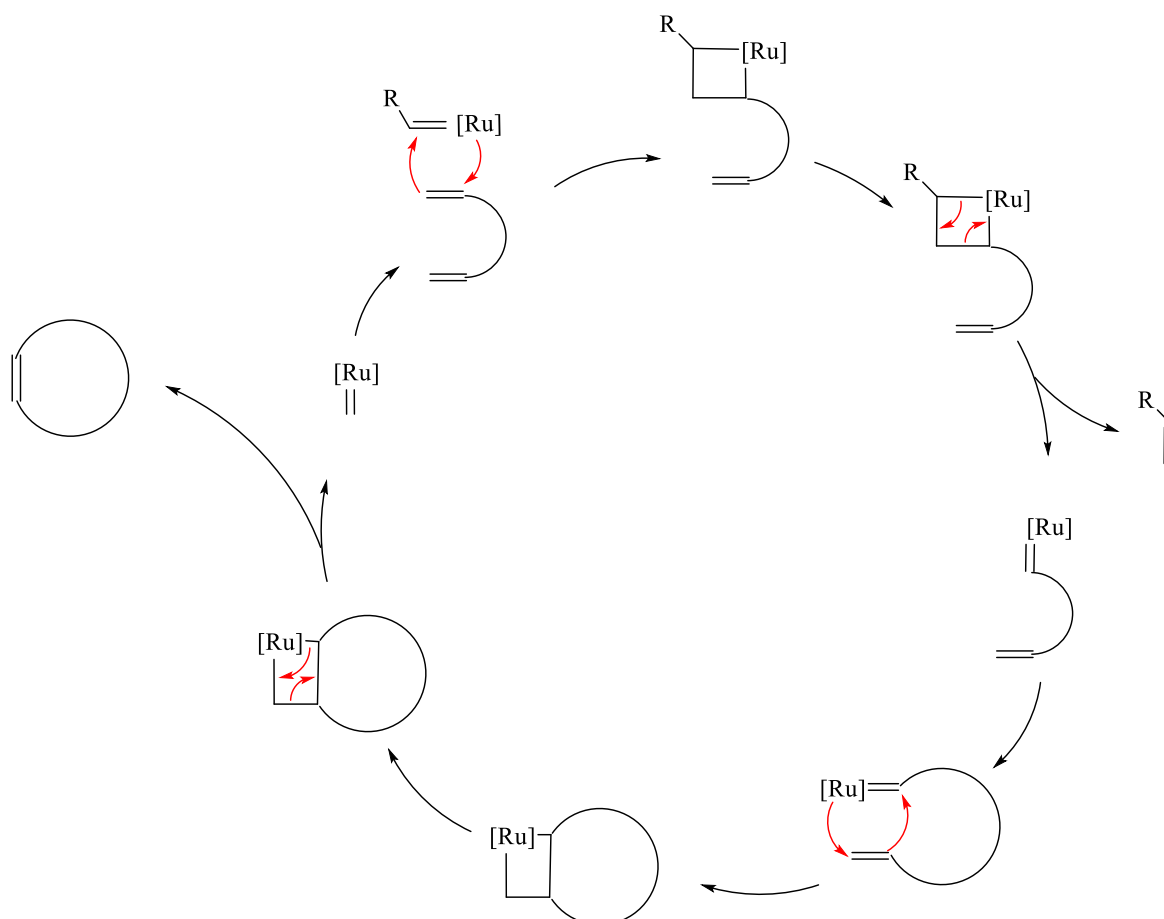


Figure 4.4: The general mechanism of the Grubbs catalyst cycle.

The outcome of the analysis of the cage data such as ¹H NMR and UV-vis appears the successful of encapsulating Pc (**59**) into the cavity (**chart 4.7, 4.8 and 4.9**). Even though the new linkers have become the same length as the dyad's linker, the compound is not symmetrical due to the presence of double bonds on three sides and a sigma bond on the fourth. Therefore, the cyclisation completion was indicated by the formation of new double bonds signals. Those signals also indicated that the protons' position around alkene bonds stated as a mixture of *cis* and *trans* isomers, which could explain the spilt of signals in aliphatic parts of the molecule's ¹H NMR spectrum. Also, the broadened signals indicated that the inner protons are affected by the high electron density of Pc and La as they become closer to the cavity centre. That could also indicate the occurrence of slower Pc rotation.

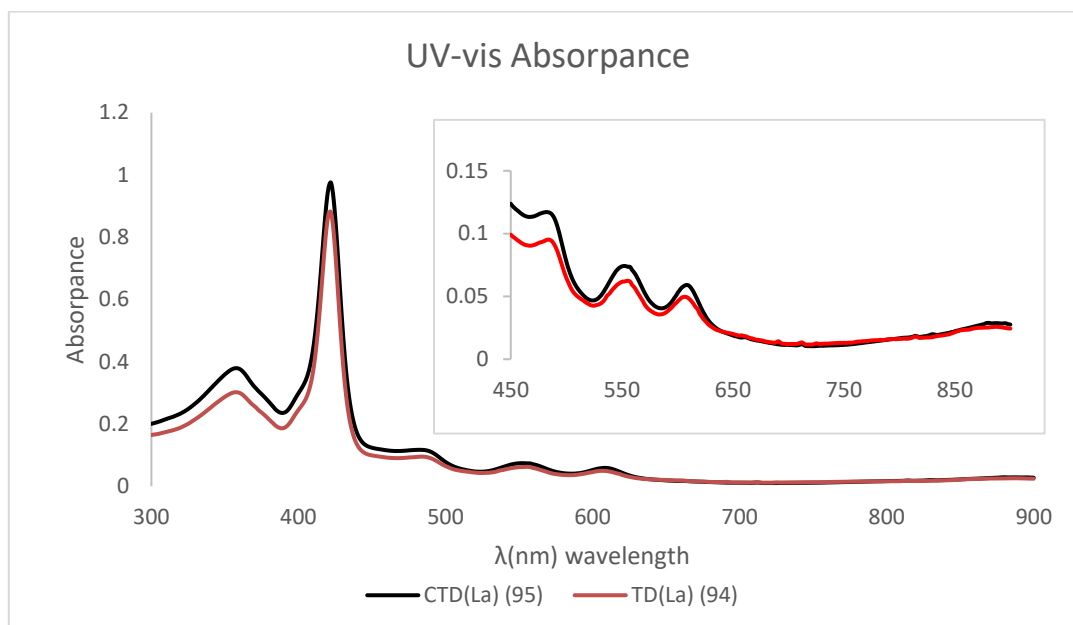
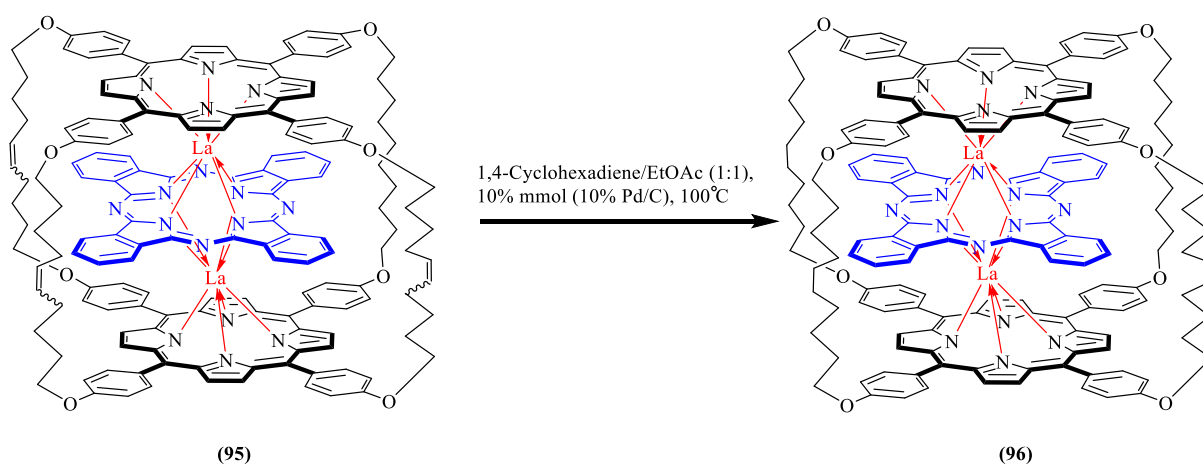


Chart 4.9: The identical peaks of TD(La) (**94**) and its cage analogue CTD (**95**) are the sign of the stability of the target model, which confirms the presence of Pc in its geometrical position in the centre of the cage.

4.1.11 Reduction of CTD

Toward increasing the symmetry, reducing the alkene bonds of CTD linkers was planned to achieve equal linkers' length. This step was achieved using hydrogen transfer methodology as a rapid, effective and safer pathway. This methodology requires a hydrogen donor that can be oxidised in the presence of a catalyst. One of the useful reagent that fulfilled the requirement was developed by Eberhardt⁸² using 1,4-cyclohexadiene and iodine as a catalyst. This method then was improved by Felix *et al.*⁸³ using palladium-carbon (Pd/C 10%) as a catalyst.

Our attempts toward reducing alkene bonds were achieved by using Felix *et al.* pathway⁸³ (**scheme 4.18**). Even though the concerns of metal exchange or alkoxy cleavage, the reaction was a straightforward step and completion was observed within 5h without any side products. The pure product was obtained by filtering the catalyst and evaporating the solvents to dryness.



Scheme 4.18: Reduction of alkene bonds pathway to achieve symmetrical cage

The analysis of ¹H NMR appeared that the reduction had occurred smoothly, and the results fulfilled the symmetry (**chart 4.10**). The duplication of the aliphatic region peaks has no longer existed, as shown in the resonance of alkoxy peaks, and aromatic peaks' splits also demonstrated the state of symmetry. Interestingly, the rest of the alkyl chains are still broadened, which may indicate the effect of Pc (**59**) on them. The UV-vis shows identical absorbance behaviours, indicating that the TD is stable (**chart 4.11**). Also, it was confirmed by MALDI-ToF-MS ($C_{160}H_{144}La_2N_{16}O_8$)⁺ m/z [M]⁺ calcd: 2694.94 found: 2694.30, which shows identical mass for the symmetrical analogues of the cage (**96**) (**chart 4.12**).

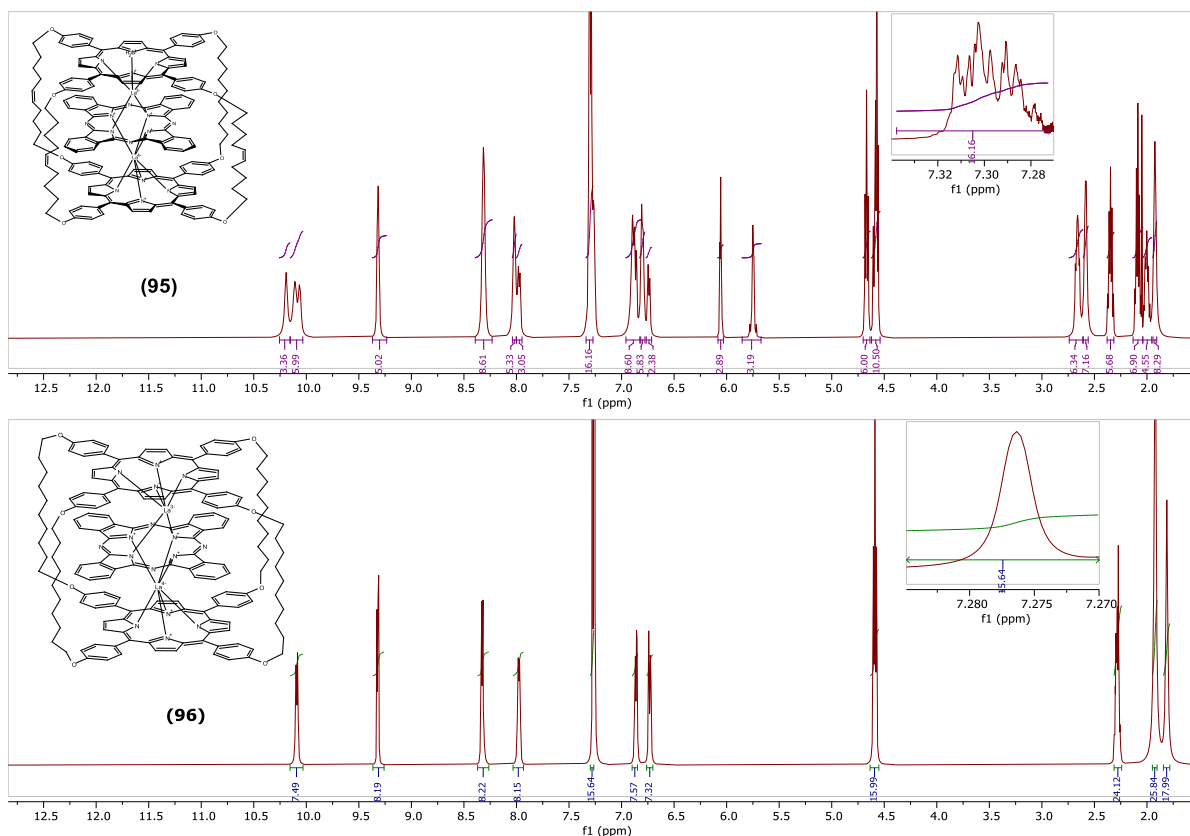


Chart 4.10: The symmetry of the cage containing Pc is achieved by reducing alkene peaks, which can be indicated from the disappearance of their peaks at 6.05 and 5.75 ppm; the peaks' shape is especially porphyrin protons (in the frame) show the (96) is symmetry.

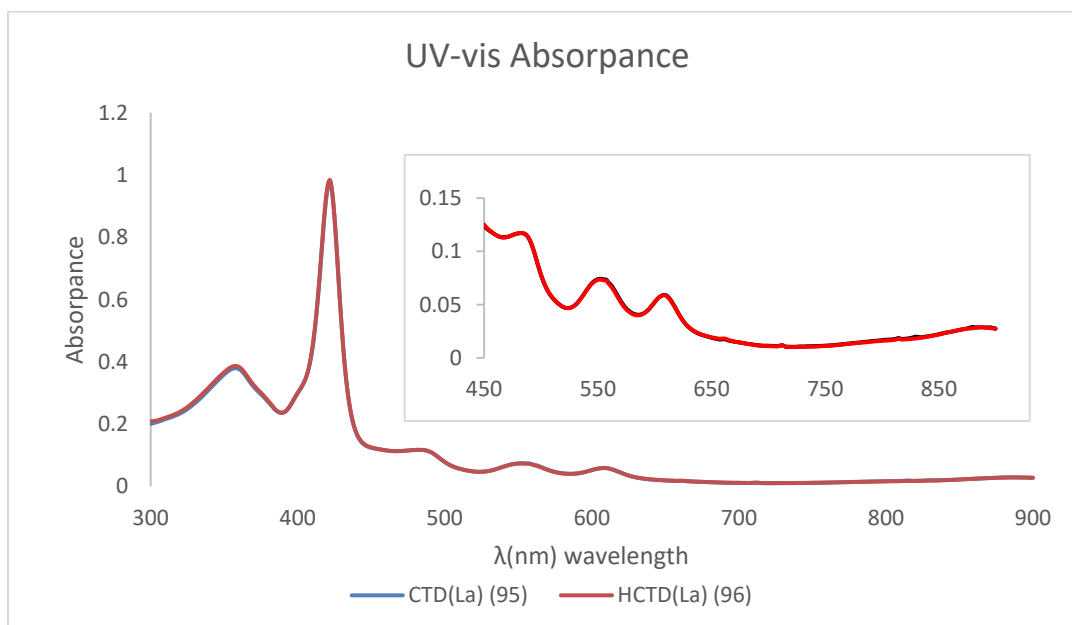


Chart 4.11: The UV-vis shows identical absorbance behaviours, indicating that the π overlaps are not affected, and the TD is stable.

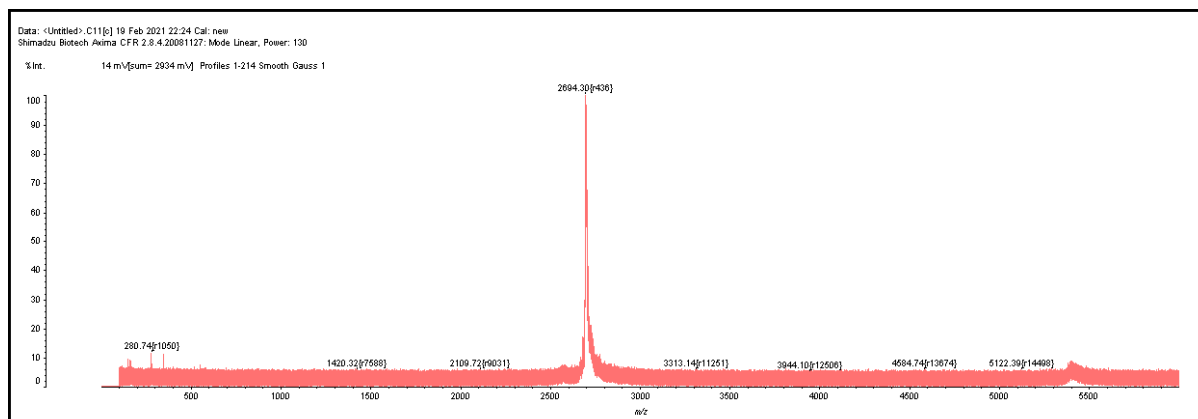


Chart 4.12: MALDI-ToF-MS shows relevant mass for the HCTD (**96**)

4.1.12 Conclusion

In conclusion, this pathway has shown the successful encapsulation of Pc into the porphyrin cage. The main challenge in the method is that the formation of an intermediate dyad takes a long time with a low yield. The steps afterwards are relatively straightforward, and the product shows stability against the light, solvents and heat. Therefore, the protocol of encapsulating **Pc** into the porphyrin cavity is new in the field and adds more stability for TDs in the same order. Also, replacing lanthanum ions with another lanthanide ions could be possible under TD formation conditions of ion size requirement. Therefore, due to the difficulty of intermediate dyad preparation, we moved to investigate another route to meet the goal with the aim of obtaining better yields.

4.2 Self-organized porphyrin cage

4.2.1 Introduction

The successful capsulation of phthalocyanine (Pc) into the porphyrin cage through TD protocol, as intermediate, leads toward investigating more possible pathways that may follow to obtain the cage in fewer steps. There are several methods to achieve porphyrin cages mentioned in the literature, but encapsulated Pc is not included. Investigating that may provide alternative pathways toward encapsulated Pc into porphyrin cages directly. There are two potential pathways that may be followed to meet the self-organised cages strategy; (i) using Lanthanide metals, as TDs were achieved by them previously, and (ii) using DABCO template to organise components. Therefore, focusing on the formation of TD on the same order of porphyrin-phthalocyanine-porphyrin will be targeted in this section.

4.2.2 Direct Triple Deckers (DTD) formation

The order of porphyrin-phthalocyanine-porphyrin triple-deckers was previously achieved by Tsivadze and co-workers. Therefore, encapsulation of Pc could be achieved by modifying their approach. One of the drawbacks of this methodology is that porphyrin and phthalocyanine are organised randomly in the presence of lanthanide metals to form double and triple-deckers in different orders (**figure 4.5**). Even though the expected yield will be low, easy access to starting materials is on the side of this investigating.

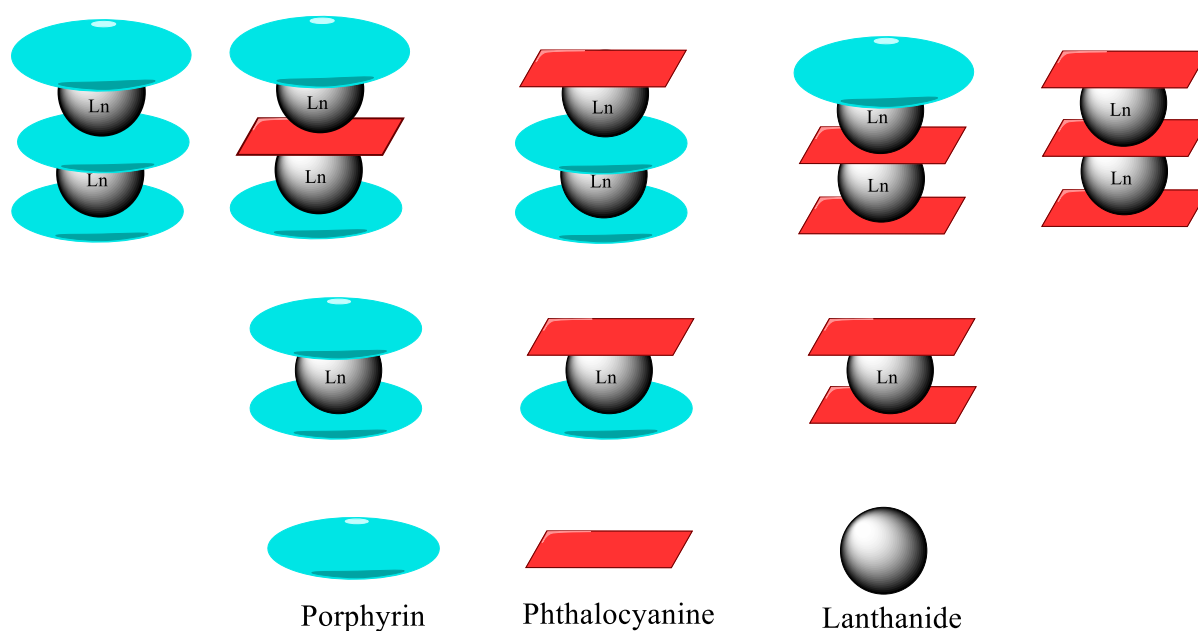
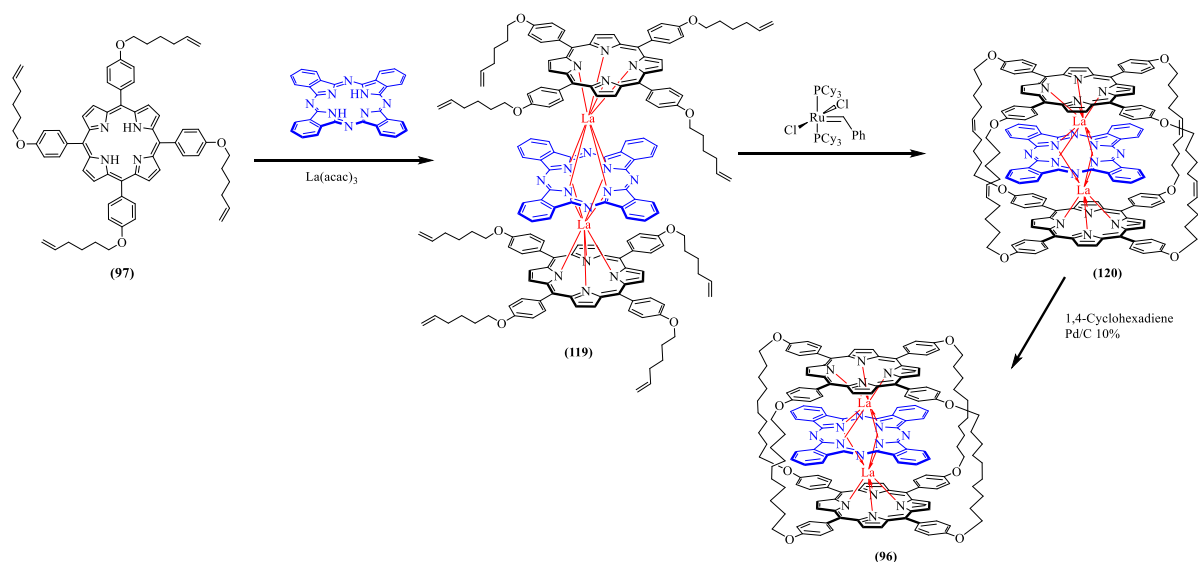


Figure 4.5: The possibility of self-organisation orders

The approach was designed to use previously synthesised tetrakis-*p*-5-hexen-1-oxy phenyl porphyrin (**97**) to achieve the porphyrin cage that hosts **Pc** (scheme 4.19). Despite the absence of the linker between porphyrin units, which reduces the control of synthesis, it may provide a new class of symmetrical triple-deckers DTDs.



Scheme 4.19: The approach toward encapsulated Pc into the cage through DTD (**119**)

The first step in this approach is preparing triple-deckers as intermediates to organise the components in the required order. As one of the possibilities that may form is triple-deckers from three porphyrin molecules, pre metalation of porphyrin may not be helpful to control the reaction. Therefore, the starting materials, (**97**), (**59**) and $\text{La}(\text{acac})_3$, were mixed in a low volume of 1-pentanol in a sealed tube. The mixture was heated in an oil bath at 200 °C for 24h; then, the solvent was removed and separated from the products achieved by column chromatography. The majority of the starting materials were converted to products. Therefore, DTD (**119**) was isolated and characterised by NMR and MALDI-ToF-MS to confirm the ratio of components in the product. As we expected that the yield cannot be guaranteed due to the formation of other analogues, therefore, the average yield of DTD was around 25%, but it seems a good achievement in one step formation.

Also, the comparison between TD (**94**) and DTD (**119**) appeared that the Pc is set between porphyrin units in the required order as planned. The differences in the symmetry were obvious in ^1H NMR (chart 4.13) and UV-vis (chart 4.14) due to the absence of the linker between porphyrin units (figure 4.6). That resulted in the lanthanum ions being positioned precisely in the centre, which affected the aromatic peaks to be slightly deshielded due to the move of electrons density.

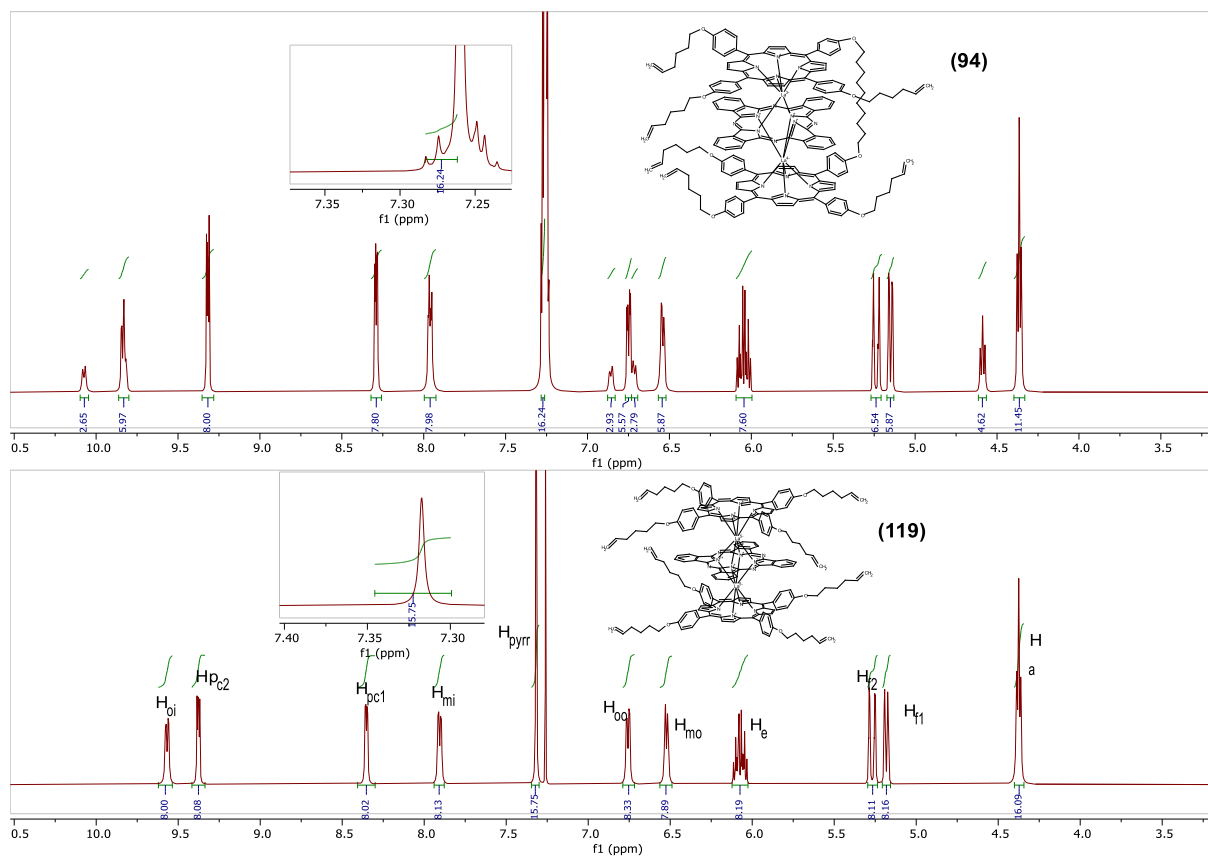


Chart 4.13: Comparison between TD top and DTD bottom appears the differences in the symmetry.

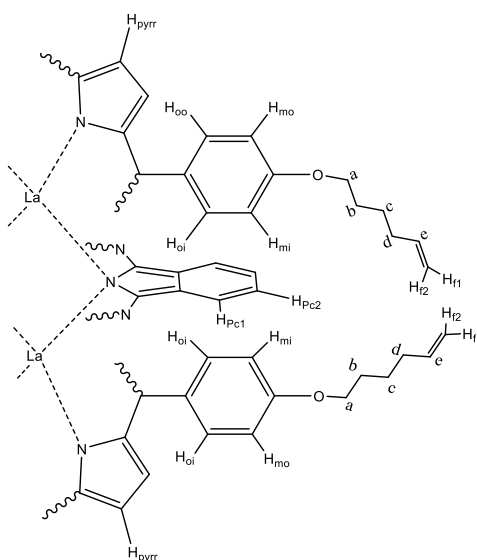


Figure 4.6: Identification of protons' location in ¹H NMR as a symmetrical environment.

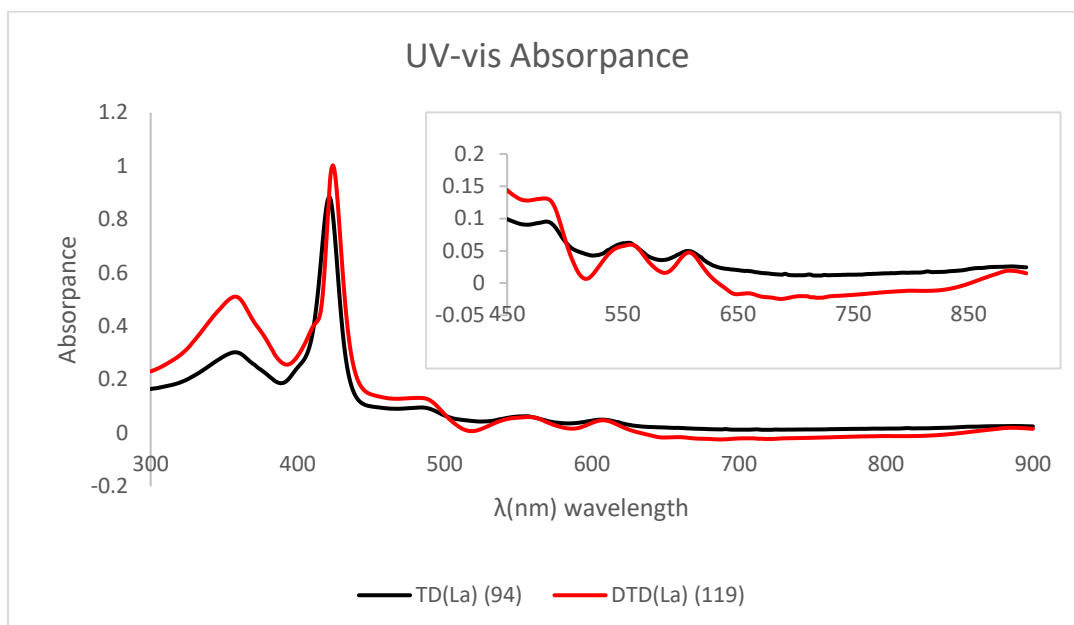
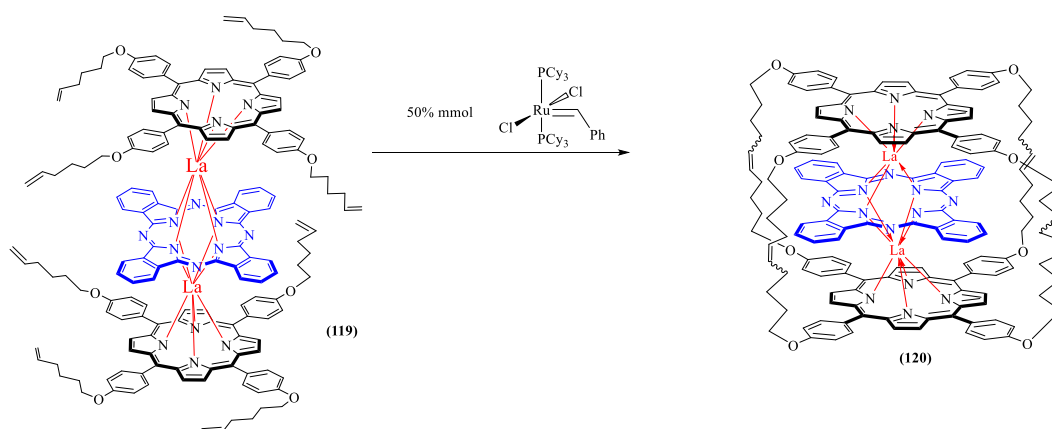


Chart 4.14: The UV-vis shows the similarity between linked TD(La) **94** (black) and open DTD(La) **119** (red) in absorbance due to the geometrical similarity between them as a heteroleptic system of Porphyrin-Phthalocyanine-Porphyrin.

4.2.3 Cyclic Direct Triple Deckers (CTD)

The formation of uncontrolled porphyrin-phthalocyanine-porphyrin triple-deckers DTD (**119**) successfully raised the question of whether the ring-closing metathesis was allowed due to the geometry positions alkenyl chains or forbidden. The original strategy was chosen because the link chain forces alignment of the two porphyrins; open systems are expected to be staggered. To investigate that, the reaction was examined on the same approach of previous CTD (**95**) using 1st generation of Grubbs catalyst^{®78} (scheme 4.20).



Scheme 4.20: The approach towards ring-closing of (**119**)

Again, the cyclisation of DTD(La) (**119**) has been obtained smoothly, which implies it becomes undoubtedly that the geometry of alkenyl chains has not affected the ability of cyclisation (metathesis). The completion was observed within 24h, which was confirmed by ¹H NMR spectroscopy as well. Interestingly, the symmetry of the aliphatic parts of the cage has been changed, which also affected the symmetry of aromatics. That may indicate the linkers are positioned differently as it was expected that the CDTD(La) (**120**) would be an isomeric mixture because the 1st generation of Grubbs catalyst is not stereoselective (chart 4.15).

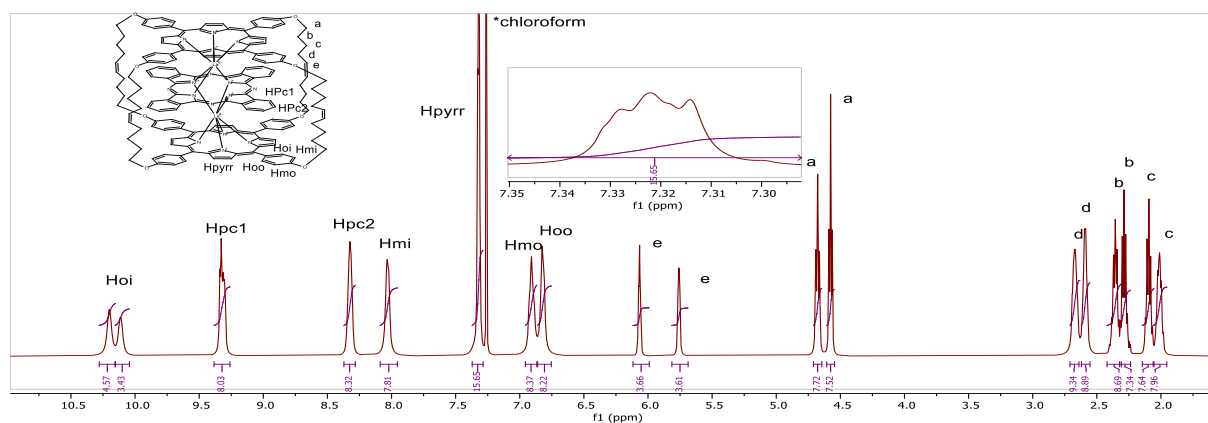


Chart 4.15: ¹H NMR appears the formation of *cis* and *trans* mixture cages

The focus on the aliphatic region appeared that the middle alkenes and their neighbours were broadened. The possible explanation is that two of the linkers face the cavity inner, which makes them affected by the diamagnetic field of phthalocyanine (**chart 4.16 and 4.17**).

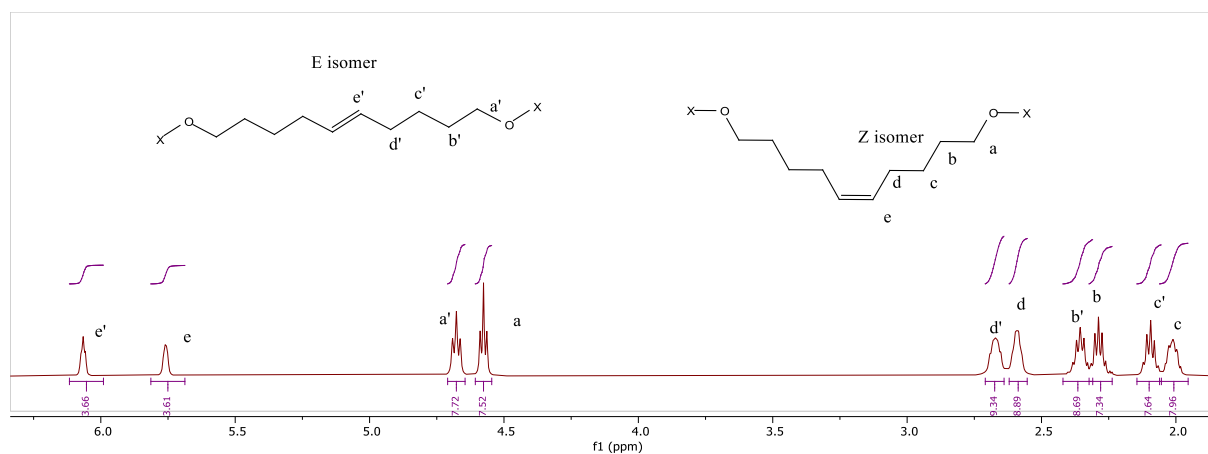


Chart 4.16: The peaks near the centre were broadened due to the effects of phthalocyanine on the linkers of CDTD(La) **120**, whereas the duplications of the peaks are caused by the new alkene bonds that formed as a mixture of *E* and *Z* isomers which affected the symmetry.

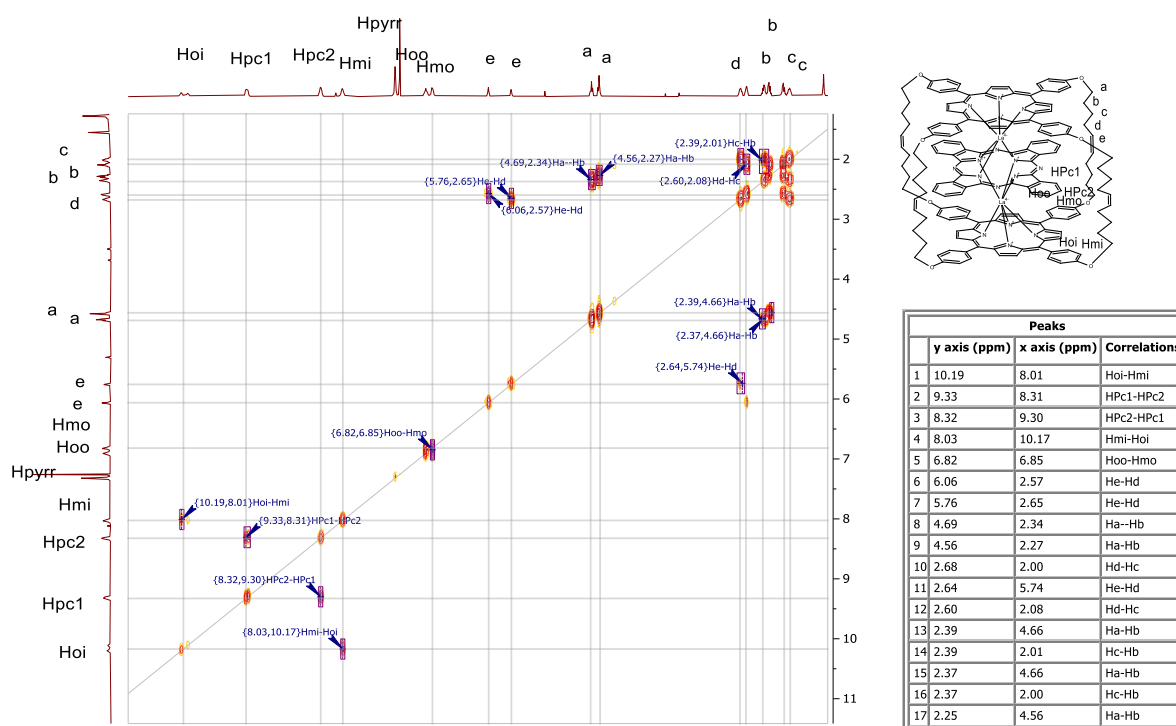
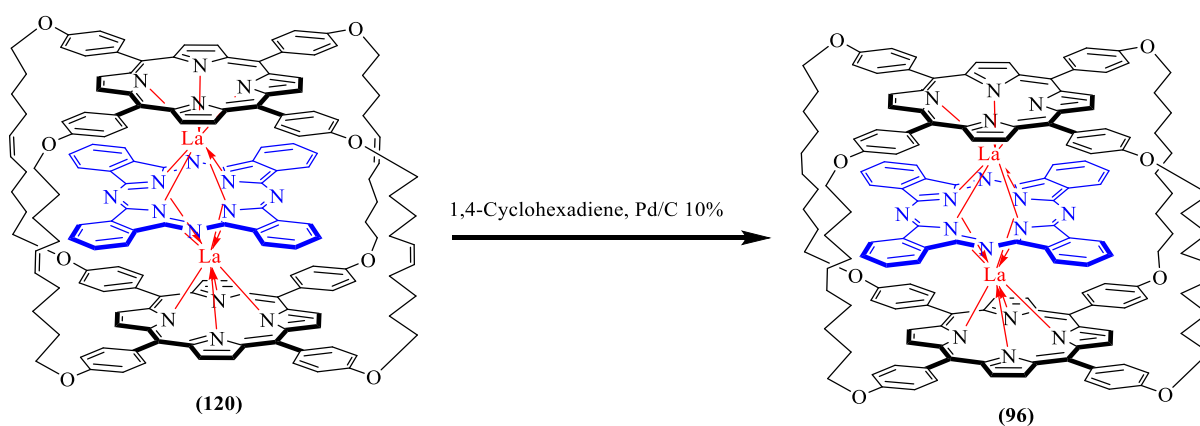


Chart 4.17: The correlations between the protons of CDTD(La) **120**

4.2.4 Reduction of alkene linkers of CDTD

For a comparison reason, reduction of alkene linker was carried in the same approach that has been used before (**scheme 4.21**). The results were identical to the expectation as the reduction shows completion nearly at the same time. The analysis appeared that reduction of CTD(La) (**95**) and CDTD(La) (**120**) resulted the same compound (**96**). Even though both cages follow different pathways to form, the same results can be achieved successfully.



Scheme 4.21: Reduction of alkene bonds pathway to achieve symmetrical cage

The comparison between both methods appears significant different in geometry. Therefore, each of them has its unique characteristic. As we reached the target in both ways, the comparison in synthetic routes appears some advantages and disadvantages. From starting material to the final product was six steps using dyad intermediate (**94**). Whereas it is just three steps to the reduction step (not including porphyrin synthesis as it comes byproduct from the first route). On the yield side, the dyad (**94**) preparation was the main challenge otherwise, it would be the best route. The first route developed about 4% of the final product, whereas the second route developed 15% (counted from initial porphyrin). The purification was on both required column chromatography and recrystallisation to obtain pure form.

4.2.5 Porphyrin cage through DABCO template

In the aim of encapsulating phthalocyanine **Pc** in the shorter pathway, the ability of 1,4-diazabicyclo[2.2.2]octane (DABCO) (**121**) to organise the cage components selectively was examined. Zinc analogues of porphyrin and phthalocyanine were prepared to allow them hosting the DABCO ligands. This method was mentioned frequently in several examples, whether using DABCO⁸⁴ (**121**) or 4,4-bipyridiene⁸ (**122**). Therefore, modifying the approach may organise the components on the order of porphyrin-phthalocyanine-porphyrin (**figure 4.7**).

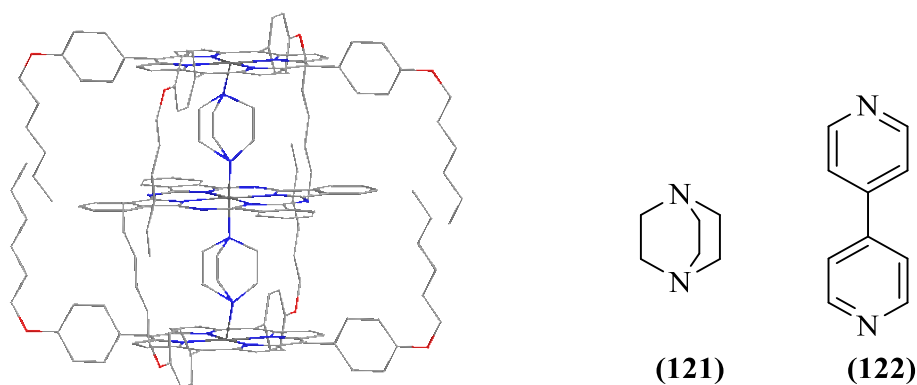
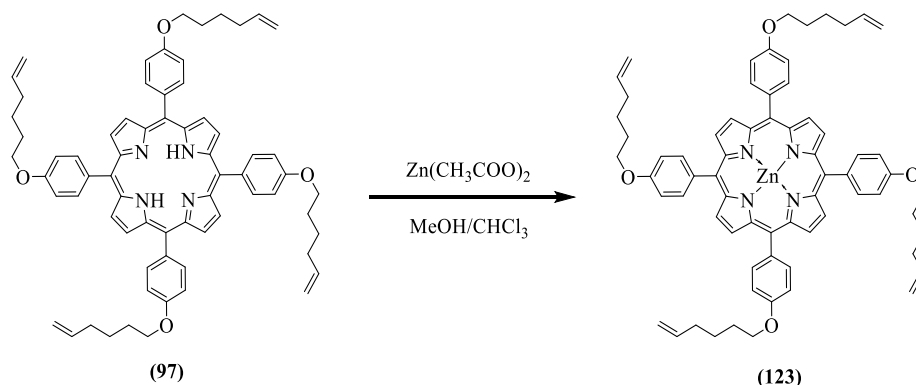


Figure 4.7: The proposed structure of TD using DABCO; The most common templates for preparing porphyrin dimer (on the left).

4.2.5.1 Preparation of zinc tetrakis p-hex-5-en-1-oxy-phenyl porphyrin

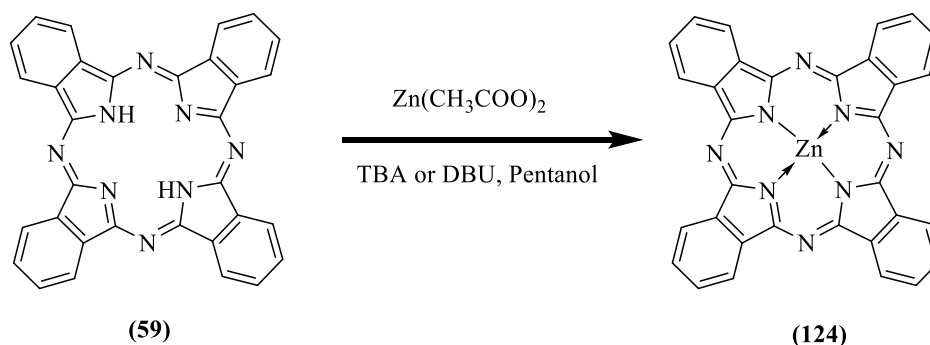
The metalation of porphyrin and phthalocyanine were carried following the general methods for that which are well known in the field. For metalating porphyrin, zinc acetate was refluxed with porphyrin in a mixture of acetone and chloroform to increase the solubility for 3h (**scheme 4.22**). The reaction was monitored by ¹H NMR for observing the completion by the disappearance of inner protons peak. Then, the solvent was removed to dryness and extracted the product from DCM/H₂O. A pure product was obtained in a quantitative yield after slow recrystallisation using DCM/MeOH.



Scheme 4.22: preparation of zinc porphyrin

4.2.5.2 Preparation of Zinc phthalocyanine

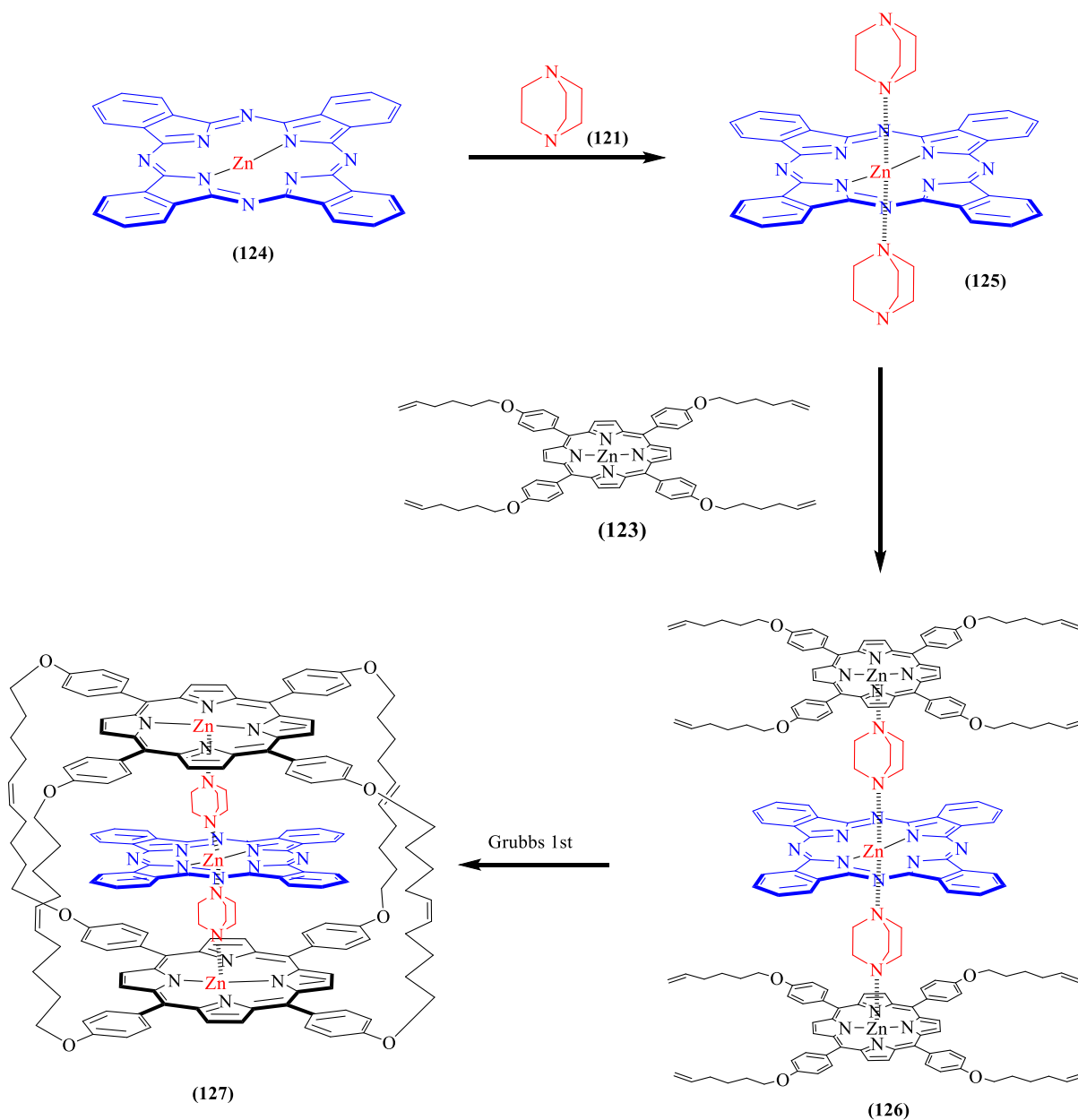
The zinc analogue of phthalocyanine was synthesised to fulfil the requirement to host DABCO ligands. This analogue was well known previously. Therefore, it was synthesised following the latest method in the field⁸⁵. This 2h method is based on reacted Pc with Zn salt in the presence of tributylamine TBA to remove acidic protons from the Pc centre. Unlike the Pc, the product is soluble which can be characterised by ¹H NMR. Also, this reaction can be prepared in a sealed tube using the same reactant and DBU as a catalyst in 2h as well (**scheme 4.23**).



Scheme 4.23: preparation of zinc phthalocyanine

4.2.5.3 Triple deckers using DABCO

In the line toward the target, 4,4-diazocyclo[2.2.2]octane (DABCO) was dissolved in dry DCM, then, ZnPc was added to the mixture and left stirring for 1h to allow them to coordinate. Then, two equivalents of pre-dissolved THxTPP(Zn) were added to the mixture then left stirring for another 1h. Grubbs catalyst was added to the mixture then left stirring for 3 days (**scheme 4.24**).



Scheme 4.24: proposed pathway toward encapsulated Pc using DABCO in one flask

The reaction was checked regularly using TLC, UV, ^1H NMR, and MS with no sign of product had been developed. Therefore, we concluded that attempting to encapsulate Pc into a porphyrin cage through DABCO may not be possible. The theoretical calculation of the distance between porphyrin units is about 13.4\AA , which is higher than the distance of CDTD.

To investigate why this pathway is inefficient, we checked the distance between porphyrin units in cage systems that were previously prepared using DABCO. Taesch *et al.*⁸⁴ found the distance between units using x-ray is between $7 - 15\text{\AA}$ when they obtained the cage using ring-closing metathesis through Grubbs 2nd generation catalyst (**figure 4.8**). Whereas, Kosher *et al.*²⁶ and Schoepff *et al.*⁸⁶ found the distance 7.53\AA and 7.09\AA , respectively, when

they obtained the cage using copper-catalysed azide-alkyne cycloaddition (CuAAC). Those cage models were obtained using one molecular of DABCO to hold two porphyrin units (**33**). In our case, we have to use two molecules of DABCO to hold Pc (**124**) between porphyrin units. Therefore, the required linkers' length would be longer than that we had used, as the distance between porphyrin units doubled. That could explain the reason of forbidding the ring-closing metathesis to be success in our proposed cage (**127**).

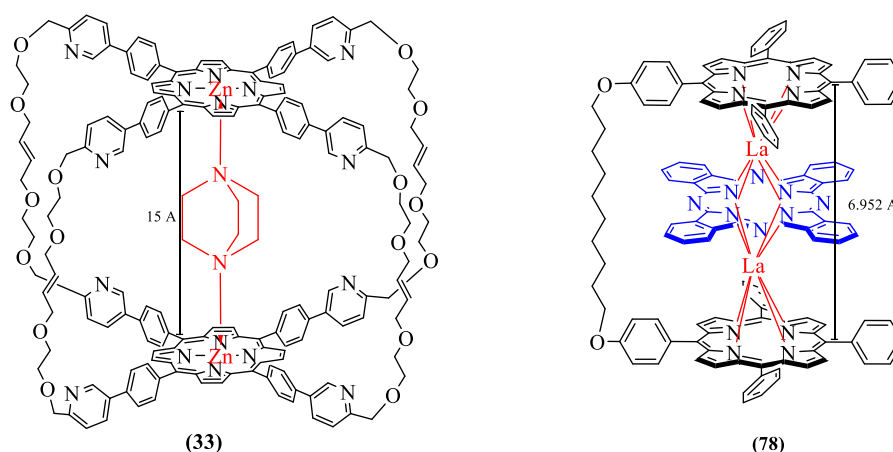


Figure 4.8: The Taesch's *et al.*⁸⁴ cage system using DABCO (**33**) which its measured distance found 15 Å (left); the distance in heteroleptic system (**78**)⁴ was found 6.95 Å (right).

4.2.6 Conclusion

In conclusion, the self-organised cages strategy shows alternative pathways toward encapsulating Pc into the porphyrin cage system in a simple way. It is successfully achieved using lanthanum metal as a template for components in order of porphyrin-phthalocyanine-porphyrin. Whereas DABCO needs more investigation, such as increasing the length of side linkers. Therefore, open TD intermediate is approved alternative way toward cage system.

4.3 Lanthanides' effect

4.3.1 introduction

The successful incorporation of Lanthanum toward encapsulating phthalocyanine into the porphyrin cage in the previous section leads to the investigation of selected elements of the lanthanide series. As assembled TDs required large metallic atoms to template the layers in the order needed, lanthanides are widely investigated in TDs' formation because they provide the required size and appropriate oxidation state.

As lanthanides are found to be set above the porphyrin and phthalocyanine rings due to their ionic radii, there are high possibilities to form triple-deckers (**figure 4.9**). The ionic radius of lanthanides is generally over the inner space size of porphyrin and phthalocyanine macrocyclic, which was around 80 pm⁸⁷.

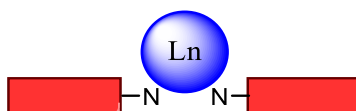


Figure 4.9: Lanthanides' position on porphyrin and phthalocyanine macrocyclic.

The ionic radius of lanthanides is decreased through the series from 1.03 Å for La to 0.86 Å for Lu⁶⁵, which was found highly affecting the formation of TDs in order of porphyrin-phthalocyanine-porphyrin. The limitation of Birin *et al.*^{3,68} methodology of forming TDs is Eu which has an atomic radius of 0.95 Å; whereas the limitation of Cammidge *et al.*⁴ methodology is Dy which has an atomic radius of 0.91 Å (**figure 4.10**). Also, TD formation based on Dy has been confirmed by Jiang *et al.*⁸⁸, which emphasised the ionic size effects. Those studies conclude that the TDs formation based on a smaller atomic radius size of Ln⁺³ cannot be achieved because the inner protons on phenyl groups on the top and bottom of porphyrin rings are facing each other which may resist the stability of the complex.

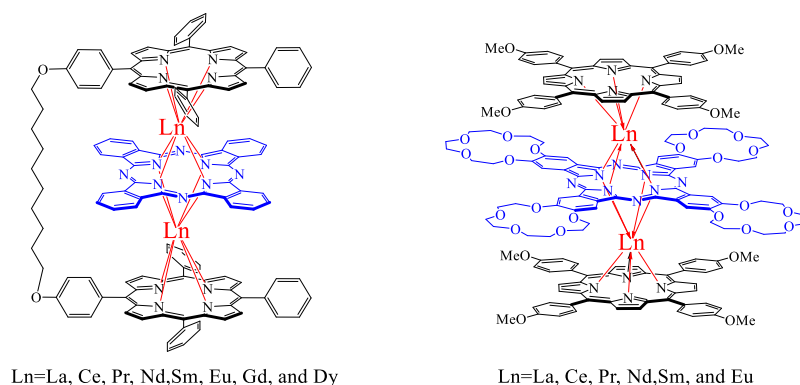


Figure 4.10: The general model systems of heteroleptic TD; Cammidge *et al.*⁴ model (left) and Birin *et al.*⁶⁸ models (right).

The studies of TD formation also consider the oxidation states of the metals besides the size. The common trivalent oxidation state of lanthanides (Ln^{+3}) is ideal for connecting three macrocyclic of porphyrin and phthalocyanine. Also, Yttrium (Y) from the third series of transition metals can form triple-deckers due to its large ionic size and stable Y^{+388} . The other oxidation states (Ln^{+2} and Ln^{+4}) are less common, but it could be the significant key point of understanding TDs formation as the double-deckers side products are always formed beside the TDs (table 4.6).

Element	Ionic radius Ln^{+3}	Oxidation state	Atom (Ln) configuration	Ion (Ln^{+3}) configuration	Magnetic status ^b
La	1.03 Å	+3	[Xe] 5d ¹ 6s ²	[Xe]	DM
Ce	1.02 Å	+3 and +4	[Xe] 4f ¹ 5d ¹ 6s ²	[Xe] 4f ¹	PM
Pr	0.99 Å	+3 and +4	[Xe] 4f ³ 5d ⁰ 6s ²	[Xe] 4f ²	PM
Nd	0.98 Å	+3 and (+4)	[Xe] 4f ⁴ 5d ⁰ 6s ²	[Xe] 4f ³	PM
Pm	0.97 Å	+3 and (+4)	[Xe] 4f ⁵ 5d ⁰ 6s ²	[Xe] 4f ⁴	PM
Sm	0.96 Å	+3, +2 and (+4)	[Xe] 4f ⁶ 5d ⁰ 6s ²	[Xe] 4f ⁵	PM
Eu	0.95 Å	+3 and +2	[Xe] 4f ⁷ 5d ⁰ 6s ²	[Xe] 4f ⁶	PM
Gd	0.94 Å	+3	[Xe] 4f ⁷ 5d ¹ 6s ²	[Xe] 4f ⁷	FM
Tb	0.92 Å	+3 and +4	[Xe] 4f ⁹ 5d ⁰ 6s ²	[Xe] 4f ⁸	PM
Dy	0.91 Å	+3 and (+4)	[Xe] 4f ¹⁰ 5d ⁰ 6s ²	[Xe] 4f ⁹	PM
Ho	0.90 Å	+3	[Xe] 4f ¹¹ 5d ⁰ 6s ²	[Xe] 4f ¹⁰	PM
Er	0.89 Å	+3	[Xe] 4f ¹² 5d ⁰ 6s ²	[Xe] 4f ¹¹	PM
Tm	0.88 Å	+3 (+2 and +4)	[Xe] 4f ¹³ 5d ⁰ 6s ²	[Xe] 4f ¹²	PM
Yb	0.87 Å	+3 and +2	[Xe] 4f ¹⁴ 5d ⁰ 6s ²	[Xe] 4f ¹³	PM
Lu	0.86 Å	+3	[Xe] 4f ¹⁴ 5d ¹ 6s ²	[Xe] 4f ¹⁴	DM

Table 4.6: Ionic radii and common oxidation states of Lanthanides' elements; unstable oxidation states are enclosed in brackets. (adapted from Mironov⁶⁵); ^b magnetic property of single ion lanthanide where DM: diamagnetic, FM: ferromagnetic, and PM: paramagnetic.

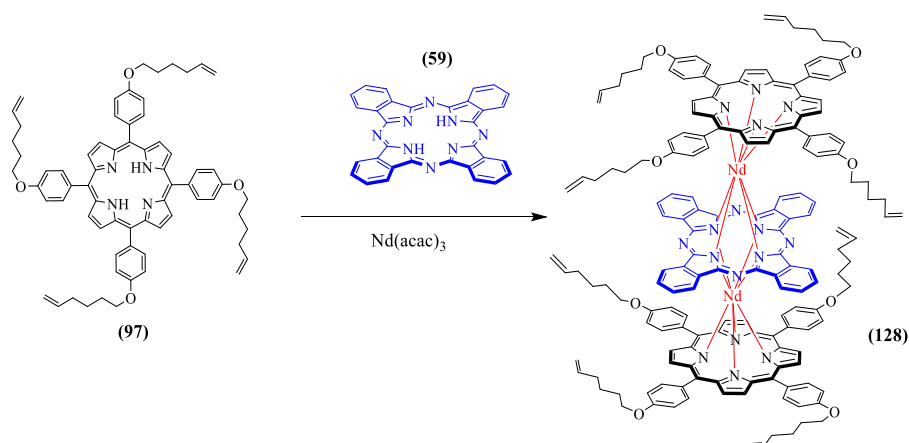
Lanthanides also have unique magnetic properties that attracted researchers to design magnetic materials such as single molecular magnets for electronic devices. Unpaired electrons at their *f* orbital play a significant role in their properties. However, *f-f* exchange coupling is found weak, but bridging them by a radical will allow them to communicate⁶⁹. In our case, the radical will be the Pc with the aim of achieving a stable TD intermediate on the same principle of self-organised methodology. The lanthanum example that we previously made in the last section will be the background of this investigation on selective Ln elements.

4.3.2 Neodymium Triple Deckers DTD(Nd)

Neodymium is the fourth element in the lanthanide series (in the case the series start with lanthanum) with atomic radii 0.98\AA and three electrons in the f^3 shell. It gains attention because of its uses in computers, known as a neodymium magnet. The strength of those magnets attracted chemists to design potential single molecular magnets based on Nd.

Neodymium triple-deckers had been investigated by Birin *et al.*⁸⁹ as open TD, and Cammidge *et al.*⁴ as a linked TD. Both studies show a phenomenon shift of protons in ^1H NMR due to the magnetic behaviour of Nd. Therefore, Nd is nominated as a potential element toward forming TD intermediate in a similar way to Lanthanum.

Our attempt toward holding Pc between porphyrin units using Nd as a template was carried in one pot in a minimum volume of 1-pentanol (**scheme 4.25**). The mixture was heated in a sealed tube at $200\text{ }^\circ\text{C}$ for four hours as the TLC analysis showed concentrated new spot was improved. The expectation of crude product is a mixture of homoleptic and heteroleptic of double-deckers and triple-deckers.



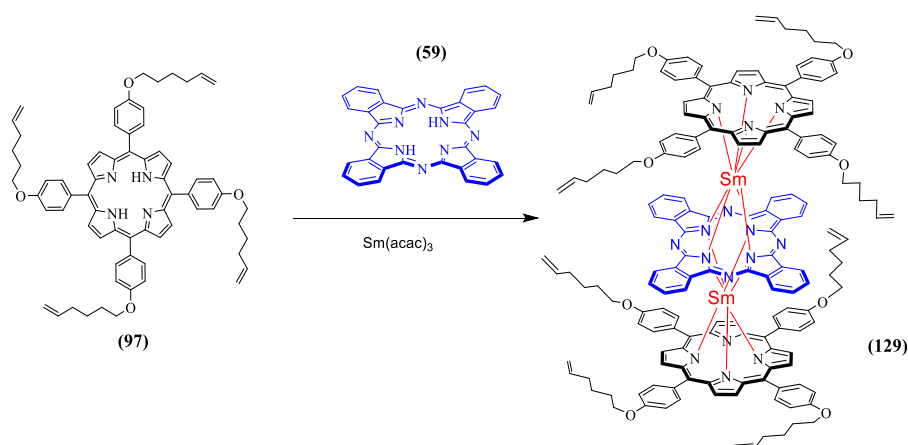
Scheme 4.25: The proposed synthesis of Nd triple-deckers.

The target compound was isolated from the mixture using column chromatography in a good yield, but its purity was questionable. Even though it was purified twice, ^1H NMR was not in a state that can be fully understood. The shielded peaks and broaden signals were indicated the presence of Nd, but Pc peaks could not be identified as they could be broadened. On the other hand, the aliphatic region is slightly shielded, but the peaks are clear (**chart 4.18**).

4.3.3 Samarium Triple Deckers DTD(Sm)

Samarium is the sixth element in the lanthanide series with an atomic radius of 0.96Å and five electrons in the f^5 shell. Its triple-deckers had also been investigated by Birin *et al.*⁸⁹ as open TD, and Cammidge *et al.*⁴ as a linked TD. Therefore, their studies guided this attempt toward forming TD intermediate in a similar way of Lanthanum.

Again, our attempt toward holding Pc between porphyrin units using Sm as a template was carried in one pot in a minimum volume of 1-pentanol (**scheme 4.26**). The mixture was heated in a sealed tube at 200 °C for 24 hours as the TLC analysis showed several new spots were formed. Also, the expectation of crude product is a mixture of homoleptic and heteroleptic of double-deckers and triple-deckers. Therefore, the crude mixture was separated by column chromatography, but the target compound could not be achieved in pure form. The confirmation of its formation was assigned from MALDI-ToF-MS, but it may need to be separated by a different kind of chromatography like bio-beads size exclusion or alumina.

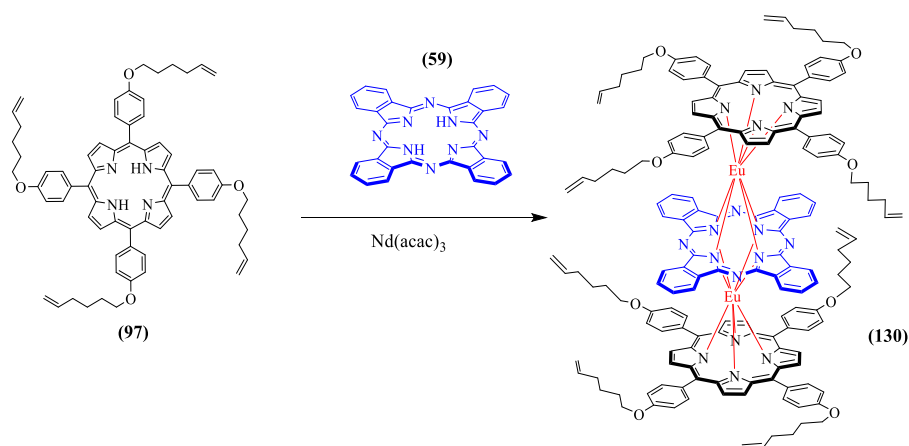


Scheme 4.26: The proposed pathway toward DTD(Sm) (129)

4.3.4 Europium Triple Deckers DTD(Eu)

Europium is the sixth element in the lanthanide series with atomic radii 0.95Å and six electrons in the f^6 shell. Its triple-deckers model had also been previously investigated by Birin *et al.*⁸⁹ as open TD, and Cammidge *et al.*⁴ as a linked TD.

In line with previous attempts, the reaction was carried in one pot in a minimum volume of 1-pentanol (**scheme 4.27**). The formation of the target compound (**130**) was confirmed by MALDI-ToF-MS ($C_{168}H_{152}Eu_2N_{16}O_8$)⁺ [M]⁺ calcd: 2827.03 found: 2827.00 (**chart 4.19**), but the impurity after second column chromatography may be a sign of instability.



Scheme 4.27: The proposed pathway toward DTD(Eu) (**130**)

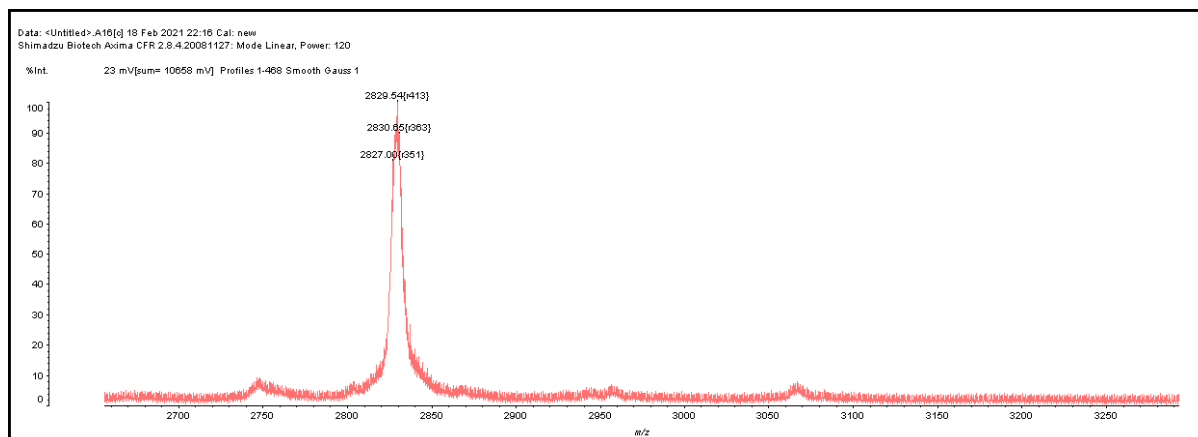


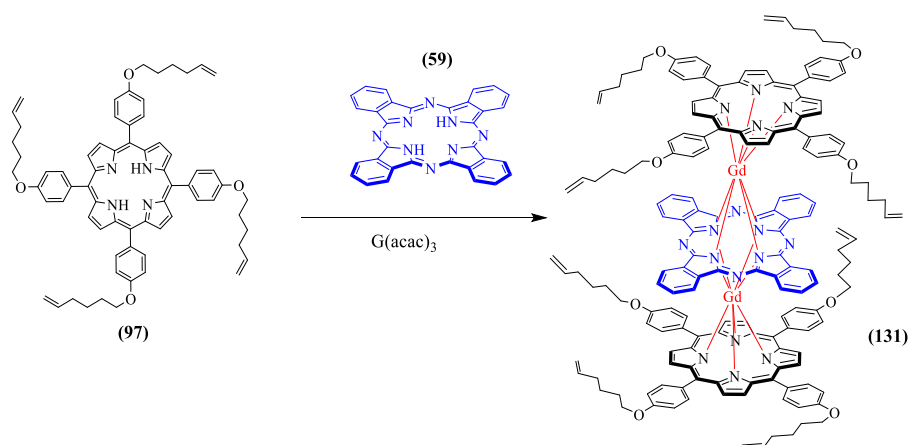
Chart 4.19: MS indicates the formation of DTD(Eu)

4.3.5 Gadolinium Triple Deckers DTD(Gd)

Gadolinium is the seventh element in the lanthanide series with atomic radii 0.94Å and seven electrons in the f^7 shell. It refers to a half-filled orbital that gains the attention because of its uses in MRI scans due to its ferromagnetic behaviour. Therefore, chemists have investigated the design of a potential single molecular magnet based on Gd for medical uses.

Preparation of gadolinium TD was firstly achieved by Weiss *et al.*⁹⁰ in good yield, but NMR data were not published. When we investigated Gd as a template for TD, the ^1H NMR chart was silent due to the ferromagnetic effect of Gd. On the other hand, the formation of DTD(Gd) (**131**) was confirmed by MALDI-ToF-MS ($\text{C}_{168}\text{H}_{152}\text{Gd}_2\text{N}_{16}\text{O}_8$)⁺ [M]⁺ calcd: 2837.04 found: 2837.77 (**chart 4.20**), which is another potential stable intermediate compound for cage system beside La.

Our approach of holding Pc between porphyrin units using Gd as a template was carried on the same method of the previous compounds. The reaction mixture was placed as one-pot in minimum volume (2-3 ml) of 1-pentanol (**scheme 4.28**). The mixture was heated in a sealed tube at 200 °C for 24 hours as the TLC analysis showed several new spots were developed. Therefore, the crude mixture was separated by column chromatography. We obtain a nice yield of about 25% in most potential alternative lanthanide metal to replace La. However, the silence of ^1H NMR is not helpful to continue forming the cage analogue because the order of components' assembly is not known, and further reaction cannot be easily monitored.



Scheme 4.28: The proposed pathway toward DTD(Gd) (**131**)

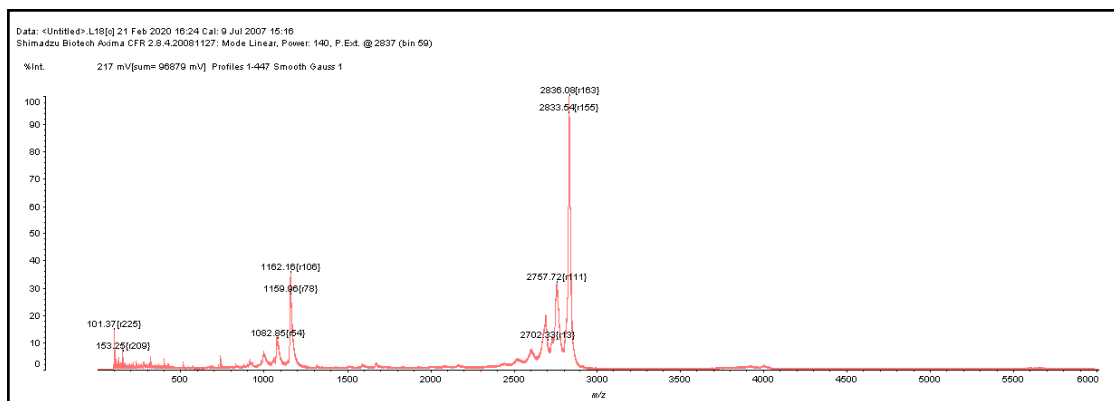
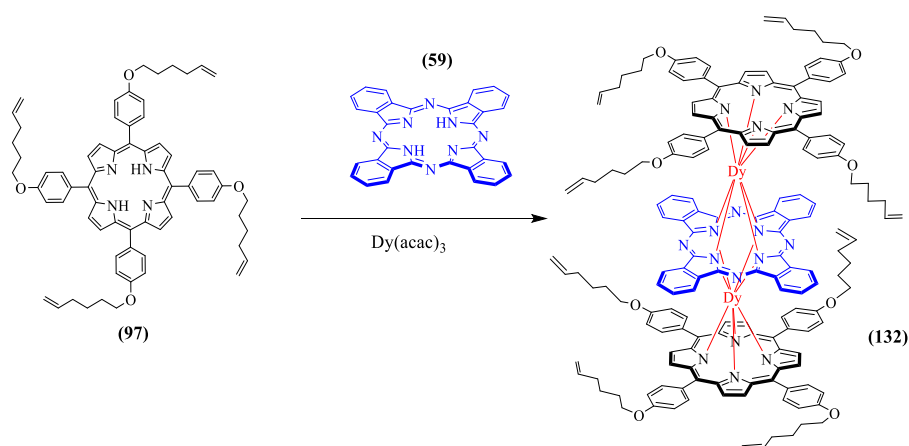


Chart 4.20: MALDI-ToF-MS shows formation on DTD(Gd) (131)

4.3.6 Dysprosium Triple Deckers DTD(Dy)

Dysprosium is the ninth element in the lanthanide series with atomic radii 0.91Å and nine electrons in the f^9 shell. It gains attention because it has the highest magnetic susceptibility compared with other lanthanides. DyTD was firstly prepared by Jiang *et al.*⁸⁸ in the different example but similar in the goal.

Therefore, DTD(Dy) (**132**) was prepared on the same principle that we previously used (**scheme 4.29**). This model is known as unstable against a daylight which is challenging. That could explain why it was not isolated in pure form, but we managed to confirm its formation by MALDI-ToF-MS ($C_{168}H_{151}Dy_2N_{16}O_8$)⁺ m/z [M-H]⁺ calcd: 2848.05 found: 2848.22 (**chart 4.21**).



Scheme 4.29: The proposed pathway toward DTD(Dy) (**132**)

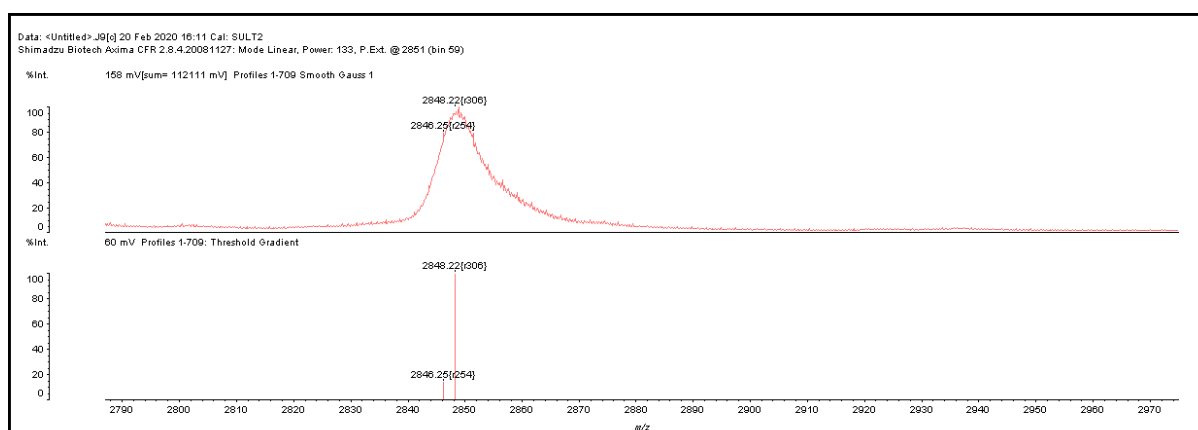
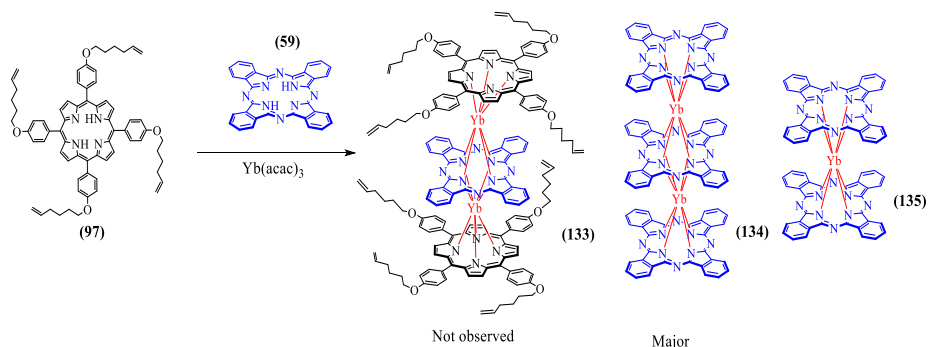


Chart 4.21: MS indicates the formation of DTD(Dy) (**132**)

4.3.7 Ytterbium Triple Deckers DTD(Yb)

Ytterbium is the thirteenth element in the lanthanide series with atomic radii 0.87\AA and thirteen electrons in the f_{13} shell. There were several attempts toward achieving TD using Yb, but its ionic radii is smaller than required to form them.

Our attempt to prepare TD intermediate on the same principle that we tried before (**scheme 4.30**) was resulted several products. The characterisation of those products was not shown any sign of the target compound. The products that we achieved were homoleptic PcTD and PcDD (**chart 4.22**).



Scheme 4.30: The proposed pathway toward DTD(Yb) (133)

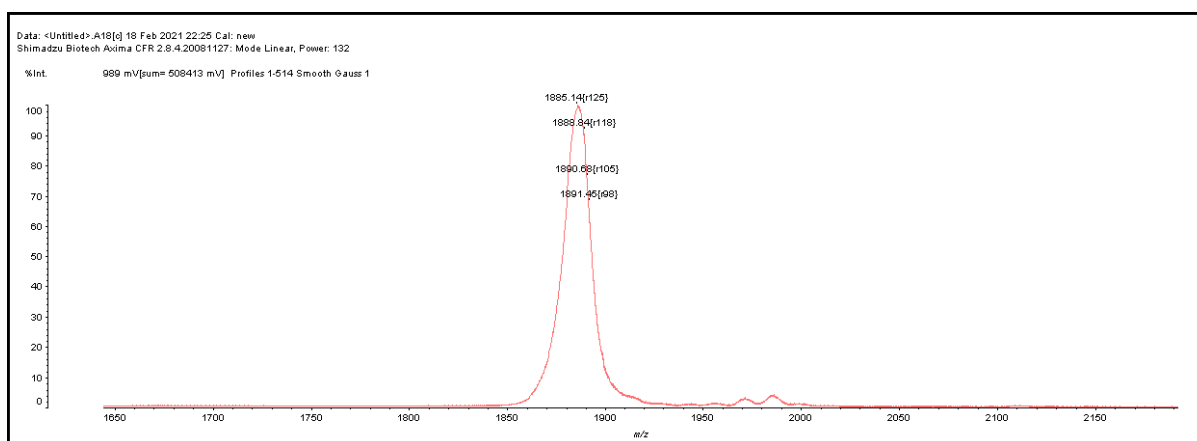
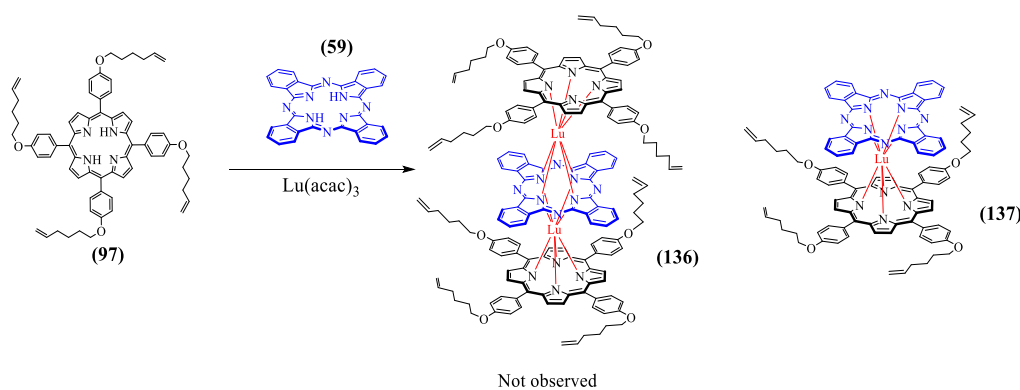


Chart 4.22: MALDI-ToF-MS confirms the formation of homoleptic triple deckers (theoretical calculation in the frame).

4.3.8 Lutetium Triple Deckers DTD(Lu)

Lutetium is the last element in the lanthanide series with atomic radii 0.86Å and fourteen electrons in the f^{14} shell. There were several attempts to achieve TD using Lu, but its ionic radii is also smaller than required to form them.

We attempted to prepare TD intermediate on the same principle that we examined before (**scheme 4.31**). However, the products that we managed to isolate were Pc homoleptic double- and triple-deckers, and heteroleptic double-deckers as indicated by MALDI-ToF-MS ($C_{100}H_{84}LuN_{12}O_4$)⁺ [M]⁺ calcd: 1692.62 found:1692.83 (**chart 4.23**). Also, we noted that the aromatic region was completely silent on ¹H NMR due to Lu magnetic status being diamagnetic (**chart 4.24**). As heteroleptic double-deckers were indicated, it could be worth trying to react with another lanthanide element to form an intermediate TD through hetero- di lanthanide.



Scheme 4.31: The proposed pathway toward DTD(Lu)

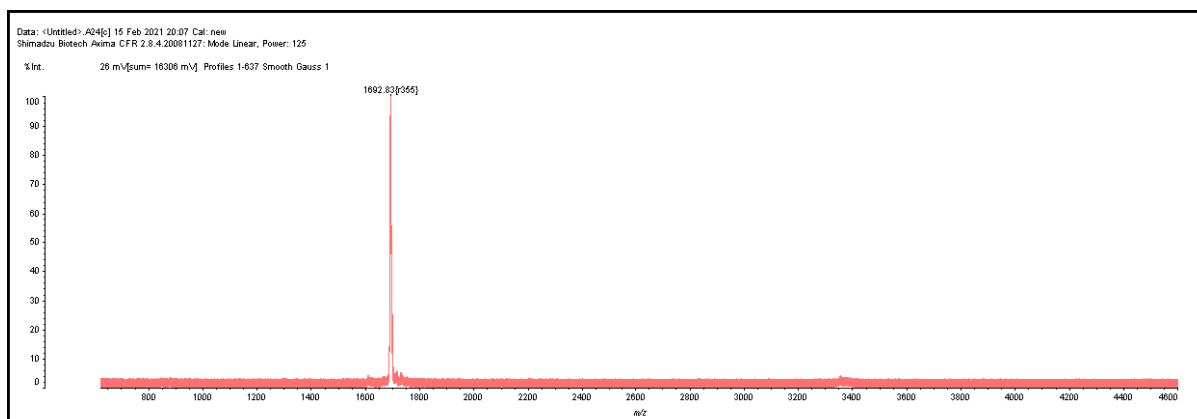


Chart 4.23: MALDI-ToF-MS confirms the formation of heteroleptic double deckers (**137**).

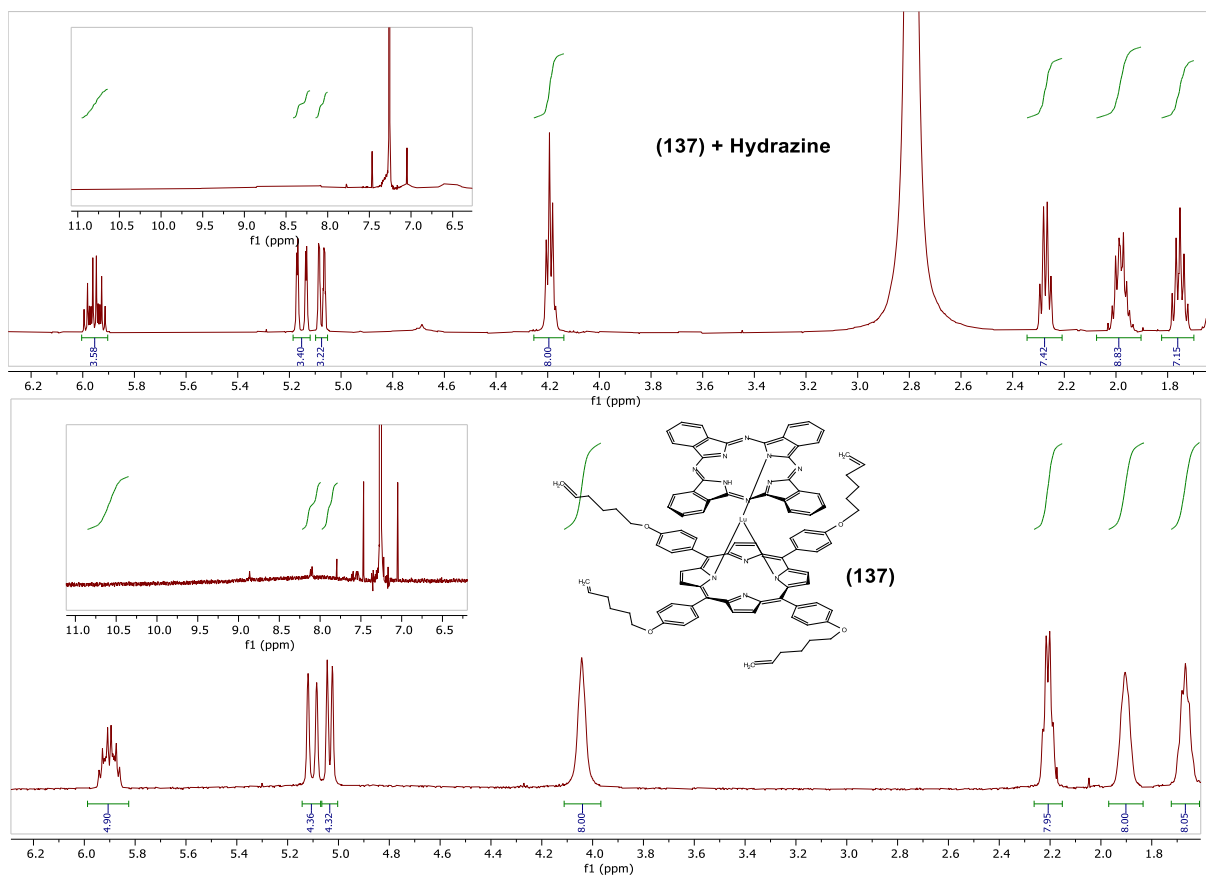


Chart 4.24: ^1H NMR for double-deckers before (bottom) and after (top) addition of hydrazine and the aromatic signals still broadened whereas the aliphatic peaks become clearer (the aromatic region in frame).

4.3.9 Conclusion and future work

The unique properties of lanthanides metals are always fascinating to investigate due to their magnetic behaviours and optical characteristics and their ability to host ligands. Our exploring on them were shown a few suitable metals that may be alternatives to obtain a cage system through the series. Nd, Eu and Gd are the most potential elements to test them as the intermediate TD was obtained. The purpose of our study was to identify and compare strategies towards encapsulating a central phthalocyanine unit within a cage formed by two capping porphyrins and bridging chains. This was successfully achieved by pre-forming porphyrin dyads, and also by the one-pot multicomponent assembly. Each strategy had advantages. The linked strategy gave control over product formation but synthesis of the key starting material (where a large part of this project's time was committed) proved challenging and difficult to scale up. Complexation to other metals was briefly investigated but lanthanum derivatives proved the easiest to prepare, purify and characterize. Encapsulation was successfully achieved using metathesis and the resulting triple-deckers appear to contain a mixture of alkene geometries. It has so far not proved possible to grow crystals suitable for characterisation by X-ray crystallography, but this is an important final stage for future work. However, reduction of the alkenes to alkanes gave identical, symmetrical systems from both routes, proving the proposed general structures of intermediates. Finally, it was the ultimate aim of this project to remove the bridging metal ions from these assemblies to give unique mechanically entrapped systems. Therefore, this project has provided a firm position from which this can be achieved in future.

Chapter 5

Experimental section

5. Experimental Section

5.1 General Methods

Reagents and solvents were obtained from commercial sources and used without further purification unless otherwise stated. Reactions and distillation were carried out under an inert atmosphere (argon or nitrogen gas), in most air-sensitive reactions, argon was preferred. Brine is a saturated aqueous solution of sodium chloride. Organic layers were dried using anhydrous magnesium sulphate. Evaporating of solvent was performed using a Buchi rotary evaporator at reduced pressure.

^1H NMR spectra were recorded either at 400 MHz on Ultrashield Plus™ 400 spectrometer or 500 MHz on a Bruker Ascend™ 500 spectrometer in 5 mm diameter tubes. Signals are quoted in ppm as δ downfield from tetramethylsilane ($\delta=0.00$) and coupling constants J given in Hertz. $^{13}\text{C}[^1\text{H}]$ NMR spectra were recorded at 100.6 MHz or 125.7 MHz on the same spectrometers. NMR spectra were performed in solution using deuterated chloroform and dichloromethane at room temperature unless otherwise stated.

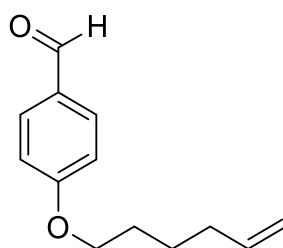
Ultraviolet-Visible absorption spectra were recorded on Hitachi U-3310 Spectrophotometer in solvent as stated. MALDI-ToF-MS mass spectra were carried out using a Shimadzu Biotech Axima instrument. Characterisation of hybrids by MALDI-ToF-MS mass spectrometry was achieved by comparison of isotopic distribution to theory. IR spectra were recorded using a Perkin-Elmer Spectrum BX FT-IR spectrometer.

Thin-layer chromatography (TLC) was performed using aluminium sheets coated with Alugram® Sil G/UV254 (Macherey-Nagel), and the compounds were visualised under short-wavelength UV-light at 245 nm or 366 nm. Column chromatography was carried out using silica gel 60Å mesh 70-230 (63-200 μm) under gravity or moderate pressure at ambient temperature. Solvent ratios are given as v:v.

Melting points were taken on a Reichart ThermoVar microscope with a thermopar based temperature control. Reactions using microwave irradiation were carried out in Biotage Initiator+ Microwave system.

5.2 Experimental procedures

1. Synthesis of *p*-5-hexen-1-oxybenzaldehyde⁹¹ (91)



Method A

A mixture of *p*-hydroxybenzaldehyde (6.1 g, 50 mmol, 1 eq.), 6-bromohex-1-ene (8.1 g, 50 mmol, 1 eq.) and potassium carbonate (3.5 g, 25 mmol, 0.5 eq.) were heated in acetone under reflux (50 ml) for 48h. Water and DCM were added, the mixture separated and the organic layer dried over MgSO₄. After filtration, the solvent was evaporated, and the residue distilled under reduced pressure (approx. 15mm Hg). The fraction distilling at 180°C afforded a colourless oil (8.72g, 86%).

Method B

A mixture of *p*-hydroxybenzaldehyde (6.1 g, 50 mmol, 1 eq.), 6-bromohex-1-ene (10 g, 60 mmol, 1 eq.) and potassium carbonate (6.1 g, 44 mmol, 0.88 eq.) were refluxed in DMSO (20 ml) for 2h at 100 C. Brine and diethylether were added, the mixture separated and the organic layer dried over MgSO₄. After filtration, the solvent was evaporated and the residue distilled under reduced pressure to give a colourless oil (8.4g, 82%).

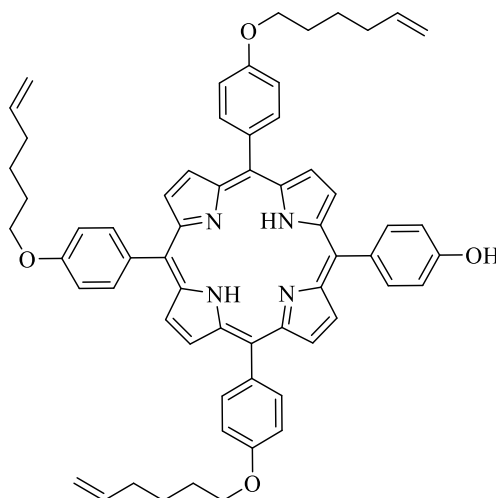
Method C

A mixture of *p*-hydroxybenzaldehyde (6.1 g, 50 mmol, 1 eq.), 6-bromohex-1-ene (10 g, 60 mmol, 1 eq.) and potassium carbonate (6.1 g, 44 mmol, 0.88 eq.) were refluxed in DMF (20 ml) for 2h at 100 C. Brine and diethylether were added, the mixture separated and the organic layer dried over MgSO₄. After filtration, the solvent was evaporated and the residue distilled under reduced pressure. The fraction distillation at 180°C afforded as a colourless oil (8.4g, 91%).

¹H NMR (500 MHz, CDCl₃) δ 9.87 (s, 1H), 7.82 (d, *J* = 8.8 Hz, 2H), 6.98 (d, *J* = 8.8 Hz, 2H), 5.82 (ddt, *J* = 17.1, 10.2, 6.7 Hz, 1H), 5.04 (dd, *J* = 17.1, 1.9 Hz, 1H), 4.98 (dd, *J* = 10.2, 1.9 Hz, 1H), 4.05 (t, *J* = 6.5 Hz, 2H), 2.17 – 2.10 (m, 2H), 1.87 – 1.79 (m, 2H) and

1.62 – 1.54 (m, 2H); ^{13}C NMR (126 MHz, CDCl_3) δ 190.89, 164.29, 138.39, 132.07, 129.87, 115.01, 114.83, 68.27, 33.42, 28.55 and 25.29; UV-vis, (DCM)/nm (log ϵ): 283 (4.18), 228 (4.18), 218 (4.21); IR (KBr, cm^{-1}): 3054, 2987, 2305, 1601, 1422, 1265, 896, 739 and 705. HRMS (ESI) ($\text{C}_{13}\text{H}_{17}\text{O}_2$) $^+$ $[\text{M}+\text{H}]^+$: calcd: 205.1223; found: 205.1413.

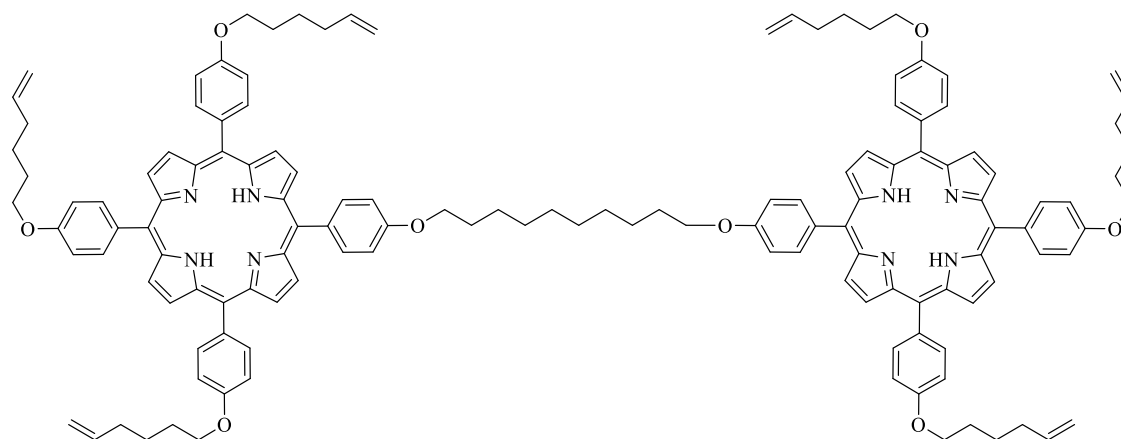
2. Synthesis of 5,10,15-Tris-[*p*-(5-hexenyl-1-oxy)phenyl]-20-(4-hydroxyphenyl) porphyrin (92)



Following a modified version of Adler's general procedure,^{48,49} freshly distilled pyrrole (3.35 g, 50 mmol, 4 eq.) was added dropwise to a mixture of *p*-5-hexenyloxybenzaldehyde (7.65g, 37.5 mmol, 3 eq.) and *p*-hydroxybenzaldehyde (1.525 g, 12.5 mmol, 1eq.) in refluxing propionic acid (150 ml). After refluxing for 30 min, the mixture was cooled to room temperature and MeOH (200 ml) added. After 3 days, the mixture was filtered and the resulting purple solid purified by column chromatography using initially DCM and then DCM/MeOH (4:1) to collect the target compound. The solvent was removed and the residue re-dissolved in DCM. Addition of MeOH precipitated the product affording the title compound as a purple solid (0.59 g, 5.1%); ¹H NMR (500 MHz, CD₂Cl₂) δ 8.89 (s, 8H), 8.11 (d, *J* = 8.5 Hz, 6H), 8.06 (d, *J* = 8.2 Hz, 2H), 7.29 (d, *J* = 8.5 Hz, 6H), 7.19 (d, *J* = 8.2 Hz, 2H), 5.95 (ddt, *J* = 17.1, 10.2, 6.7 Hz, 3H), 5.13 (d, *J* = 17.1 Hz, 3H), 5.05 (d, *J* = 10.2 Hz, 3H), 2.29 – 2.23 (m, 2H), 2.04 – 1.95 (m, 6H), 1.78 – 1.70 (m, 6H), -2.81 (s, 2H); ¹³C NMR (126 MHz, CDCl₃) δ 159.05, 155.47, 138.77, 135.81, 135.74, 134.95, 134.61, 119.99, 119.66, 115.00, 113.76, 112.85, 68.22, 33.71, 29.09 and 25.66; IR (KBr, cm⁻¹): 3427, 3054, 2987, 2305, 1643, 1421, 1265, 896, 738 and 705; UV-vis, (DCM)/nm (log ε): 422 (5.27), 455 (4.10), 519 (4.16), 556 (4.04), 593 (3.83), 650 (3.89); MALDI-ToF-MS (C₆₂H₆₁N₄O₄)⁺ m/z [M+H]⁺ calcd: 925.46 found: 925.91 (100%).

potassium carbonate (120 mg, 0.86 mmol, 4 eq.) and excess of dibenzo18-crown-6 (130 mg, 0.36 mmol, 1.67 eq.) were stirred in microwave at 100C for 1 min. The reaction crude was dissolved by DCM and water was added. The mixture separated and the organic layer dried over MgSO_4 . The crude mixture recrystallized using a mixture of DCM/MeOH and purple crystals of the title compound solid was obtained (200 mg, 80%) ^1H NMR (500 MHz, Chloroform-d) δ 8.88 (s, 8H), 8.15 – 8.08 (m, 8H), 7.27 (d, $J = 8.5$ Hz, 8H), 5.94 (ddt, $J = 16.9, 10.2, 6.7$ Hz, 3H), 5.20 – 5.10 (m, 3H), 5.11 – 5.03 (m, 3H), 4.25 (t, $J = 6.4$ Hz, 8H), 3.45 (t, $J = 6.9$ Hz, 2H), 2.33 – 2.22 (m, 6H), 2.00 (dp, $J = 8.2, 6.4$ Hz, 8H), 1.94 – 1.86 (m, 2H), 1.76 (tt, $J = 9.9, 6.4$ Hz, 6H), 1.63 (dt, $J = 15.4, 7.3$ Hz, 2H), 1.52 – 1.45 (m, 7H), -2.73 (s, 2H). MALDI-ToF-MS ($\text{C}_{72}\text{H}_{80}\text{N}_4\text{O}_4\text{Br}$) $^+$ m/z $[\text{M}]^+$ calcd: 1143.54 found: 1143.15 (100%).

4. Synthesis of Porphyrin C₁₀ dyad (93)



Method A

Following a modified version of Williamson's general procedure⁹² and Cammidge *et al.* method⁴, a mixture of **5** (203 mg, 0.21 mmol, 2 eq.) and 1,10-dibromodecane (32 mg, 0.10 mmol, 1 eq.) were dissolved in acetone (25 ml) and excess of potassium carbonate (50 mg, 0.36 mmol, 2.26 eq.) was added. The mixture was heated in sealed tube in an oil bath at 70°C for 6 days. The reaction was quenched by water (50 ml) and DCM was added to recover organic material. The mixture separated and the organic layer dried over MgSO₄. The crude mixture was purified by column chromatography using DCM/pet.ether (1.5:1). A purple solid of title compound was obtained (48 mg, ~22%).

Method B

Following a modified version of Williamson's general procedure⁹² and Cammidge *et al.* method⁴, a mixture of **5** (54 mg, 0.058 mmol, 1.35 eq.) and **19** (50 mg, 0.043 mmol, 1 eq.) were dissolved in acetone (12 ml). An excess of potassium carbonate (200 mg, 1.45 mmol, 33 eq.) and dibenzo-18-crown-6 (100 mg, 0.27 mmol, 6.5 eq) were added. The mixture was heated in sealed tube in an oil bath at 70°C for 9 days. The reaction was quenched by water (150 ml) and DCM was added to recover organic material. The mixture separated and the organic layer dried over MgSO₄. After filtration, the solvent was evaporated and the residue was purified by column chromatography using DCM/pet.ether (1.5:1). A purple solid of title compound was obtained (28 mg, ~32%).

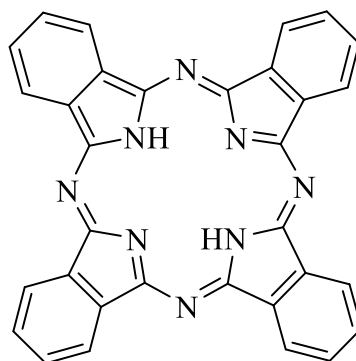
Method C

Following a modified version of Williamson's general procedure⁹² and a modified version of Smith, RG *et al.* method⁹³, a mixture of **5** (195 mg, 0.211 mmol, 1.45 eq.) and **19** (171 mg, 0.149 mmol, 1 eq.) were dissolved in DMSO (8 ml). An excess of potassium carbonate (200 mg, 1.49 mmol, 10 eq.) and dibenzo-18-crown-6 (268 mg, 0.74 mmol, 5 eq.) were added. The mixture was heated in sealed tube in an oil bath at 100°C for 24h. The reaction was quenched with water (50 ml) and DCM was added to recover organic material. The mixture separated and the organic layer dried over MgSO₄. After filtration, the solvent was evaporated and the residue was purified by column chromatography using DCM. A purple solid of title compound was obtained from second fraction (39 mg, ~13%).

Method D:

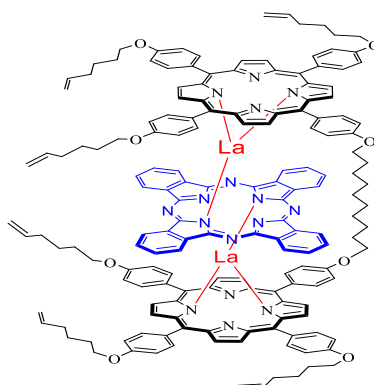
Following a modified version of Williamson's general procedure⁹² and a modified version of Smith, RG *et al.* method⁹³, a mixture of **5** (150 mg, 0.211 mmol, 2 eq.) and 1,10-dibromodecane (29 mg, 0.096 mmol, 1 eq.) were dissolved in DMSO (8 ml). An excess of potassium carbonate (200 mg, 1.49 mmol, 10 eq.) and dibenzo-18-crown-6 (100 mg, 0.27 mmol, 2.8 eq.) were added. The mixture was stirred under N₂ in oil bath at 100°C for 8h. The reaction was quenched with water (50 ml) and DCM was added to recover organic material. The mixture separated and the organic layer dried over MgSO₄. After filtration, the solvent was evaporated and the residue was purified by column chromatography using DCM. A purple solid of title compound was obtained in second fraction (55 mg, ~28%)

mp. 243°C; ¹H NMR (400 MHz, CDCl₃) δ 8.83 – 8.75 (m, 16H), 8.07 – 7.97 (m, 16H), 7.25 – 7.16 (m, 8H), 7.18 – 7.11 (m, 8H), 5.85 (dtt, *J* = 16.8, 10.1, 6.6 Hz, 6H), 5.05 (ddq, *J* = 17.1, 8.4, 1.7 Hz, 6H), 4.97 (ddd, *J* = 10.4, 7.3, 2.3, 1.2 Hz, 6H), 4.21 (t, *J* = 6.8 Hz, 4H), 4.18 (t, *J* = 6.6 Hz, 4H), 4.12 (t, *J* = 6.4 Hz, 8H), 2.25 – 2.12 (m, 13H), 2.00 – 1.85 (m, 15H), 1.74 – 1.58 (m, 14H), 1.47 – 1.37 (m, 10H), -2.82 (s, 4H).; ¹³C NMR (101 MHz, CDCl₃) δ 158.95, 138.29, 135.74, 134.32, 120.26, 120.08, 114.98, 112.82, 67.76, 33.72, 33.69, 29.07, 26.44, 25.64. (s); IR (KBr, cm⁻¹): 3072, 2936, 1639, 1606, 1506, 1470, 1350, 1284, 1244, 1173, 1108, 966, 910, 801 and 735; UV-vis, (DCM)/nm (log ε): 422 (5.23), 455 (4.16), 519 (4.32), 557 (4.21), 593 (3.93), 651 (3.97) and 949 (3.59); MALDI-ToF-MS (C₁₃₄H₁₃₇N₈O₈)⁺ m/z [M]⁺ calcd: 1987.06 found: 1987.17 (100%).

5. Phthalocyanine [75,94](#) (59)

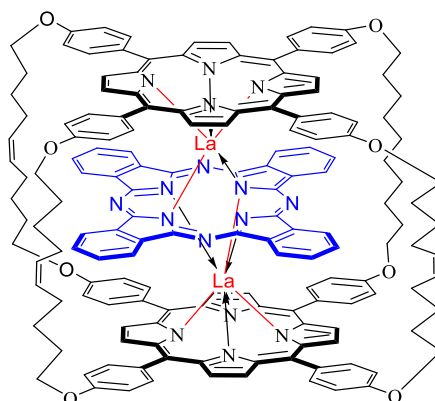
Following a general procedure using lithium as a template, a solution of phthalonitrile (1.28 g, 10 mmol) in 1-pentanol (12 ml) was heated to 120 °C for 1h. Lithium (200 mg, 4 mmol) was washed by MeOH and added to the reaction mixture and continued for another 1 h. Acetic acid was added (20 ml) and refluxed for 1h. The reaction mixture was cooled down to room temperature, methanol (50 ml) was added to precipitate the product and the dark blue solid of the pure phthalocyanine collected by vacuum filtration (1.20g, 93%); UV-vis (THF, λ_{max} , nm (rel. int.)): 690 (0.603), 654 (0.659), 377 (0.592); MALDI-ToF-MS ($\text{C}_{32}\text{H}_{16}\text{N}_8$)⁺ m/z [M]⁺ calcd: 514.17 found: 514.75 (100%).

6. Synthesis of Triple decker TD(La) (94)



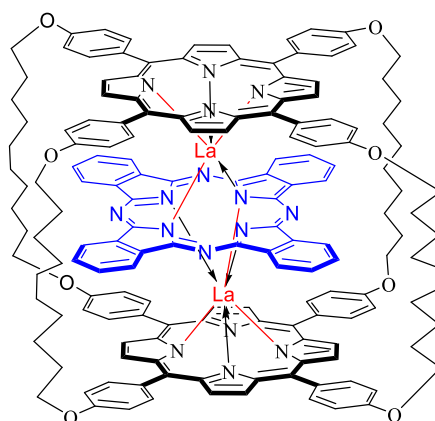
Following a modified version of Cammidge methodology⁴, a mixture of dyad (35 mg, 0.017 mmol, 1eq), lanthanum(III) acetylacetonate hydrate (16 mg, 0.036 mmol) and phthalocyanine (9 mg, 0.017 mmol, 1eq) were refluxed in 10 ml of octanol for 4h at 200C under Ar. Solvent was removed and the residual separated by column chromatography using CHCl₃/hexane (1:1) then crude recrystallized from DCM/MeOH. The title product was collected as dark brown solids (15 mg, 31 %); mp. >350 C; ¹H NMR (500 MHz, CDCl₃) δ 10.00 (d, *J* = 7.9 Hz, 2H), 9.80 – 9.72 (m, 6H), 9.25 (dd, *J* = 5.3, 2.9 Hz, 7H), 8.22 (dd, *J* = 5.7, 2.5 Hz, 7H), 7.89 (dd, *J* = 7.9, 3.2 Hz, 8H), 7.18 (s, 16H), 6.79 (d, *J* = 8.1 Hz, 2H), 6.71 – 6.61 (m, 8H), 6.47 (dd, *J* = 7.8, 2.5 Hz, 7H), 5.98 (ddt, *J* = 17.0, 10.2, 6.7 Hz, 6H), 5.17 (dq, *J* = 17.2, 1.7 Hz, 6H), 5.11 – 5.07 (m, 6H), 4.52 (t, *J* = 7.3 Hz, 4H), 4.29 (t, *J* = 6.2 Hz, 12H), 2.31 (q, *J* = 7.1 Hz, 13H), 2.06 (dd, *J* = 15.2, 6.5 Hz, 8H), 1.82 (dt, *J* = 15.1, 7.4 Hz, 22H); UV-vis (DCM, λ_{max}, nm (rel. int.)): 890 (0.025), 609 (0.049), 558 (0.061), 488 (0.092), 422 (0.881), and 358 (0.301); MALDI-ToF-MS (C₁₆₆H₁₅₀La₂N₁₆O₈)⁺ m/z [M]⁺ calcd: 2772.99 found: 2773.00

7. Synthesis of Cyclic Triple Deckers CTD(La) (95)



A modified version of a general methodology of GrubbsTM metatheses⁷⁸, solution of TD(La) (41mg, 0.014 mmol, 1eq) in dry DCM (100 ml) was degassed by N₂ for 10 min. A degassed solution of 1st generation of GrubbsTM (13 mg, 0.015 mmol, 1eq) in dry DCM (20 ml) was added to a reaction mixture using cannula then left stirring for 20h. After completion, the reaction was quenched by Butyl vinyl ether 10 ml and opened to air. The solvent removed to dryness. The residual was purified by column chromatography using DCM then DCM/EtOAc (99:1). A dark brown solid of title compound was obtained in first fraction (35 mg, 85%); m.p.>350C; ¹H NMR (500 MHz, CDCl₃) δ 10.19 (s, 3H), 10.09 (d, *J* = 22.5 Hz, 5H), 9.31 (d, *J* = 3.9 Hz, 8H), 8.31 (s, 8H), 8.02 (s, 5H), 7.97 (d, *J* = 8.4 Hz, 3H), 7.34 – 7.27 (m, 16H), 6.96 – 6.82 (m, 8H), 6.80 (d, *J* = 7.8 Hz, 6H), 6.74 (d, *J* = 8.1 Hz, 2H), 6.08 – 6.03 (m, 3H), 5.85 – 5.67 (m, 3H), 4.67 (t, *J* = 7.2 Hz, 6H), 4.58 (dt, *J* = 8.7, 6.9 Hz, 10H), 2.67 (d, *J* = 11.1 Hz, 6H), 2.58 (d, *J* = 5.6 Hz, 6H), 2.35 (q, *J* = 6.8 Hz, 6H), 2.28 (p, *J* = 6.6 Hz, 10H), 2.13 – 2.04 (m, 6H), 2.00 (p, *J* = 6.8 Hz, 6H), 1.92 (s, 8H), 1.81 (s, 4H). ¹³C NMR (126 MHz, CDCl₃) δ 158.63, 158.58, 158.53, 147.84, 142.77, 136.48, 135.27, 131.18, 130.29, 130.02, 130.00, 128.17, 128.15, 123.48, 119.64, 119.56, 77.23, 69.07, 68.73, 68.09, 32.57, 29.71, 29.47, 29.27, 29.02, 28.88, 28.57, 27.24, 26.65, 26.51. UV-vis (DCM, λ_{max}, nm (rel. int.)): 880 (0.028), 609 (0.059), 553 (0.074), 482 (0.117), 422 (0.975), and 358 (0.379); MALDI-ToF-MS (C₁₆₀H₁₃₈La₂N₁₆O₈)⁺ m/z [M]⁺ calcd: 2688.90 found: 2688.89.

8. Synthesis of Hydrogenated Cyclic Triple Deckers HCTD(La) (96)



Pathway 1

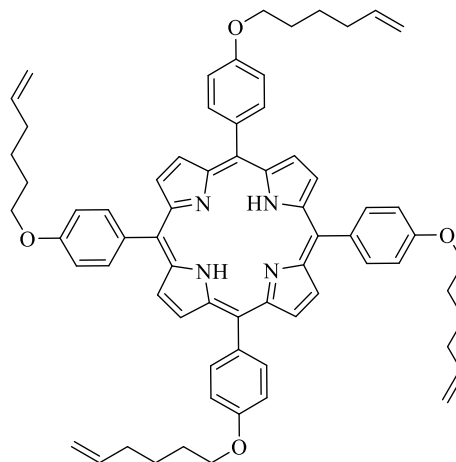
Following a modified version of general hydrogen transferred methodology developed by Meienhofer *et al.*⁸³, a mixture of CTD (10 mg, 3.72 μmol , 1 eq) and Pd/C 10% (10 mg) were dissolved in 1,4-cyclohexadiene (1 ml, 10.9 mmol, 700 eq). The mixture was heated in sealed vessel in an oil bath at 100°C for 24h. The catalyst was filtered, and the solvent was evaporated to dryness. A dark brown solid of title compound was obtained (9.9 mg, 99%).

Pathway 2

Following a modified version of general hydrogen transferred methodology developed by Gregg *et al.*⁹⁵, A mixture of CDTD (22 mg, 8.2 μmol , 1 eq) and Pd/C 10% (5 mg) were dissolved in a mixture of 1,4-cyclohexadiene (1 ml, 10.9 mmol, 700 eq) and EtOAc (1 ml). The mixture was heated in sealed vessel in an oil bath at 100°C for 5h. The catalyst was filtered, and the solvent was evaporated to dryness. A dark brown solid of title compound was obtained (22 mg, 96%).

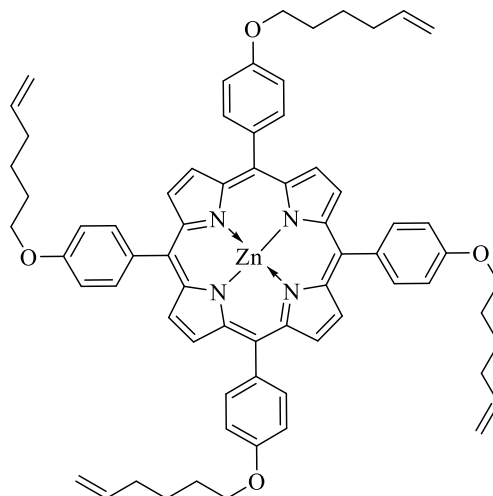
^1H NMR (500 MHz, CDCl_3) δ 10.13 – 10.03 (m, 8H), 9.32 (dd, $J = 5.3, 3.0$ Hz, 8H), 8.33 (dd, $J = 5.6, 2.5$ Hz, 8H), 7.98 (d, $J = 7.8$ Hz, 8H), 7.28 (s, 16H), 6.86 (dd, $J = 8.0, 2.8$ Hz, 8H), 6.76 – 6.70 (m, 8H), 4.59 (t, $J = 7.2$ Hz, 16H), 2.28 (qd, $J = 7.3, 4.5$ Hz, 24H), 1.92 (d, $J = 4.2$ Hz, 26H), 1.81 (s, 18H). UV-vis (DCM, λ_{max} , nm (rel. int.)): 880 (0.028), 610 (0.052), 557 (0.072), 487 (0.115), 422 (0.983), and 365 (0.358); MALDI-ToF-MS ($\text{C}_{160}\text{H}_{144}\text{La}_2\text{N}_{16}\text{O}_8$)⁺ m/z [M]⁺ calcd: 2694.94 found: 2694.30.

9. Synthesis of 5,10,15 and 20 Tetrakis [*p*-(5-hexenyl-1-oxy)phenyl] porphyrin THxTPP (97)



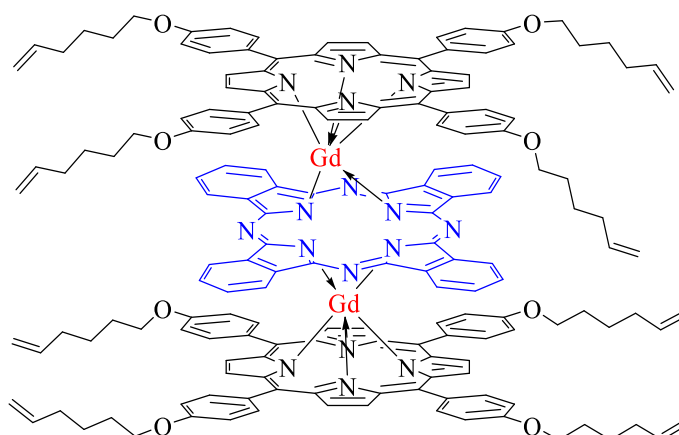
The title compound was synthesized along with THxTPPOH (92). It was isolated from first fraction of column chromatography using eluent DCM/Hexane (1:1) followed by slow crystallization using (DCM/MeOH). The title compound was obtained as a purple solid (0.7g, 8%); ¹H NMR (500 MHz, Chloroform-*d*) δ 8.87 (s, 8H), 8.13 – 8.09 (m, 8H), 7.30 – 7.24 (m, 8H), 5.94 (ddt, *J* = 16.9, 10.2, 6.6 Hz, 4H), 5.14 (dq, *J* = 17.1, 1.6 Hz, 4H), 5.06 (ddt, *J* = 10.2, 2.2, 1.2 Hz, 4H), 4.26 (t, *J* = 6.4 Hz, 8H), 2.31 – 2.23 (m, 8H), 2.04 – 1.97 (m, 8H), 1.79 – 1.72 (m, 8H), -2.73 (s, 2H). ¹³C NMR (101 MHz, CDCl₃) δ 158.92, 138.63, 135.61, 134.52, 119.80, 114.86, 112.70, 77.34, 77.22, 77.02, 76.70, 68.09, 33.58, 28.96, 25.53; UV-vis (DCM, λ_{max}, nm (rel. int.)): 649 (0.030), 598 (0.033), 562 (0.051), 518 (0.064), and 422 (0.935); MALDI-ToF-MS (C₆₈H₇₀N₄O₄)⁺ *m/z* [M]⁺ calcd: 1007.30 found:1007.31.

10. Synthesis of 5,10,15 and 20 Tetrakis [*p*-(5-hexenyl-1-oxy)phenyl] 21,22 Zinc Porphyrin (123)



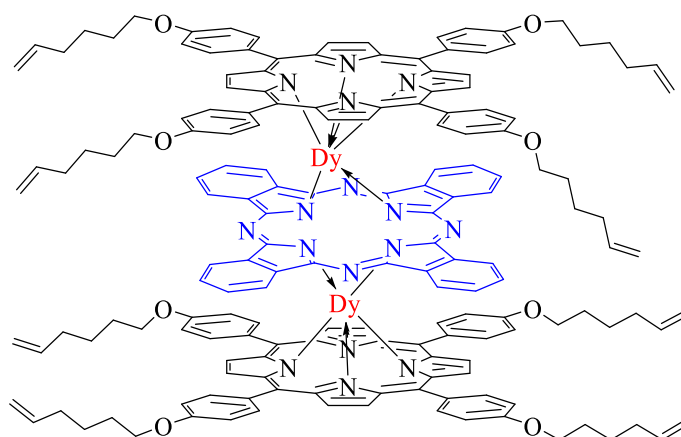
Following a general procedure of porphyrin metalation, a mixture of THTPP (0.818g, 0.81 mmol, 1eq.) and zinc acetate (0.2g, 1 mmol, 1.25eq.) were refluxed in acetone (50 ml) for 3h. Checked completion by ^1H NMR, then, solvent were removed and residual were recrystallised from DCM/MeOH afforded a light purple crystals (0.79g, 91%); mp. 249 C; ^1H NMR (500 MHz, Chloroform-*d*) δ 8.98 (s, 8H), 8.14 – 8.09 (m, 8H), 7.30 – 7.21 (m, 8H), 5.94 (ddt, $J = 17.0, 10.2, 6.7$ Hz, 4H), 5.14 (dq, $J = 17.2, 1.7$ Hz, 4H), 5.06 (ddd, $J = 10.2, 2.2, 1.2$ Hz, 4H), 4.26 (t, $J = 6.4$ Hz, 8H), 2.31 – 2.23 (m, 8H), 2.05 – 1.96 (m, 8H), 1.76 (tt, $J = 10.0, 6.5$ Hz, 8H). ^{13}C NMR (126 MHz, CDCl_3) δ 158.89, 150.66, 138.79, 135.54, 135.25, 132.04, 120.97, 115.00, 112.71, 77.73, 77.42, 77.36, 77.22, 77.16, 76.91, 68.21, 33.73, 29.11, 25.67; UV-vis (DCM, λ_{max} , nm (rel. int.)): 586 (0.043), 551 (0.069), and 423 (0.918); MALDI-ToF-MS ($\text{C}_{68}\text{H}_{68}\text{N}_4\text{O}_4\text{Zn}$) $^+$ m/z $[\text{M}]^+$ calcd: 1068.45 found:1068.46.

12. Synthesis of Direct Triple deckers DTD(Gd) (131)



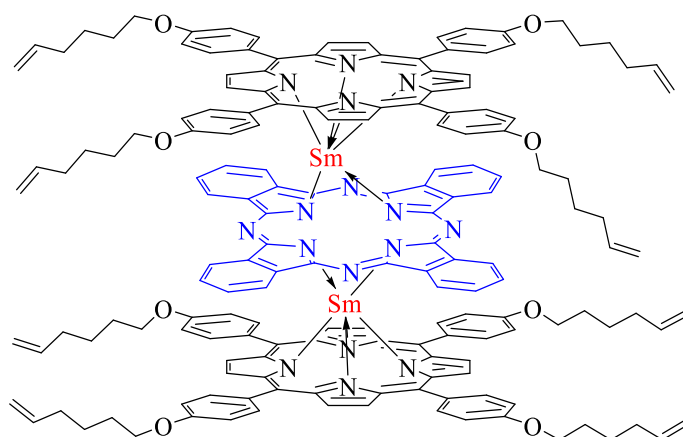
A Pentanol (2 ml) was added to a mixture of THxTPP (100 mg, 0.099 mmol, 2eq), phthalocyanine (25 mg, 0.048 mmol, 1 eq) and Gd(acac)₃ (50 mg, 0.123, 2.5 eq) then heated to 160 C for 24h. The solvent was removed under high vacuum and the residual was separated by column chromatography DCM/EtOAc/Petroleum ether (4:1:45) then DCM/EtOAc (99:1). A title compound was isolated in second fraction as dark brown crystals (25 mg, 25%); ¹H NMR & ¹³C NMR are not achieved due to ferromagnetic effect of Gd broaden signals; MALDI-ToF-MS (C₁₆₈H₁₅₂Gd₂N₁₆O₈)⁺ m/z [M]⁺ calcd: 2837.04 found: 2837.77

13. Synthesis of Direct Triple deckers DTD(Dy) (132)



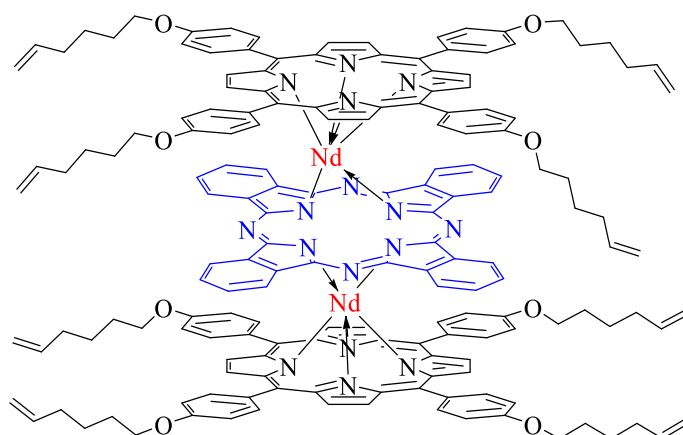
A Pentanol (2 ml) was added to a mixture of THxTPP (100 mg, 0.099 mmol, 2eq), phthalocyanine (25 mg, 0.048 mmol, 1 eq) and Dy(acac)₃ (57 mg, 0.123 mmol, 2.5 eq) then heated to 160 C in oil bath for 24h. The solvent was removed under high vacuum and the residual was separated by column chromatography DCM/EtOAc/Petroleum ether (4:1:45) then DCM/EtOAc (99:1). A title compound was isolated in second fraction as dark brown crystals (19.5 mg, 20%); ¹H NMR & ¹³C NMR are not achieved due to instability of the compounds; MALDI-ToF-MS (C₁₆₈H₁₅₁Dy₂N₁₆O₈)⁺ m/z [M-H]⁺ calcd: 2848.05 found: 2848.22

14. Synthesis of Direct Triple deckers DTD(Sm) (129)



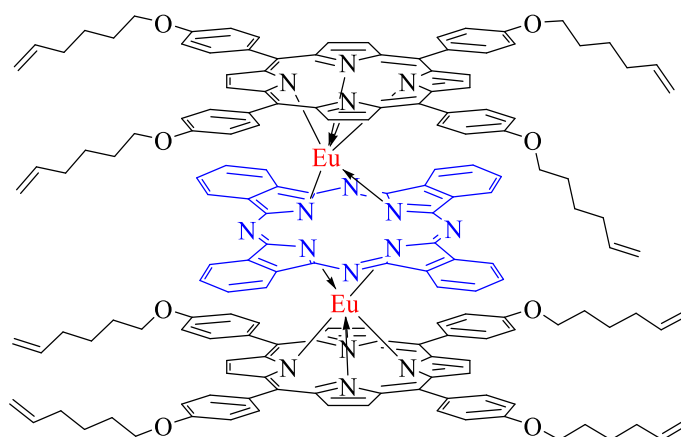
A Pentanol (2 ml) was added to a mixture of THxTPP (55 mg, 0.054 mmol, 2eq), phthalocyanine (14 mg, 0.027 mmol, 1 eq) and Sm(acac)₃ (24.4 mg, 0.054 mmol, 2 eq) then heated to 200 C in oil bath for 24h. The solvent was removed under high vacuum and the residual was separated by column chromatography DCM/Hexane (3:1) then DCM/EtOAc (9:1). A title compound was isolated in second fraction as dark brown crystals (11 mg, 20%); ¹H NMR & ¹³C NMR are not achieved due to instability of the compounds; MALDI-ToF-MS (C₁₆₈H₁₅₁Sm₂N₁₆O₈)⁺ m/z [M-H]⁺ calcd: 2824.03 found: 2823.94

15. Synthesis of Direct Triple deckers DTD(Nd) (128)



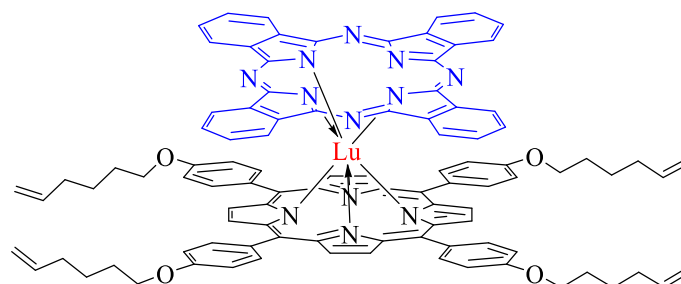
A Pentanol (2 ml) was added to a mixture of THxTPP (50 mg, 0.049 mmol, 2eq), phthalocyanine (12.5 mg, 0.024 mmol, 1 eq) and Nd(acac)₃ (21.9 mg, 0.049 mmol, 2 eq) then heated to 200 C in oil bath for 4h. The solvent was removed under high vacuum and the residual was separated by column chromatography DCM/Hexane (3:2). A title compound was isolated in second fraction as dark brown crystals (12 mg, 25.8%); ¹H NMR & ¹³C NMR are not achieved due to instability of the compounds; MALDI-ToF-MS (C₁₆₈H₁₅₂Nd₂N₁₆O₈)⁺ m/z [M]⁺ calcd: 2805.01 found: 2805.49

16. Synthesis of Direct Triple deckers DTD(Eu) (130)



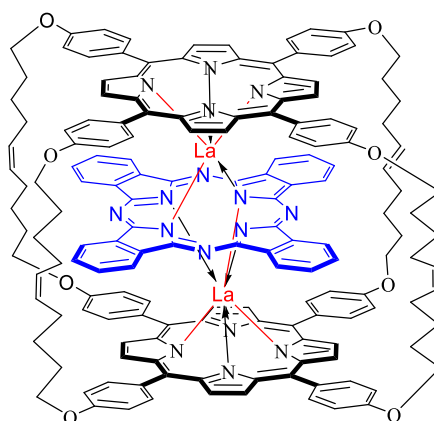
A Pentanol (2 ml) was added to a mixture of THxTPP (56.8 mg, 0.056 mmol, 1.93 eq), phthalocyanine (19.8 mg, 0.038 mmol, 1.52 eq) and $\text{Eu}(\text{acac})_3$ (26.3 mg, 0.058 mmol, 2 eq) then heated to 200 C in oil bath for 24h. The solvent was removed under high vacuum and the residual was separated by column chromatography DCM/EtOAc/Petroleum ether (4:1:45) then DCM/EtOAc (99:1). A title compound was isolated in second fraction as dark orange crystals (8 mg, 15%); ^1H NMR & ^{13}C NMR are not achieved due to instability of the compounds; MALDI-ToF-MS ($\text{C}_{168}\text{H}_{152}\text{Eu}_2\text{N}_{16}\text{O}_8$)⁺ m/z [M]⁺ calcd: 2827.03 found: 2827.00.

17. Synthesis of heteroleptic double deckers DD(Lu) (137)



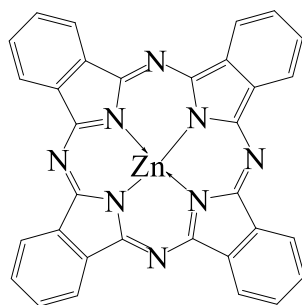
A Pentanol (2 ml) was added to a mixture of THxTPP (57 mg, 0.056 mmol, 2 eq), phthalocyanine (18 mg, 0.035 mmol, 1.6 eq) and Lu(acac)₃ (21 mg, 0.044 mmol, 1.7 eq) then heated to 200 C for 24h. The solvent was removed under high vacuum and the residual was separated by column chromatography DCM/Hexane (2:1). A title compound was isolated in second fraction as light orange crystals (10 mg, 18.4%); ¹H NMR & ¹³C NMR are not achieved due to broaden aromatic signals; MALDI-ToF-MS (C₁₀₀H₈₄LuN₁₂O₄)⁺ m/z [M]⁺ calcd: 1692.62 found:1692.83.

18. Synthesis of Cyclic Direct Triple Deckers (CTDD) (120)

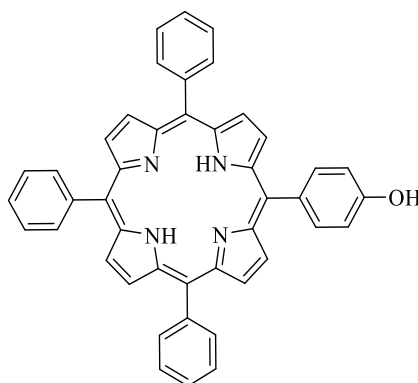


A modified version of a general methodology of GrubbsTM metatheses⁷⁸, solution of (DTD(La) **119**) (60mg, 0.021 mmol, 1eq) in dry DCM (100 ml) was degassed by N₂ for 10 min. A degassed solution of 1st generation of GrubbsTM (9 mg, 0.010 mmol, 0.5 eq) in dry DCM (20 ml) was added to a reaction mixture using cannula then left stirring for 21h. After completion, the reaction was quenched by opened to air. The solvent removed to dryness. The residual was purified by column chromatography using DCM then DCM/EtOAc (99:1) then DCM/EtOAc (9:1). A dark brown solid of title compound was obtained in second fraction (25 mg, 41.6%); ¹H NMR (500 MHz, CDCl₃) δ 10.20 (s, 5H), 10.11 (s, 3H), 9.38 – 9.26 (m, 8H), 8.37 – 8.28 (m, 8H), 8.03 (d, *J* = 7.9 Hz, 8H), 7.37 – 7.29 (m, 16H), 6.96 – 6.87 (m, 8H), 6.82 (d, *J* = 7.8 Hz, 8H), 6.07 (td, *J* = 4.0, 2.0 Hz, 4H), 5.76 (dd, *J* = 5.0, 2.7 Hz, 4H), 4.68 (t, *J* = 7.1 Hz, 8H), 4.58 (t, *J* = 6.3 Hz, 8H), 2.67 (t, *J* = 5.2 Hz, 9H), 2.59 (dd, *J* = 7.5, 4.2 Hz, 9H), 2.35 (h, *J* = 6.8 Hz, 9H), 2.28 (q, *J* = 6.7 Hz, 7H), 2.09 (p, *J* = 7.1 Hz, 8H), 2.02 (ddt, *J* = 8.9, 6.4, 3.3 Hz, 8H). ¹³C NMR (126 MHz, CDCl₃) δ 158.77, 158.67, 153.52, 147.96, 136.62, 135.50, 135.38, 134.18, 131.31, 130.42, 130.14, 129.64, 128.30, 123.65, 119.79, 119.71, 114.10, 113.43, 109.31, 77.41, 77.16, 76.91, 69.20, 68.23, 32.70, 32.08, 29.85, 29.81, 29.51, 29.15, 29.01, 27.37, 26.79, 26.64, 22.84, 14.28, 1.18; UV-vis (DCM, λ_{max}, nm (rel. int.)): 888 (0.030), 609 (0.064), 553 (0.080), 481 (0.124), 422 (0.982), and 358 (0.388); MALDI-ToF-MS (C₁₆₀H₁₃₆La₂N₁₆O₈)⁺ m/z [M]⁺ calcd: 2686.88 found: 2686.88.

19. Synthesis of Pc(Zn) (124)

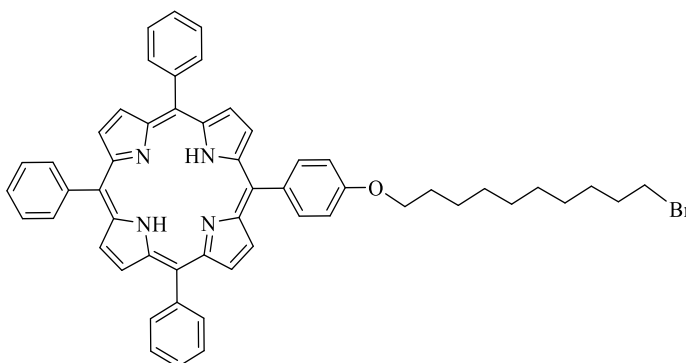


Following the general methodology of Pc metalation⁸⁵, zinc acetate (145 mg, 1.18 eq) and phthalocyanine **59** (290 mg, 1 eq) were dissolved in Octanol (3 ml). Catalytic amount of DBU was added to the mixture in sealed tube then left stirred at 200C for 2h. The reaction mixture cooled down to rt, then MeOH (20 ml) was added. The crude was filtered and washed several times by MeOH. Greenish blue crystals of title compound were obtained (320 mg, 98.3%); MALDI-ToF-MS (C₃₂H₁₆N₈)⁺ m/z [M]⁺ calcd: 576.08 found: 576.11.

20. Synthesis of 5-(4-hydroxyphenyl)-10,15,20-tris(phenyl) porphyrin TPPOH (112)

To a mixture of p-Hydroxybenzaldehyde (3.05g, 25 mmol) and benzaldehyde (7.96g, 75 mmol) in propionic acid (200 ml), a freshly distilled pyrrole (7.17g, 107 mmol) was added and refluxed for (30 min). The reaction mixture was cooled down and 150 ml of MeOH was added. The reaction mixture was filtered and washed with methanol. A column chromatography was applied (silica gel, DCM/pet.ether (1:1)). A slow recrystallization from (MeOH/DCM) obtained purple solid of TPPOH 0.81g (5.2%); M.p>350°C. ¹H NMR (500 MHz, CDCl₃) δ 8.88 (d, *J* = 4.7 Hz, 2H), 8.84 (d, *J* = 4.6 Hz, 6H), 8.22 (d, *J* = 8.0 Hz, 6H), 8.08 (d, *J* = 8.5 Hz, 2H), 7.79 – 7.73 (m, 9H), 7.21 (d, *J* = 8.5 Hz, 2H), -2.77 (s, 2H). MALDI-ToF-MS (C₄₄H₃₀N₄O)⁺ m/z [M]⁺ calcd: 630.24 found: 630.25.

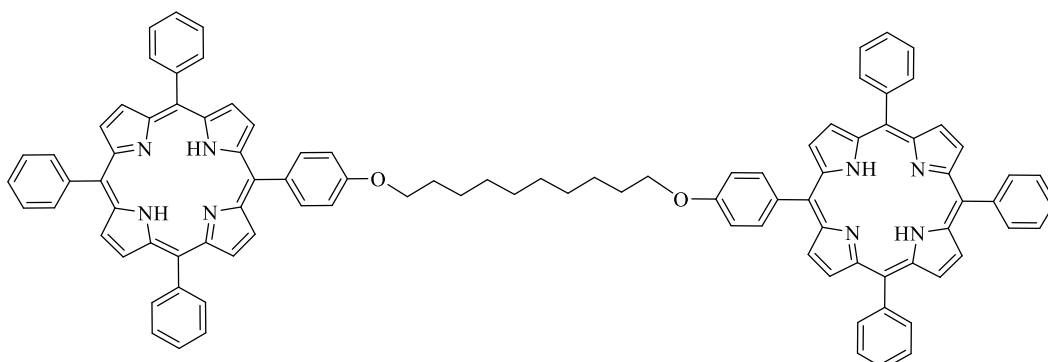
21. Synthesis of (TPPO(CH₂)₁₀Br) (113)



Method A:

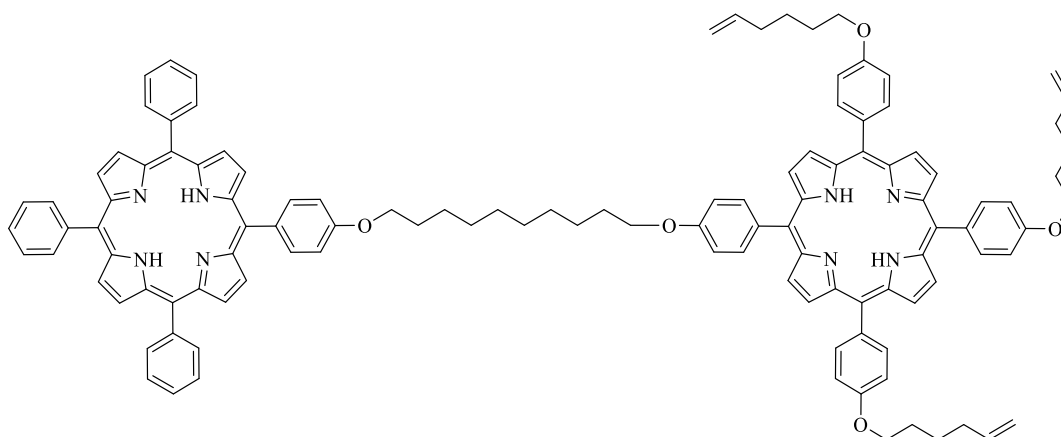
Following a modified version of Williamson's general procedure⁹² and Cammidge *et al.* methodology⁴, A mixture of 24 (100 mg, 0.16 mmol, 1 eq) and 1,10-dibromodecane (100 mg, 0.333mmol, ~2.1 eq) were dissolved in 25 ml of acetone. Excess of K₂CO₃ (60mg, 0.434mmol) and dibenzo-6-crown-18 (0.1 g, 0.2 mmol) were added to the mixture then stirred at rt for 48h under N₂. The crude mixture was poured to 50 ml of distilled water and organic layer recovered by DCM (50 ml). The organic layer was washed several times then dried over MgSO₄. The titled compound was obtained in first fraction from column chromatography DCM/Hexane (1:1) followed by a slow recrystallization from (MeOH/DCM) as a pure purple solid (72.6mg, 53.81%) m.p>350°C. ¹H NMR (500 MHz, CDCl₃) δ 8.89 (d, *J* = 4.7 Hz, 2H), 8.83 (s, 6H), 8.22 (d, *J* = 6.3 Hz, 6H), 8.14 – 8.09 (m, 2H), 7.80 – 7.72 (m, 9H), 7.28 (d, *J* = 7.8 Hz, 2H), 4.26 (t, *J* = 6.5 Hz, 2H), 3.44 (t, *J* = 6.9 Hz, 2H), 1.93 – 1.86 (m, 4H), 1.44 – 1.34 (m, *J* = 3.8 Hz, 8H), 0.90 – 0.82 (m, 4H), -2.76 (s, 2H). ¹³C NMR (126 MHz, CDCl₃) δ 134.57 (s), 127.78 – 127.55 (m), 126.68 (s), 112.76 (s), 77.23 (s).

22. Synthesis of Dyad (TPPO(CH₂)₁₀TPPO)⁴

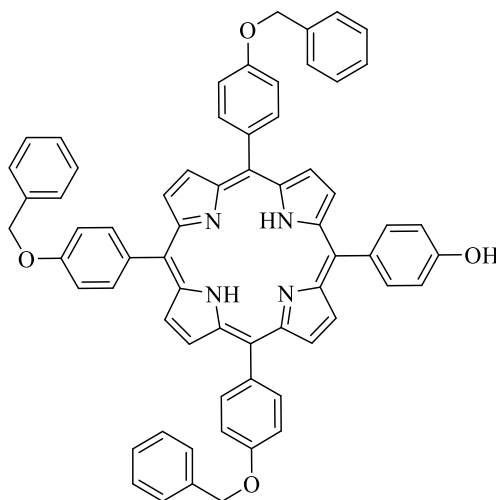


Following a modified version of Williamson's general procedure⁹² and Cammidge *et al.* methodology⁴, A mixture of **24** (200 mg, 0.317 mmol, 2.03 eq) and 1,10-dibromodecane (47 mg, 0.156 mmol, 1 eq) were dissolved in 10 ml of DMF. Excess of K₂CO₃ (0.22 g, 1.6 mmol) and dibenzo-6-crown-18 (0.1 g, 0.2 mmol) were added to the mixture then heated at 60 °C for 24h under N₂. The crude mixture was poured to 50 ml of brain and organic layer recovered by EtOAc (50 ml). The organic layer was washed several times then dried over MgSO₄. The solvent was removed to dryness, then redissolved in DCM. The crude separated by column chromatography using (EtOAc/DCM/Hexane 1:9:40). The target compound was obtained from second fraction and recrystallization from (MeOH/DCM), a pure purple solid of title compound (57 mg, ~26 %) m.p.>350°C. ¹H NMR (500 MHz, CDCl₃) δ 8.89 (d, *J* = 4.7 Hz, 2H), 8.83 (s, 6H), 8.22 (d, *J* = 6.3 Hz, 6H), 8.14 – 8.09 (m, 2H), 7.80 – 7.72 (m, 9H), 7.28 (d, *J* = 7.8 Hz, 2H), 4.26 (t, *J* = 6.5 Hz, 2H), 3.44 (t, *J* = 6.9 Hz, 2H), 1.93 – 1.86 (m, 4H), 1.44 – 1.34 (m, *J* = 3.8 Hz, 8H), 0.90 – 0.82 (m, 4H), -2.76 (s, 2H). ¹³C NMR (126 MHz, CDCl₃) δ 134.57 (s), 127.78 – 127.55 (m), 126.68 (s), 112.76 (s), 77.23 (s). MALDI-ToF-MS (C₉₈H₇₉N₈O₂)⁺ m/z [M+H]⁺ calcd: 1399.62 found: 1400.33.

23. Synthesis of asymmetrical Porphyrin C₁₀ dyad (114)

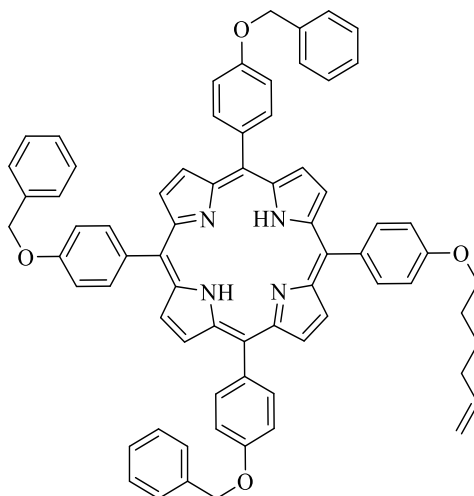


Following a modified version of Williamson's general procedure⁹² and simulating a modified version of Lucas's work⁹⁴, a mixture of **15** (10 mg, 0.21 mmol, 2 eq.) and (10 mg, 0.10 mmol, 1 eq.) were dissolved in acetone (10 ml), then an excess of potassium carbonate (50 mg, 0.36 mmol, 2.26 eq.) and dibenzo-6-crown-18 were added. The mixture was stirred in room temperature for 3 days. The reaction was quenched by water (150 ml) and DCM was added to recover organic material. The mixture separated and the organic layer dried over MgSO₄. The crude mixture was purified by column chromatography using DCM. A purple solid of title compound was obtained (107 mg, 49%) in first fraction. ¹H NMR (500 MHz, CD₂Cl₂) δ 8.92 – 8.80 (m, 16H), 8.07 (d, *J* = 8.4 Hz, 8H), 8.02 (d, *J* = 8.3 Hz, 8H), 7.29 – 7.21 (m, 8H), 7.16 (d, *J* = 8.4 Hz, 8H), 5.99 – 5.85 (m, 6H), 5.13 – 5.06 (m, 6H), 5.06 – 4.99 (m, 6H), 4.22 (q, *J* = 6.7 Hz, 8H), 4.12 (t, *J* = 6.4 Hz, 8H), 2.28 – 2.22 (m, 6H), 2.23 – 2.17 (m, 8H), 2.02 – 1.94 (m, 10H), 1.94 – 1.87 (m, 8H), 1.76 – 1.70 (m, 6H), 1.69 – 1.62 (m, 12H), -2.80 (s, 4H); ¹³C NMR (126 MHz, CD₂Cl₂) δ 206.45, 159.21, 159.15, 159.10, 138.87, 135.66, 135.62, 134.35, 134.31, 119.95, 114.55, 114.53, 112.83, 112.81, 112.79, 112.74, 68.44, 68.21, 68.13, 41.42, 36.21, 33.85, 33.60, 30.67, 29.59, 28.96, 28.68, 27.76, 26.29, 25.87, 25.56, 22.43 and 20.52 (s); IR (KBr, cm⁻¹): 3072, 2936, 1639, 1606, 1506, 1470, 1350, 1284, 1244, 1173, 1108, 966, 910, 801 and 735; UV-vis, (DCM)/nm (log ε): 422 (5.23), 455 (4.16), 519 (4.32), 557 (4.21), 593 (3.93), 651 (3.97) and 949 (3.59); MALDI-ToF-MS (C₁₁₆H₁₀₈N₈O₅)⁺ m/z [M]⁺ calcd: 1692.84 found: 1693.29

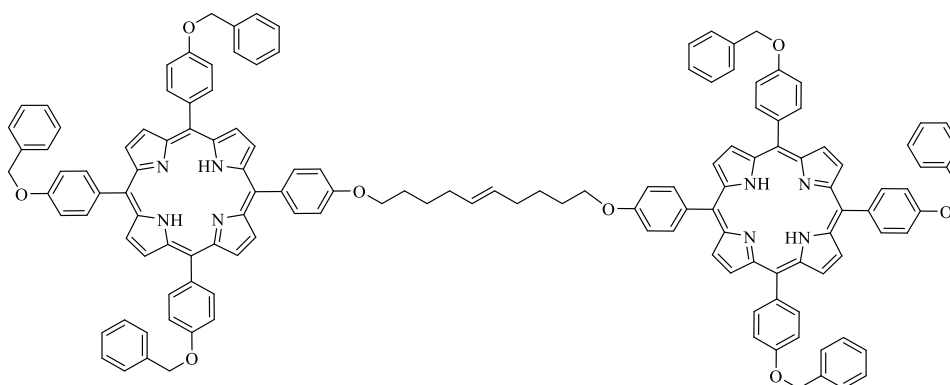
24. Synthesis of 5,10,15-Tris-[*p*-(benzyle)phenyl]-20-(4-hydroxyphenyl) porphyrin (115)

Following a modified version of Adler's general procedure^{48,49}, freshly distilled pyrrole (6.7 g, 100 mmol, 4 eq.) was added dropwise to a mixture of *p*-5-hexenyloxybenzaldehyde (15.91 g, 75 mmol, 3 eq.) and *p*-hydroxybenzaldehyde (3.05 g, 25 mmol, 1eq.) in refluxing propionic acid (350 ml). After refluxing for 30 min, the mixture was cooled down to room temperature and MeOH (400 ml) added. After one day, the crude mixture was filtered and washed several times by MeOH. The crude was dissolved in DCM (10 ml) and loaded on column chromatography. DCM was eluted first fraction, and the title compound was eluted using DCM/EtOAc (9:1) from second fraction afforded (2.1 g, 8.86%); MALDI-ToF-MS ($C_{65}H_{48}N_4O_4$)⁺ m/z [M]⁺ calcd: 948.36 found: 948.35.

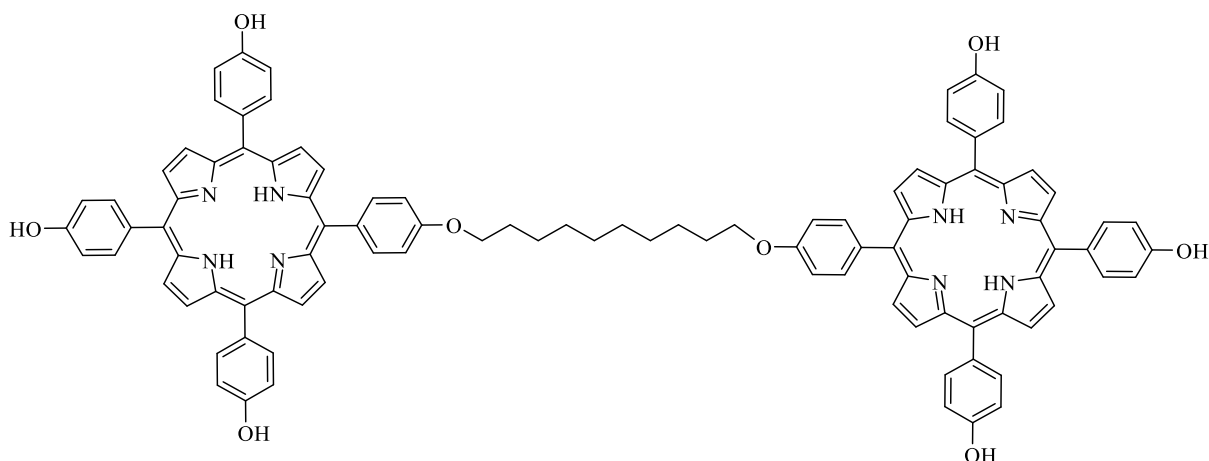
25. Synthesis of 5,10,15-Tris-[p-(benzyle)phenyl]-20-(4-hexe-5-ene-oxyphenyl) porphyrin (116)



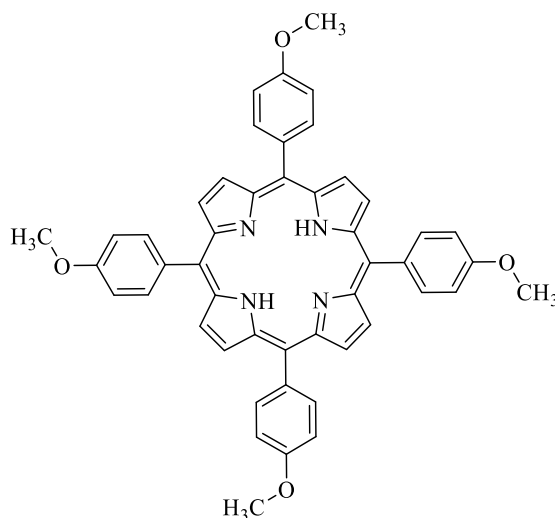
Following a modified version of Williamson's general procedure⁹², a mixture of **27** (1.8 g, 1.89 mmol, 1 eq.) and 6-bromo-1-hexene (1 ml, 1.22 g, 7.48 mmol, 4 eq.) were dissolved in DMF (20 ml), then an excess of potassium carbonate (1.4 g, 0.36 mmol, 2.26 eq.) was added. The mixture was stirred under N₂ at 100°C for 18h. The reaction was quenched by brine (3×50ml) and organic materials recovered by EtOAc. The mixture separated and the organic layer dried over MgSO₄. After recrystallisation from DCM/MeOH, purple solid of title compound was obtained (1.8 g, 92.3%). ¹H NMR (500 MHz, CDCl₃) δ 8.87 (s, 8H), 8.15 – 8.11 (m, 6H), 8.12 – 8.08 (m, 2H), 7.67 – 7.62 (m, 6H), 7.51 (t, *J* = 7.6 Hz, 6H), 7.43 (t, *J* = 7.5 Hz, 3H), 7.40 – 7.34 (m, 6H), 7.28 (d, *J* = 8.4 Hz, 2H), 5.94 (ddt, *J* = 16.9, 10.3, 6.6 Hz, 1H), 5.36 (s, 6H), 5.14 (dq, *J* = 17.2, 1.7 Hz, 1H), 5.06 (ddd, *J* = 10.2, 2.2, 1.2 Hz, 1H), 4.27 (t, *J* = 6.4 Hz, 2H), 2.27 (q, *J* = 7.2 Hz, 2H), 2.05 – 1.98 (m, 2H), 1.80 – 1.72 (m, 2H), -2.75 (s, 2H). ¹³C NMR (126 MHz, CDCl₃) δ 158.67, 137.07, 135.65, 128.76, 128.18, 127.77, 113.10, 77.27, 77.02, 76.76, 70.41, 33.58, 31.25, 29.71, 29.47, 28.96. MALDI-ToF-MS (C₇₁H₅₇N₄O₄)⁺ *m/z* [M-H]⁺ calcd: 1029.44 found: 1029.12.

26. Synthesis of 5,10,15-Tris-[*p*-(benzyle)phenyl]-20-(4-hydroxyphenyl) porphyrin (117)

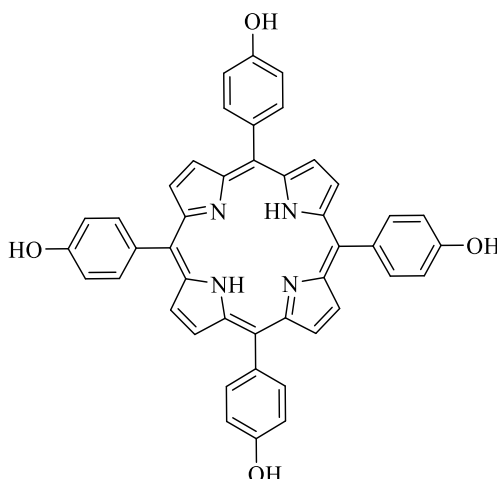
A modified version of a general methodology of GrubbsTM metatheses, solution of 28 (0.430 g, 0.40 mmol, 2 eq) in dry DCM (40 ml) was degassed by N₂ for 10 min. A degassed solution of 1st generation of GrubbsTM (67 mg, 0.081 mmol, 0.2 eq) in dry DCM (10 ml) was added to a reaction mixture using cannula then left stirring for 48h. After completion, the reaction was quenched by opened to air. The solvent removed to dryness, and the residual was purified by column chromatography using DCM then DCM/EtOAc (9:1). A purple solid of title compound was obtained from second fraction afforded (0.420 g, 91.3%); ¹H NMR (500 MHz, CDCl₃) δ 8.87 (s, 16H), 8.16 – 8.08 (m, 16H), 7.64 (d, *J* = 7.3 Hz, 12H), 7.51 (t, *J* = 7.6 Hz, 12H), 7.43 (t, *J* = 7.0 Hz, 6H), 7.37 (d, *J* = 8.4 Hz, 12H), 7.32 (t, *J* = 8.1 Hz, 2H), 7.28 (d, *J* = 8.5 Hz, 2H), 6.36 (t, *J* = 7.0 Hz, 1H), 6.32 (t, *J* = 7.0 Hz, 1H), 5.36 (s, 12H), 4.30 (t, *J* = 6.4 Hz, 2H), 4.27 (t, 2H), 2.43 (q, *J* = 7.1 Hz, 2H), 2.28 (dt, *J* = 19.9, 7.2 Hz, 2H), 2.09 – 2.03 (m, 2H), 2.04 – 1.98 (m, 2H), 1.85 (p, *J* = 7.4 Hz, 2H), 1.78 – 1.69 (m, 2H), -2.75 (s, 4H).

27. Synthesis of 5,10,15-Tris-[*p*-(benzyle)phenyl]-20-(4-hydroxyphenyl) porphyrin (118)

Following a modified version of general hydrogen transferred methodology developed by Meienhofer *et al.*⁸³, a mixture of 29 (0.4 g, 0.19 mmol, 1 eq) and Pd/C 10% (10 mg) were dissolved in 1,4-cyclohexadiene (1 ml, 10.9 mmol, 57 eq). The mixture was heated in sealed vessel in an oil bath at 100°C for 2d. The catalyst was filtered, and the solvent was evaporated to dryness. A green solid of title compound was obtained (400 mg, 99%); MALDI-ToF-MS ($C_{98}H_{78}N_8O_8$)⁺ m/z [M]⁺ calcd: 1494.59 found:1494.01.

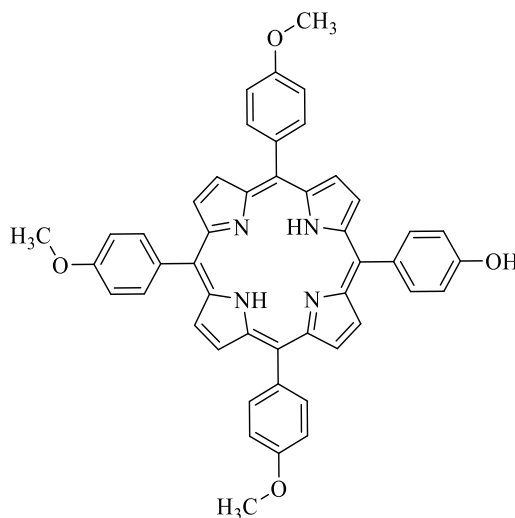
28. Synthesis of 5,10,15,20-Tetra-*p*-(methoxy)phenyl porphyrin (TMeTPP)⁴⁹(81)

Following a modified version of Adler's general procedure,^{48,49} freshly distilled pyrrole (3.35 g, 50 mmol, 1 eq.) was added dropwise to *p*-methoxybenzaldehyde (6.806g, 50 mmol, 1 eq.) in refluxing propionic acid (150 ml). After refluxing for 30 min, the mixture was cooled down to room temperature and MeOH (200 ml) added. After one days, the mixture was filtered and washed several times by MeOH. A purple solid of title compound was obtained (3 g, 32.6%); ¹H NMR (500 MHz, Chloroform-*d*) δ 8.86 (s, 8H), 8.15 – 8.10 (m, 8H), 7.31 – 7.27 (m, 8H), 4.10 (s, 12H), -2.75 (s, 2H); MALDI-ToF-MS (C₄₈H₃₇N₄O₄)⁺ m/z [M-H]⁺ calcd: 733.29 found: 733.39.

29. Synthesis of 5,10,15,20-Tetra-*p*-(hydroxy)phenyl porphyrin⁹⁶ (102)

Following a modified version of McOmin *et al.* general procedure⁷¹ Boron tribromide (2.85 g, 11.42 mmol, 8 eq.) was added dropwise to TMeTPP (11) (1.051 g, 1.429 mmol, 1 eq.) in dry DCM (25 ml) under flow of N₂ at -10C then left stirred at rt overnight. After completion, water (50 ml) added and neutralised using TEA. A purple solid of title compound was obtained (0.92 g, 95.83%); MALDI-ToF-MS (C₄₄H₃₁N₄O₄)⁺ m/z [M+H]⁺ calcd: 679.23 found: 679.23.

**30. Synthesis of 5,10,15-Tris-[*p*-(methoxy)phenyl]-20-(4-hydroxyphenyl) porphyrin⁹⁷
(103)**



Method A:

Following a modified version of Adler's general procedure,^{48,49} freshly distilled pyrrole (3.35 g, 50 mmol, 4 eq.) was added dropwise to a mixture of *p*-methoxybenzaldehyde (5.10 g, 37.5 mmol, 3 eq.) and *p*-hydroxybenzaldehyde (1.525 g, 12.5 mmol, 1eq.) in refluxing propionic acid (150 ml). After refluxing for 30 min, the mixture was cooled down to room temperature and MeOH (200 ml) added. After one day, the mixture was filtered and purified by column chromatography using chloroform. The target compound was collected from second fraction using chloroform/MeOH (19:1). A purple solid of title compound was obtained (0.35 g, 3.8%); ¹H NMR (500 MHz, Chloroform-*d*) δ 8.86 (d, *J* = 4.6 Hz, 8H), 8.15 – 8.10 (m, 6H), 8.04 (dd, *J* = 8.0, 6.4 Hz, 2H), 7.31 – 7.27 (m, 6H), 7.13 (d, *J* = 8.2 Hz, 2H), 4.10 (s, 6H), 4.09 (s, 3H), -2.75 (s, 2H); MALDI-ToF-MS (C₄₇H₃₆N₄O₄)⁺ *m/z* [M-H]⁺ calcd: 720.27 found: 720.33.

6. References

- (1) Lindoy, L. F.; Atkinson, I. M. *Self-assembly in supramolecular systems*; Royal Society of Chemistry, 2000.
- (2) Lehn, J. M. *Angewandte Chemie International Edition in English* **1990**, *29*, 1304.
- (3) Birin, K. P.; Poddubnaya, A. I.; Gorbunova, Y. G.; Tsivadze, A. Y. *Macrocyclic Chemistry* **2017**, *10*, 514.
- (4) González-Lucas, D.; Soobrattee, S. C.; Hughes, D. L.; Tizzard, G. J.; Coles, S. J.; Cammidge, A. N. *Chemistry – A European Journal* **2020**, *26*, 10724.
- (5) Bruns, C. J.; Stoddart, J. F. *The nature of the mechanical bond: from molecules to machines*; John Wiley & Sons, 2016.
- (6) De Bo, G. *Chemical science* **2018**, *9*, 15.
- (7) Mondal, P.; Rath, S. P. *Coordination Chemistry Reviews* **2020**, *405*, 213117.
- (8) Totten, R. K.; Ryan, P.; Kang, B.; Lee, S. J.; Broadbelt, L. J.; Snurr, R. Q.; Hupp, J. T.; Nguyen, S. T. *Chemical Communications* **2012**, *48*, 4178.
- (9) Kubo, Y.; Kitada, Y.; Wakabayashi, R.; Kishida, T.; Ayabe, M.; Kaneko, K.; Takeuchi, M.; Shinkai, S. *Angewandte Chemie International Edition* **2006**, *45*, 1548.
- (10) Wakabayashi, R.; Kaneko, K.; Takeuchi, M.; Shinkai, S. *New Journal of Chemistry* **2007**, *31*, 790.
- (11) Hajjaj, F.; Tashiro, K.; Nikawa, H.; Mizorogi, N.; Akasaka, T.; Nagase, S.; Furukawa, K.; Kato, T.; Aida, T. *Journal of the American Chemical Society* **2011**, *133*, 9290.
- (12) Ooyama, Y.; Enoki, T.; Ohshita, J.; Kamimura, T.; Ozako, S.; Koide, T.; Tani, F. *RSC advances* **2017**, *7*, 18690.
- (13) Anderson, H. L.; Sanders, J. K. M. *Journal of the Chemical Society, Chemical Communications* **1989**, 1714.
- (14) Anderson, S.; Anderson, H. L.; Sanders, J. K. M. *Journal of the Chemical Society, Perkin Transactions 1* **1995**, 2255.
- (15) Rickhaus, M.; Jirasek, M.; Tejerina, L.; Gotfredsen, H.; Peeks, M. D.; Haver, R.; Jiang, H.-W.; Claridge, T. D. W.; Anderson, H. L. *Nature Chemistry* **2020**, *12*, 236.
- (16) Kang, B.; Totten, R. K.; Weston, M. H.; Hupp, J. T.; Nguyen, S. T. *Dalton Transactions* **2012**, *41*, 12156.
- (17) Walter, C. J.; Anderson, H. L.; Sanders, J. K. M. *Journal of the Chemical Society, Chemical Communications* **1993**, 458.
- (18) Kagan, N. E.; Mauzerall, D.; Merrifield, R. B. *Journal of the American Chemical Society* **1977**, *99*, 5484.
- (19) Hunter, C. A.; Sanders, J. K. M.; Stone, A. J. *Chemical Physics* **1989**, *133*, 395.
- (20) García-Simón, C.; Garcia-Borràs, M.; Gómez, L.; Parella, T.; Osuna, S.; Juanhuix, J.; Imaz, I.; Maspoch, D.; Costas, M.; Ribas, X. *Nature Communications* **2014**, *5*, 5557.
- (21) **!!! INVALID CITATION !!! 21,22.**
- (22) Jongkind, L. J.; Caumes, X.; Hartendorp, A. P. T.; Reek, J. N. H. *Accounts of Chemical Research* **2018**, *51*, 2115
- (23) García-Simón, C.; Gramage-Doria, R.; Raoufmoghaddam, S.; Parella, T.; Costas, M.; Ribas, X.; Reek, J. N. H. *Journal of the American Chemical Society* **2015**, *137*, 2680.
- (24) Sawai, T.; Yamaguchi, Y.; Kitamura, N.; Date, T.; Konishi, S.; Taga, K.; Tanaka, K. *Applied Physics Letters* **2018**, *112*, 202902.
- (25) Cândida, M.; Shohoji, B. L.; Franco, M. L. T. M. B.; Lazana, M. C. R. L. R.; Nakazawa, S.; Sato, K.; Shiomi, D.; Takui, T. *AIP Conference Proceedings* **2000**, *503*, 333.

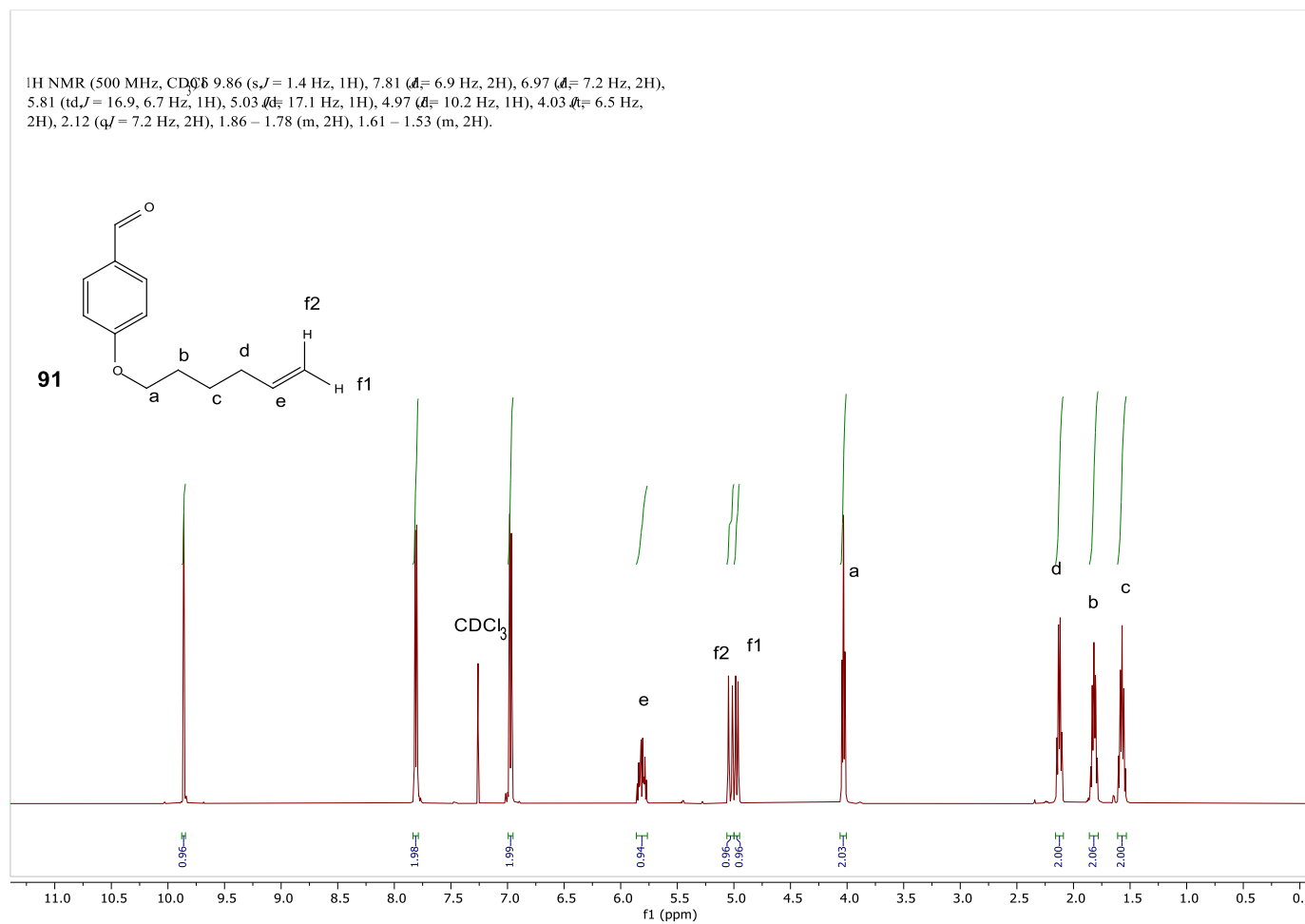
- (26) Kocher, L.; Durot, S.; Heitz, V. *Chemical Communications* **2015**, *51*, 13181.
- (27) Zhang, J.; Li, Y.; Yang, W.; Lai, S.-W.; Zhou, C.; Liu, H.; Che, C.-M.; Li, Y. *Chemical Communications* **2012**, *48*, 3602.
- (28) Zhang, J.; Zheng, X.; Jiang, R.; Yu, Y.; Li, Y.; Liu, H.; Li, Q.; Shuai, Z.; Li, Y. *RSC Advances* **2014**, *4*, 27389.
- (29) Durot, S.; Flamigni, L.; Taesch, J.; Dang, T. T.; Heitz, V.; Ventura, B. *Chem. Eur. J* **2014**, *20*, 9979.
- (30) Ding, H.; Meng, X.; Cui, X.; Yang, Y.; Zhou, T.; Wang, C.; Zeller, M.; Wang, C. *Chemical Communications* **2014**, *50*, 11162.
- (31) Dang, T. T.; Durot, S.; Monnereau, L.; Heitz, V.; Barbieri, A.; Ventura, B. *Dalton Transactions* **2017**, *46*, 9375.
- (32) Zhang, C.; Wang, Q.; Long, H.; Zhang, W. *Journal of the American Chemical Society* **2011**, *133*, 20995.
- (33) Ge, Y.; Huang, S.; Hu, Y.; Zhang, L.; He, L.; Krajewski, S.; Ortiz, M.; Jin, Y.; Zhang, W. *Nature Communications* **2021**, *12*, 1136.
- (34) Singh, S.; Aggarwal, A.; Farley, C.; Hageman, B. A.; Batteas, J. D.; Drain, C. M. *Chemical Communications* **2011**, *47*, 7134.
- (35) Rogers, L.; Burke-Murphy, E.; Senge, M. O. *European Journal of Organic Chemistry* **2014**, *2014*, 4283.
- (36) Vicente, M.; Smith, K. *Current organic synthesis* **2014**, *11*, 3.
- (37) Sauvage, J. P. *Molecular machines and motors*; Springer, 2001; Vol. 99.
- (38) Balzani, V.; Credi, A.; Venturi, M. *Molecular devices and machines; A journey into the nanoworld*; Wiley-vch: Weinheim, 2004.
- (39) Shemin, D.; Wittenberg, J. *Journal of Biological Chemistry* **1951**, *192*, 315.
- (40) Brody, T. *Nutritional biochemistry*; Elsevier, 1998.
- (41) Krebs, H. A.; Johnson, W. A. *Biochem J* **1937**, *31*, 645.
- (42) Hollingsworth, J., Louisiana State University, 2012.
- (43) Gouterman, M.; Wagnière, G. H.; Snyder, L. C. *Journal of Molecular Spectroscopy* **1963**, *11*, 108.
- (44) Zhang, A.; Kwan, L.; Stillman, M. J. *Organic & Biomolecular Chemistry* **2017**, *15*, 9081.
- (45) Rothmund, P. *Journal of the American Chemical Society* **1935**, *57*, 2010.
- (46) Calvin, M.; Ball, R. H.; Aronoff, S. *Journal of the American Chemical Society* **1943**, *65*, 2259.
- (47) Giovannetti, R. *Macro to nano spectroscopy* **2012**, *1*, 87.
- (48) Adler, A. D.; Longo, F. R.; Shergalis, W. *Journal of the American Chemical Society* **1964**, *86*, 3145.
- (49) Adler, A. D.; Longo, F. R.; Finarelli, J. D.; Goldmacher, J.; Assour, J.; Korsakoff, L. *The Journal of Organic Chemistry* **1967**, *32*, 476.
- (50) Lindsey, J. S.; Hsu, H. C.; Schreiman, I. C. *Tetrahedron letters* **1986**, *27*, 4969.
- (51) Jonathan S. Lindsey, I. C. S., Henry C. Hsu, Patrick C. Kearney, and Anne M. Marguerettaz *Journal of organic chemistry* **1987**, *52*.
- (52) Geier, G. R.; Lindsey, J. S. *Tetrahedron* **2004**, *60*, 11435.
- (53) Sun, Z.; Jiao, S.; Li, F.; Wen, J.; Yu, Y.; Liu, Y.; Cao, M.; Li, L.; Zhou, Y.; She, Y. *Asian Journal of Organic Chemistry* **2019**, *8*, 542.
- (54) Bradshaw, J. S.; Krakowiak, K. E.; Izatt, R. M. *The Chemistry of Heterocyclic Compounds, Aza-Crown Macrocycles*; John Wiley & Sons, 1993; Vol. 51.
- (55) Alkorbi, F.; Díaz-Moscoso, A.; Gretton, J.; Chambrier, I.; Tizzard, G. J.; Coles, S. J.; Hughes, D. L.; Cammidge, A. N. *Angewandte Chemie International Edition* **2021**, *60*, 7632.

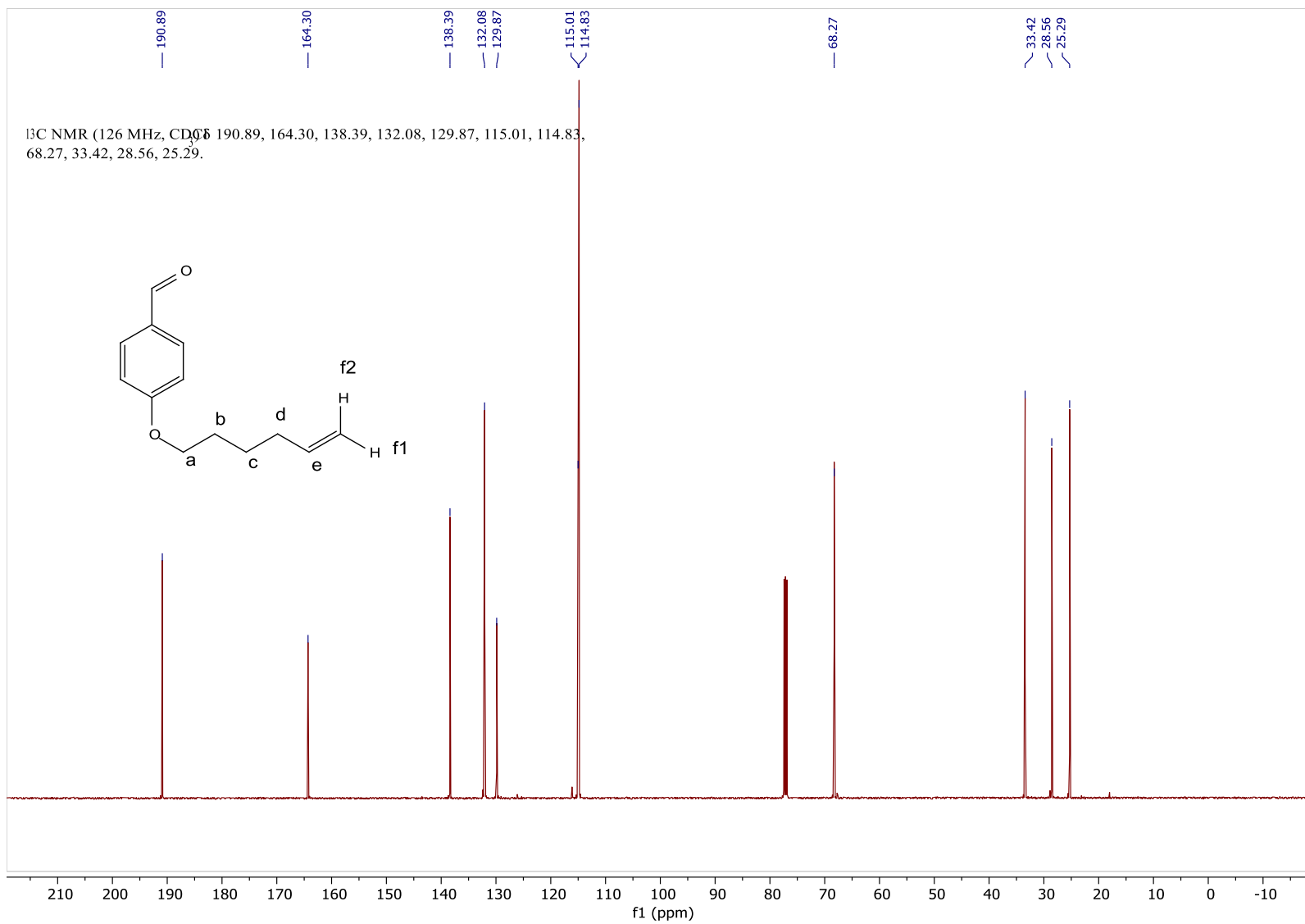
- (56) Alharbi, N.; Díaz-Moscoso, A.; Tizzard, G. J.; Coles, S. J.; Cook, M. J.; Cammidge, A. N. *Tetrahedron* **2014**, *70*, 7370.
- (57) Sun, X.; Li, D.; Chen, G.; Zhang, J. *Dyes and pigments* **2006**, *71*, 118.
- (58) Orian, L.; Carlotto, S.; Di Valentin, M.; Polimeno, A. *The Journal of Physical Chemistry A* **2012**, *116*, 3926.
- (59) Faure, S.; Stern, C.; Guillard, R.; Harvey, P. D. *Journal of the American Chemical Society* **2004**, *126*, 1253.
- (60) Dexter, D. L. *The Journal of Chemical Physics* **1953**, *21*, 836.
- (61) Cammidge, A. N.; Scaife, P. J.; Berber, G.; Hughes, D. L. *Organic letters* **2005**, *7*, 3413.
- (62) Ingram, G.; Zheng-Hong, L. *PHOTOE* **2014**, *4*, 040993.
- (63) Fleischer, E. B.; Wang, J. H. *Journal of the American Chemical Society* **1960**, *82*, 3498.
- (64) Prushan, M. *Semantic Scholar* **2005**.
- (65) Mironov, A. F. *Russian Chemical Reviews* **2013**, *82*, 333.
- (66) Bochkarev, M. N.; Pushkarev, A. P. *Organic Photonics and Photovoltaics* **2016**, *4*.
- (67) Werts, M. H.; Nerambourg, N.; Pélégry, D.; Le Grand, Y.; Blanchard-Desce, M. *Photochemical & Photobiological Sciences* **2005**, *4*, 531.
- (68) Birin, K. P.; Gorbunova, Y. G.; Yu. Tsivadze, A. *Journal of Porphyrins and Phthalocyanines* **2009**, *13*, 283.
- (69) Liu, F.; Velkos, G.; Krylov, D. S.; Spree, L.; Zalibera, M.; Ray, R.; Samoylova, N. A.; Chen, C.-H.; Rosenkranz, M.; Schiemenz, S.; Ziegs, F.; Nenkov, K.; Kostanyan, A.; Greber, T.; Wolter, A. U. B.; Richter, M.; Büchner, B.; Avdoshenko, S. M.; Popov, A. A. *Nature Communications* **2019**, *10*, 571.
- (70) Benton, F. L.; Dillon, T. E. *Journal of the American Chemical Society* **1942**, *64*, 1128.
- (71) McOmie, J.; Watts, M.; West, D. *Tetrahedron* **1968**, *24*, 2289.
- (72) Biggs, R. A.; Ogilvie, W. W. In *Comprehensive Organic Synthesis (Second Edition)*; Knochel, P., Ed.; Elsevier: Amsterdam, 2014, p 802.
- (73) Ashby, E.; Argyropoulos, J. *The Journal of Organic Chemistry* **1985**, *50*, 3274.
- (74) Kornblum, N.; Jones, W. J.; Anderson, G. J. *Journal of the American Chemical Society* **1959**, *81*, 4113.
- (75) Galanin, N.; Shaposhnikov, G. *Russian Journal of General Chemistry* **2012**, *82*, 764.
- (76) Zheng, W.; Wan, C.-Z.; Zhang, J.-X.; Li, C.-H.; You, X.-Z. *Tetrahedron Letters* **2015**, *56*, 4459.
- (77) Linstead, R. P.; Lowe, A. R. *Journal of the Chemical Society (Resumed)* **1934**, 1022.
- (78) Scholl, M.; Ding, S.; Lee, C. W.; Grubbs, R. H. *Organic Letters* **1999**, *1*, 953.
- (79) Dias, E. L.; Nguyen, S. T.; Grubbs, R. H. *Journal of the American Chemical Society* **1997**, *119*, 3887.
- (80) Sanford, M. S.; Love, J. A.; Grubbs, R. H. *Journal of the American Chemical Society* **2001**, *123*, 6543.
- (81) Fürstner, A.; Grela, K. *Angewandte Chemie International Edition* **2000**, *39*, 1234.
- (82) Eberhardt, M. K. *Tetrahedron* **1967**, *23*, 3029.
- (83) Felix, A. M.; Heimer, E. P.; Lambros, T. J.; Tzougraki, C.; Meienhofer, J. *The Journal of Organic Chemistry* **1978**, *43*, 4194.
- (84) Taesch, J.; Heitz, V.; Topić, F.; Rissanen, K. *Chemical Communications* **2012**, *48*, 5118.

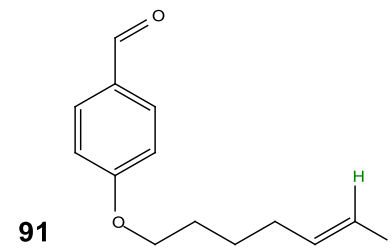
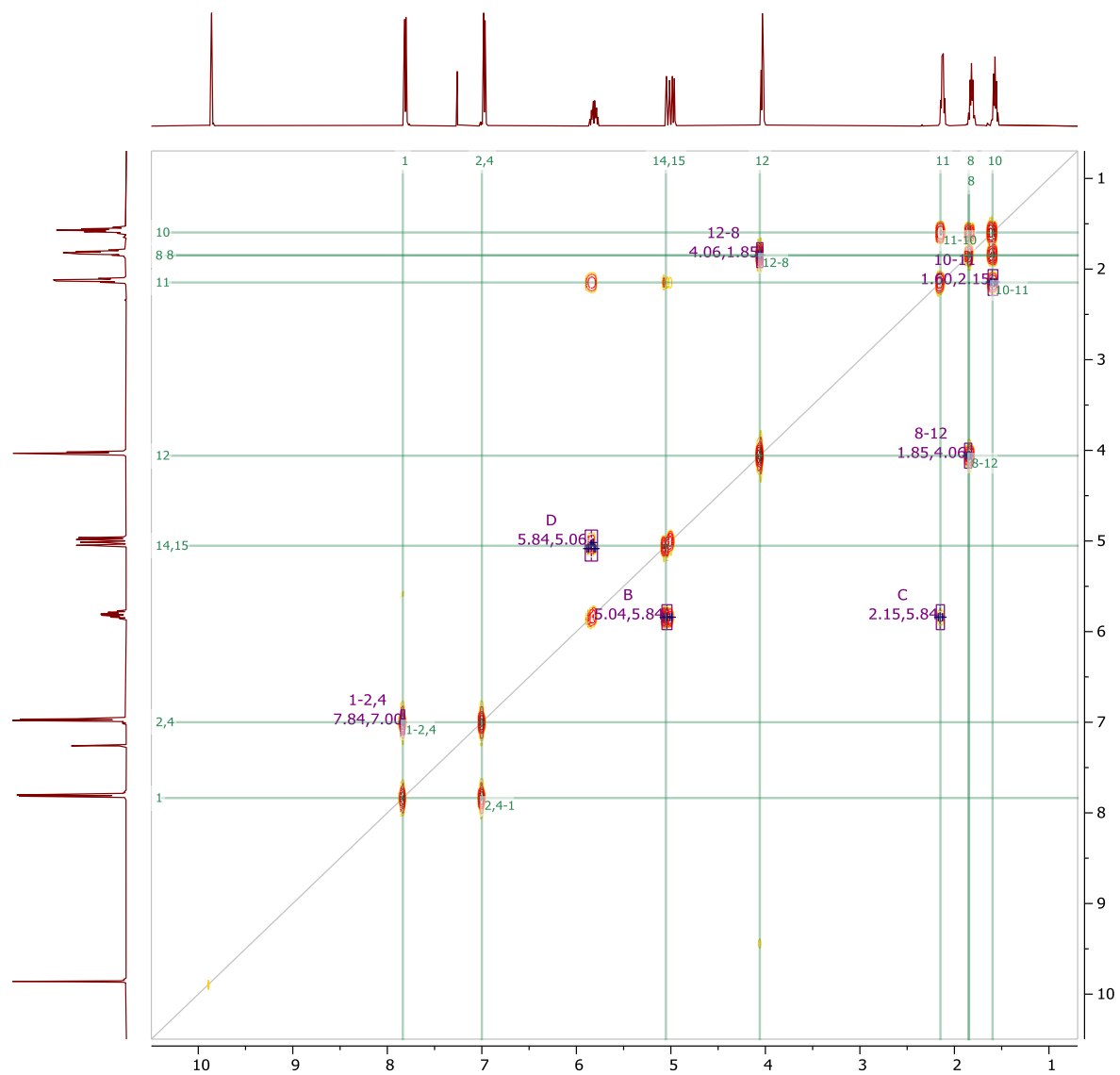
- (85) Denekamp, I. M.; Veenstra, F. L. P.; Jungbacker, P.; Rothenberg, G. *Applied Organometallic Chemistry* **2019**, *33*, e4872.
- (86) Schoepff, L.; Kocher, L.; Durot, S. p.; Heitz, V. r. *The Journal of organic chemistry* **2017**, *82*, 5845.
- (87) Walker, V. E.; Castillo, N.; Matta, C. F.; Boyd, R. J. *The Journal of Physical Chemistry A* **2010**, *114*, 10315.
- (88) Wang, K.; Zeng, S.; Wang, H.; Dou, J.; Jiang, J. *Inorganic Chemistry Frontiers* **2014**, *1*, 167.
- (89) Birin, K. P.; Gorbunova, Y. G.; Tsivadze, A. Y. *Dalton Transactions* **2011**, *40*, 11474.
- (90) Tran-Thi, T.-H.; Mattioli, T. A.; Chabach, D.; De Cian, A.; Weiss, R. *The Journal of Physical Chemistry* **1994**, *98*, 8279.
- (91) Mazumder, M. A. J. *Int. J. Electrochem. Sci* **2016**, *11*, 4050.
- (92) Williamson, A. W. *Quarterly Journal of the Chemical Society of London* **1852**, *4*, 229.
- (93) Smith, R. G.; Vanterpool, A.; Kulak, H. J. *Canadian Journal of Chemistry* **1969**, *47*, 2015.
- (94) González Lucas, D., University of East Anglia, 2014.
- (95) Quinn, J. F.; Razzano, D. A.; Golden, K. C.; Gregg, B. T. *Tetrahedron Letters* **2008**, *49*, 6137.
- (96) Berenbaum, M. C.; Akande, S. L.; Bonnett, R.; Kaur, H.; Ioannou, S.; White, R. D.; Winfield, U. J. *British Journal of Cancer* **1986**, *54*, 717.
- (97) Liu, J.; Chen, H.; Li, Y.; Chen, Y.; Mao, L.; Xu, A.; Wang, C. *Journal of Chemical Research* **2011**, *35*, 698.

7. APPENDIXES

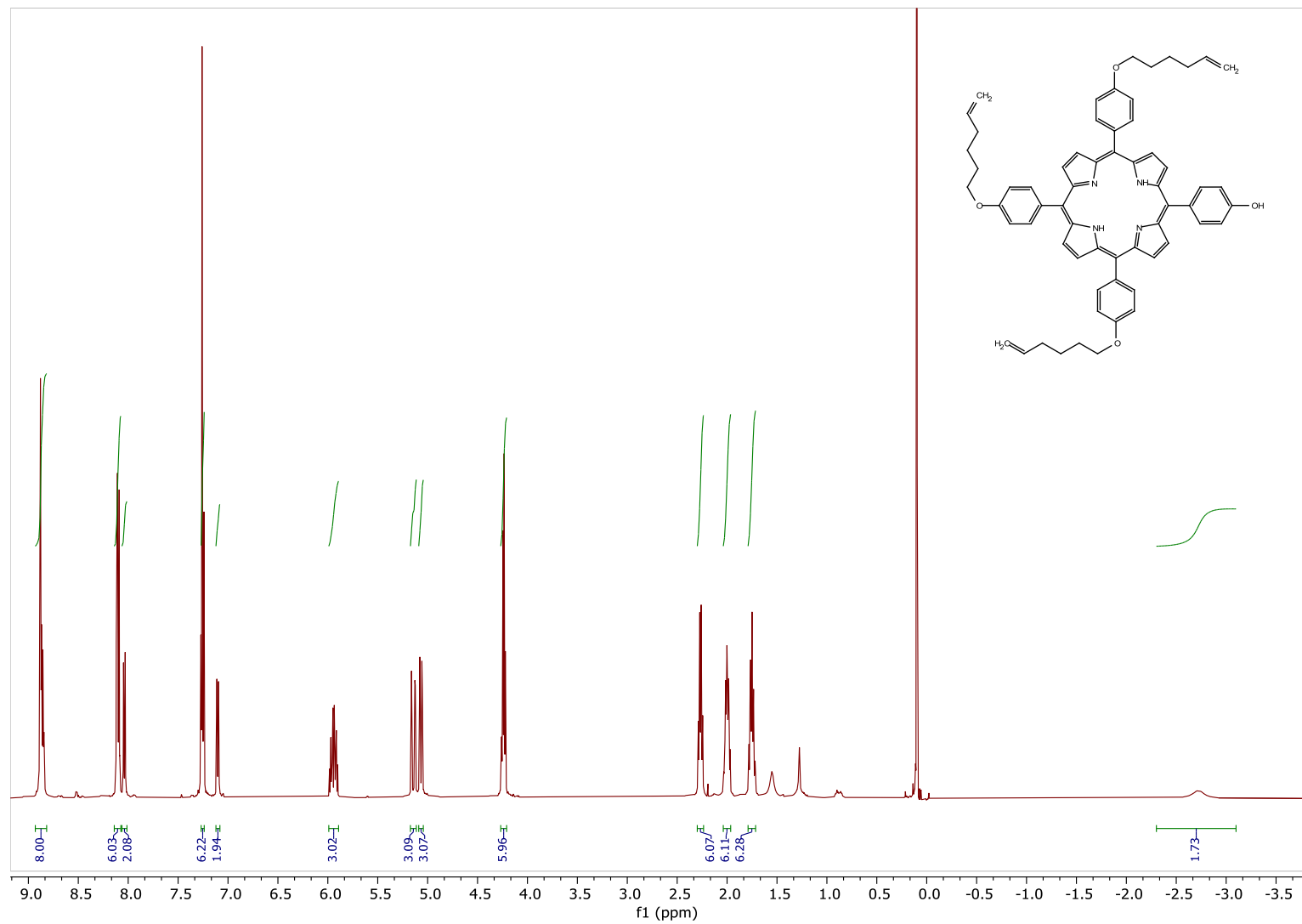
1. *P*-5-hexenyl-1-oxybenzaldehyde (91)

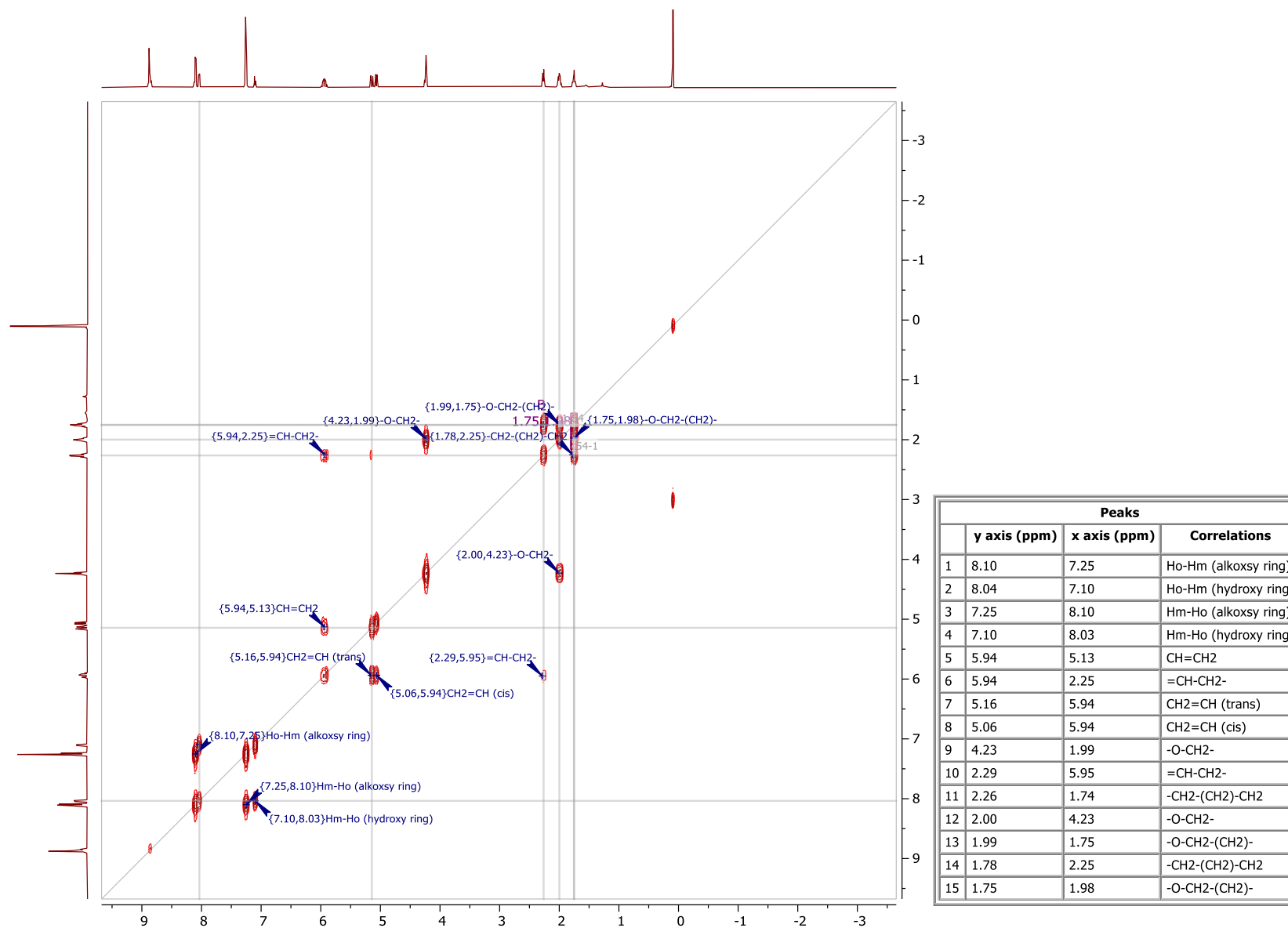


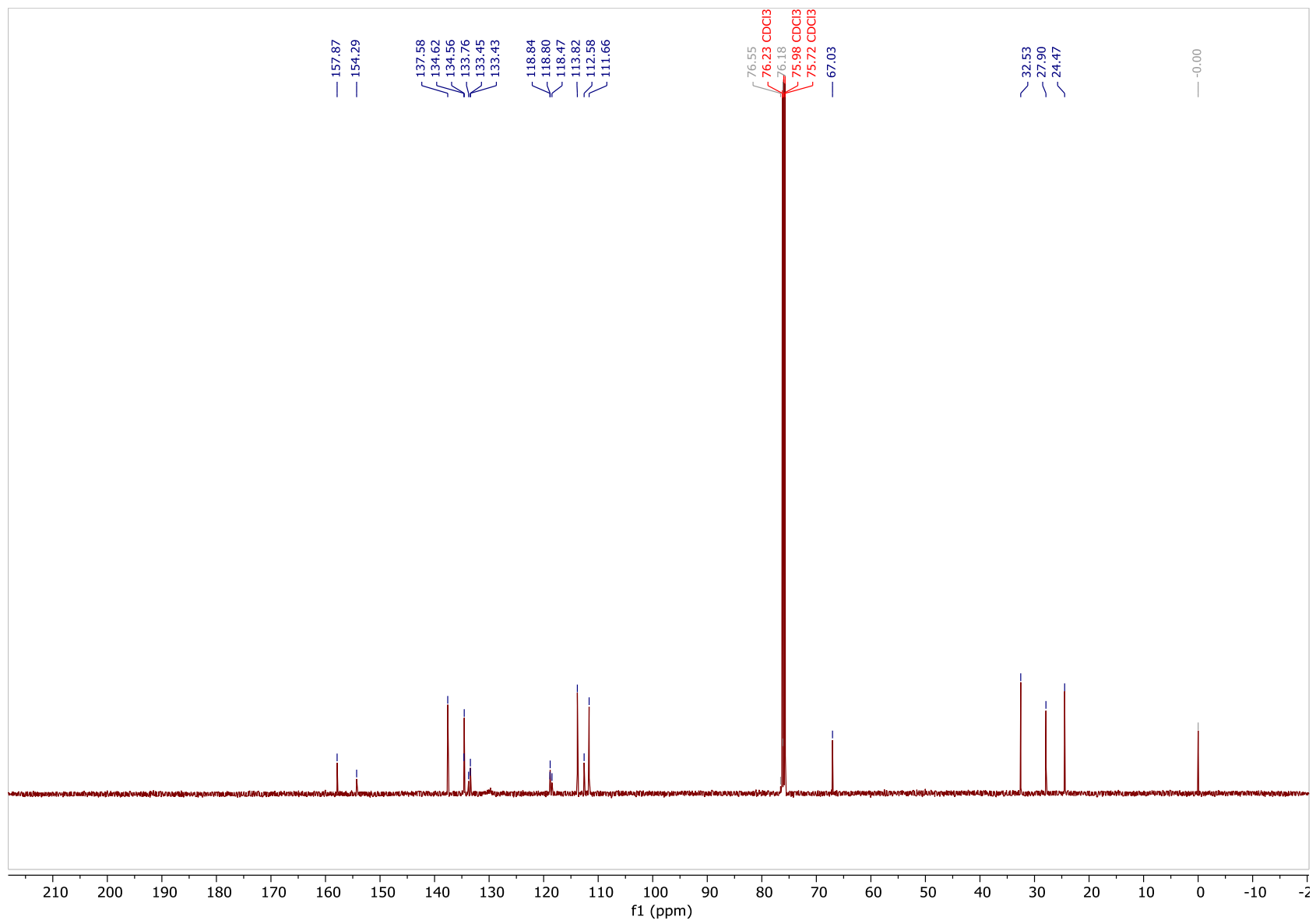




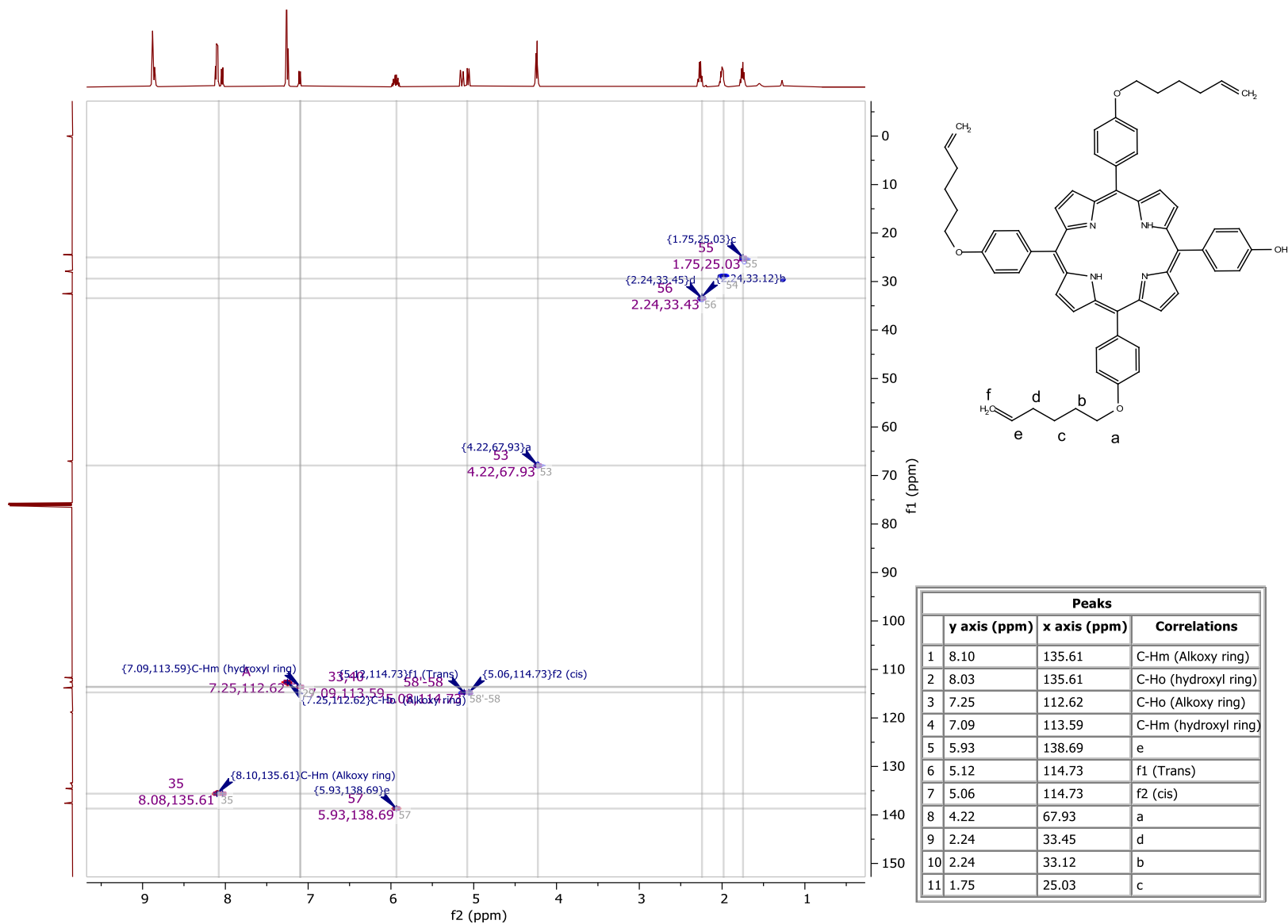
Peaks		
y axis (ppm)	x axis (ppm)	Correlations
1	7.84	Ho--Hm
2	7.01	Hm--Ho
3	5.07	CH=CH2 (trans)
4	4.99	CH=CH2 (cis)
5	4.07	-O-CH2-(CH2)-
6	2.17	-CH2-(CH2)-CH2-
7	2.13	=CH-CH2-
8	1.87	-O-CH2-(CH2)-
9	1.61	-CH2-(CH2)-CH2-

2. 5,10,15-Tris-[*p*-(5-hexenyl-1-oxy)phenyl]-20-(4-hydroxyphenyl)porphyrin (92)

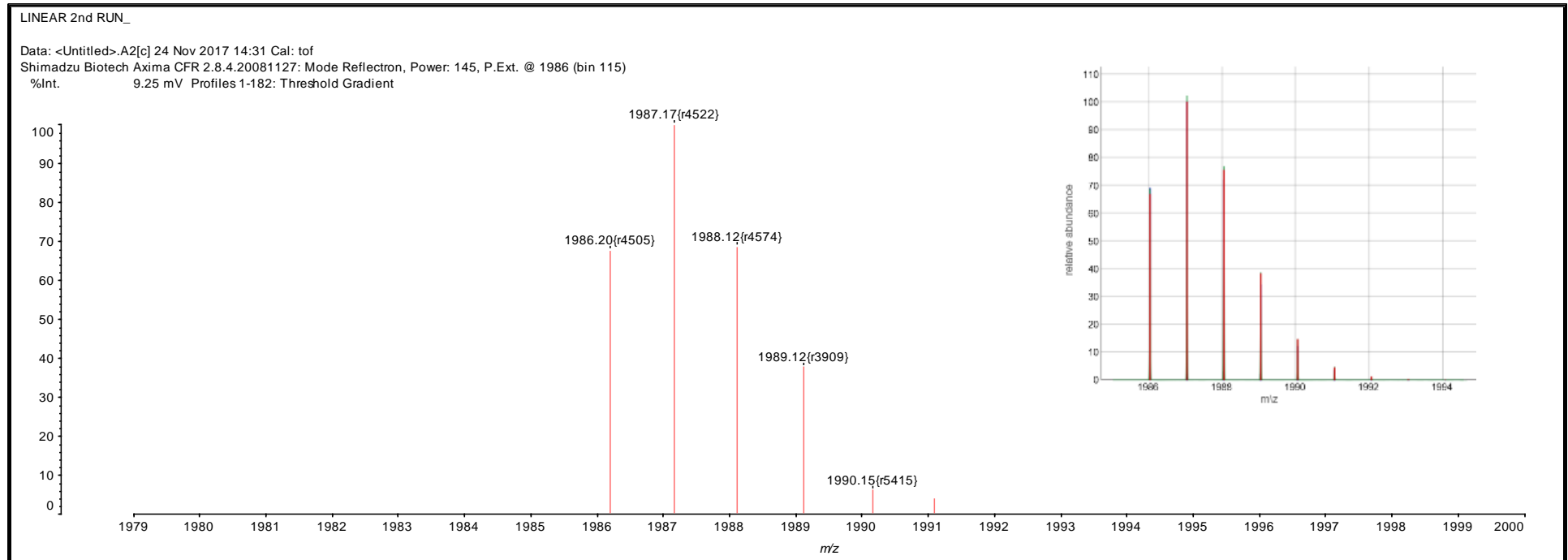


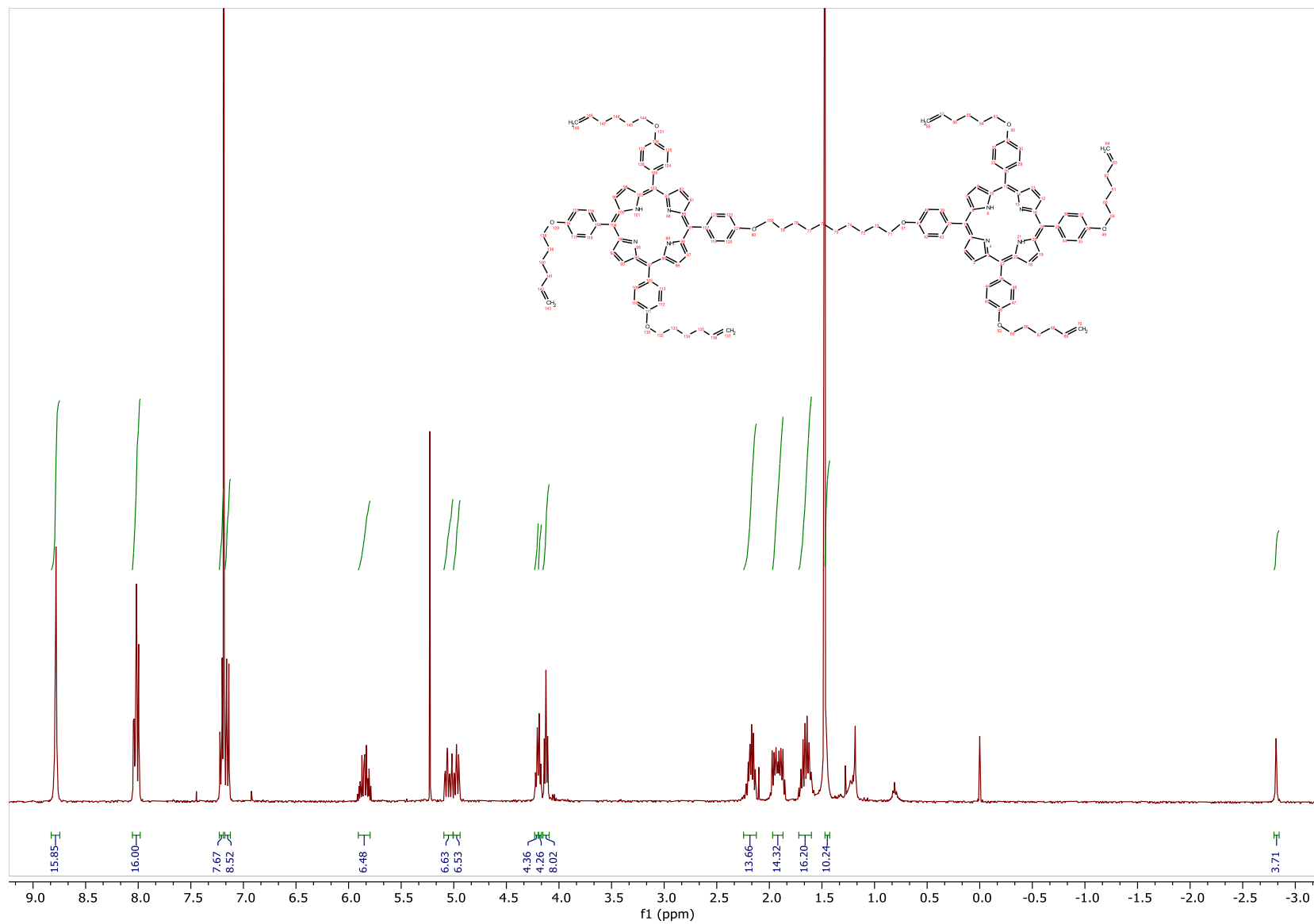


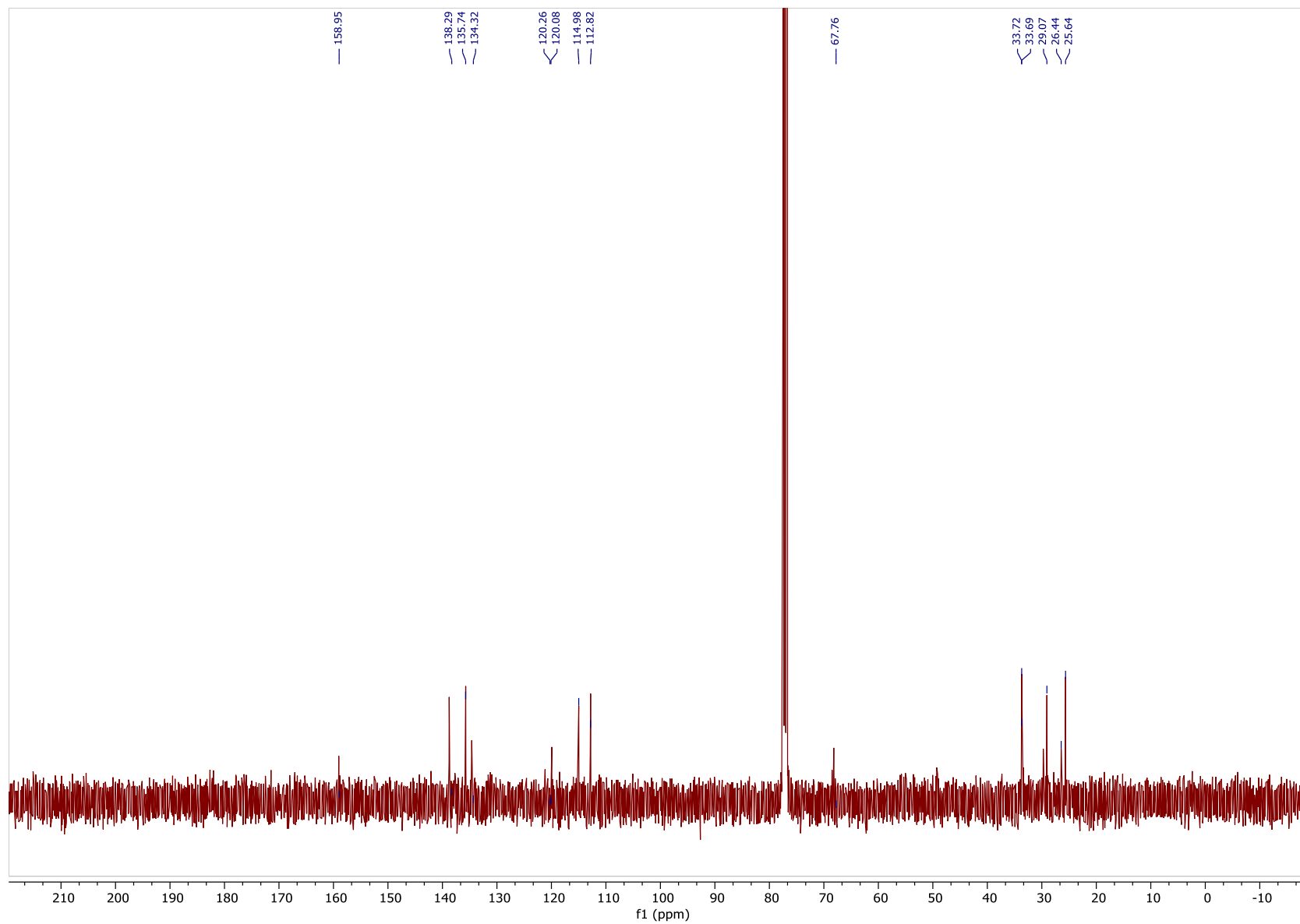
(141)



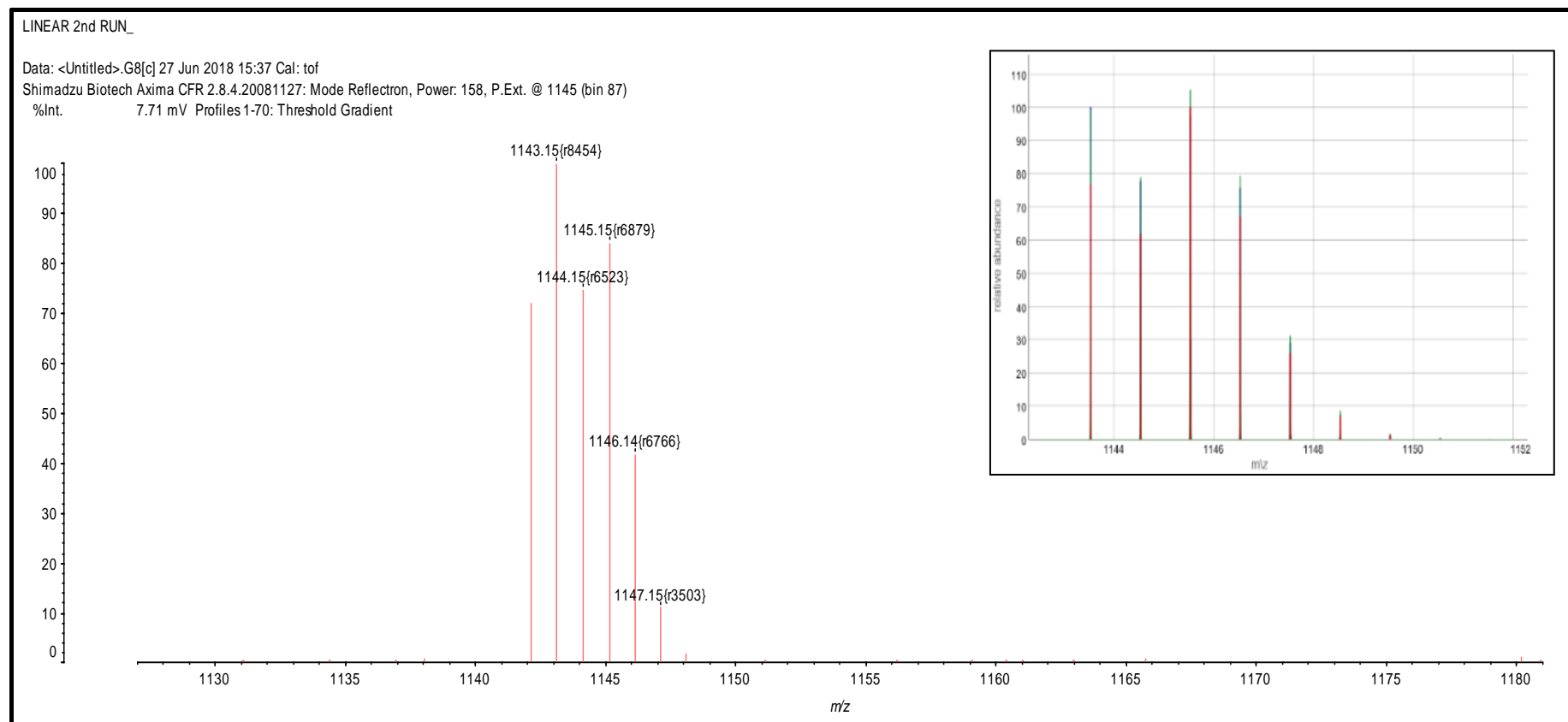
3. Dyad (93)



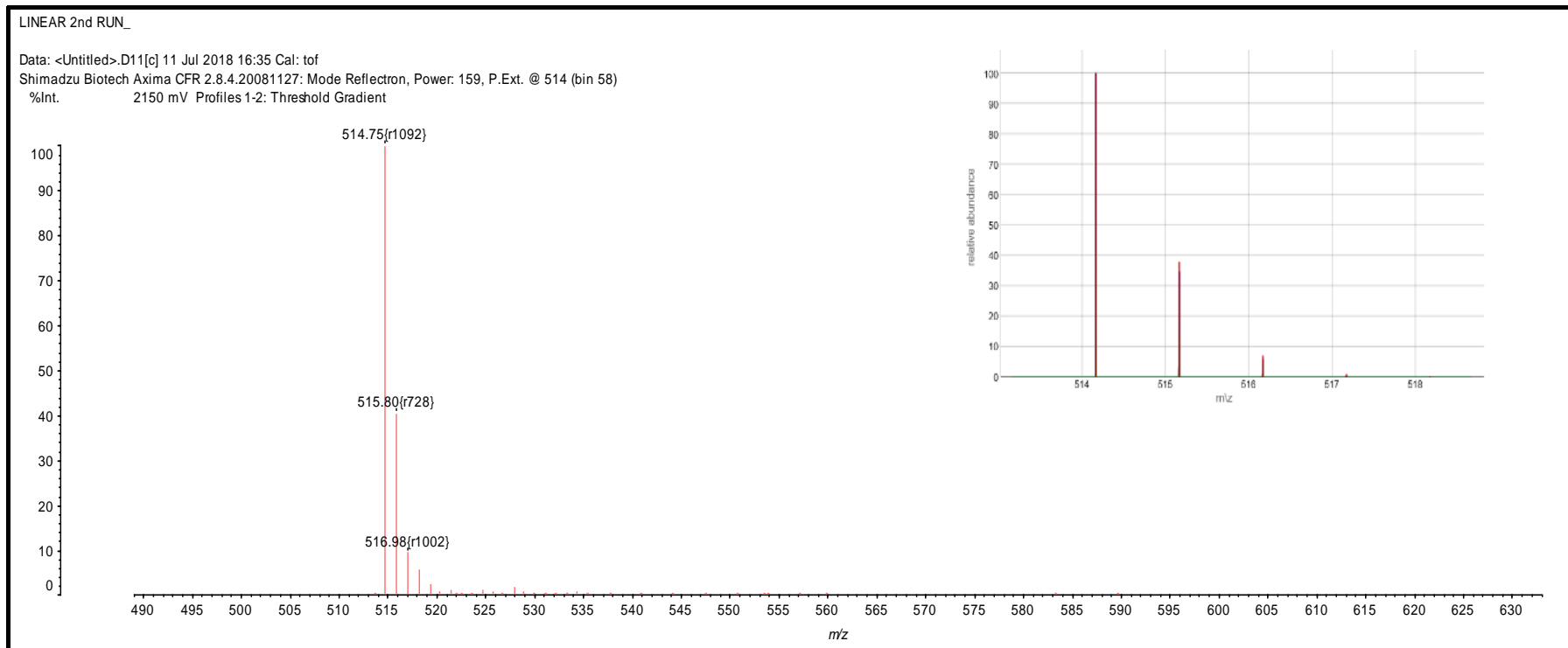




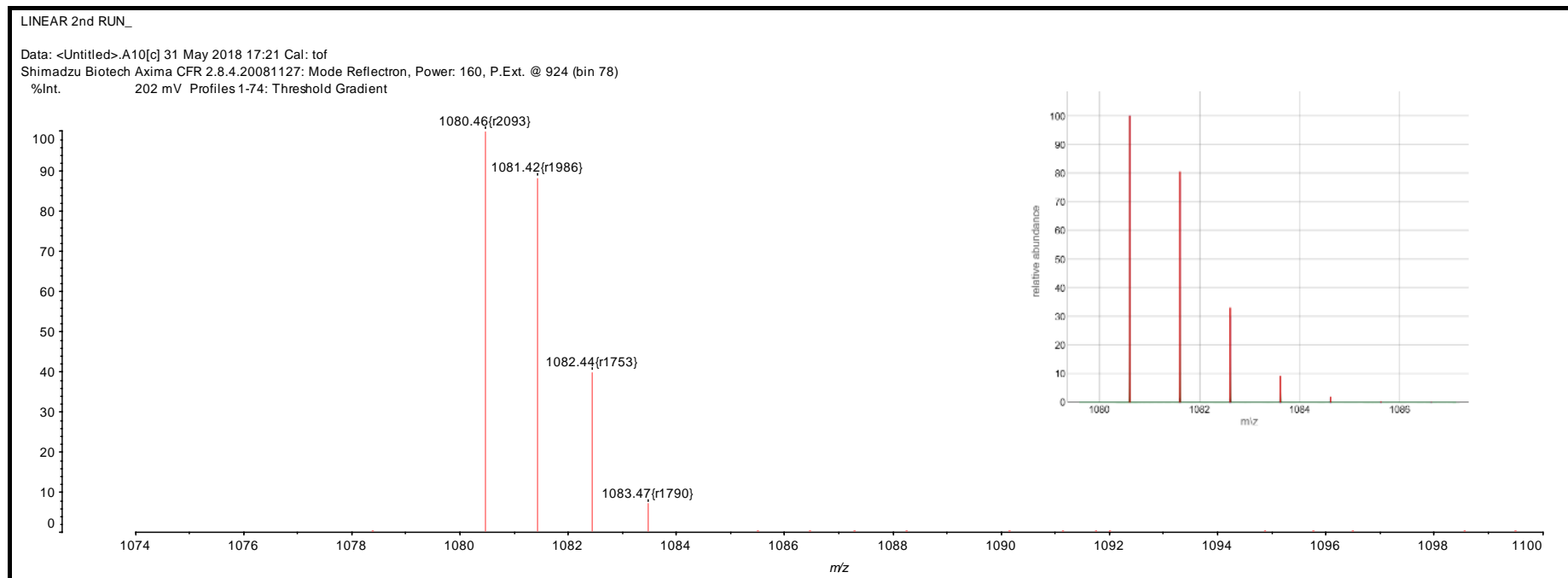
4. Mono Bromide Chain Porphyrin (107)



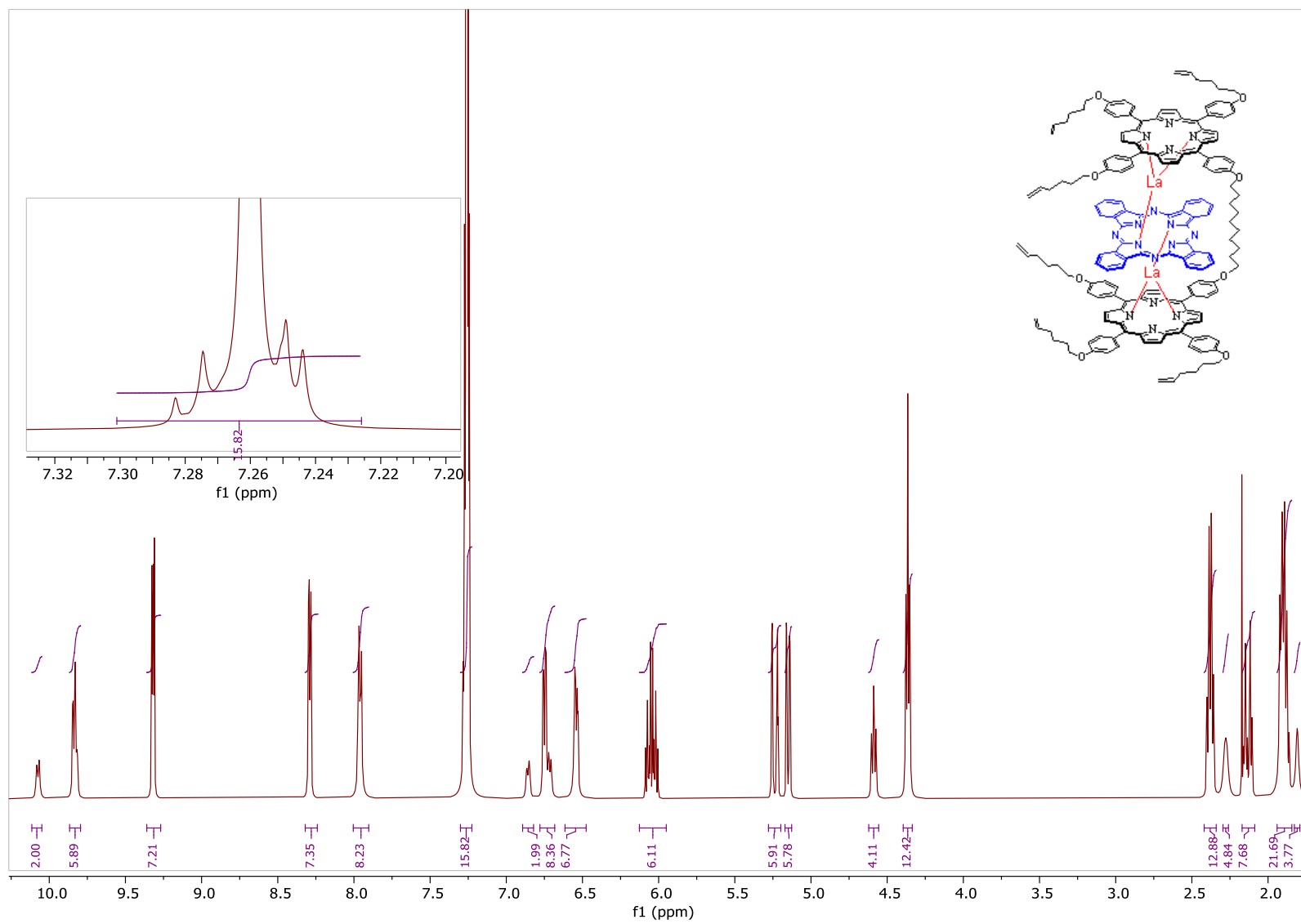
5. Phthalocyanine (59)

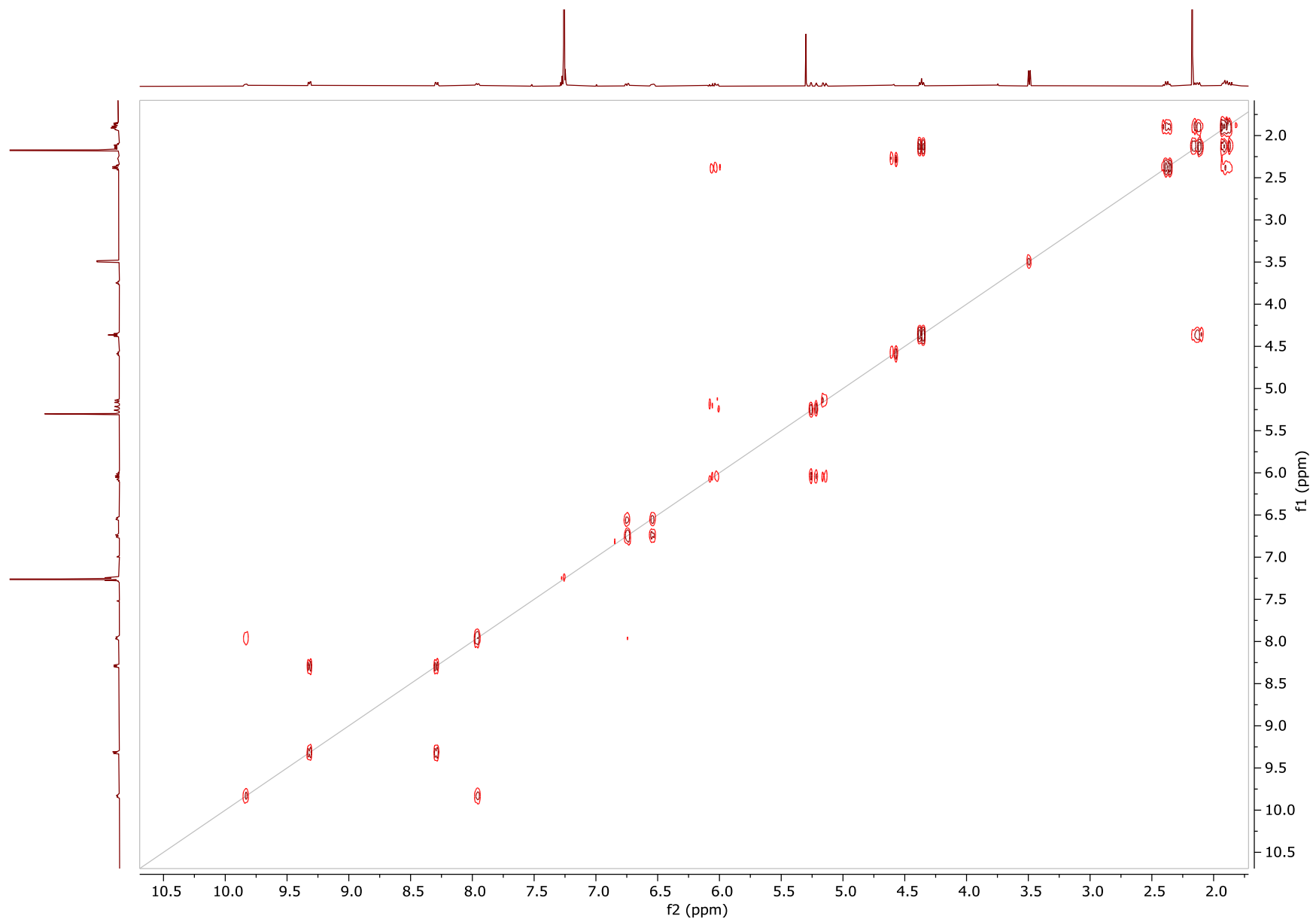


7. HydroxyalkylPorphyrin (109)

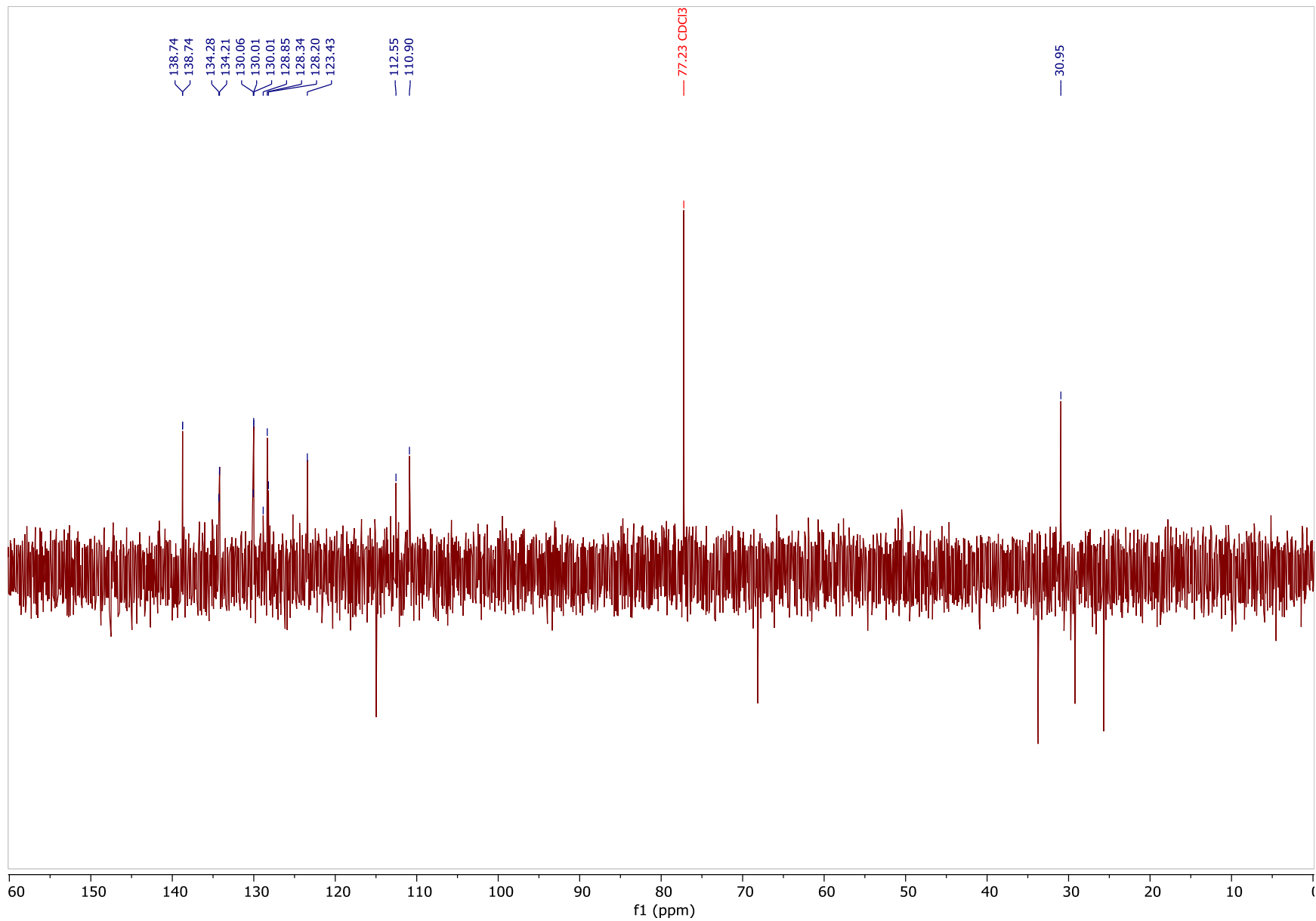


8. TD(La) (94)

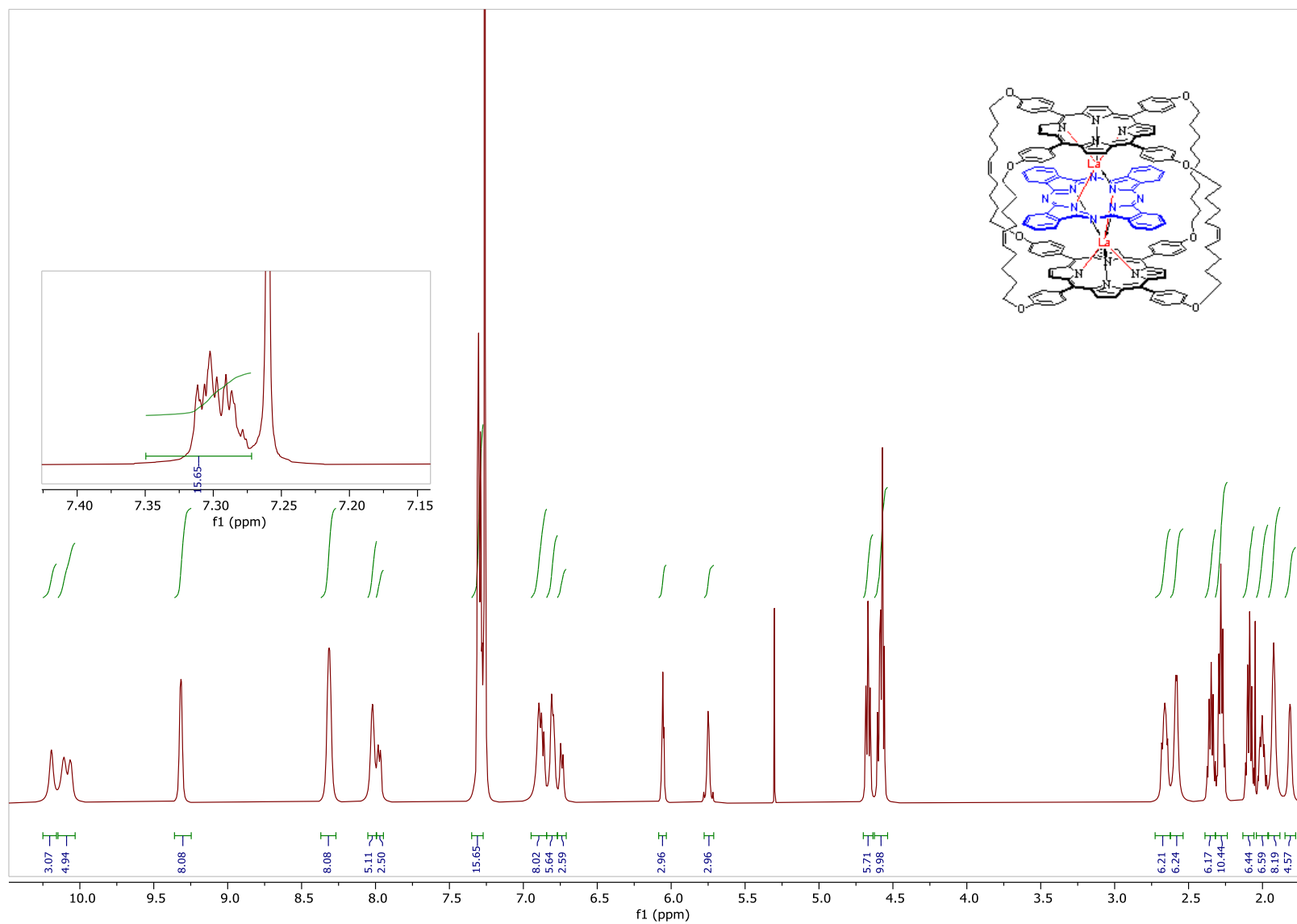


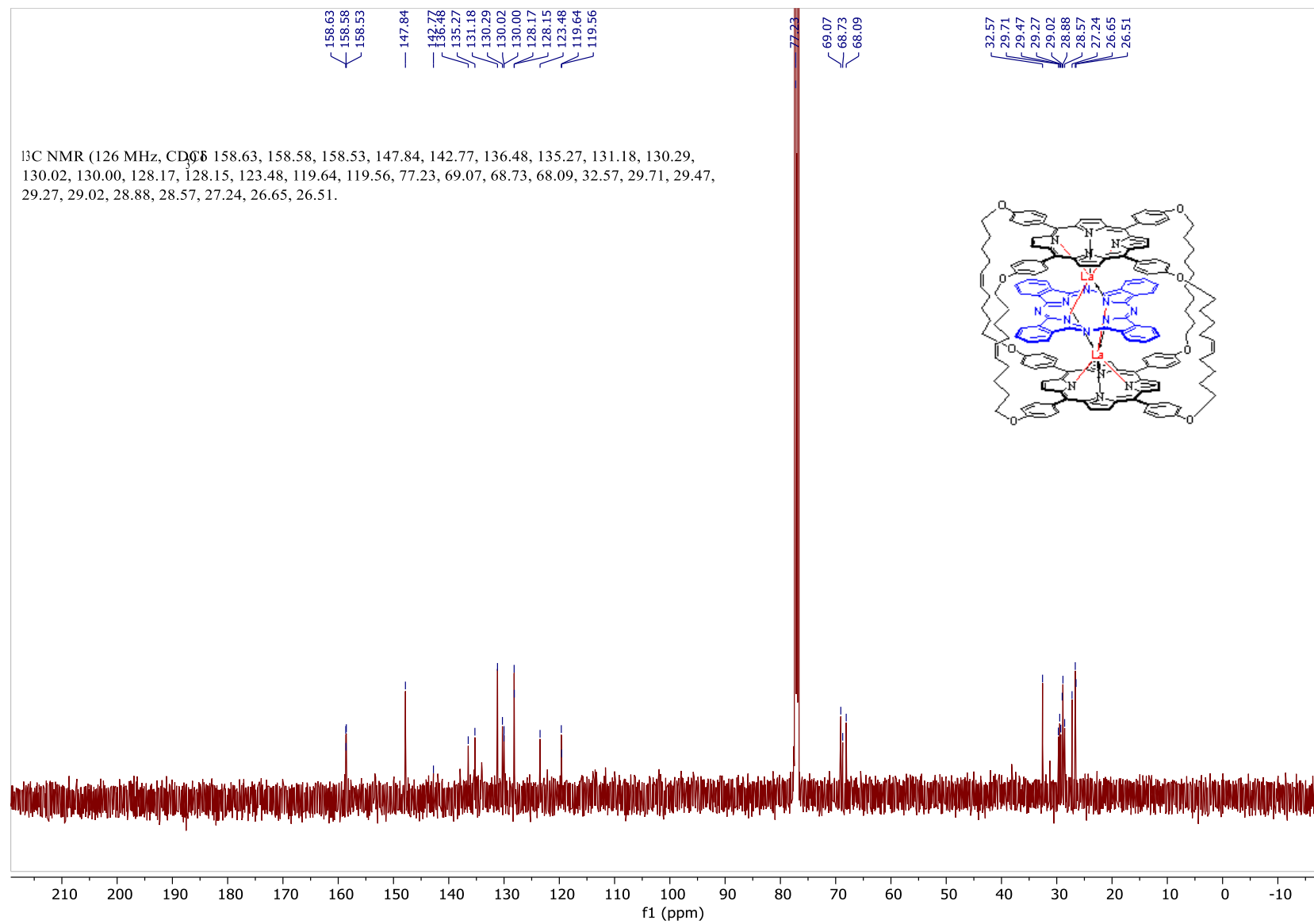


(150)

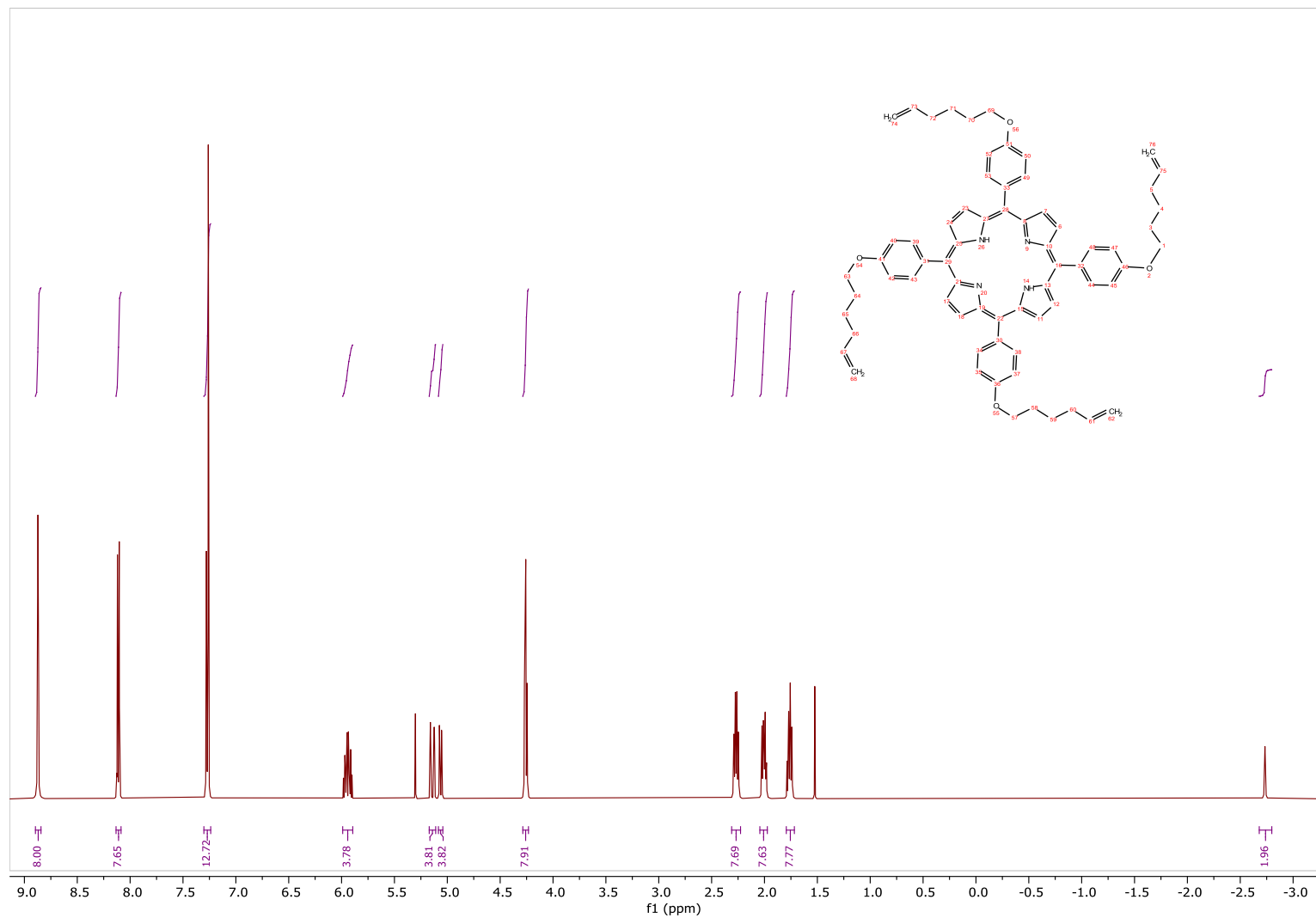


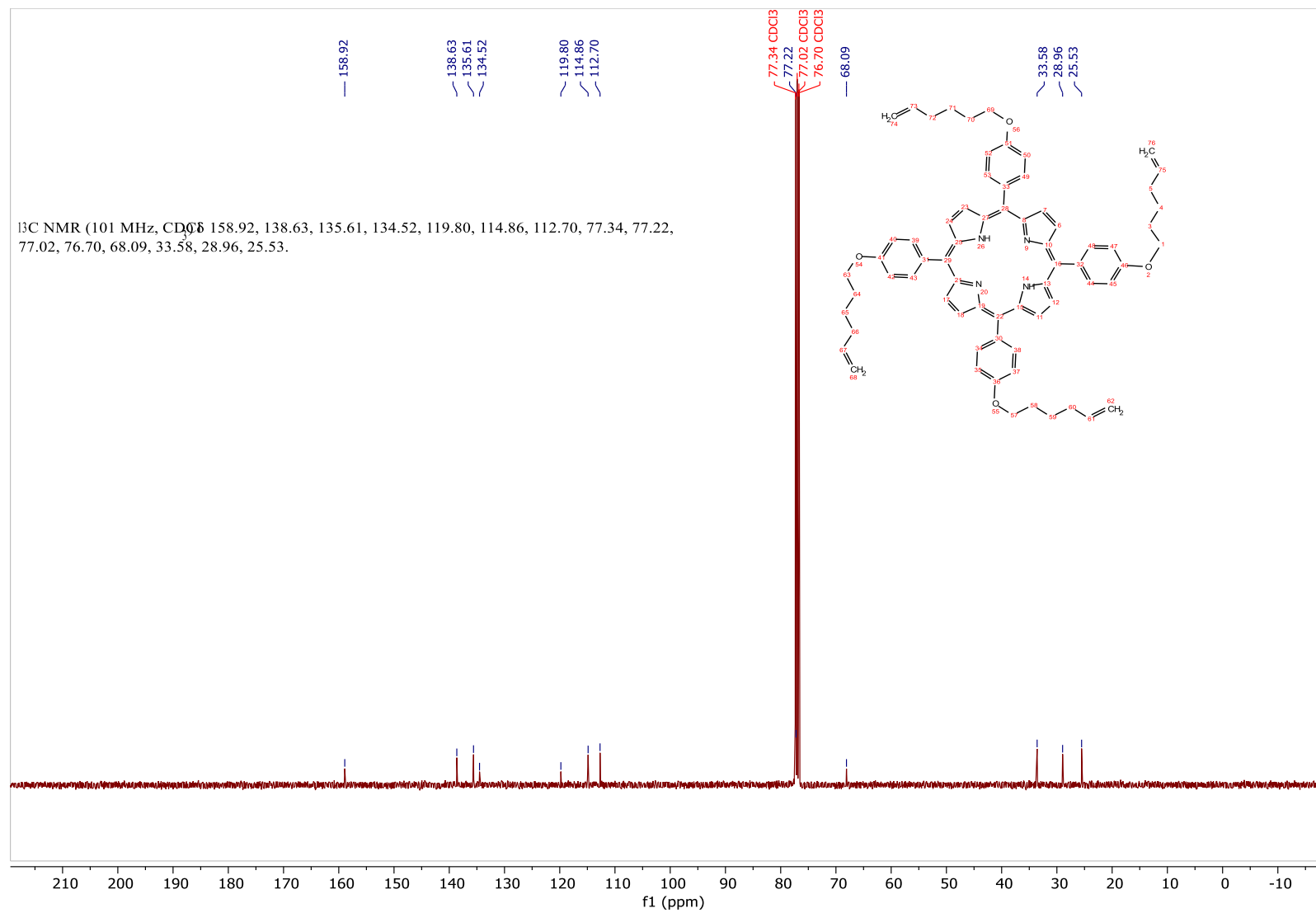
9. CTD(La) (95)



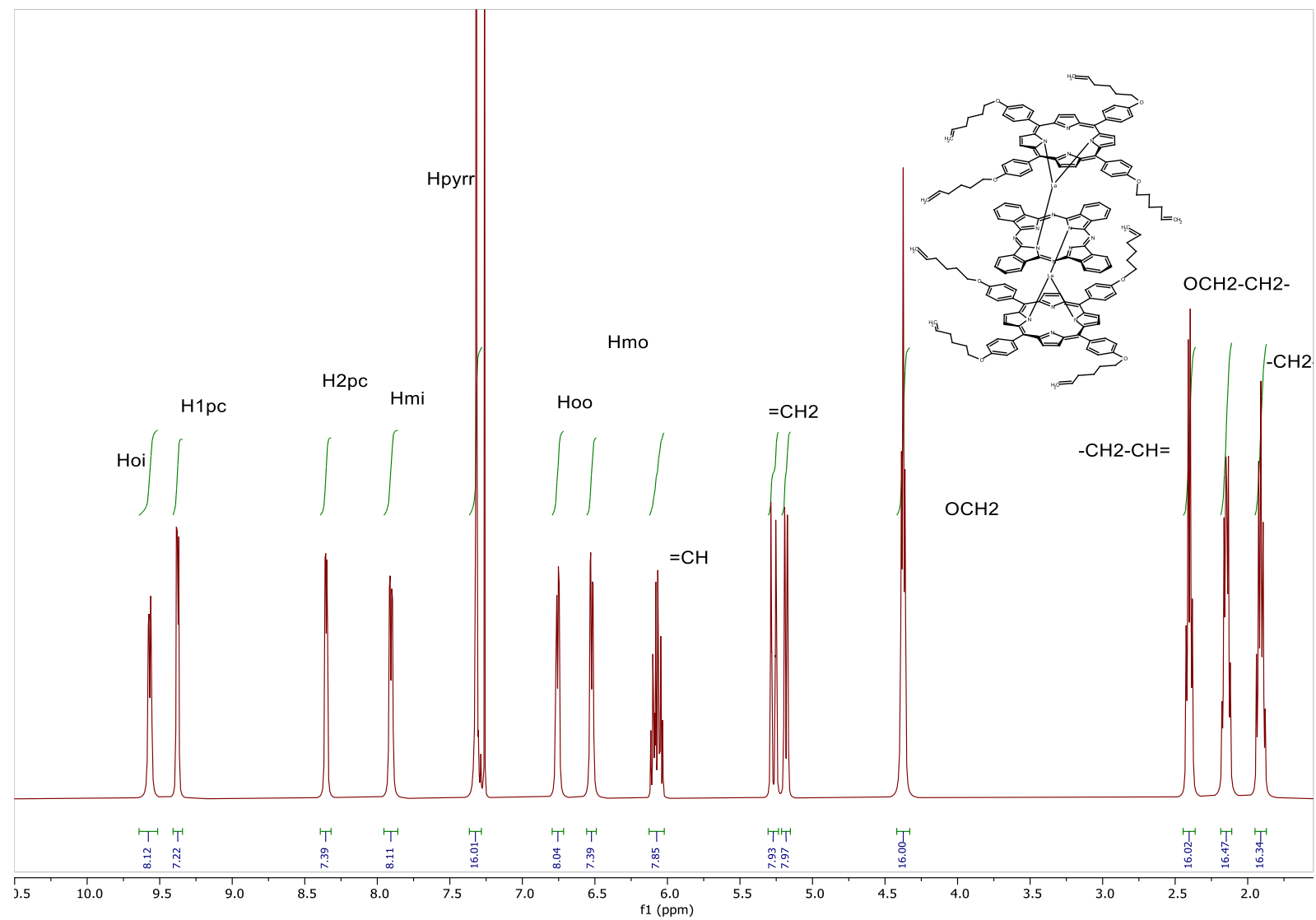


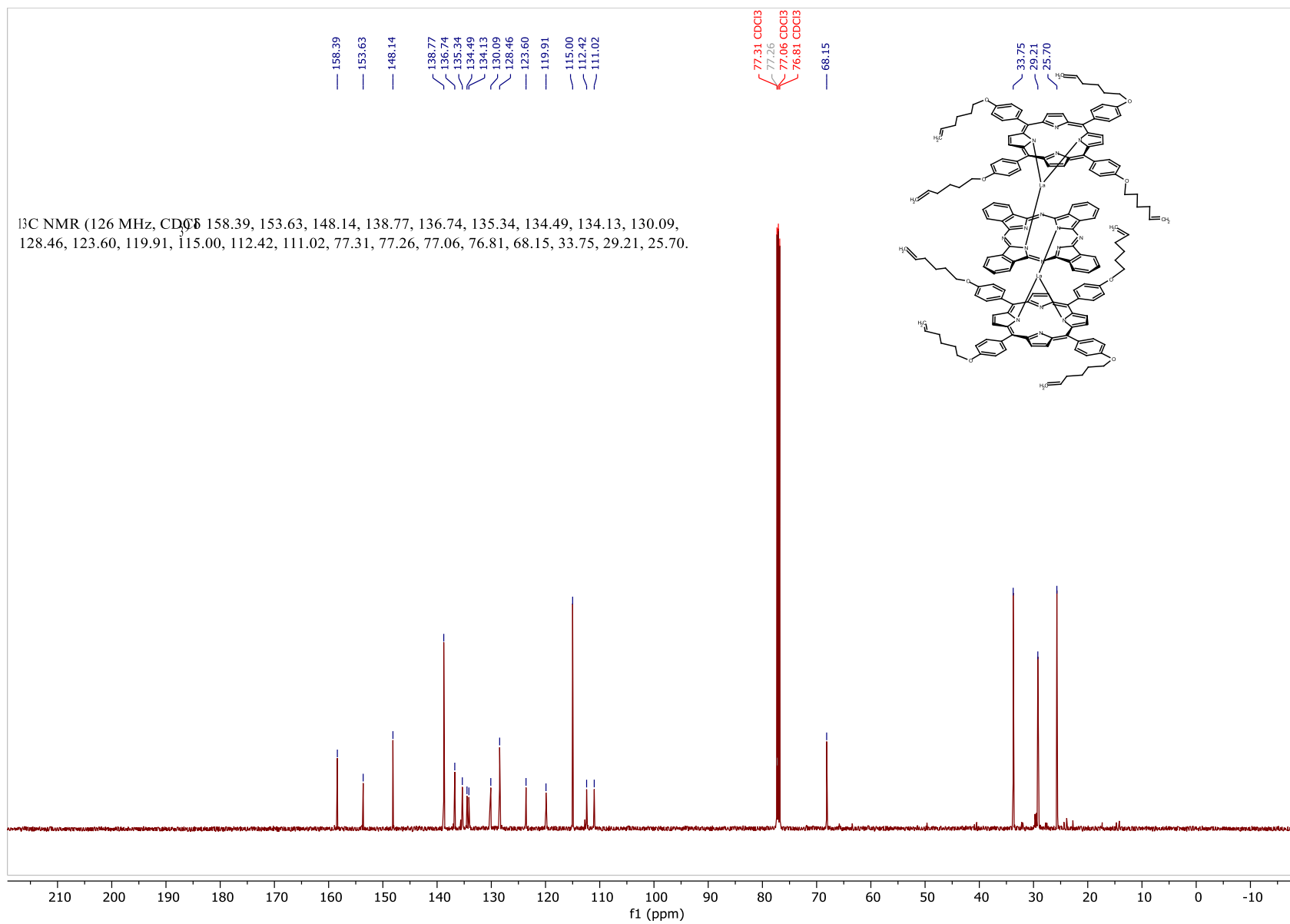
10. THxTPP (97)

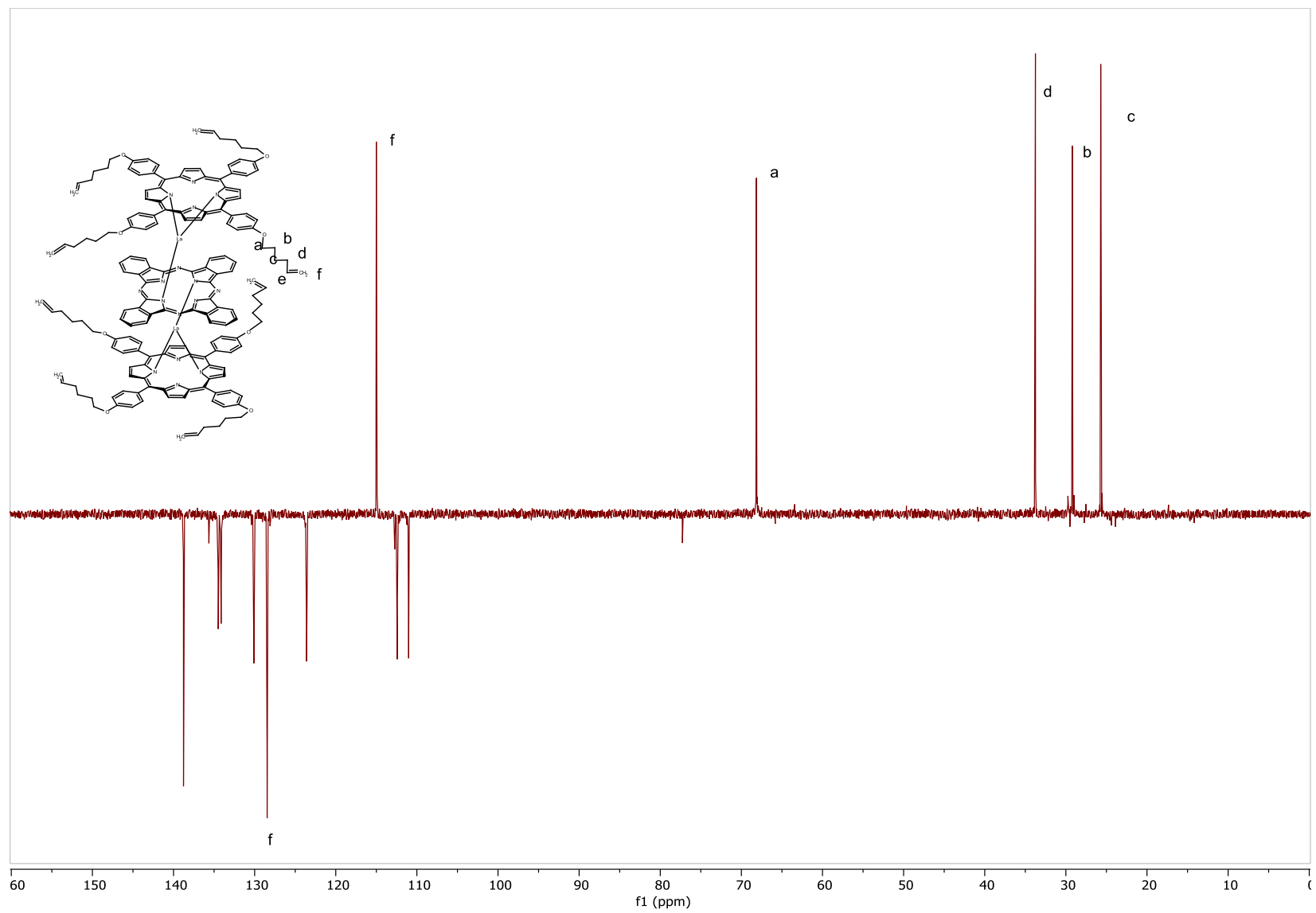




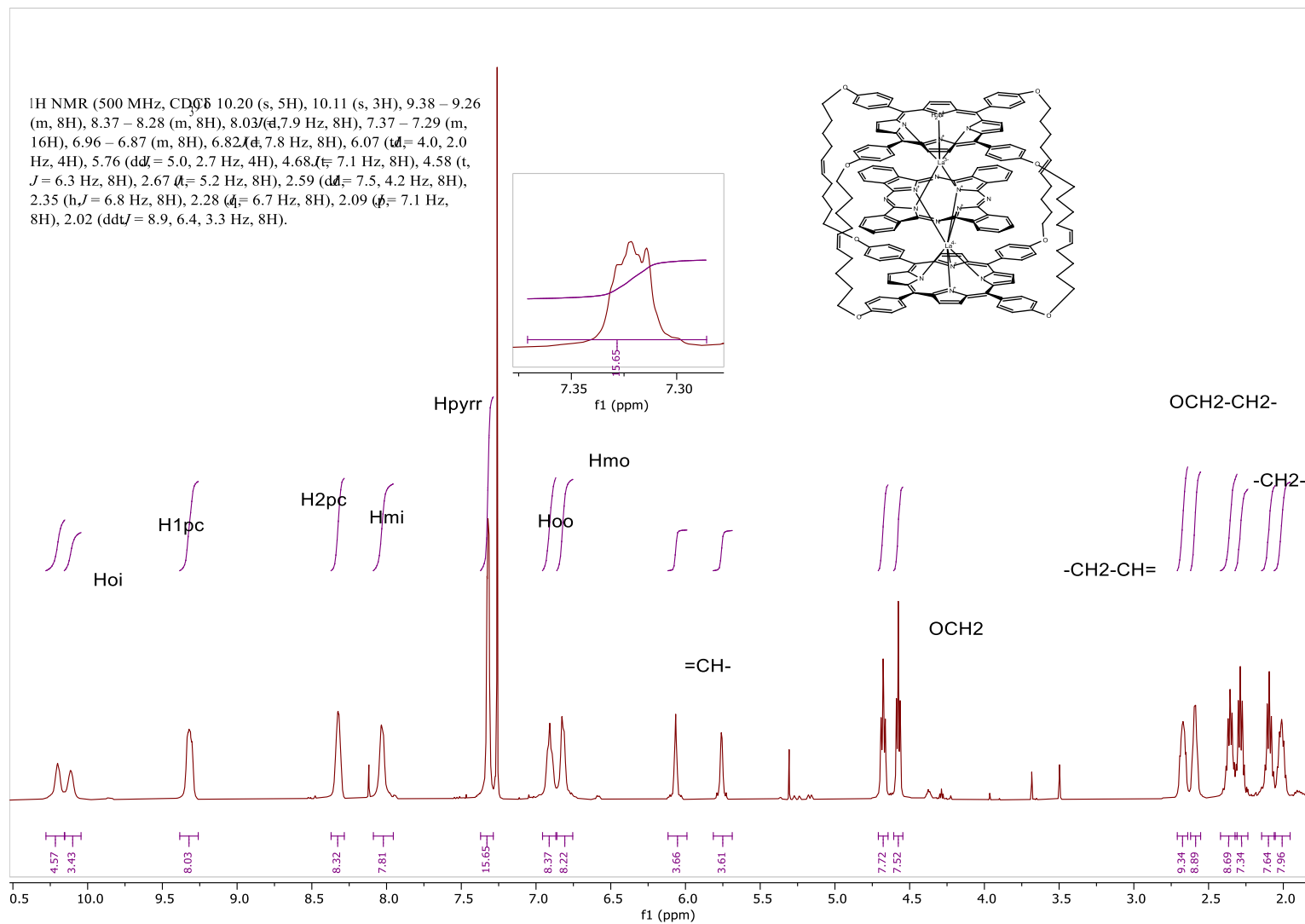
11.DTD(La) (119)

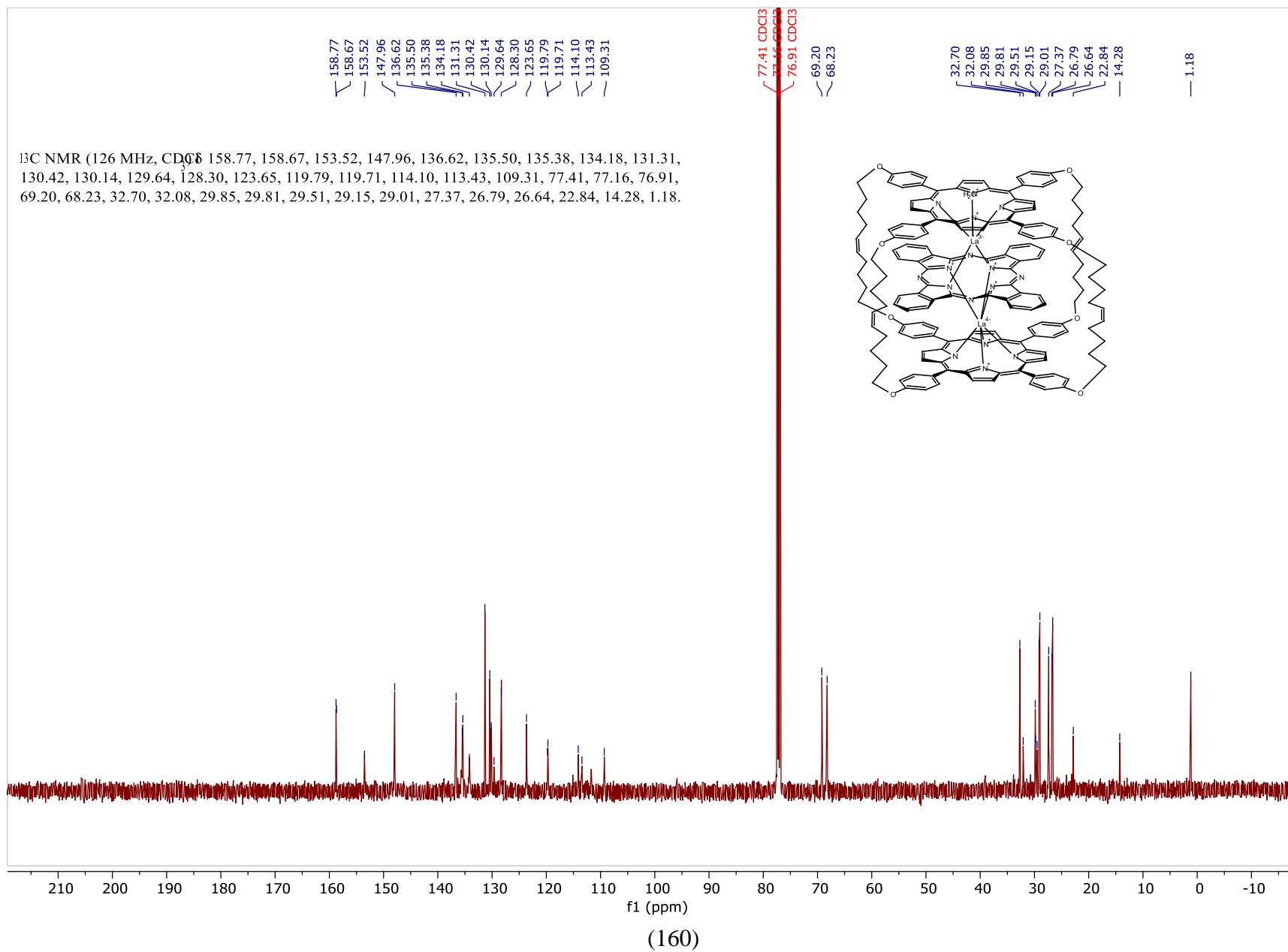


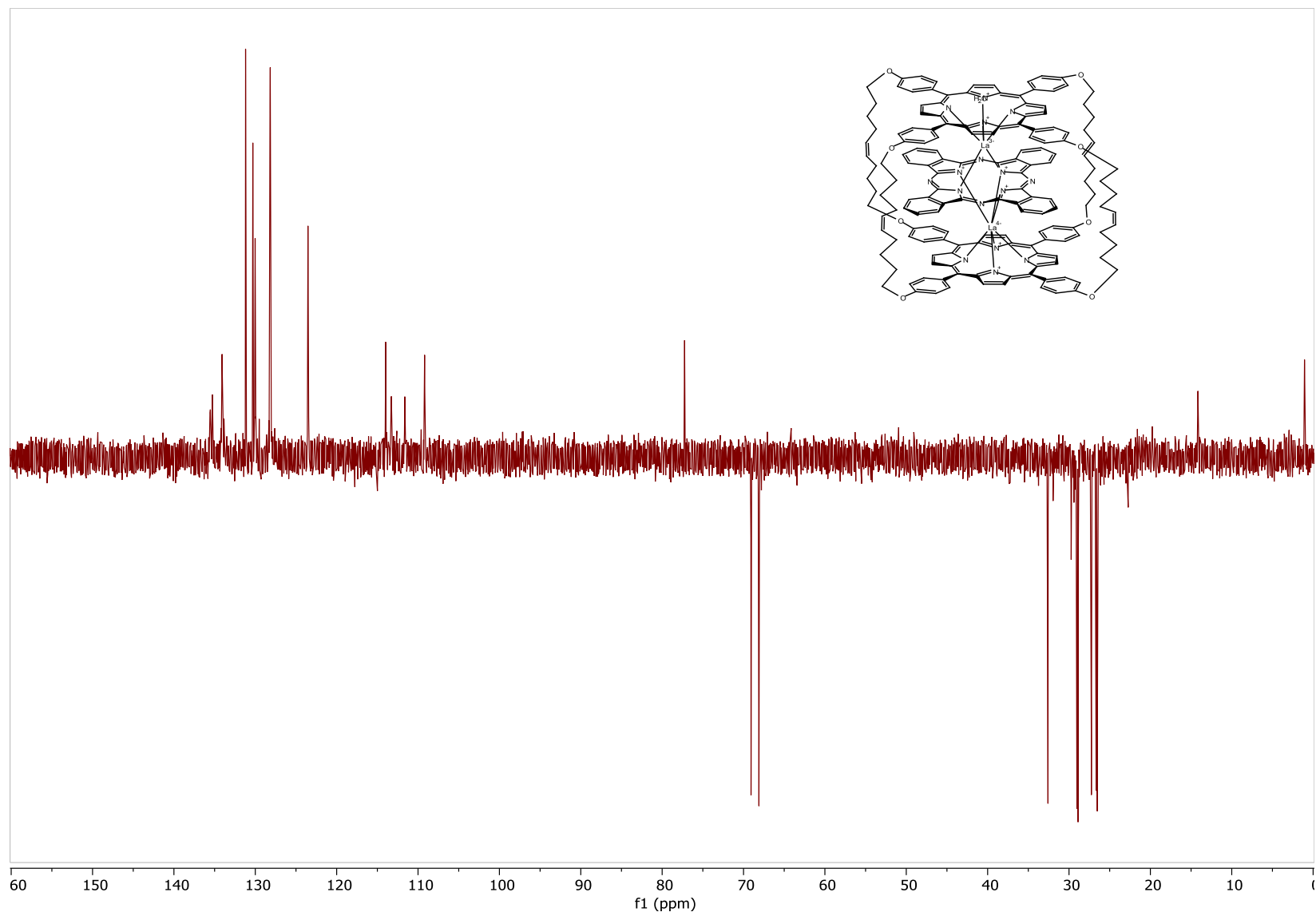




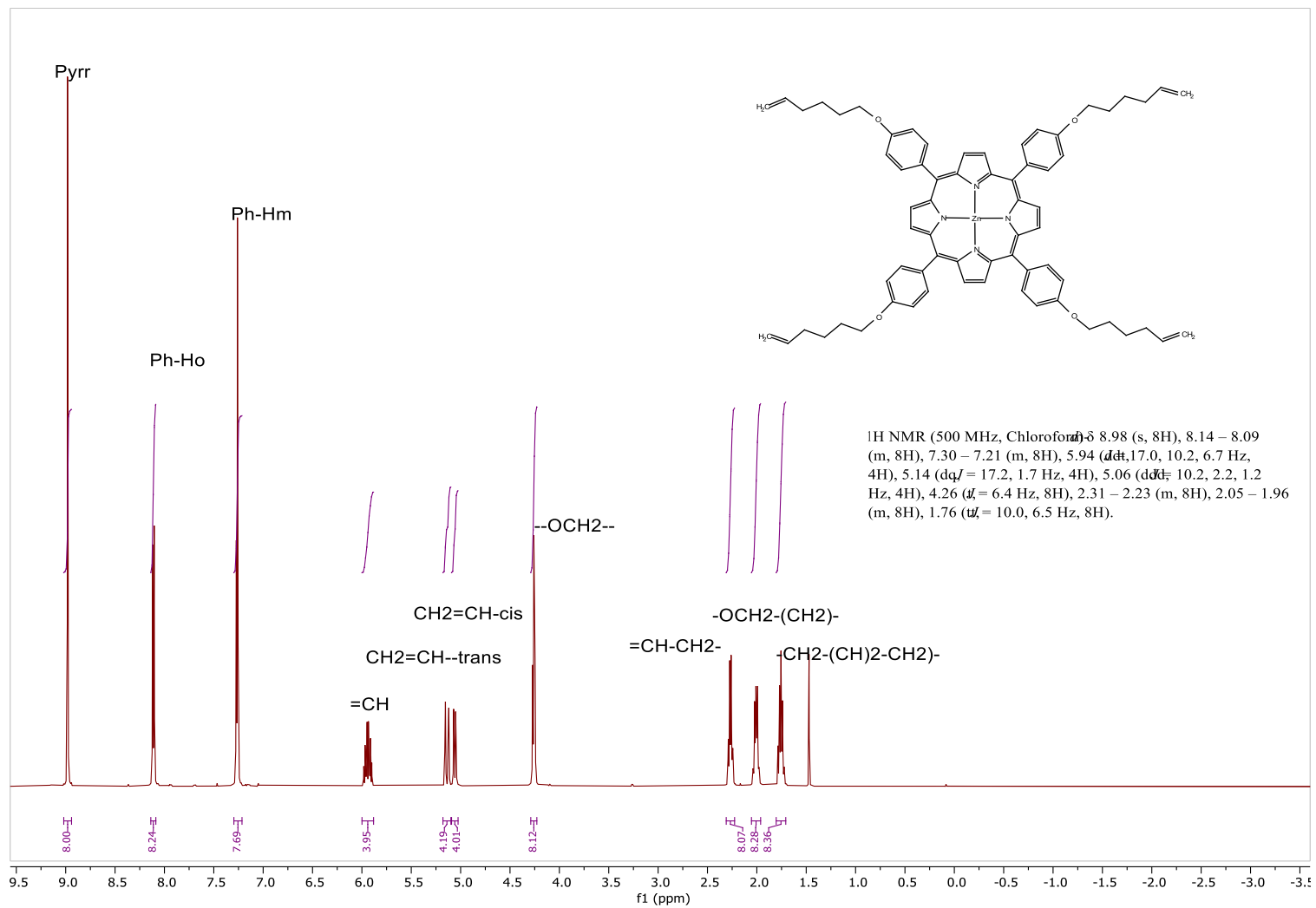
12.CDTD(La) (120)

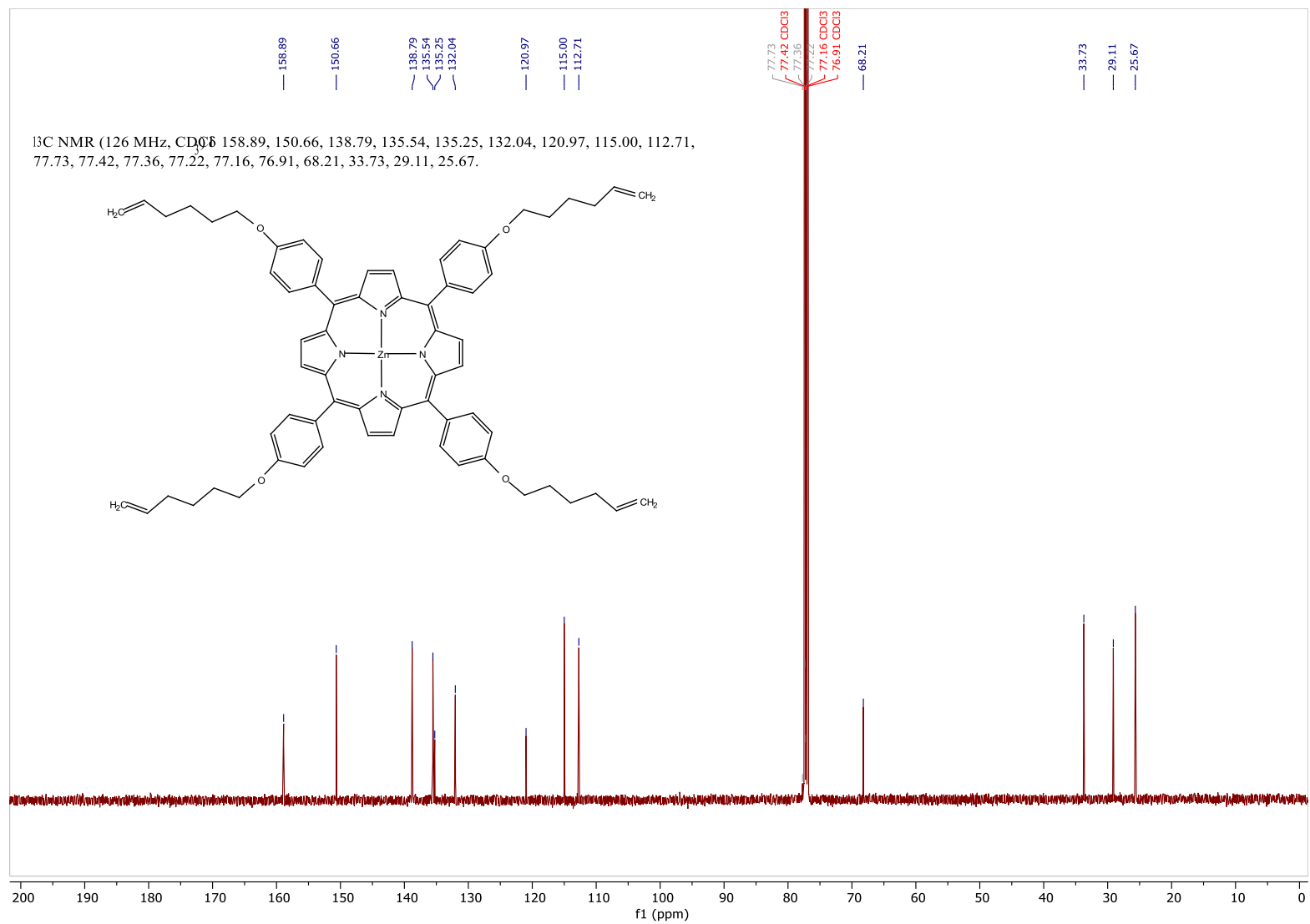






13. THxTPP(Zn) (124)





14. Asymmetrical dyad (114)

